Identification of Central, Stretch Reflex, and Intrinsic Contributions to Human Postural Control

Pouya Amiri

Doctor of Philosophy

Department of Biomedical Engineering

McGill University

Montreal, Quebec, Canada

August 2019

A thesis submitted to McGill University in partial fulfillment of the requirements of the degree of Doctor of Philosophy

To my parents, Masoumeh and Hatam

For their love and support

ABSTRACT

This thesis deals with the identification of central, stretch reflex, and intrinsic contributions to human postural control. Standing is an important functional task that involves complex interactions among central nervous, peripheral nervous, and musculoskeletal systems. The body is inherently unstable in standing, so ankle torque must be continuously modulated to maintain stability. This is achieved by: (1) a central controller, activating muscles in response to sensory information, (2) intrinsic stiffness, due to mechanical properties of muscles and joint, and (3) reflex stiffness, resulting from stretch reflex activation of muscles. This thesis aims to answer two questions: 1) What is the contribution of ankle intrinsic stiffness to postural control? 2) What are the contributions of central and stretch reflex mechanisms to postural control?

The first part of this thesis deals with quantifying ankle intrinsic stiffness in a range of postural operating conditions. It makes five major contributions: (i) It develops a method to identify time varying ankle intrinsic stiffness in standing. In doing so, it demonstrates that the commonly used mass-spring-damper model of ankle intrinsic stiffness is not sufficient in standing, and a more complex model is needed to describe the stiffness accurately. (ii) It quantifies ankle intrinsic stiffness in a range of postural operating conditions, including normal standing, forward lean, backward lean, toe-up, and toe-down standing. (iii) It demonstrates that in each operating condition, intrinsic stiffness changes systematically as a function of center of pressure in one of three ways, associated with distinct muscle activation patterns. (iv) It shows that mean ankle intrinsic stiffness varies with the operating conditions; the stiffness is highest in forward lean, where the mean center of pressure is close to the anterior limits of stability and is lowest in backward lean, where the mean center of pressure is close to the posterior limits of stability. (v) Finally, it demonstrates that intrinsic stiffness varies widely with the operating conditions, from as little as 0.08 to as much as 0.75 of the critical stiffness. Thus, the intrinsic stiffness can be substantial, but it is never adequate in itself to provide postural stability.

The second part of the thesis develops a multiple-input, single-output, closed-loop method to identify active contributions to postural control, generated by the central controller and stretch reflex. It makes five major contributions: (i) The new method quantifies the relative contributions of central controller, stretch reflex, and intrinsic stiffness to ankle torque in human postural control.

(ii) Application of the method to data of perturbed normal standing shows that active elements contribute on average 85% to the total torque and thus are much larger than the passive contributions, generated by intrinsic stiffness. (iii) Ankle plantar-flexors generate the largest portion of the active torque in response to central activation, while the plantar-flexors torque in response to stretch reflex activation is variable among subjects and substantial in some cases. In addition, ankle dorsi-flexors central torque is significant in a few cases. (iv) Although there is high inter-subject variability in the contribution of individual ankle plantar-flexors to the central torque, medial gastrocnemius often contributes the most, while soleus and lateral gastrocnemius make smaller but substantial contributions. (v) The EMG-torque dynamics of the ankle plantar-flexors are different for central and stretch reflex activation: *central EMG-torque dynamics* has higher DC gain and smaller bandwidth. Altogether, these results demonstrate that active central torque provides most of the torque required for postural control, while the stretch reflex and intrinsic stiffness generate smaller but still substantial torques.

The methods developed in this thesis provide the means (a) to quantify time varying ankle intrinsic stiffness in a variety of postural conditions, and (b) to decompose the contributions of central control, stretch reflex, and intrinsic stiffness to ankle torque in standing. These methods provide the tools to investigate healthy human postural control and its adaptability to different experimental conditions. In addition, the methods can be used to objectively diagnose the etiology of balance impairments, and consequently design targeted interventions for patients. Particularly, the methods are useful to investigate and assess the risk of falls in the elderly and develop strategies for fall prevention. Moreover, the findings can be used for the design of assistive devices such as orthotics and prosthetics.

The application of the developed methods to experimental data generated results with important implications: (i) Ankle intrinsic stiffness and its contribution undergo large changes in standing; failure to account for such changes in any study of postural control generates misleading results. (ii) Intrinsic stiffness can change over a large range in normal standing, but, its overall contribution is much smaller than the active contributions, since the intrinsic stiffness mostly has modest values in the normal standing condition. (iii) Muscle activation strategy for postural control is not unique but is very subject dependent. Consequently, in any investigation of postural control, it is important to record the EMG activity of all major ankle muscles and account for all muscles'

contributions to the ankle torque. Otherwise, important contributions may be neglected. (iv) Central and stretch reflex EMG-torque dynamic relations are very different and must not be assumed to be the same in any study of postural control and probably in any type of functional tasks. Altogether, the results of this thesis demonstrate that any investigation, which treats human postural control as a stationary process with fixed contributions from different components, will provide misleading results. A correct understanding of the underlying mechanism of postural control is possible, when it is regarded as a dynamic process, where the relative contributions of different elements are continuously changing.

RÉSUMÉ

Cette thèse examine l'identification des contributions centrales, réflexes et intrinsèques au contrôle postural humain. Rester debout est une tâche importante qui requis des interactions complexes entre les système nerveux central, système nerveux périphérique et système musculo-squelettique. Le corps est intrinsèquement instable en position verticale; le moment de torsion de la cheville doit donc être modulé continuellement pour maintenir la stabilité. Ceci est réalisé par: (1) un contrôleur central, activant les muscles en conséquence des informations sensorielles, (2) la raideur intrinsèque, à cause de propriétés mécaniques des muscles et des articulations, et (3) la raideur réflexe, résultant de l'activation du réflexe des muscles. Cette thèse vise à répondre à deux questions: 1) Quelle est la contribution de la raideur intrinsèque de la cheville au contrôle postural? et 2) Quelles sont les contributions du contrôle central et du réflexe au contrôle postural?

La première partie de cette thèse portait sur la quantification de la raideur intrinsèque de la cheville dans diverses conditions opératoires posturales. Elle a apporté cinq contributions majeures: (i) le développement d'une méthode d'identification de la raideur intrinsèque instationnaire de la cheville. Ce faisant, il a été démontré que le modèle masse-ressort-amortisseur couramment utilisé pour décrire la raideur intrinsèque de la cheville était insuffisant durant l'acte de rester debout, et qu'il fallait un modèle plus complexe pour décrire la raideur; (ii) la quantification la raideur intrinsèque de la cheville dans diverses conditions opératoires posturales, y compris la posture normale, l'inclinaison vers l'avant, l'inclinaison vers l'arrière, la posture normale avec diverse inclinaison des pieds; (iii) la démonstration que dans chaque condition, la raideur intrinsèque change systématiquement en fonction du centre de pression de l'une des trois façons associée à des schémas d'activation musculaire distincts; (iv) la démonstration que la raideur intrinsèque moyenne de la cheville variait avec les conditions, étant plus élevée en l'inclinaison vers l'avant, où le centre de pression moyen était proche des limites antérieures de stabilité et étant plus faible en l'inclinaison vers l'arrière, où le centre de pression moyen était proche des limites de stabilité postérieur; (v) enfin, la démonstration que la raideur intrinsèque variait considérablement avec les conditions opératoires posturales, allant de 0.08 à 0.75 fois la raideur critique. Ainsi, la raideur intrinsèque pourrait être substantielle, mais elle n'a jamais suffi à assurer la stabilité posturale.

La deuxième partie de la thèse a développé une méthode en boucle fermée à entrées multiples sortie simple, permettant d'identifier les contributions actives au contrôle postural, générée par le contrôleur central et le réflexe. Elle a apporté cinq contributions majeures: (i) la nouvelle méthode a quantifié les contributions relatives du contrôleur central, du réflexe et de la raideur intrinsèque au moment de torsion de la cheville dans le contrôle postural humain; (ii) l'application de la méthode aux données de posture normale perturbée a montré que les éléments actifs contribuaient en moyenne 85% du moment de torsion total et étaient donc beaucoup plus importants que les contributions passives, générées par la raideur intrinsèque; (iii) les fléchisseurs plantaires de cheville généraient la plus grande partie du moment de torsion actif en réponse à l'activation centrale, tandis que le moment de torsion de fléchisseurs plantaires en réponse à l'activation du réflexe était variable selon les sujets et substantiel dans certains cas. De plus, le moment de torsion central dorso-fléchisseur de la cheville était significatif dans peu de cas; (iv) bien que la contribution des fléchisseurs plantaires individuels de la cheville au moment de torsion central variait fortement entre les sujets, le gastrocnémien médial souvent contribuait plus, alors que le gastrocnémien latéral et soléus contribuaient moins mais restait substantielle; (v) la dynamique de EMG-moment de torsion des fléchisseurs plantaires de la cheville était différente pour l'activation central et réflexe: la dynamique de EMG-moment de torsion central avait un gain statique plus élevé et une bande passante réduite. Ces résultats démontrent que le moment de torsion central actif contribuait la majeure partie du moment torsion nécessaire du contrôle postural, alors que le réflexe et la raideur intrinsèque génèrent des moments de torsion plus faibles, mais néanmoins importants.

Les méthodes développées dans cette thèse fournissent les moyens (a) de quantifier la raideur intrinsèque instationnaire de la cheville dans diverses conditions posturales, et (b) de décomposer les contributions du contrôle central, du réflexe et de la raideur intrinsèque au moment de torsion de la cheville en position debout. Ces méthodes fournissent les outils nécessaires pour étudier le contrôle postural humain sain et son adaptabilité à diverses conditions expérimentales. En outre, les méthodes peuvent être utilisées pour diagnostiquer objectivement l’étiologie des troubles de l’équilibre et, par conséquent, concevoir des interventions ciblées pour les patients. Les méthodes sont particulièrement utiles pour étudier et évaluer le risque de chute chez les personnes âgées et

pour développer des stratégies de prévention des chutes. En plus, les résultats peuvent être utilisés pour la conception de dispositifs d'assistance tels que les orthèses et les prothèses.

Ici, l'application des méthodes développées aux données expérimentales a produit des résultats avec des implications importantes: (i) la raideur intrinsèque de la cheville et sa contribution subissent de grandes modifications durant l'acte de rester debout; l'absence de prise en compte de tels changements dans toute étude du contrôle postural génère des résultats erronés; (ii) la raideur intrinsèque peut changer largement durant l'acte de rester debout. Cependant, sa contribution totale est beaucoup plus petite que les contributions actives, car la raideur intrinsèque a généralement des valeurs modestes dans des conditions posturales normales; (iii) la stratégie d'activation musculaire pour le contrôle postural n'est pas unique, mais dépend fortement du sujet. Par conséquent, dans toute étude du contrôle postural, il est important d'enregistrer l'activité EMG de tous les principaux muscles de la cheville et de comptabiliser toutes les contributions de ces muscles au moment de torsion de la cheville. Sinon, des contributions importantes pourraient être négligées; (iv) le dynamique de EMG-moment de torsion réflexe et le dynamique de EMG-moment de torsion central sont très différentes et ne doivent pas être supposées identiques dans aucune étude du contrôle postural et probablement dans tout type de tâches fonctionnelles. En totalité, les résultats de cette thèse démontrent que toute enquête, qui considère le contrôle postural humain comme un processus stationnaire avec une contribution fixe de différentes composantes, donnera des résultats erronés. Une bonne compréhension du mécanisme du contrôle postural est possible, lorsque celui-ci est considéré comme un processus dynamique, dans lequel l'importance de différents éléments change continuellement.

ACKNOWLEDGMENTS

I wish to express my sincere gratitude to my supervisor, Professor Robert E. Kearney, for his invaluable advice, support, and continuous guidance throughout my PhD. I have been always amazed by Dr. Kearney's vision, knowledge, and experience in different subjects of engineering. He has guided me through different stages of my PhD research, nonetheless, he always gave me the freedom to choose the problems and to find solutions to tackle them, which, in my opinion, is essential for a PhD student, who wishes to continue doing research in the future. In addition, Dr. Kearney has always been very approachable and patient with me and I have learned so many things from him that will help me throughout both my academic and personal life and for that I am very grateful.

I would like to thank the members of my PhD committee, Dr. Joyce Fung, and Dr. Satya Prakash for their constructive comments and excellent feedback on my research and progress during my PhD.

I wish to express my gratitude to my colleagues at REKLAB, where I spent most of my time during my PhD. I would specifically like to thank my friend, Abolfazl Mohebbi, who has contributed to this thesis and has been the co-author of one of my articles. His knowledge and ideas have been always very helpful. I would also like to thank Mahsa Golkar and Ehsan Sobhani, my awesome friends, who have always provided me with great ideas and enjoyable moments in the lab. Finally, I want to thank my other colleagues Guy Tsror, Kian Jalaleddini, Lara Kanbar, Johan Vargas, and Diego Guarin, with whom I shared great time inside and outside of the lab.

I would also like to thank the awesome people at the department of biomedical engineering at McGill University, who have made my PhD life easy. My gratitude extends to Ms. Pina Sorrini, Mrs. Trang Q. Tran, and Ms. Sabrina Teoli for their help to resolve different administrative matters during my PhD. They have all been very friendly and approachable. In addition, I want to thank Dr. Ross Wagner for his help to resolve technical difficulties in the lab.

Finally, I wish to express my utmost gratitude to my parents, Hatam and Masoumeh, for their love and endless support throughout different stages of my life. I can not thank them enough and

the least I can do it to dedicate this thesis to them. I am also thankful to my amazing sister, Pegah, who has been very encouraging and supportive during my PhD.

Finally, I want to thank the sources of funding, which have made this research possible. These include, the NPRP grant #6-463-2-189 from the Qatar National Research Fund (a member of Qatar Foundation), MOP grant #81280 from the Canadian Institutes of Health Research (CIHR), and Lloyd Carr-Harris foundation.

TABLE OF CONTENTS

ABSTRACT ..... **III**
RÉSUMÉ ..... **VI**
ACKNOWLEDGMENTS ..... **IX**
TABLE OF CONTENTS ..... **XI**
LIST OF TABLES ..... **XV**
LIST OF FIGURES ..... **XVI**
CHAPTER 1 INTRODUCTION **1**
1.1 THESIS OUTLINE **3**
1.2 CONTRIBUTION OF THE AUTHORS **4**
CHAPTER 2 REVIEW OF THE LITERATURE PERTAINING TO POSTURAL CONTROL 7
2.1 SOME COMMON NOTIONS IN HUMAN POSTURAL CONTROL **7**
2.2 POSTURAL CONTROL **10**
2.3 POSTURAL CONTROL STRATEGIES **11**
2.4 VIEWS ON POSTURAL CONTROL **13**
2.4.1 Stiffness control 13
2.4.2 Feedback control 14
2.4.3 Feedforward control 14
2.4.4 Intermittent, ballistic-like control 15
2.5 CLOSED-LOOP POSTURAL CONTROL **16**
2.5.1 Feedback postural control 16
2.5.2 Models of human body dynamics in standing 18
2.5.3 Sensory systems in postural control 19
2.6 MULTISENSENSORY INTEGRATION IN HUMAN POSTURAL CONTROL **23**
2.7 APPROACHES TO MODEL SENSORY REWEIGHTING IN POSTURAL CONTROL 24
2.8 ANKLE JOINT STIFFNESS AND ITS ROLE IN POSTURAL CONTROL **27**
2.8.1 Ankle joint 27
2.8.2 Dynamic Joint stiffness 28
2.8.3 Variation of ankle stiffness with the operating points 32
2.8.4 Ankle stiffness in standing 33
CHAPTER 3 IDENTIFICATION OF HUMAN POSTURAL CONTROL **39**
3.1 IDENTIFICATION OF ANKLE JOINT STIFFNESS IN CONTROLLED SUPINE CONDITIONS **39**
3.1.1 Identification in quasi-stationary experiments 40
3.1.2 Identification in time varying conditions 41
3.2 THE PROBLEM WITH CLOSED-LOOP IDENTIFICATION **42**
3.3 METHODS FOR CLOSED-LOOP IDENTIFICATION **45**
3.3.1 The direct approach 46
3.3.2 The indirect approach 46

3.3.3 The joint input-output approach 48
3.4 REVIEW OF THE STUDIES OF POSTURAL CONTROL IDENTIFICATION 49
3.4.1 Indirect approach 49
3.4.2 Joint input-output approach 51
3.4.3 Direct approach 51
3.5 RATIONALE 53
CHAPTER 4 MEASUREMENT OF SHANK ANGLE DURING STANCE USING LASER RANGE FINDERS 55
4.1 ABSTRACT 56
4.2 INTRODUCTION 57
4.3 THEORY 58
4.4 METHODS 61
4.4.1 Sensor selection 61
4.4.2 Data acquisition 62
4.4.3 Linear calibration 62
4.4.4 Static angular testing 62
4.4.5 Dynamic testing 63
4.4.6 Stance experiments 64
4.5 RESULTS 65
4.6 DISCUSSION 68
CHAPTER 5 EXPERIMENTAL METHODS TO STUDY HUMAN POSTURAL CONTROL 69
5.1 ABSTRACT 70
5.2 INTRODUCTION 70
5.2.1 Standing apparatus 73
5.2.2 Virtual reality device and environment 73
5.2.1 Kinetic measurements 74
5.2.2 Kinematic measurements 75
5.2.3 Data acquisition 75
5.2.4 Safety mechanisms 75
5.3 PROTOCOL 76
5.3.1 Experiments 76
5.3.2 Experimental protocols 78
5.4 IDENTIFICATION OF HUMAN POSTURAL CONTROL 79
5.4.1 Non-parametric identification of the dynamic relation of body angle to visual perturbations 79
5.4.2 Parametric identification of ankle intrinsic stiffness in standing 82
5.5 REPRESENTATIVE RESULTS: 87
5.5.1 Pseudo random ternary sequence (PRTS) and TrapZ signals 87
5.5.2 Identification of the body angle to visual perturbations system 89
5.5.3 Identification of ankle intrinsic stiffness parameters 91
5.6 DISCUSSION 94
CHAPTER 6 ANKLE INTRINSIC STIFFNESS CHANGES WITH POSTURAL SWAY 98

6.1 ABSTRACT 99
6.2 INTRODUCTION 99
6.3 METHODS 100
6.3.1 Participants 100
6.3.2 Standing apparatus 101
6.3.3 EMG 103
6.3.4 Experiments 103
6.3.5 Data acquisition 103
6.3.6 Postural activity 104
6.3.7 Data segmentation and grouping 105
6.3.8 Intrinsic stiffness estimation 105
6.4 RESULTS 108
6.4.1 Quiet vs perturbed standing 108
6.4.2 Shank movement in response to foot perturbation 108
6.4.3 Intrinsic stiffness model 109
6.4.4 Low frequency ankle intrinsic stiffness 111
6.5 DISCUSSION 116
6.5.1 The intrinsic stiffness model 116
6.5.2 Intrinsic stiffness 116
6.5.3 Functional significance of the modulation of ankle intrinsic stiffness in stance 118
CHAPTER 7 PATTERNS OF MUSCLE ACTIVATION AND MODULATION OF ANKLE INTRINSIC STIFFNESS IN STANDING 120
7.1 ABSTRACT 121
7.2 INTRODUCTION 121
7.3 METHODS 123
7.3.1 Participants 123
7.3.2 Dual-actuator apparatus 124
7.3.3 EMG collection 126
7.3.4 Data acquisition 126
7.3.5 Experiments 126
7.3.6 Data analysis 128
7.3.7 Statistical analysis 130
7.4 RESULTS 131
7.4.1 Typical experimental trial 131
7.4.2 Performance of the EIM 131
7.4.3 Intrinsic stiffness modulation 132
7.4.4 Intrinsic stiffness across operating conditions 136
7.5 DISCUSSION 138
7.5.1 Intrinsic stiffness in inclined surface standing 139
7.5.2 Intrinsic stiffness in lean 140
7.5.3 Functional importance of intrinsic stiffness modulations 141
CHAPTER 8 IDENTIFICATION OF CENTRAL, STRETCH REFLEX, AND INTRINSIC CONTRIBUTIONS TO HUMAN POSTURAL CONTROL 142
8.1 ABSTRACT 143
8.2 INTRODUCTION 144

8.3 METHODS **146**
8.3.1 Subjects 146
8.3.2 Standing Apparatus 146
8.3.3 EMG Recording 147
8.3.4 Data Acquisition 147
8.3.5 Experiments 147
8.3.6 Human Postural Control Model 148
8.3.7 EMG decomposition 151
8.3.8 Identification 152
8.4 RESULTS **156**
8.4.1 Experimental data 156
8.4.2 EMG decomposition 158
8.4.3 Typical identification results 160
8.4.4 Identification results for all subjects 164
8.4.5 Central, stretch reflex, and intrinsic contributions 165
8.4.6 Soleus reflex and central EMG-torque dynamics 166
8.5 DISCUSSION **167**
8.5.1 EMG decomposition 168
8.5.2 Identification performance 168
8.5.3 EMG-torque dynamics 169
8.5.4 Central and reflex EMG-torque dynamics 170
8.5.5 Central, reflex, and intrinsic contributions to ankle torque 171
8.6 CONCLUSIONS **172**
CHAPTER 9 DISCUSSION AND CONCLUSIONS **173**
9.1 SUMMARY OF ACCOMPLISHMENTS **173**
9.2 DISCUSSION **175**
9.3 ORIGINAL CONTRIBUTIONS **181**
9.3.1 Intrinsic stiffness in standing 181
9.3.2 Identification of central, stretch reflex, and intrinsic contributions to human postural control 182
9.4 FUTURE WORK **183**
9.4.1 Development of a global ankle intrinsic stiffness model for standing 184
9.4.2 Identification of stretch reflex stiffness in standing 184
9.4.3 Identification of intrinsic stiffness from the residual of the EMG-torque model 185
9.4.4 Adaptation of human postural control 185
9.4.5 Application of the EMG-torque model to standing experiments with continuous perturbations 185
REFERENCES **187**

LIST OF TABLES

Table 5.1 Table of materials 74

Table 6.1 Anthropometric data of the subjects (STD = standard deviation). For gender, M stands for male and F stands for female..... 101

Table 6.2 EIM and IBK model performance for all subjects. Min and max stand for minimum and maximum. IQR shows the interquartile range. 111

Table 6.3 Changes of K_{EIM} with COP for the left and right ankles of subjects. The ratio of maximum K_{EIM}^{N} (K_{EIM}^{max}) to minimum K_{EIM}^{N} (K_{EIM}^{min}) and the range (maximum-minimum) of the estimated parameters, including K_{EIM}^{N}, background torque ($\overline{TQ}_A$), and COP (X_{cop}); and the results of linear regressions analysis for the relation between K_{EIM}^{N} and X_{cop} for all subjects. P value is the probability of the slope being zero. The last column shows mean and standard deviation (std) of each parameter. To find the mean and standard deviation for slope, intercept, and R-squared, only the lines with a non-zero slope (i.e. with p-value<0.05) were used. 114

Table 7.1 Anthropometric data of the subjects (STD = standard deviation). 123

Table 8.1 Identification results for all subjects; S stands for subject; L and R shows left and right ankles. p and BW show the number of poles and bandwidth of the identified TFs. %VAF correspond to the the total active torque. 164

LIST OF FIGURES

Figure 2.1 Determination of COP in standing: the balance between the GRF torque and ankle torque about the ankle axis of rotation in standing 8

Figure 2.2 Free body diagram of a SIP, assuming a torsional spring with stiffness K is opposing the gravity toppling torque. 10

Figure 2.3 Closed-loop human postural control; the body is inherently unstable and subject to gravity torque (g) and disturbances ($dint$ and $dext$). Corrective muscle forces are generated by 1- an active controller with two components: a central controller and spinal stretch reflex; and 2- a passive controller, the intrinsic mechanical joint stiffness. Muscle activation due to stretch reflex and central contributions is reflected by EMG. Only the signals shown in red can be measured, whereas other signals cannot be measured in standing experiments. 17

Figure 2.4 Vestibular organ including the three semicircular canals, and the otolith organ (which includes utricle and saccule); the cochlea is also shown. 20

Figure 2.5 Talocrural joint 27

Figure 2.6 Ankle major dorsi-flexor and plantar-flexor muscles [144] 28

Figure 2.7 Stretch reflex circuit in the arm muscles. Taken and modified from [14]. 31

Figure 2.8 Reflex stiffness model for quasi-stationary conditions; taken from [175]. 32

Figure 3.1 Time invariant, parallel cascade model of ankle joint stiffness under quasi-stationary conditions. Taken from [171]. 40

Figure 3.2 General representation of (A) an open-loop system and (B) a closed-loop system 43

Figure 4.1 Shank rotation and the related horizontal and vertical displacements during stance 59

Figure 4.2 Implementation configurations for shank angle measurement using a range finder; (a) attached sensor, (b) vertical, and (c) horizontal strategies; the blue square and line show the range finder and its beam. 60

Figure 4.3 (a) Calibration: the range finder, points to a block in known distances; (b) Static testing: the ranger finder points to a goniometer with known angles. 63

Figure 4.4 (a) Controlled dynamic testing: the range finder is attached to a frame, to measure the movement of the standing apparatus pedal (b) stance experiment: a subject, standing on the standing apparatus, with the laser measuring the linear displacement of a point on the shank.... 64

Figure 4.5 (a) Calibration result: mean of the measured voltages and corresponding distances and the best line fit; (b) static experiment: estimated angles (mean± standard deviation) vs. true angles (green bars) 66

Figure 4.6 Dynamic experiment results: estimated angle using range finder data compared to the potentiometer angle for a sawtooth input with peak to peak amplitude of 1.72 degrees..... 67

Figure 4.7 Shank, foot, and ankle angles, and the corresponding joint torque in (left) quiet and (right) perturbed stance experiments 67

Figure 5.1 Postural control model: the body is inherently unstable and subject to destabilizing gravity torque (g) and disturbances. Stable upright posture is maintained by corrective muscle forces, generated by a central controller, spinal stretch reflexes, and intrinsic mechanical joint stiffness. Muscle activation due to stretch reflex and central contributions is evident in the EMG activity. Only the signals in red can be measured, whereas black signals cannot be measured. .. 71

Figure 5.2 Generation of PRTS and TrapZ signals. (A) PRTS signal. A stimulus is created from a 242-length PRTS sequence, which includes values of 0, 1, and 2, corresponding to fixed velocities of 0, +v, and -v for a fixed duration of Δt. The velocity is integrated to generate the position, which is used as the perturbation signal. The period of the perturbation signal is equal to $3m - 1\Delta t$, where m is the stage number of the shift registrar, determining the sequence of the velocity. (B) TrapZ signal. The signal starts at zero; after a random time interval (δ), it ramps up or down to its maximum ($+A$) or minimum value ($-A$) with a constant velocity; the signal goes back to zero after a random time interval (W) and the whole loop starts again. 88

Figure 5.3 Typical experimental trial with TrapZ visual perturbation; the peak-to-peak perturbation amplitude is 0.087 rad, and the velocity is 0.105 rad/s. (A) VR perturbation angle, showing the rotation of the field of view in sagittal plane. (C) Ankle angle, which is the same as shank angle, as the foot does not move. (E) Body angle. (G) Ankle torque. (B, D, F, H) Raw

rectified EMG of SOL, MG, LG, and TA; SOL and LG are continuously active, while MG shows burst of activity associated with body sway, and TA is silent. 89

Figure 5.4 Frequency response of the dynamic relation of body angle to visual perturbation estimated from the data presented in Figure 3. Gain (top panel) shows ratio of the amplitude of the output to the input as a function of frequency; it shows a low pass behavior. Phase (middle panel) shows the difference between the input and output phase as a function of frequency. Coherence (bottom panel) provides an index measuring how much of the output power is linearly related to the input power at each frequency. A coherence of 1 shows perfect linear input-output relationship; however, the presence of noise or nonlinearity reduces it. 90

Figure 5.5 Typical PRBS position perturbation trial; the peak-to-peak perturbation amplitude is 0.02 rad, and the switching interval is 200 ms. (A) Foot angle, which is the same as the position perturbations since the foot moves with the pedal. (C) Ankle angle; the random changes are due to shank movement with sway. (E) Body angle, obtained assuming the body acts as an inverted pendulum. (G) Ankle torque measured form the load cells data. (B, D, F, H) Raw EMG of SOL, MG, LG, and TA; the TS muscles are all continuously active, while the large peaks reflect stretch reflex activity; TA is mostly silent..... 92

Figure 5.6 An individual pulse from the trial shown in Figure 5, on an expanded time scale. (A) Foot angle, (B) foot velocity, (C) SOL EMG, and (D) ankle torque. The vertical dotted lines separate the response into the pre-response (25 ms), intrinsic response (65 ms), and reflex response (300 ms); positive torque and angles correspond to dorsiflexion. The data for this figure are taken from Amiri and Kearney [37]. 93

Figure 5.7 Estimated normalized intrinsic stiffness as a function of COP position for the left and right side of a typical subject, obtained from the data shown in Figure 5. Bars indicate the 95% confidence intervals of the stiffness values. The data for this figure are taken from Amiri and Kearney [37]. 94

Figure 6.1 Experimental apparatus, (B) Schematic of the forces, measured by the load cells and the equation to calculate ankle torque and COP location; (C) The shank angle (θ_S) was estimated by measuring its linear discplacement Δ and dividing it by the range finder height, h, above the ankle axis of rotation; foot angle (θ_F) was measured by the actuator potentiometer; ankle

angle (θ_A) was obtained using equation (3); (D) The laser range finders used to measure shank and body movements 102

Figure 6.2 Typical experimental trial. Left column shows 15 seconds of a typical trial, (A) Foot angle, (C) Foot velocity, (E) Soleus EMG, and (G) Ankle torque; The right column shows an individual pulse, encompassed by the red dashed box in the left column, on an expanded time scale: (B) Foot angle, (D) Foot velocity, (F) Soleus EMG, and (H) Ankle torque. The vertical dotted lines separate the response into the pre-response (0 to 25 ms), intrinsic response (26 to 90 ms), and reflex response (91 to 390 ms); positive torque and angles correspond to dorsiflexion. 104

Figure 6.3 Typical group of intrinsic responses to dorsiflexing (DFP, left column) and plantar-flexing pulses (PFP, right column). (A,B) Foot angle, (C,D) Shank angle, (E,F) Ankle torque. Individual responses are shown in blue and their ensemble averages in red. Background torque range is 11 - 14 Nm for subject 1's left ankle. 109

Figure 6.4 Torques predicted by the IBK model and EIM for typical dorsiflexing (DFP) and plantarflexing (PFP) pulses. (A,B) Foot angle, (C,D) Experimental, IBK model, and EIM torques, (E,F) Residual torques for the IBK model and EIM. The results belong to Subject 1's left ankle at background torque 22.5 Nm. 110

Figure 6.5 Relation between normalized intrinsic stiffness and COP position. Each panel shows the left (blue) and right (red) stiffness for one subject; bars indicate the 95% confidence intervals of the stiffness values. Note that S7R was discarded. 112

Figure 6.6 The influence of ankle muscle activity on the joint stiffness of subject 8's left ankle, (S8, left column) and subject 9' left ankle (S9, right column); (A, B) the EMG activity of the TS and TA muscles, and (C, D) the corresponding joint stiffness. In (A, B) the bars show the min and max and the circle shows the median of the background EMG activity at each background torque. In the bottom row, K_{EIM}^{N} is shown with its 95% confidence interval. 115

Figure 6.7 Range of combined normalized stiffness (left minimum stiffness + right minimum stiffness to left maximum stiffness + right maximum stiffness) for all subjects. 118

Figure 7.1 (A) Experimental apparatus, (B) The shank angle (θs) was estimated by measuring its linear discplacementand Δ dividing it by the range finder height above the ankle axis of rotation, h; foot angle (θF measured by the actuator potentiometer, (C) A participant during the experiments 125

Figure 7.2 Typical experimental trial. Left column shows 15 seconds of a typical trial, (A) Foot angle, (C) Foot velocity, (E) Soleus EMG, and (G) Ankle torque; The right column shows an individual pulse, encompassed by the red dashed box in the left column, on an expanded time scale: (B) Foot angle, (D) Foot velocity, (F) Soleus EMG, and (H) Ankle torque. The vertical dotted lines separate the response into the pre-response segment (0 to 25 ms), intrinsic responses segment (26 to 90 ms), and reflex response segment (91 to 390 ms); positive torque and angles correspond to dorsiflexion. 128

Figure 7.3 Torques predicted by the EIM for typical dorsiflexing (DFP) and plantarflexing (PFP) pulses. (A,B) Foot angle, (C,D) Experimental and EIM torques, (E,F) Residual torques for the EIM. The results belong to Subject 2's left ankle at background torque 19.5 Nm. 132

Figure 7.4 Modulation of (A) TS muscles background EMG, (B) Ankle background angle, (C) TA muscle background EMG, and (D) normalized intrinsic stiffness with COP position for S4L. The red curves show normal standing, blue curves show toe-down and the light green curves show toe-up. In addition, the dark green curves show backward lean (BWD) and purple curves show forward lean (FWD). TS and TA-TS inside the parenthesis in the legend show the muscle activation pattern used in the tasks. 133

Figure 7.5 Modulation of (A) TS muscles background EMG, (B) Ankle background angle, (C) TA muscle background EMG, and (D) normalized intrinsic stiffness with COP position for S8L. The red curves show normal standing, blue curves show toe-down and the light green curves show toe-up. In addition, the dark green curves show backward lean (BWD) and purple curves show forward lean (FWD). TS, TA and TA-TS inside the parenthesis in the legend show the muscle activation pattern used in the tasks. 134

Figure 7.6 Number of cases for each muscle activation pattern in each postural task; TS, TA-TS, and TA stand for TS-only pattern, TA-TS pattern, and TA-only pattern, respectively. L and R shows the number of cases happening for left and right ankles. 136

Figure 7.7 Range of combined normalized stiffness (left minimum stiffness + right minimum stiffness to left maximum stiffness + right maximum stiffness) for all subjects in normal standing, toe-up and toe-down experiments, and forward (shown by Fwd lean) and backward (shown by Bwd lean) lean. 137

Figure 7.8 Results of Dunn-Sidak multiple pairwise comparison of normalized low frequency stiffness. The circles show the mean ranks for each operating condition and the bars show two standard errors. The black horizontal lines and stars indicate pairs of operating condtions, which were significantly different ($p \leq 0.005$). 138

Figure 8.1 (A) Experimental standing apparatus, (B) The shank angle (θs) was estimated by measuring its linear displacement (Δ) and dividing it by the range finder height, h, above the ankle axis of rotation; foot angle (θf) was measured by the actuator potentiometer; ankle angle (θA) was obtained using (8.1). 146

Figure 8.2 Postural control model: the body, an inverted pendulum, is unstable and subject to destabilizing gravity torque (g) and disturbances ($tqdist$); therefore, corrective muscle forces are generated by a central controller, stretch reflexes, and intrinsic mechanical stiffness to achieve stable upright posture. The stretch reflex and central contributions are captured by muscle EMG activity. The red signals are measured, whereas the black signals cannot be measured. 149

Figure 8.3 Box-Jenkins structure for central and reflex EMG-torque relationships..... 152

Figure 8.4 Sample experimental data; (A, B) ankle angle, (C, D) SOL rectified EMG, (E, F) MG rectified EMG, (G, H) LG rectified EMG, (I, J) TA rectified EMG, (K, L) ankle torque; left column shows the data of S1L, and right column shows the data of S4L. 158

Figure 8.5 Decomposition of TS muscles EMG to central and reflex components for S1L; (A) foot angle, (B) SOL, (C) MG, and (D) LG normalized EMG, (E) ankle torque. Blue shows estimated reflex EMG, and red shows the estimated central EMG. 159

Figure 8.6 Cross-correlation between the estimated reflex and central EMG for (A) SOL (B) MG (C) LG of S1L. CC stands for cross-correlation..... 160

Figure 8.7 Identification results for S1L (A) ankle angle, (B) TS central input, (C) TA central input, (D) TS reflex input, (E) predicted TS central torque, (F) predicted TA torque, (G) predicted

TS reflex torque, (H) measured torque (blue) and total predicted active torque (red), (I) residual torque. 161

Figure 8.8 Ankle angle vs. residual torque in an expanded time scale for S1L..... 162

Figure 8.9 TS muscle central torques for S1L; (A) SOL, (B) MG, (C) LG, and (D) total TS central torque. 163

Figure 8.10 FR of the identified transfer functions for S1L, (A) Gain, (B) Phase. 163

Figure 8.11 %VAF of the preidcted torque components; (A) %VAF of the total active (blue) and the residual (red) torques, (B) %VAF of the TS central ($tqSOLc$, cayan), TA central ($tqTAc$, purple), and TS reflex ($tqTSr$, orange) torque; (C) %VAF SOL (light purple), MG (green), and LG (yellow) central torque; L and R show left and right sides. Si (i=1,…,9) shows subject i... 166

Figure 8.12 Comparison of SOL central and reflex BW and DC gain; (A) BW, and (B) DC gain; the results are shown for left and right ankles. The individual points show the values for the individual cases, whereas identical markers belong to the same case. 167

CHAPTER 1 INTRODUCTION

Movement is an essential element of our lives which allows us to interact with the world. We start to learn to move very early and gradually develop the ability to perform a variety of motor tasks. We often consider important activities of our daily living, such as standing and walking, to be simple and overlook their complexity. However, all these tasks are realized through intricate interactions among many elements of the central nervous system, the peripheral nervous system, and the musculoskeletal system. Understanding the role of each system and the complex interactions among them, which permits the versatility of human motor control, is important. It provides the knowledge of the healthy motor control system and forms the basis to discover the etiology of many diseases that hinder the normal motor function. Knowledge of the source of a motor impairment can be followed by targeted interventions, aimed directly at the source of the disability in order to restore or improve the lost or affected function. This is crucial, since it ameliorates the quality of lives of many individuals with movement problems.

A very important functional activity of daily life is standing, which requires a robust postural control system. The major challenge in standing is to control the inherently unstable human body, which is subject to a variety of internal and external perturbations. Postural stability is provided through the continuous control of muscle forces, needed to maintain the body's upright posture and reject disturbances that endanger postural stability. Several systems must work in concert to provide these corrective muscle forces, required for postural stability: a central controller, which activates the muscles in response to information provided from three main sensory modalities including visual, vestibular, and somatosensory systems; spinal stretch reflexes, which generate muscle activation and forces through spinal circuits; and the intrinsic mechanical stiffness of muscles and joints. Remarkably, the role of each system and the way they interact can quickly change to adapt to different environmental conditions and postural tasks. It has been proposed that the importance of the visual, vestibular, and somatosensory sensory inputs change according to the accuracy of the information they provide [1, 2]. For example, when we are standing in a dark room with no visual input, the postural control adapts to provide stability using vestibular and somatosensory inputs.

Understanding the role of the different sub-systems in human postural control and how they interact is challenging. Experimental studies of standing provide valuable information regarding postural control. Mathematical methods complement the experimental results and help to disentangle the function of the individual sub-systems that contribute to standing. However, in general, quantifying human postural control is difficult for four reasons. First, the contributions of all sub-systems appear together and cannot be measured separately; there is only access to biomechanical variables (e.g. joint torques and angles, muscle EMGs, body center of mass, and center of pressure) that provide information regarding the overall postural control. Second, postural sway, the persistent low frequency movement of the body in standing, generates large non-stationarities in the measured signals, making the analysis difficult. Third, body sway is associated with continuous modulation of operating conditions that alter the dynamics of the sub-systems. Fourth, in standing, experimental data is acquired under closed-loop conditions, where open-loop identification methods fail and specific approaches must be employed to deliver unbiased estimates of the systems. This thesis deals with quantifying the contribution of passive and active mechanisms to human postural control. Thus, the first part deals with the identification of ankle intrinsic stiffness in a variety of postural conditions and characterizing its behavior. The second part deals with active mechanisms, by developing a method to identify central and stretch reflex contributions to human postural control.

When the body is exposed to small perturbations in standing, movement happens primarily about the ankle joint; this is referred to as “ankle strategy” [3]. It is evident that ankle plays a fundamental role in postural control; in particular, ankle intrinsic stiffness is believed to contribute substantially to postural control. Ankle intrinsic stiffness quantifies the joint’s instantaneous resistance to movement; it results from the passive visco-elastic properties of muscles and connective tissues about the joint, combined with the inertial properties of the limbs. There is ample evidence that ankle intrinsic stiffness changes dramatically with ankle operating conditions, defined by ankle torque and ankle position [4-7]. These both vary significantly with postural sway. Thus, it is reasonable to expect that intrinsic stiffness changes in standing. However, such changes have been generally overlooked in the balance control literature [8-11]. Consequently, a thorough investigation is necessary to check if and how ankle intrinsic stiffness changes with postural sway in standing. Moreover, the stiffness may change when the operating conditions change, making

the control of posture more challenging, such as when standing on inclined surfaces. However, there is little known about the behavior of ankle intrinsic stiffness when the requirements of the postural task change.

Quantifying the contributions of central and stretch reflex mechanisms and intrinsic stiffness to human postural control is challenging [12]. This is because ankle intrinsic and reflex torques are smaller than the central torque and the measured ankle torque is the sum of all; consequently, the low signal-to-noise ratio for the stiffness torques makes it challenging to decompose the ankle torque into its individual components [13]. In addition, determining the relative contributions of the three pathways to postural control, using only kinematic and kinetic data, requires utilizing identification methods that can generate unbiased estimates of a system with several nonlinear time-varying pathways from data acquired in closed-loop conditions.

With this overview, the overall objectives of this thesis were to:

1. Develop a method to identify ankle intrinsic stiffness in standing, while accounting for its changes with postural sway.
2. Use the new method to estimate ankle intrinsic stiffness and characterize its modulation with postural operating conditions.
3. Develop a method to decompose ankle torque to its central, stretch reflex, and intrinsic contributions in standing, using EMG as inputs and ankle torque as output.

1.1 THESIS OUTLINE

Chapter 2 provides a detailed review of human postural control, its individual elements, their interactions, and the hierarchy that achieves maintenance of postural stability.

Chapter 3 reviews issues related to the identification of human postural control with a focus on the difficulties arising from closed-loop effects and the methods to address them.

Chapter 4 describes the design and implementation of a new laser-based motion capture system that I developed to measure shank angles in standing.

Chapter 5 provide a detailed descriptions of the methods to study human postural control. We prepared this chapter to review and demonstrate the basic requirements and methods for the study

human postural control; it has been accepted for publication in the Journal of Visualized Experiments (JOVE) in 2019, in an article entitled "Experimental Methods to Study Human Postural Control". The manuscript is supplemented by a video, filmed in our lab and is authored by Pouya Amiri, Abolfazl Mohebbi, and Robert E. Kearney.

Chapter 6 describes a new method to estimate time-varying ankle intrinsic stiffness in standing and uses it to demonstrate that ankle intrinsic stiffness changes significantly with postural sway. This chapter has been published in the Journal of Biomechanics in 2019 and authored by Pouya Amiri, and Robert E. Kearney.

Chapter 7 characterizes ankle intrinsic stiffness during different operating conditions of standing and demonstrates that ankle intrinsic stiffness changes with postural sway in a manner dependent on muscle activation patterns. This chapter was submitted to the Journal of Neurophysiology, and is authored by Pouya Amiri, and Robert E. Kearney.

Chapter 8 introduces a novel multiple-input, single-output, closed-loop method to identify EMG-torque dynamics of ankle muscles in standing. The method decomposes the ankle torque to the components arising from its central, stretch reflex, and intrinsic mechanisms. This chapter will be submitted shortly to IEEE Transactions on Neural Systems and Rehabilitation Engineering (TNSRE) and is authored by Pouya Amiri, and Robert E. Kearney.

Chapter 9 provides a summary of the original contributions of the thesis and discusses their significance. The chapter concludes with recommendation for future work.

1.2 CONTRIBUTION OF THE AUTHORS

Chapters 1, 2, 3, and **9** were written by Pouya Amiri (PA), with advice, critical review, and editorial input from his supervisor, Professor Robert E. Kearny (REK).

Chapter 4: PA designed the experiments, developed the analysis method, analyzed the experimental data and interpreted the results, drafted the initial manuscript for the IEEE EMBC conference, and submitted the final manuscript. Luke J. MacLean helped with the experiments, the analysis and interpretation of the results. REK provided supervision at all steps of the work, including the design of the study objectives, designing the experiments, analysis of the

experimental data, and interpretation of the results. He also provided critical review and editorial comments on the manuscript.

Chapter 5: PA designed the experiments with mechanical and visual perturbations, analyzed the experimental data and interpreted the results. PA drafted the manuscript for the JOVE, revised the manuscript in response to reviewers' comments, and made the final submission. PA also performed the interviews for the filming, made videos of computer screen, giving the analysis procedure instructions, and performed all the experimental steps, which was filmed by videographer of the JOVE. Abolfazl Mohebbi (AM) designed the visual perturbations and analyzed the corresponding experimental data, helped in the preparation and revision of the manuscript, performed interview for the filming, made videos of computer screen and helped to show the experimental protocol for the video. REK provided the supervision in all steps of the work, including the design of the experiments and analysis of the data, and interpretation of the results. He also provided advice and editorial comments to develop the initial manuscript, and to respond to the journal reviewers to prepare the revised version. He also helped for the preparation of the filming scripts and participated in the interview for the video.

Chapter 6: PA designed and performed the experiments, developed the identification method, performed the analysis of the experimental data, interpreted the results and drafted the initial manuscript, responded to the reviewers' comments and revised the manuscript accordingly for final submission to the Journal of Biomechanics. REK supervised all aspects of the work, including the design of the experiments, development of the identification algorithm, analysis of the experimental data and interpretation of the results, preparation of the manuscript, and its revisions in response to the journal reviewers.

Chapter 7: PA designed and performed the experiments in different postural experiments, performed the analysis of the experimental data, interpreted the results and drafted the initial manuscript for submission to the Journal of Neurophysiology. REK supervised all aspects of the work, including design of the experiments, and analysis of the experimental data and interpretation of the results, critical review and editorial comments in preparation of the manuscript.

Chapter 8: PA designed and performed the experiments, developed the closed-loop identification method and applied it to the experimental data of nine subjects, interpreted the results

and drafted the initial manuscript for submission to the IEEE TNSRE Journal. REK supervised all aspects of the work; this included the design of the experiments, and development of the closed-loop identification method, analysis of the experimental data, and interpretation of the results; he also provided critical review and editorial comments for the preparation of the journal manuscript.

CHAPTER 2 REVIEW OF THE LITERATURE PERTAINING TO POSTURAL CONTROL

This chapter reviews the literature and modeling approach pertaining to human postural control. The chapter provides an overview of the different postural strategies and control frameworks that have been proposed to explain human upright posture. Major contributing sub-systems in the postural control are discussed, starting with a brief overview of the structure of three main sensory systems and their possible contributions to postural control. Then, the process of multisensory integration, which is fundamental to the adaptability of human postural control, is discussed. Finally, joint stiffness and its possible contributions to human postural control are considered.

2.1 SOME COMMON NOTIONS IN HUMAN POSTURAL CONTROL

It will be useful to first define a number of common terms that are used in the study of human postural control.

Base of support

The base of support (BOS) refers to the area of the body that is in contact with the support surface [14]. The BOS is important to postural control, as it defines the area that must encompass projection of the body center of gravity to ensure stability.

Center of mass

The center of mass (COM) is a unique point in an object, about which the moment of gravity of its distrusted mass sums to zero. Application of a force to the COM of an object generates linear acceleration and no rotation. For a multi-body system, such as human body, the COM is not unique and changes with body configuration.

Center of pressure

The center of pressure (COP) is the point, about which the moment of the disturbed forces applied to the sole of foot from BOS (during standing and walking) sums to zero. Consequently, the distributed forces can be replaced with a unique force equal to their sum, applied at COP, with no moment. If ankle torque (T_A) and ground reaction force (GRF) are known, the COP position

can be determined in standing. Since, the foot is stationary, the measured ankle torque and the torque generated by GRF about the ankle axis of rotation must be equal. Figure 2.1 shows a free body diagram of the foot in the sagittal plane during standing; the following relation holds:

$$T_A = GRF_y x_{cop} + GRF_x h_f \tag{2.1}$$

where GRF_x and GRF_y are the horizontal and vertical components of the GRF and x_{cop} is the horizontal distance of the COP to the ankle axis of rotation, and h_f is the vertical distance between the ankle axis of rotation and foot sole. In the case of the ankle strategy, GRF_x will be negligible (since the body horizontal acceleration is small), while GRF_y will be close to the body weight; thus, (2.1) becomes [12, 15]:

$$T_A = mgx_{cop} \tag{2.2}$$

where m is the body weight, and g is the gravitational acceleration. This relationship clearly shows that the ankle torque is directly correlated with the position of COP (x_{cop}).

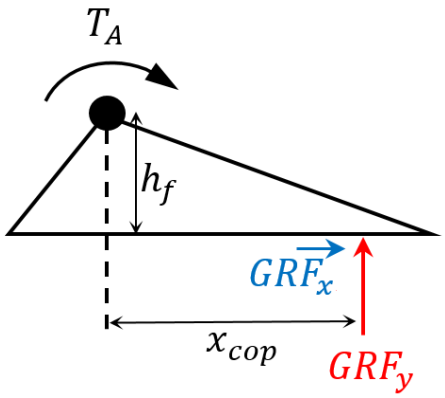

Figure 2.1 Determination of COP in standing: the balance between the GRF torque and ankle torque about the ankle axis of rotation in standing

Quiet and perturbed standing

Quiet standing refers to standing when there is no external (mechanical or sensory) perturbation, all sensory inputs are available and accurate, and the BOS is stationary. However, if any of the

above conditions are violated, for example, if the visual scene or BOS moves or an external force is applied to the body, the conditions is referred to as *perturbed standing*. Controlled perturbed standing experiments are generally used to evoke postural responses and study postural control.

Postural sway

Quiet standing is characterized by a low amplitude, random, low frequency movement of the body, which is highly correlated with the modulation of ankle torque. This low frequency non-stationarity is referred to as postural sway [16, 17]. Postural sway persists in perturbed standing and is generally larger than quiet standing.

Critical stiffness

When an ankle strategy is used for postural control, the body is generally modelled as a single-link inverted pendulum. In such condition, the minimum elastic stiffness required to achieve postural stability is called the critical stiffness [9, 10]. Assuming that only a torsional spring with stiffness K at ankle opposes the gravity toppling torque, as illustrated in Figure 2.2, the equation of motion of the single-link inverted pendulum is:

$$K\theta - mgh\sin(\theta) = I\ddot{\theta} \tag{2.3}$$

where θ is the body angle with respect to the vertical, m is the body mass, I is the body moment of inertia about the ankle, g is the gravitational acceleration, and h is the height of the body COM with respect to the ankle axis of rotation. If it is assumed that there are only small displacements from the equilibrium position so that $\sin(\theta) \sim \theta$ and that the body is static conditions ($\ddot{\theta} = 0$), the critical stiffness K_c is given by:

$$K_c = mgh \tag{2.4}$$

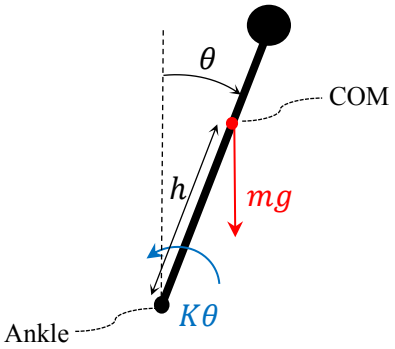

Figure 2.2 Free body diagram of a SIP, assuming a torsional spring with stiffness K is opposing the gravity toppling torque.

2.2 POSTURAL CONTROL

Postural control has two main objectives: postural *stability* and *orientation.* Postural stability (also called balance) is the ability to maintain the body COM inside the BOS. Postural orientation is the alignment of body segments with respect to each other and the alignment of the body with respect to the environment [18]. Although, postural control seems an easy task for healthy individuals, it is the result of complex interactions of many elements of the central (CNS) nervous, peripheral nervous (PNS), and musculoskeletal systems. This complexity stems from the versatility of postural control; the roles and importance of the different sub-systems are not fixed but change according to the environment, biomechanical constraints, cognitive abilities, perception, and sensory strategies [19]. For example, postural control is different in a dark room than in a bright room, due to the removal of visual cues. Similarly, the control strategy is different on a wide BOS than on a narrow beam, where the body COM must be kept with a smaller BOS – a more difficult task. Similarly, when there is a fear of falling (e.g. standing on a high ledge), the postural control strategy may differ from that under normal conditions.

Understanding postural control when there are deteriorations or changes in CNS, PNS, and musculoskeletal system due to ageing and/or diseases, is even more complex [14]. In such conditions, the heterogeneity of these changes makes it difficult to determine the underlying source of the postural control impairment. Each subject will require specific interventions to improve balance. This is why falls are a major cause of disability in the elderly and despite a large literature on postural control and fall prevention, we are still unable to address the problem effectively [19].

Postural stability is an important goal of postural control. In standing, the body resembles an inverted pendulum, which is inherently unstable and is subject to a variety of internal perturbations (such as voluntary movements, respiration, heartbeat, etc.), and external disturbances, such as a push or movement of the BOS. Such perturbations will displace the body from its equilibrium position, resulting in an increase in destabilizing torque due to gravity, displacing the body further away from its equilibrium. To oppose this, corrective muscle forces must be generated by the coordinated action of the CNS, PNS, and musculoskeletal systems. Three main subsystems contribute to the generation of these stabilizing forces:

1- The central controller (brain) activates muscles in response to the information regarding the position of the body segments with respect to each other and to the environment, provided by somatosensory, visual and vestibular systems.
2- The spinal cord may generate muscle activation through spinal circuits (stretch reflexes), resisting movements of the joints.
3- The intrinsic mechanical stiffness of joints will generate torques in response to their movement.

Postural stability will be maintained, provided that the muscle corrective forces keep the horizontal projection of the body COM within the BOS [20]. Indeed, it has been proposed that the CNS uses the position of body COM as the main control variable to achieve postural stability [21]. Recently, this view has been extended and it has been shown that not only the position, but also the COM velocity must be considered to assess postural stability [22]. Thus, if the COM projection is within BOS but it is moving with a high velocity toward the limits of stability, it may be necessary to change the postural control strategy to maintain balance.

2.3 POSTURAL CONTROL STRATEGIES

Individuals achieve postural stability using an ankle strategy [23], a hip strategy [3], or a combination of both [24]. If stability can not be achieved using these strategies, then a step is taken to realign the BOS under the COM [25]. Factors which determine the postural control strategy include the properties of the BOS, the amplitude of external perturbations, and the perception of stability.

Ankle strategy

In the ankle strategy, postural control is achieved by rotating the body primarily about the ankle, while keeping knee and hip extended [3]. Since the lower limbs and upper body move together, the body can be regarded as a single-link inverted pendulum. The ankle strategy is utilized when the BOS is firm, external perturbations are small, subjects have sufficient strength, and do not fear falling [26]. This strategy is associated with a specific muscle activation pattern [3, 23, 27]; muscle activation starts in the distal lower limb muscles and is followed by activation of the proximal upper body muscles. Thus, when the body is displaced forward (in response to a backward BOS translation or a plantar-flexing rotation of the BOS), the ankle plantar-flexors, hamstrings, and para-spinal muscles are activated sequentially. Conversely, when the body is displaced backward (due to a forward BOS translation or a dorsi-flexing rotation of the BOS), the muscles located on the front of the body, including tibialis anterior, quadriceps, and abdominals are activated in order [3].

Hip strategy

Under demanding conditions, e.g. when the BOS is compliant, or it is firm, but smaller than foot, when perturbations are large, when subjects are weak or fear falling, postural stability cannot be achieved using the ankle strategy [26]. In such cases, a hip strategy is used in which movements occur about both ankle and hip joints to keep the COM projection within the BOS [3]. This strategy is characterized by anti-phase movements of hip and ankle joints [24, 28]. The hip strategy involves the simultaneous activation of proximal upper body muscles [3]. In contrast to the ankle strategy, in the hip strategy, when the body sways forward, the proximal muscles located in front of the body, including abdominals and quadriceps are activated; and when the body sways backward, the proximal muscles on the back of the body, including para-spinal muscles and hamstrings are mostly active [3].

Stepping strategy

If neither the ankle nor hip strategies are able to keep the body COM within the BOS, a step is taken. This realigns the BOS to encompasses the COM projection and provide stability [14]. It was originally believed that stepping strategy was used only when the COM moved outside the

BOS in response to large perturbations [29]. However, it was later showed that stepping is also used when the COM was well within the BOS [25].

Co-existence of ankle and hip strategies

It was initially suggested that the CNS uses either the ankle or hip strategy in a mutually exclusive manner [18]. However, it was later demonstrated that both strategies are always used in combination [30]. Creath et al. showed that during quiet standing, ankle and hip movements were in phase at frequencies below ~1 Hz, showing dominance of ankle strategy. However, at higher frequencies, the movements were out-of-phase, which is the characteristic of hip strategy [24]. In addition, it was initially suggested that the frequency at which the ankle strategy switched to hip strategy was set by the CNS. However, more recent studies suggest the antiphase movement is not centrally generated, but rather associated with the mechanics of body [28, 31]. In fact, Kiemel et al. demonstrated that the one neural input (composed of the combined activation of several distal and proximal muscles) led to both ankle and hip movements; consequently, they concluded that the in-phase movement of the joints was neurally generated, while the out-of-phase pattern was caused by plant dynamics [32].

2.4 VIEWS ON POSTURAL CONTROL

Here, I discuss different views on postural control, their merits, and the most widely accepted strategy, the feedback control paradigm, which is the basis of the methods developed in this thesis.

2.4.1 Stiffness control

Winter et al. initially proposed that postural control is achieved under open-loop conditions, where ankle stiffness alone provides postural stability. In this view, the only role of the CNS is to set the tone (activation) of ankle muscles to render the ankle stiffness required for stability during quiet standing [17, 33, 34]. They observed that in quiet standing, the delay between the COP (which is highly correlated with ankle torque) and body COM was too short to allow any active contribution from the CNS. Consequently, they concluded that ankle intrinsic stiffness (sometimes called passive stiffness) was responsible for postural stability [17, 33]. Thus, they estimated the stiffness in standing using linear regression between the ankle angle and torque and reported that the stiffness was larger than the critical stiffness for quiet standing [17, 33].

However, this line of thinking has been criticized and now is widely discredited for several reasons. First, the relationship between COP and COM in quiet standing is determined by the plant (body) dynamics and provides no insight into the underlying control mechanism (more details are given in 3.4) [15]. Second, muscle activity is continuously modulated with postural sway; consequently, the ankle torque must be generated by a combination of intrinsic stiffness and active mechanisms. Moreover, many researchers have quantified ankle intrinsic stiffness in standing and demonstrated that it is not adequate in itself to provide postural stability [1, 9, 10, 32, 35-40].

2.4.2 Feedback control

Today, it is widely accepted that the postural stability is maintained by feedback control [1, 12, 32, 41-55], where muscle activation is generated in response to deviations of the body from its equilibrium position. Information regarding the body position is transduced by three main sensory systems: somatosensory/proprioceptive, visual and vestibular systems. In response, muscle activities are modulated to produce the forces required to maintain postural stability and keep the desired orientation. This view of postural control also accounts for the contribution of the intrinsic stiffness to postural control. However, the stiffness contribution has been reported to be small, generating only around 10-15% of the required torque for postural control [1, 32, 49, 56].

2.4.3 Feedforward control

The feedforward postural control hypothesis states that central, pre-programmed control achieves standing stability, that is the CNS anticipates perturbations, using sensory cues and generates appropriate corrective muscle responses, rather than relying on continuous sensory feedback [57]. Using a closed-loop identification method, Fitzpatrick et al. estimated the feedback gain from the body sway angle to the generated EMG in gastrocnemius muscles in standing and reported a gain close to unity; they concluded that the feedback gain was too low to achieve stability, thus, feedforward mechanisms might exist to aid with the postural control [47]. Yet, they provided no convincing evidence for anticipatory (feedforward) control. Following this, Gatev et al. showed that significant non-causal (anticipatory) cross-correlation existed between the body COM and EMG during standing, and concluded that muscle activity leads the body COM movement in an anticipatory manner [57]. However, any analysis based on cross-correlation between muscle EMG and body COM in standing will generate an anticipatory component due to

closed-loop nature of the postural control, so should not be interpreted as an indication of feedforward control [12]; this is discussed in detail in Chapter 3. Indeed, the non-causal cross-correlation between EMG and body COM can be easily replicated in simulation of standing, using a simple closed loop controller with position and velocity feedback [58]. As Chapter 3 will explain, the non-causality is generated due to the noise in closed-loop system [59]. There are important roles for feedforward control when anticipation is possible, for example, prior to voluntary movements while standing [23, 60, 61]; however, there is little evidence to support the existence of postural feedforward control in response to unpredictable perturbations.

2.4.4 Intermittent, ballistic-like control

Several researchers have proposed that postural stability is achieved through an intermittent, ballistic-like control [62-65]. The idea is that rather than being controlled continuously, upright posture is realized through intermittent activation of ankle muscles. This view has been supported by the observation that medial gastrocnemius is activated intermittently during standing [66, 67]. The intermittent control paradigm has been suggested to function in an anticipatory or closed-loop framework. Thus, Loram et al. suggested that standing is controlled by periodic predictive update of muscle activation with an intrinsic low rate, which is independent of the body inertia (load); and claimed that the update rate was a constraint imposed by the neuromuscular system [64]. Bottaro et al. postulated that the sway in standing was produced by a sliding mode postural controller, which generates chattering when sensory thresholds are passed [63, 65]. Finally, Asai et al. showed that an intermittent, proportional-derivative controller with a dead zone around the nominal equilibrium state could replicate postural sway [62].

In this thesis, the continuous feedback control is considered to be the most plausible framework to explain human postural control. This is owing to the fact that the other proposed theories do not seem feasible and lack sufficient evidence. There is overwhelming evidence that the stiffness control theory is not correct; the feedforward control scheme does not explain the postural responses that are evoked by external perturbations; and the intermittent control does not explain the continuous activity of soleus muscle in standing.

2.5 CLOSED-LOOP POSTURAL CONTROL

The focus of the current thesis is on human postural control in the context of a closed-loop feedback control. Thus, in this section, I will provide a detailed description of the elements of the closed-loop postural system, define their hierarchy, and discuss their interactions.

2.5.1 Feedback postural control

Figure 2.3 shows a simple model of closed-loop human postural control. The body is the plant to be controlled; it is modelled as an inverted pendulum subject to a variety of internal disturbances (such as heartbeat, respiration, or voluntary movements) and external perturbations (such as a push or the movement of the BOS). These perturbations displace the body from its equilibrium, resulting in an increase in destabilizing gravitation torque. Thus, ankle torque must be continuously controlled to keep the body near its set-point. The torque is generated by both active and passive mechanisms. Active refers to the forces that are generated as a result of the modulation of muscle neural activation; passive refers to muscle forces that are generated with no change in muscle activation [40]. Active forces are modelled as arising from two sub-systems: a central controller, and a spinal stretch reflex component. Passive forces are modelled as arising from the muscles intrinsic stiffness [40].

The central controller activates muscles in response to feedback from: 1- Somatosensory system, which generates information regarding the BOS, and joint angles and velocities; 2- Visual system, which provides information regarding the body position with respect to the environment; and 3- Vestibular system, which generates information regarding the head angular velocity, linear acceleration and orientation with respect to the gravity [19, 68]. The central controller uses a complex multisensory integration process to combine the feedback from the three systems to generate descending commands that activate the muscles and produce forces required for postural control [69]. The process of sensory transmission, processing, and transduction is associated with a long delay, which differs for each sensory system. These delays were reported to be around 80-100 ms for somatosensory system [70, 71], 50-60 ms for the vestibular system [70, 72], and around 200 ms for the vision [73].

The stretch reflex pathway acts with a shorter delay, reported to be around 40 ms [74-76]. This controller acts when joint movements are sensed by muscle spindles and other receptors, triggering a spinal response that generates a burst of activity in the muscle, resisting its stretch [26].

Finally, the passive controller, associated with the intrinsic mechanical stiffness of the joint, generates resistive torque with no delay and no change in muscle activation [77].

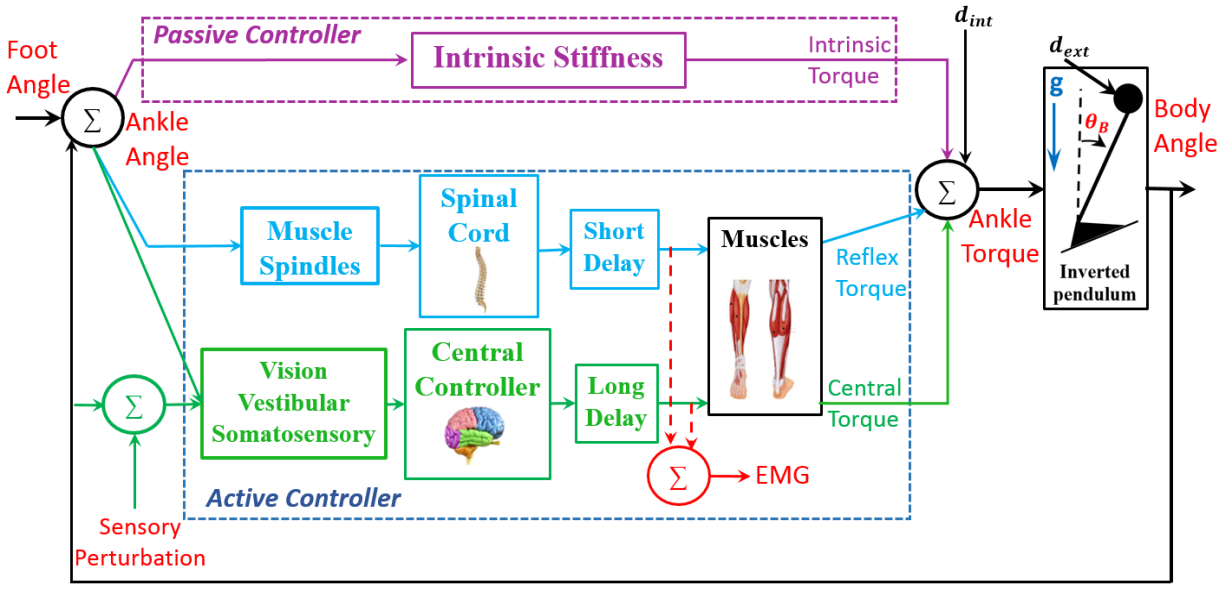

Figure 2.3 Closed-loop human postural control; the body is inherently unstable and subject to gravity torque (g) and disturbances (d_{int} and d_{ext}). Corrective muscle forces are generated by 1- an active controller with two components: a central controller and spinal stretch reflex; and 2- a passive controller, the intrinsic mechanical joint stiffness. Muscle activation due to stretch reflex and central contributions is reflected by EMG. Only the signals shown in red can be measured, whereas other signals cannot be measured in standing experiments.

In the following sections, I will discuss the components illustrated in Figure 2.3 including: the body, the plant, the sensory systems and their role in postural control. I will then discuss multisensory integration, which permits the postural control system to adapt to new environmental and experimental conditions. Finally, joint stiffness and its role in postural controller will be discussed.

2.5.2 Models of human body dynamics in standing

To develop accurate models of human postural control, it is necessary to identify the dominant postural strategy and model the components of postural control accordingly. There is a wide body of literature dealing with postural control using the ankle strategy, where the human body is modelled as a single-link inverted pendulum (SIP). In a SIP, the ankle angle and COP position are highly correlated. Consequently, cross-correlation between the two can be used to verify whether the ankle strategy is used in a particular experimental condition [17]. High correlation values suggest a dominant ankle strategy; lower correlation values suggests that hip is involved.

Some researchers have used more complex, multi-segment models to study postural control [24, 32, 41, 42, 51, 78, 79]. Recent studies, trying to develop methods to objectively quantify postural control (with the aim of understanding the impairments due to diseases) indicate that the differences in postural control of younger adults, the elderly, and individuals with Parkinson's disease were more evident when a double-link inverted pendulum (DIP) model of balance control was used [50, 51]. This approach makes both the standing experiments and data analysis more complex. Experimentally, quantification of the DIP postural control requires the application of independent perturbations at the ankle and hip and measurement of their movements [80]. The analysis of multi-segment coordination is more involved, because mathematical models must account for the control contributions of both ankle and hip joints, as well as, for their interactions [41].

Investigating bilateral coordination in balance control also requires more complex experimental and analysis procedures. Most studies of balance control have used a single platform to apply simultaneous mechanical perturbations to both feet. For the examination of bilateral effects, each ankle must be perturbed separately which requires the development of devices capable of applying separate independent perturbations to each ankle. The analysis also must be performed separately for each side. This approach has been used to examine the bilateral contribution of proprioceptive information in postural control of healthy individuals [52]. Using such approach is particularly useful to investigate disease-related balance asymmetries that cannot be detected visually or by functional outcome measures. For example, using bilateral perturbations and system identification, it has been shown that post-stroke patients rely mostly on their non-paretic leg to maintain balance and that the contribution to control of balance was not tightly

coupled to the weight carried by each leg [81]. A similar balance asymmetry also has been reported in individuals with Parkinson's disease [55, 82, 83].

Correct understanding of the mechanism of postural control requires designing appropriate experiments that evoke a dominant postural strategy. The strategy can be verified by examining the relationship between lower limb and upper body movements. Subsequently, a single joint controller with an SIP model of body or a double joint controller with a DIP model of body must be employed. Generally, the SIP is preferred, since the experiments, the analysis, and the interpretation are all simpler. However, if there is significant use of hip or the study is aimed at understanding the hip strategy, the more complicated multi-segment approach is required. If the objective is to study bilateral coordination, simultaneous independent mechanical perturbations are applied to both ankles, and each leg should be investigated separately.

2.5.3 Sensory systems in postural control

Feedback control of posture requires feedback of the body positon with respect to the environment, as well as of the positions of body segments with respect to each other. The major sensory systems contributing to postural control are: vestibular, visual, and somatosensory. In the following, I will first describe each sensory system, discuss its role in postural control, and then describe the sensory integration strategies.

Vestibular system

The vestibular organ, located inside the inner ear, is composed of three semicircular canals and the otolith, as Figure 2.4 illustrates. The semicircular canals act as band-pass filters for 3D angular velocity of the head [84, 85]. The otolith also has a band-pass response to head linear acceleration [85, 86]. This information is used by CNS to detect direction and the amplitude of the angular velocity and linear acceleration of the head.

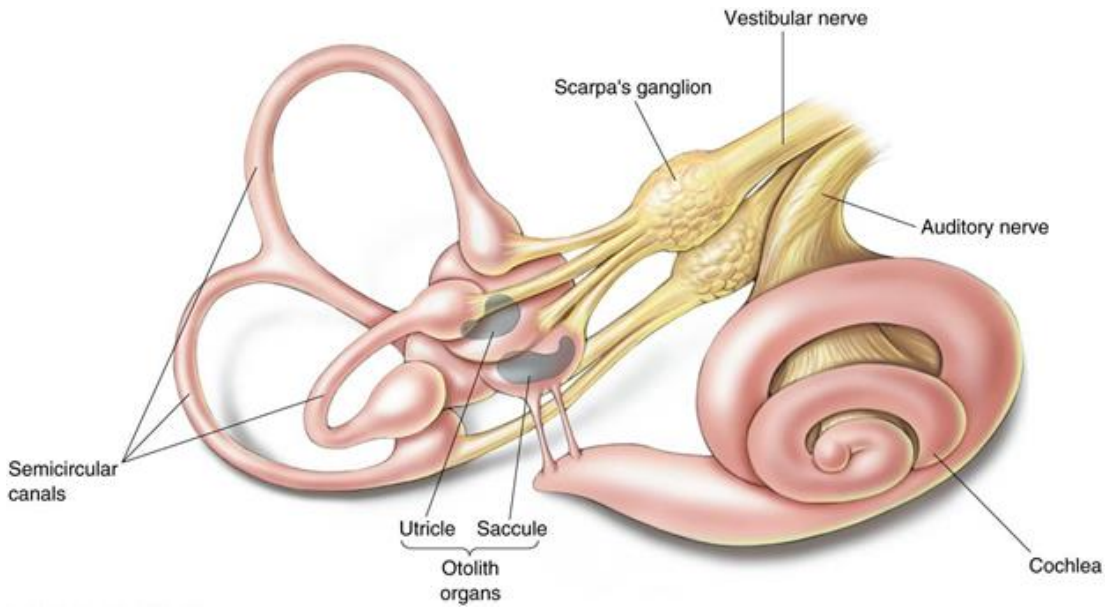

Figure 2.4 Vestibular organ including the three semicircular canals, and the otolith organ (which includes utricle and saccule); the cochlea is also shown.

It is generally not feasible to perturb only one sensory system in standing, since postural sway engages all the sensory systems, and their contributions to postural control will be intertwined and difficult to disentangle. However, it is possible to primarily target one system. Some studies perturbed the vestibular system in postural control by forward and backward weighted head displacement and reported that the responses were not large [87]. However, this approach may not be appropriate for the study of vestibular system in postural control, since it has been demonstrated that balance adapts to passive and active head rotations, and it seems that the vestibular responses to head rotations are inhibited [88]. In addition, the rotation of the head does not perturb the vestibular system in isolation, but also evokes responses of the somatosensory receptors in the neck and head. Another method is to apply direct electrical stimulation to the mastoid processes, which will perturb the only vestibular system and generate a sensation of head velocity [89]. It has been shown that electrical stimulation evokes lower leg muscle activation response in standing with delays between 60-120 ms [72], providing evidence that the vestibular system could contribute to postural control, especially in perturbed standing. In addition, it has been reported that damage to vestibular system results in balance related problems and dizziness [90, 91], and higher rate of fall incidents in the elderly [92]. These effects are stronger in the acute stages of

vestibular damage and the sensorimotor system generally starts to adapt and compensate for the loss, and vestibular rehabilitation can be helpful in recovery [93-95].

Somatosensory system

Somatosensory receptors are distributed in joints, muscles, and skin throughout the body; they provide information regarding the position of body segments with respect to each other and the environment. A variety of somatosensory receptors continuously monitor muscle length, velocity, force, joint position, and the GRF.

Muscle spindles are the somatosensory receptors that monitor muscle length and velocity continuously. The spindles, located at the belly of the skeletal muscles have a characteristic frequency response that shows a flat gain at low frequencies up to 1 Hz, with a steep increase in gain for frequencies between 1-20 Hz [96]. Therefore, spindles are effective in low frequencies, but are more important for fast transients induced by perturbations in standing [97]. Joint receptors, located at the joint capsules, also detect joint position, however, they are thought to be most important at the end of the joint range of motion [98, 99].

Cutaneous receptors are other somatosensory organs that may be important for postural control, since they provide information regarding the interaction between the body and the world [68]. In particular, Ruffini and Merkel cells measure sustained pressure applied to the feet, so provide information about low frequency content of postural control [100-102]. Messiers and Pacinian corpuscles are sensitive to dynamic deformation and vibration of skin [100, 103-105]; therefore, they detect transient BOS perturbations [106, 107].

Another somatosensory receptor, implicated in postural control, is the Golgi tendon organ (GTO). GTOs are located at the junction of the muscle-tendon, continuously monitor the active tension at the muscle, and is especially more sensitive to high frequencies (>1 Hz) [108]. Loram et al. postulated that the GTO is the main sensory system contributing to postural control, because they observed paradoxical movement of plantar-flexors in standing that would obscure the measurement of body sway by muscle spindles [109]. It has also been recently shown that the addition of a torque (force) feedback to a model of postural controller significantly improves the model performance to explain experimental data, providing some evidence regarding the role of GTO in postural control [13, 48].

A variety of experimental studies have investigated the contribution of somatosensory receptors to postural control. Vascular ischemia and cooling of lower limbs reduce the flow of somatosensory inputs and result in increased sway during standing [110-112], providing evidence that somatosensory inputs contribute to the postural control. The most popular method to perturb the somatosensory system in postural studies has been to apply BOS translations [3, 113, 114] or rotation [1, 55]. This experimental procedure generates somatosensory responses in postural control, since it primarily changes the GRF and the joint angles. In addition, the application of vibration to neck, eye, and ankle muscles in standing have shown to increase postural sway [115, 116]. A light touch of the hand fingers to a stable surface causes a reaction in the lower leg muscles and generates corrective stabilizing forces in standing [117, 118]. Therefore, there is a wide variety of evidence showing the somatosensory inputs from all parts of the body are important in postural control.

Visual system

The visual system contributes to postural control by providing references of verticality from environment, needed for the control of body orientation; it also detects the movement with respect to the environment [26].

The contribution of vision to postural control has been examined in different ways. The simplest experiments demonstrated that removing visual input (by closing the eyes) increased postural sway, indicating that the visual system generates information for postural control [119, 120]. However, the visual input is not absolutely necessary for postural control; healthy individuals keep their balance easily without vision, e.g. in a dark room.

Removing visual input is not a very informative method to understand its role in postural control. Therefore, researchers have taken advantage of the inability of the visual system to distinguish between self-motion and the movement of the environment to study vision in standing. The experiments generally caused an illusion of body movement by moving the walls or an artificial visual surround and examined the resulting postural responses [32, 121-125]. It has been reported that the postural response to visual field rotation is nonlinear, because the ratio of the body sway to the movement of visual field perturbation decreases as the perturbation amplitude increases [124, 125]. In addition, the postural responses to visual perturbations are complex and

depend on the velocity of the visual scene movement. Thus, Day et al. showed that unidirectional visual rotations generated an early response to the perturbation (<190 ms), which was attenuated as the rotation velocity increased; there was also a later response (>700 ms) that aligned the body with respect of the gravity [126]. In addition, Mergner et al. found that the postural responses to visual perturbations were affected by the threshold of other sensory cues [125]. Visual postural responses have long delays (close to 200 ms) [73] and it is relatively easy to keep balance without vision; therefore, it seems that the sensory cues from somatosensory and vestibular systems are more important for postural control.

2.6 MULTISENSENSORY INTEGRATION IN HUMAN POSTURAL CONTROL

Human postural control is continuously faced with new environments and tasks, and it is remarkable how quickly the control system adapts to the new requirements [68]. This is achieved by combining the sensory inputs from different systems in an optimal manner to provide postural stability; this is referred to as multi-sensory integration.

There are two theories regarding multisensory integration in human postural control. The intermodal theory of sensory organization states that there is never any conflict or inaccuracy in the sensory information; therefore, the sensory information from all sources contributes equally to postural control, and as a result, the CNS does not prioritize any source of sensory information [127]. However, this theory cannot explain the adaptation of postural control that occurs in many conditions; for example, individuals with complete bilateral vestibular loss can eventually learn to control their balance in a dark room (no vision), demonstrating that they rely largely only on somatosensory inputs.

In contrast, the sensory (re-)weighting theory, states that the CNS uses information from all the sensory systems for postural control, but the sensory contributions are not necessarily equally weighted. Thus, for a particular environmental condition and postural task, the CNS adapts by prioritizing the information from more accurate (or less variable) sensory sources [1, 2, 48, 60, 128-132]. The benefits of adaptive integration of sensory information for postural control include improved certainty in the neural representation of the orientation and motion of the body, achieving a robust control of posture when there is a dysfunction in any of the sensory system contributing

to the postural control, the ability to resolve conflicting sensory information (for example the self-motion and motion of the environment, when the visual system is unable to distinguish between the two) [2].

The sensory reweighting theory requires the postural control system to know the accuracy of the information provided by each sensory modality. Generally, the sensory systems with a larger working range will have higher input variability and consequently have a higher threshold for movement detection. The vestibular system possesses the highest variability, since it is designed to work over a large range and contribute to many tasks. The semicircular canals can detect velocities from -400 to 400 °/s over a wide range of frequencies, and otolith detects sustained head orientation from -180 to 180° [2]. Ankle proprioceptors generate inputs with less variability and can detect changes in the joint angle over a smaller range, close to 60° [2]. It is difficult to quantify the variability of visual input, since it depends on many factors, such as visual scene properties, contrast, and the distance between the eye and the scene [2].

Fitzpatrick and McCloskey documented the threshold of the proprioceptive, visual and vestibular systems under conditions mimicking balance control. Consistent with the working range, the reported thresholds were 0.1° and 0.1°/s for somatosensory, 0.3° and 0.1-0.3°/s for visual, and 1° and 1°/s for vestibular systems [133]. Therefore, it is to be expected that in normal condition of standing, postural control will depend primarily on somatosensory system; in perturbed standing, the CNS adapts to use the sensory systems which are less affected by the perturbations. For example, Peterka showed that in quiet standing, the contributions of proprioceptive, visual and vestibular systems were 50, 33, and 17%, respectively. In the absence of visual input (eyes closed), the contribution of proprioceptive and vestibular inputs were 68% and 32%, respectively. Finally, when the BOS was rotated, the visual and vestibular system contributed 77% and 23% [1].

2.7 APPROACHES TO MODEL SENSORY REWEIGHTING IN POSTURAL CONTROL

Understanding the complex mechanism of human postural control requires the development of computational models that can replicate the observed experimental data and explain the role of the different sub-systems. Accurate models are particularly useful for the study of multisensory

integration, since they provide the means to examine each system's role. This is important, since it is not possible to perturb only one sensory system independently and postural sway will excite all the sensory systems. In addition, modelling methods allow the study of the adaptation of postural control to different environmental conditions and tasks. Three approaches have been developed for the study of multisensory integration in postural control.

PID control method

The first modeling approach, the PID control method, postulates that a simple linear controller (with proportional-derivative (and sometimes an integral) coefficients) combines the sensory inputs to achieve postural stability and the desired orientation [1]. In this framework, each of the three sensory systems provides input regarding the body's state in its own reference system; the global error is obtained as the weighted sum of the different sensory inputs and the desired body state. For example, the desired ankle angle for upright standing is the right angle between the foot and shank; so any deviation from a right ankle angle is an error for the proprioceptive system. The sensory weights and the controller coefficients are estimated such that the model output replicates the experimental data. This method has gained much interest, since its relative simplicity makes it useful in clinical setting [2].

The PID modeling approach has been used to investigate multisensory integration and adaptability of the postural control system in a variety of experimental conditions. It has also been employed to quantify changes in postural control with aging and disease [1, 48, 49, 51, 52, 55, 134]. Peterka was the first to use this approach to investigate sensory reweighting in human postural control [1]. To investigate the adaptation of postural control to changes in available sensory cues, he performed experiments in six conditions, where different combinations of visual or BOS rotation perturbations were applied to the standing subjects. He found that unperturbed sensory systems were assigned higher weights. More specifically, for small perturbation amplitudes, postural sway was small and control was achieved using mostly somatosensory and visual inputs. However, for larger visual and BOS rotation, the vestibular information was assigned a higher gain. Interestingly, subjects with severe bilateral vestibular loss could not use this sensory reweighting toward using vestibular system for larger perturbation amplitudes, and usually experienced instability and fall.

The PID control approach has provided valuable information regarding postural control and has been recently organized into a framework for clinical research [48]. However, it does not automatically predict reweighting of the sensory inputs and must be applied to any new experimental condition to estimate the corresponding controller and sensory parameters. In addition, it assumes perfect measurement of postural variables by the sensory systems, ignoring the dynamic response of sensory organs. There are two other approaches that automatically deal with sensory reweighting, although they are more complicated.

Kalman filtering and internal models

The second approach uses Kalman filtering and internal models [135-138]. This approach has two main components: a sensory integration center, and an internal model. The sensory integration center generates an accurate representation of the environmental and experimental conditions by correcting for the sensory prediction error, the difference between the estimated (using Kalman filtering) and measured sensory information. Internal models of body biomechanics, noise, and motor commands are required for this prediction, which will be used with an optimal feedback control system. These models have shown to be able to replicate postural control behaviors across different standing conditions with visual and mechanical perturbations. For example, van der Kooij et al. used this model to replicate the dependency of body sway response to visual surround perturbation amplitude [137].

Disturbance estimation and compensation model

The third approach is the disturbance estimation and compensation (DEC) method, proposed by Mergner [69]. The DEC method assumes that three sensory inputs are instrumental for adaptive postural control: vestibular input, joint angle, and joint torque. At the first level, the transduced sensory information from these sensory systems are fused together to provide accurate measurement of physical variables, such as head orientation. At the second level, referred to as "meta level", the sensory information is used to generate an estimate of the external disturbance, which is then used in a local proprioceptive feedback loop to reject the disturbances. Mergner has shown this method can adaptively model response to external perturbations in a variety of conditions, as well as to anticipate self-produced disturbances [69].

2.8 ANKLE JOINT STIFFNESS AND ITS ROLE IN POSTURAL CONTROL

The ankle joint plays a central role in postural control; thus, it is essential to be familiar with its structure, musculature, and stiffness.

2.8.1 Ankle joint

The ankle is a synovial joint located in the lower limb, which connects the foot and leg. The ankle joint is central in the control of movement, as the GRF is transmitted to the lower limb through the ankle. In standing with the ankle strategy, it is evident that ankle plays a pivotal role, since movement primarily happens around the ankle. In walking and running, the ankle is responsible to generate large push off torques, required to propel the body. High prevalence of ankle injuries (e.g. ankle sprain) that happen for athletes, is an evidence of these large torques transmitted to the ankle during movement [139].

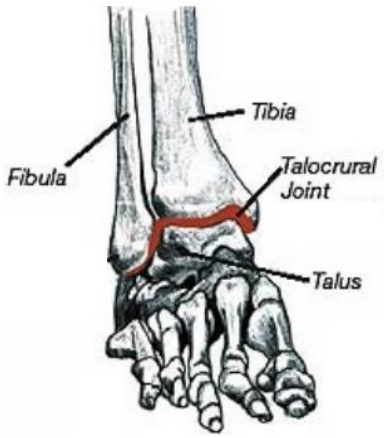

Figure 2.5 Talocrural joint

The Ankle consists of three joints: the talocrural, the subtalar, and the inferior tibiofibular [140]. The three joints are formed between the tibia and fibula in the leg and the talus in the foot. They allow 3D movement of the foot with respect to the leg. The talocrural joint, illustrated in Figure 2.5, allows movement in sagittal plane; Ankle rotation in sagittal plan is referred to as dorsiflexion (DF) and plantarflexion (PF); DF refers to the movement that brings the foot toward the shank and PF is the opposite. The subtalar joint allows inversion-eversion of the foot; inversion and eversion refers to the movement that tilt the sole of the foot towards or away from the midline

of the body, respectively. The inferior tibiofibular allows slight lateral movements of the malleolus for its rotation during DF of ankle [141].

Several skeletal muscles span the ankle, each with a specific functional role [142]. The Triceps Surae (TS) muscle group generates PF torques and consists of the three largest ankle muscles, Soleus (SOL), medial Gastrocnemius (MG) and lateral Gastrocnemius (LG). These muscles are located at the back of the shin and are attached to the calcaneus through Achilles tendon, as shown in Figure 2.6. The tibilias Anterior (TA) generates torques that dorsi-flex the ankle, it is located in front of the shin, and inserts into the medial cuneiform and first metatarsal bones of the foot (Figure 2.6). The TS muscles are much larger than TA and generate higher forces [143]; this suits function, since PF torques required in standing, walking, and running are much larger than the DF torques.

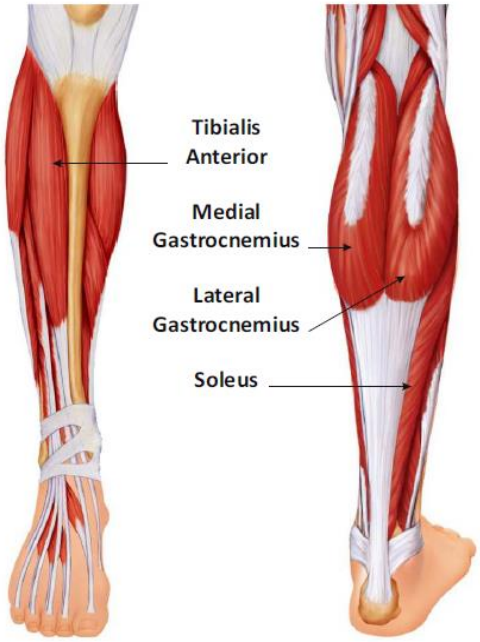

Figure 2.6 Ankle major dorsi-flexor and plantar-flexor muscles [144]

2.8.2 Dynamic Joint stiffness

Joint stiffness describes the dynamic relationship between joint angle and the torque acting about it. The stiffness provides a quantitative measure of the joint resistance to movement before the appearance of voluntary interventions [77, 145]. Thus, it is important in the study of human

movement, since it defines the joint (resisting) torque response to external position perturbations; it also determines the load that the CNS must overcome to generate movement.

Joint stiffness has intrinsic and stretch reflex components [74, 77]. The intrinsic stiffness generates resistive torque against joint movement with no change in muscle activation. Thus, it is crucial in functional tasks, such as postural control, where it reduces the burden on the CNS by providing a significant portion of the torque needed to keep the body in an upright posture [9, 10]. For athletes, the cutting maneuvers generate very large torques, tending to cause over-eversion/inversion, the intrinsic stiffness seems very important in preventing ankle sprains [146]. Reflex stiffness, on the other hand, is much more complicated and its role in functional tasks and movement control is not clearly understood [147, 148]. The stretch reflex contributions are generally quite variable among different subjects. It has been reported that stretch reflexes have important role in human movement, such as force generation for voluntary movements [148], force generation in gait [149], and regulation of balance [150]. However, reflex stiffness has been usually investigated by the analysis of muscle EMGs, which provides no direct insight into its mechanical contribution.

Intrinsic stiffness

Intrinsic stiffness is the joint mechanical resistance to movement that is generated by passive visco-elastic properties of active muscles, connective tissues, and joint, and the inertial properties of the limbs [77]. Intrinsic stiffness acts with no delay, so generates resistive torque as soon as there is a movement in the joint. It does not require any change in muscle activation.

Intrinsic stiffness has been extensively investigated in a variety of experimental conditions and at different joints. Two types of model have been used to study the intrinsic stiffness: 1- Non-parametric impulse response function (IRF) or frequency response models [151-158], and 2- Parametric second order mass-spring-damper (IBK) model, which contains Inertia (I), viscosity (B), and elasticity (k) [7-11, 159-163] or state-space models [164]. Each type of model has its own pros and cons. Non-parametric models do not constrain the structure of the stiffness, therefore, provide more flexibility. However, they are difficult to interpret and relate to physical meaningful variables. In contrast, parametric models provide a convenient, physically meaningful way to

quantify the joint stiffness. In addition, they are simple and more suitable for practical applications such as controller design.

Reflex stiffness

Reflex stiffness generates resistance against joint movement; it is generated through spinal loops, where muscle spindles trigger a reaction that causes a burst of activity and consequently generate force to oppose the movement. When a muscle is stretched, muscle spindles (located in parallel to the muscle extrafusal fibers) are also stretched, and excite their Ia afferents; the activation of these afferents depolarizes their synapse to alpha moto-neurons of the same muscle in spine and generates activity in the muscle. This is illustrated in Figure 2.7 for the elbow muscles, where a tap on the tendon of the biceps brachii muscle in the upper arm generates a stretch reflex response. Due to the limited conduction velocity of nerves, there is a delay between the muscle stretch and the burst of activity in the muscle that was reported to be around 35-40 ms in ankle [74, 75, 165]. The Ia afferents also excite Ia interneurons that inhibit the antagonist muscles of the joint (Figure 2.7). In addition, the excitation of the Ia afferents generates a signal, which is sent to the brain; in response a long latency reflex response is generated [75, 166]. This is also referred to as functional stretch reflex, since it is a more modifiable reflex and its gain may be changed by supra-spinal centers to suite the task [114].

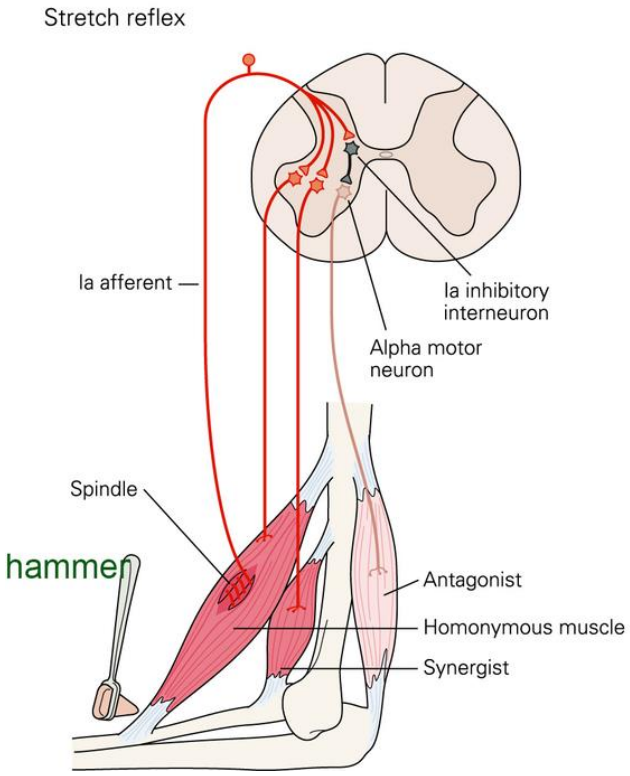

Figure 2.7 Stretch reflex circuit in the arm muscles. Taken and modified from [14].

Ankle reflex stiffness has been generally modelled using the nonlinear Hammerstein structure, shown in Figure 2.8 [167-169]. The reflex stiffness is modelled as a velocity dependent pathway that generates a torque when TS is stretched by a dorsiflexing movement of the joint [165]. A plantar-flexing movement, on the other hand, does not generate a reflex response, since reflex responses in TA are very small [170]. This direction dependency is modelled using a static nonlinearity, which resembles a half-wave rectifier, whose input is the delayed velocity of the joint movement [7]. The delay accounts for the reflex delay. The output of the nonlinearity then goes through a linear low-pass dynamics that models the muscle and sensor behavior [74]. In quasi-stationary experiments, the Hammerstein structure is considered time invariant (TI). In this model, the nonlinear elements are approximated by a set of basis functions, such as Chebyshev polynomials [171] and B-splines [172]. The linear TI dynamics have been modeled using IRF [74], transfer function [173], and state-space [174] structures.

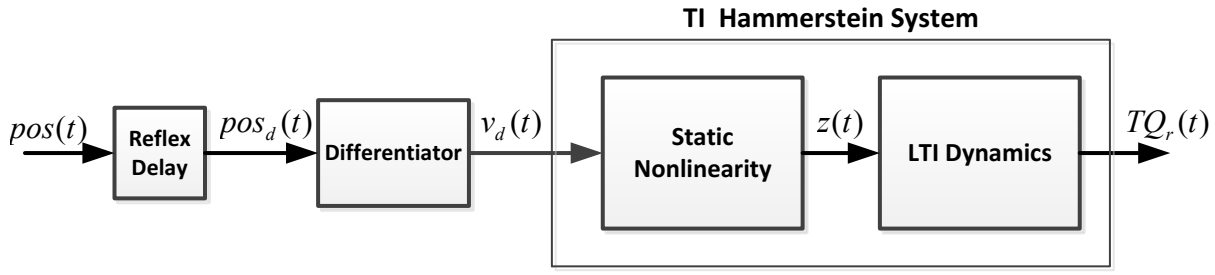

Figure 2.8 Reflex stiffness model for quasi-stationary conditions; taken from [175].

2.8.3 Variation of ankle stiffness with the operating points

Ankle joint stiffness has been shown to change dramatically with the joint operating point (OP), defined by joint mean position [5-7], muscle activation level [4, 7, 159, 160, 176, 177], joint velocity [163], and perturbation properties [178]. These modulations have been mostly demonstrated in quasi-stationary conditions, where controlled small perturbations are applied to the ankle about a fixed OP and the associated stiffness is estimated. This is repeated for different OPs to characterize how stiffness is modulated. In functional tasks, however, the joint OP changes continuously and cannot be controlled; thus, the stiffness will not be constant and TV identification methods that account for continuous changes must be used [179-182].

Ankle joint stiffness has been shown to change significantly with mean ankle position and torque in quasi-stationary studies. Mirbagheri et al. identified ankle intrinsic and reflex stiffness at a wide range of mean ankle positions and torques in quasi-stationary supine conditions [7]. They demonstrated that the intrinsic and reflex stiffness increased when the joint was moved from plantarflexion to dorsiflexion. The modulation of stiffness with activation level, however, was more complex. The intrinsic stiffness increased when ankle mean torque (muscle activation level) increased; whereas, the reflex stiffness increased initially from zero to small mean torques and then dropped significantly at higher torque values. Similar results for dependence of ankle intrinsic stiffness on joint position and activation levels were shown in other studies [4-6].

Ankle stiffness has also been shown to change with perturbation properties. The intrinsic stiffness was demonstrated to decrease as perturbation amplitude increased [178]. The reflex stiffness, however, was shown to have a highly nonlinear behavior [76]. The reflex response (both

the EMG and torque) is generally significant for discrete dorsi-flexing pulse perturbations (with short width) that stretch the TS muscles; in such conditions, the amplitude of the response increases with pulse velocity [76]. However, if the pulses are superimposed on top of a continuous random joint movement, the amplitude of the reflex response decreases [76]; as the mean absolute velocity of the joint movement goes up, the reflex responses start to become smaller and gradually diminish [76].

Similar changes to the ones observed in quasi-stationary experiments, have been shown during time varying experiments, where ankle OP continuously changes. Intrinsic stiffness has been shown to change during large imposed joint movements [183, 184] and voluntary isometric contractions [180, 185]. In addition, the stiffness was demonstrated to change when activation and joint angle change together. For example, Rouse et al. showed that ankle intrinsic stiffness changed by a factor of 4 in the stance phase of gait [186], and Lee and Hogan documented the changes of the intrinsic stiffness in swing phase of gait [158]. Moreover, it was shown that the reflex EMG gain changed significantly with imposed joint movements and when TS muscles activation changed isometrically [187, 188]. Similar changes were shown for reflex torque during imposed walking movement [189].

2.8.4 Ankle stiffness in standing

Identification of ankle stiffness in standing is challenging due to several reasons. First, the inherent postural sway generates large non-stationarities in the position and torque signals, making the identification difficult. In addition, the sway is associated with continuous changes in ankle OP (ankle angle and torque) that modulates the stiffness, resulting in time varying stiffness. Moreover, it has been shown that the centrally generated torque are much larger than the stiffness torque [1]; this, in effect, translates to low signal-to-noise ratio for the stiffness torque, making the identification of stiffness pathways difficult [13]. Finally, postural control data is acquired in closed-loop conditions, where open-loop methods fail and more sophisticated methods must be used to obtain unbiased estimates of the systems.

Intrinsic stiffness in standing

One method used to estimate ankle intrinsic stiffness in standing is to analyze the intrinsic torque response to pulse perturbations of ankle position. Application of a fast pulse perturbation

generates an instantaneous intrinsic torque, followed by a delayed active torque (reflex and central torque). Due to the short length of the pulse, the non-stationarities are small and ankle OP does not change significantly during the pulse response. Consequently, it is reasonable to assume that the stiffness is constant. In addition, closed-loop effects are not significant, since there is not sufficient time for central and reflex pathways to generate a torque response to the pulse. Therefore, the dynamic relationship between the ankle position and the intrinsic torque response provides an estimate of the dynamic ankle intrinsic stiffness in standing. This relation has been generally modelled using an IBK model [8-10, 39, 40, 190].

Numerous studies have used this method to quantify ankle intrinsic stiffness in standing and generally reported the value of elastic component of the intrinsic stiffness (i.e. K) relative to the critical stiffness. Loram et al. applied very small ankle perturbations (0.055 degree) to ensure they did not to disturb postural control and reported the intrinsic stiffness to be 91% [9]. Following Loram's work, Casadio et al. used a larger perturbaion amplitude (1 degree) and found the lower bound for intrinsic stiffness in standing was 64% [10]. Others have examined the modulation of ankle intrinsic stiffness in standing with a range of perturbation amplitudes. Loram et al. reported that the intrinsic stiffness in standing ranged from 13%-67% corresponding to perturbations with amplitude between from 0.03 to 7 degree [8]. Vlutters et al. reported that the intrinsic stiffness ranged from 44% to 93% with perturbation amplitudes ranging from 0.005 to 0.08 rad (0.29 to 4.58 degree); they showed a logarithmic function with a negative slope explained the intrinsic stiffness-perturbation amplitude relation [11]. Sakanaka et al. also showed that the stiffness decreased from 80% to 45% as the pertrubation amplitude increased from 0.1 to 0.6 degree [40]. They demonstrated that these changes with amplitude exist in normal standing. However, when the body sway was increased artificially by continusouly rotating the BOS, intrinsic stiffness did not change with perturbation amplitude [40]; they proposed this behaviour was the result of muscle tixotrophy properties, which is the temporary reduction in muscle stiffness due to large movement [191, 192]. In spite of the differences in the reported stiffness values, all these studies consistenly showed that ankle intrinsic stiffness was not adequate in itself for postural control (always smaller than the critical stiffness). However, it is large enough to make substantial contributions to the task [8-10, 39, 40, 190].

Ankle OP, including ankle torque and angle change continuously with sway; therefore, it is likely that joint stiffness changes significantly in standing. Despite this, aforementioned studies did not account for possible modulation of the intrinsic stiffness in standing and estimated the average intrinsic stiffness. Loram et al. investigated the modulation of the stiffness with sway but found no consistent relationship and concluded that intrinsic stiffness was constant in standing [9]. Sakanaka et al., however, showed that the intrinsic stiffness increased with ankle torque when sway was artificially increased by continuous rotation of the BOS [40]. However, no study has systematically demonstrated the possible changes of ankle intrinsic stiffness with sway in normal standing.

Ankle intrinsic stiffness was also identified in experiments where a continuous rotation of BOS was used as perturbation. These studies generally used time invariant closed-loop identification methods and assumed the intrinsic stiffness was constant. Estimating the intrinsic stiffness was reported to be difficult due to its possibly small contributions (low signal-to-noise ratio). Consequently, the stiffness was even sometimes ignored in their models, as they could not estimate its value reliably [1, 32, 49, 56]. One study recently demonstrated that the including EMG signals in addition to kinematic and kinetic measurements is required to decompose active and passive contributions (when continuous perturbations are used) and consequently find reliable estimates of intrinsic stiffness in standing [13].

Stretch reflex in standing

It is generally believed that reflexes become smaller with movement. For example, the reflexes in standing are smaller than prone or supine conditions, and are even smaller in walking and running [148]. However, there is no conclusive information regarding the nature, role, and contribution of reflexes in functional tasks, such as standing. This seems to be the consequence of the complexity of reflex pathways, since they are affected by many interacting factors. The changes in reflex in functional tasks are not caused simply by changes in OP, but are believed to be induced by complex neural pathways, triggered by both the CNS and PNS. The nervous system is suggested to use pre-synaptic inhibition as a versatile tool to control the excitability of reflex pathways [193]. Thus, inhibitory neurons, which synapse with the Ia-sensory afferents terminals, can reduce the

gain of the reflex pathway. As such, the reflex pathways can be facilitated or depressed according to the task requirement.

Another problem in quantifying reflex contributions in functional tasks is the lack of solid experimental and analytical methods. Analytically, as explained previously, it is difficult to develop mathematical methods that can identify time-varying nonlinear reflex stiffness with non-stationary data acquired in closed-loop experiments. Experimentally, stretch reflexes are difficult to evoke in standing and walking; strong well-designed actuators are needed to apply fast perturbations to rotate the joints and generate reflexes in standing; in walking and running, this is even more difficult, because the foot is not always in contact with the BOS and portable actuators must be used. Consequently, researchers have relied heavily on Hoffman reflexes (H-reflex) to investigate the excitability of reflex pathways in functional tasks [194-196]. The H-reflex is induced by direct electrical stimulation of Ia-sensory afferents, which in turn excites the synapse between the afferent and alpha-motoneurons and generates a burst of activity in the muscle. The efficacy of the reflex pathways is generally measured by the amplitude of the EMG evoked in the muscle. In standing, the excitability of reflex pathways is investigated by H-reflex in the soleus muscle due to the importance of soleus in postural control and the ease of generating H-reflex in it. The results obtained using H-reflexes, however, must be interpreted with care, since the H-reflex bypasses muscle spindles by directly stimulating the Ia-sensory afferent [149]. However, the stretch reflex, evoked by rotation of a joint, does not suffer this drawback and should be used when possible. Morita et al. showed that the sensitivity of pre-synaptic inhibition is different between stretch reflex and H-reflex [197]. Shimba et al. demonstrated that the amplitude of H-reflexes decreased from prone conditions to standing, while the EMG evoked by stretch reflexes increased in standing [198]; therefore, care must be taken when interpreting the results of these studies.

Reflexes have been shown to decrease significantly when going from sitting, supine and prone conditions to standing. Cecen et al. demonstrated that soleus H-reflexes were significantly smaller in standing compared to sitting and prone conditions, while soleus background activity was kept at minimum in the three conditions [199]. Similarly, Shimba et al. compared soleus H-reflexes in supine conditions with no background muscle activity to passive standing with no muscle activity achieved by using an orthosis. They showed that spinal excitability, measured by the amplitude of

H-reflex was smaller in standing than in supine conditions [198]. H-reflex has been shown to be linearly correlated with background EMG activity [200-202]; however, the EMG was similar between the two conditions, so other mechanisms must have contributed to the depression of H-reflexes. The authors suggested that the change in the sensitivity of H-reflex pathways could have been induced by supra-spinal input or the PNS, i.e. the input from somatosensory or vestibular systems. It has been shown that the direct electrical stimulation of the vestibular system depresses H-reflex amplitude [203, 204]. The importance of somatosensory inputs on H-reflexes also have been demonstrated. For example, Nakazawa et al. performed experiments where subject stood on a force platform in a water tank, while different loads were applied to their knee and ankle joint of one leg. The results showed that the soleus H-reflex were lower when the joints were loaded [205]; As the background EMG was constant between the loaded and unloaded conditions, these results showed the input from joint afferents and cutaneous inputs might have changed H-reflex sensitivity. In another study, Kawashima et al. showed that standing with different hip angles and a constant ankle angle changed H-reflex sensitivity of soleus H-reflex in standing; it was concluded that the inputs from the neural pathways between hip and ankle caused this modulation [206].

H-reflex sensitivity also have been shown to change with postural sway [207, 208]. These changes have been initially ignored in standing; consequently, large variability was observed in the amplitude of H-reflexes in standing; It was assumed that individuals with larger sway in standing had smaller highly variable H-reflexes [209, 210]. However, Tokuno et al. showed that the amplitude of H-reflex changes systematically with the position of COP [208]. When COP was located anteriorly, the H-reflex amplitude was larger compared to the situation where the COP was close to the ankle axis of rotation [208]. In a later study, Tokuno et al. looked into the H-reflex modulation with both the position and velocity of sway and demonstrated that both variables independently affect the sensitivity of H-reflexes [207]. The H-reflex amplitude was larger when the body was swaying forward compared to backward direction. In addition, they showed that the reflex was more sensitive to the sway direction than the position of the COP; thus, concluded that H-reflex sensitivity in standing was modulated in a direction dependent manner. These findings suggest that the excitability of reflex pathways changes in a functionally appropriate manner; thus, when the COP is located anteriorly and the body is swaying forward, a larger soleus reflex can push the body back toward its equilibrium and reduce sway; on the other hand, when the COP is

located close to the ankle axis of rotation and the body is swaying backward, reflexes can cause instability, therefore, they are depressed.

A drawback with the literature of reflexes in standing is that most studies relied on examining the amplitude of the evoked reflex EMG to draw conclusions regarding its modulation and role in the task. Unfortunately, this method does not provide concrete evidence regarding the functional importance of reflexes in standing, because EMG is a measure of the reflex activation in the muscle but not its mechanical contribution. In fact, there is a complex relationship between EMG and muscle force (torque), which changes with muscle length and contraction velocity [211]. As an example of this complexity, it has been shown that in supine and standing, stretch reflex EMG and torque may not show similar trends; it was shown that increasing muscle background activation did not change the amplitude of reflex EMG, while it was associated with a decrease in reflex torque [7, 74, 212].

A few studies have tried to investigate the mechanical contribution of stretch reflexes in standing. Bock et al. provided some evidence of functional importance of the reflexes by directly measuring the reflex torque in response to ankle DF pulse rotations; consistent with Tokuno et al. [207, 208], they showed that reflexes are modulated by postural sway; the stretch reflex EMG increased with ankle background torque; however, surprisingly, the reflex torque decreased with background torque [212]. In addition, the reflex torque decreased when the body was swaying forward [212]. The second finding corroborates the direction dependency of reflexes in standing shown by Tokuno and provide some evidence that the reflexes are modulated in standing to suit the postural control. Lang also estimated the reflex torque gain in response to individual dorsiflexion pulse of ankle position in normal standing and in forward and backward lean [213, 214]. It was demonstrated that the gain heavily changed with postural sway. The gain was maximum at intermediate ankle torques (happening in normal standing), but it became smaller in large ankle torques in forward lean, as well as, small ankle torques in backward lean. These studies provide some evidence of modulation of reflex mechanical contribution in standing; however, there is a need to systematically analyze the reflex responses in standing.

CHAPTER 3 IDENTIFICATION OF HUMAN POSTURAL CONTROL

This chapter deals with the identification of human postural control system. Joint stiffness identification is closely related to the identification of postural control, so I start by reviewing the challenges faced in the identification of ankle joint stiffness and then describe the experimental and analytical methods developed to deal with them. Then, I will discuss the complexities that arise in the identification of postural control, most importantly closed-loop effects. I will provide an overview of the difficulty faced in general closed-loop identification and the methods to deal with it. The chapter concludes with a review of the literature related to the identification of human postural control.

3.1 IDENTIFICATION OF ANKLE JOINT STIFFNESS IN CONTROLLED SUPINE CONDITIONS

Identification of ankle joint stiffness is challenging for several reasons: 1) Intrinsic and reflex torques cannot be measured directly, and only their sum can be measured. 2) Reflex stiffness has a non-linear structure. 3) Intrinsic and reflex stiffness change dramatically with the joint operating point (OP), defined by its torque and angle. 4) Large non-stationarities in ankle torque during movement make the identification difficult. 5) The ankle torque is controlled in closed-loop conditions; consequently, open-loop identification methods can not be used and specific methods must be utilized. To make the identification of the joint stiffness easier, several considerations are often imposed in the design of experiments.

Researchers have relied on quasi-stationary experiments to characterize ankle stiffness. In such experiments, the subjects generally are positioned in supine conditions and very strong, high performance actuators are used to apply perturbations to the ankle about a fixed OP. This means ankle joint mean position is fixed, muscle activation is held (almost) constant by keeping the ankle torque constant, and perturbation properties are invariable throughout the experiment. Imposing these conditions ensures that the stiffness remains constant in each trial and the measured signals are all stationary; therefore, the stiffness can be treated as a time invariant (TI) system. In addition, provided that the actuators are able to render very large torques, they can move the ankle joint irrespective of the torque generated by ankle. Consequently, joint stiffness can be treated as an

open-loop system with the position as the input and the torque as the output. This provides means to study ankle joint mechanics in a variety of joint OPs.

Under these conditions, joint stiffness can be modelled using a parallel cascade structure (PCS), comprising a linear TI (LTI) intrinsic stiffness pathway in parallel with a nonlinear TI reflex pathway, as illustrated in Figure 3.1. The input to the PCS is the joint position and the output is total ankle torque ($\widetilde{tq}$), the sum of intrinsic (tq_I) and reflex (tq_R) torque, voluntary torque (tq_v), and measurement noise (n). The intrinsic pathways can be modelled using a TI impulse response function (IRF) or a mass-spring-damper (IBK) model. The reflex pathway is composed of a delay, a differentiator, and a TI Hammerstein structure. Several methods have been developed to identify the intrinsic and reflex pathways under quasi-stationary conditions.

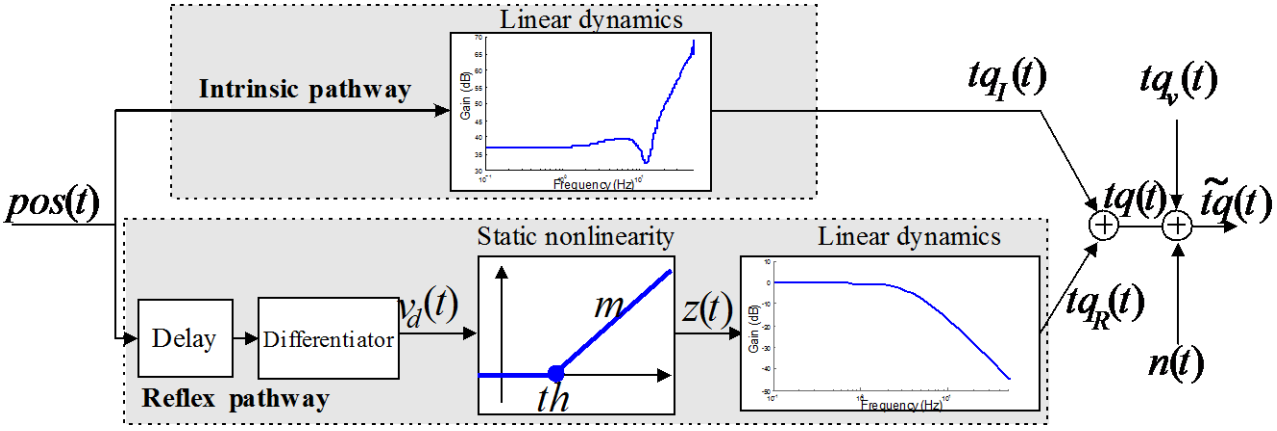

Figure 3.1 Time invariant, parallel cascade model of ankle joint stiffness under quasi-stationary conditions. Taken from [171].

3.1.1 Identification in quasi-stationary experiments

The first set of methods employ an iterative approach to estimate the intrinsic and reflex stiffness [7, 74, 215]. These methods model the intrinsic stiffness as a TI IRF, whose memory is selected to be less than the reflex response delay; this ensures that the intrinsic torque is not biased by the reflex response. Then they first estimate the intrinsic IRF and use it to predict the intrinsic torque. The predicted intrinsic torque then is removed from the total torque to provide an estimate of the reflex torque. The estimated reflex torque is then used to obtain an estimate of the reflex

stiffness and predict the reflex torque. The predicted reflex torque is removed from the total torque to estimate the intrinsic torque. This new estimate of the intrinsic torque is then used to refine the intrinsic stiffness estimate and the procedure is repeated. The iteration continues until there is no improvement in the total variance accounted for (VAF) of the stiffness predicted torque. The reflex pathway has been estimated using Hunter-Korenberg correlation-based method [74] and separable least square method [215]; although, neither method has guaranteed convergence [216].

The subspace method was developed to identify ankle joint stiffness without the need for iteration. The intrinsic stiffness is modelled as an TI IBK structure [174] or a TI IRF [171]; the linear element of the reflex pathway is modelled as state-space system, whose input is generated from delayed joint velocity after going through a Chebyshev expansion of the static nonlinear element of the Hammerstein structure [217]. Orthogonal projection is used to decompose the ankle torque to its intrinsic and reflex components and consequently estimate each pathway [218].

3.1.2 Identification in time varying conditions

The methods for ankle stiffness identification discussed so far were developed for quasi-stationary conditions, where stiffness is almost constant. These methods fail when the ankle OP changes with time, because the stiffness parameters will change with OP; thus, other methods have been developed to identify ankle stiffness, when there are large time varying (TV) changes in the joint position and/or activation.

TV identification methods model the modulation of ankle stiffness as a function of time. The most common approach is the ensemble-based method, which uses input-output data from many trials with the same TV experimental conditions to quantify the modulation of the stiffness parameters at each instant in time [158, 219-221]. This method has been used to identify ankle stiffness in controlled TV conditions [219-221] and during walking [158]. The major difficulty with ensemble-based methods is that it requires collecting hundreds of input-output trials in the same experimental conditions, which is challenging.

Another set of TV identification approaches model the changes in the stiffness parameters using basis function expansion of time. This drastically reduces the number of model parameters compared to ensemble-based methods. This method has been used to quantify the modulation of ankle stiffness during imposed walking movements [222]. Temporal expansion methods (and

ensemble-based methods) provide a good understanding of the modulation of the stiffness in a given experimental condition, but provide no direct information regarding the underlying cause of the observed changes. In addition, the temporal expansion method works best for slow movement and will fail to follow the stiffness modulation for faster movements. Finally, neither of the two methods can predict the system response to new trajectories.

Linear parameter varying (LPV) identification methods assume that the system parameters change as a function of a scheduling variable (SV) that changes with time. The SV is generally a physical variable that can be measured or estimated. LPV methods have been used to model ankle intrinsic stiffness during imposed movements at rest [183], to identify ankle intrinsic and reflex stiffness in large passive ankle movements [175], and to identify ankle stiffness during TV isometric voluntary contractions [180]. Compared to TV models, LPV models provide a better understanding of the changes of system parameters with physical entities; they need less data to yield robust parameter estimates, and can predict the response of the system to new input realizations. However, measurement/estimation or even knowledge of the right SV may be difficult.

The aforementioned methods provide valuable information regarding the stiffness in TV conditions. However, they are difficult to apply for the identification of ankle stiffness in functional tasks, such as standing, as explained in section 2.8.4. Nevertheless, they provide insight into the neuro-mechanics of ankle joint across a variety of experimental conditions, which is essential to assess its role in more complicated functional tasks, where many systems interact.

3.2 THE PROBLEM WITH CLOSED-LOOP IDENTIFICATION

The main problem in system identification using data acquired in closed-loop is the correlation between the input and the unmeasurable noise [59, 80]. To explain this, consider Figure 3.2A which shows an open-loop LTI system, where u is the measured input to the plant (P), y is the measured noisy output and $\tilde{y}$ is the true output, and v is colored additive output noise. Figure 3.2B shows the same system in closed-loop, where r is the external input or reference signal, and C is the controller. The following input-output relationship holds for both systems:

$$y(t) = \tilde{y}(t) + v(t) = P(q)u(t) + v(t) \tag{3.1}$$

where t is the time ($t = 0, \dots, N$) and q is the shift operator. The objective is to use the measured signals, including $u, y,$ and r to identify P in both conditions.

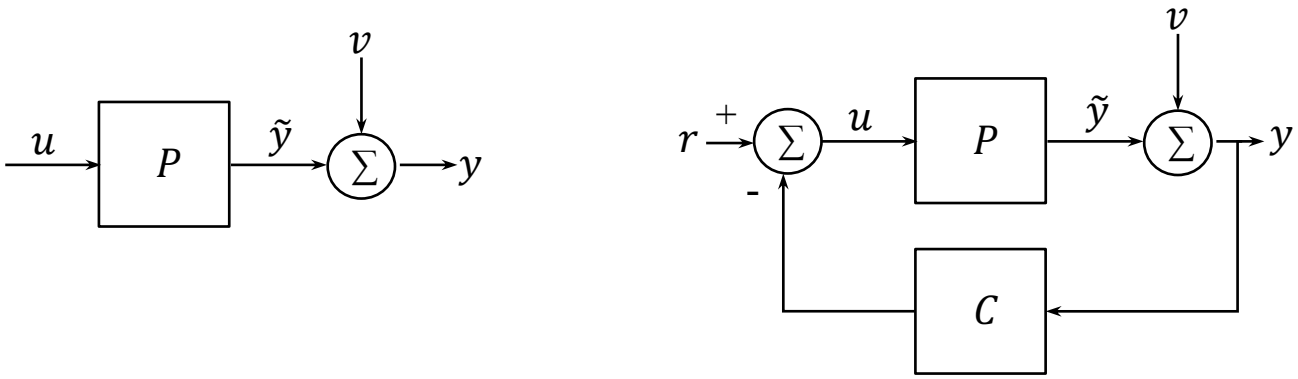

(A) (B)

Figure 3.2 General representation of (A) an open-loop system and (B) a closed-loop system

In open-loop conditions, provided that there is no correlation between the input, u, and the additive noise, v, and there is enough data, several well-developed methods exist to identify P. These includes frequency response (FR) estimation using spectral analysis [80], IRF estimation using cross-correlation analysis [216], and subspace approaches such as PI-MOESP [223].

However, in the closed-loop case, the input and output are related by:

$$u(t) = r(t) - C(q)y(t) \xrightarrow{y=\tilde{y}+v} u(t) = r(t) - C(q)(\tilde{y}(t) + v(t)) \tag{3.2}$$

This relationship clearly shows that u and v are correlated, therefore, using an open-loop identification method, based on correlation/spectral analysis between u and y provides biased estimate. To see this, note that for closed-loop conditions, the following holds (Figure 3.2B):

$$y(t) = \big(r(t) - C(q)y(t)\big)P(q) + v(t) \rightarrow y(t) = \frac{r(t)P(q) + v(t)}{1 + C(q)P(q)} \tag{3.3}$$

$$u(t) = r(t) - \big(u(t)P(q) + v(t)\big)C(q) \rightarrow u(t) = \frac{r(t) - C(q)v(t)}{1 + C(q)P(q)} \tag{3.4}$$

Therefore, the direct relation between u and y results in:

$$\frac{y(t)}{u(t)} = \frac{r(t)P(q) + v(t)}{r(t) - C(q)v(t)} \tag{3.5}$$

It is evident that this relation depends on the plant, the controller, external input, and unmeasurable noise. Similarly, we can use the following estimator to find the FR between u and y:

$$\hat{G}\big(e^{j\omega}\big) = \frac{\Phi_{uy}(e^{j\omega})}{\Phi_{uu}(e^{j\omega})} \tag{3.6}$$

where Φ_{uu}, Φ_{uy} and ω are the input auto-spectrum, input-output cross-spectrum, and the frequency. The input auto-spectrum and input-output cross-spectrum can be estimated using (3.3) and (3.4). Substituting the results into (3.6) yields [77, 224]:

$$\hat{G}\big(e^{j\omega}\big) = \frac{P\big(e^{j\omega}\big)\Phi_{rr}(\omega) - C\big(e^{-j\omega}\big)\Phi_{vv}(\omega)}{\Phi_{rr}(\omega) + |C(e^{j\omega})|^2\Phi_{vv}(\omega)} \tag{3.7}$$

where $\hat{G}$ is the estimated FR between u and y. It is evident that $\hat{G}$ is not a correct estimate of the plant P and the resulting dynamic relationship strongly depends on the properties of the reference and noise signals. If there is no output noise, i.e. $v(t) = 0$, then an estimate of the plant is obtained, showing the main problem in closed-loop identification is the noise. If there is no reference signal, i.e. $r(t) = 0$, then an estimate of the inverse of the controller is obtained. In any other case, the estimate is a combination of the plant and the controller dynamics that will depend on the relative power of the external input and the noise.

The cross-correlation analysis is the time-domain counterpart of the spectral analysis, where the estimate of the IRF is obtained by solving the following equation using linear least square method [216]:

$$R_{uy} = \boldsymbol{R}_{uu} h \tag{3.8}$$

where R_{uy} is the vector of the cross-correlation values between u and y, h is the vector of the IRF with a length of M (memory of the system), and $\boldsymbol{R}_{uu}$ is the regressor, containing the auto-correlation value of the input. Unbiased estimates of h is obtained, provided the estimates of R_{uy} are accurate. However, this will only be the case if u and y are not correlated, which is not the case in closed-loop conditions [224]. Similarly, it can be shown that correlations between the input and noise will cause subspace identification to fail [224, 225].

3.3 METHODS FOR CLOSED-LOOP IDENTIFICATION

Methods for closed-loop identification can be divided into three categories based on the assumptions made about the feedback pathway [59]:

1. The direct approach: ignores the feedback and treats the closed-loop identification in the same manner as an open-loop identification; thus, the input and output of the system of interest are used directly for identification.
2. The indirect approach: first identifies the closed-loop dynamic relationship between the reference input and the output. Then, it uses *a-priori* knowledge of the plant and controller structures to estimate their parameters.
3. The joint input-output approach: This approach considers the input and the output of a system to be jointly driven by an external input and identifies two dynamic closed-loop dynamic relationships. Then, it uses the estimates of the closed-loop systems to estimate the system of interest.

Below I will provide a more detailed description of each method. The methods are presented for a single-input, single-output (SISO) system, but they can be extended to the multiple-input, multiple-output (MIMO) structures, needed to study multi-segment postural [41].

3.3.1 The direct approach

The direct approach does a direct identification between u and y with the objective of identifying the plant P (in Figure 3.2B). This will generate unbiased estimates only if a prediction error method (PEM) is used [59]. In this approach, the input u and output y are related by [226]:

$$y(t) = P(q,\theta)u(t) + H(q,\theta)e(t) \tag{3.9}$$

where H is a noise model, e is an unknown random white sequence, θ is the vector of the parameters of the plant P and the noise model H, which must be estimated in the identification. This approach generally employs transfer function representations for P and H, whose structures (i.e. number of poles and zeros) are selected before the parameter estimation [226]. However, PEM has also been used to identify IRF [227] and state-space [228] models in closed-loop conditions.

Parameter estimation is done by minimizing the prediction error provided by:

$$\varepsilon(t,\theta) = y(t) - \hat{y}(t|\theta) = H^{-1}(q,\theta)[y(t) - P(q,\theta)u(t)] \tag{3.10}$$

where $\hat{y}$ is the one-step-ahead prediction of the model. Usually, the parameters are estimated through a numerical search scheme (e.g. nonlinear gradient-descent algorithm) that minimizes the sum of squared prediction error in (3.10) [226].

The direct approach using PEM gives consistent, accurate results, provided the parameterizations of the noise and system dynamic models are adequate [59]. Moreover, this method is applied directly to input-output data and makes no assumption about the nature of the feedback. Consequently, it provides unbiased system estimates with arbitrary (e.g. nonlinear or TV) feedback. Consequently, it should be considered as the first choice for closed-loop identification.

3.3.2 The indirect approach

In the indirect approach, first the closed-loop dynamic relation between the external input and the output is determined. Then, in a second step, the estimated closed-loop transfer function and *a-priori* knowledge about the controller are used to obtain the plant dynamics.

The closed-loop transfer function describes the relationship between the external input r and the output y, shown in Figure 3.2B, as:

$$y(t) = G_c(q)r(t) + H_c(q)v(t) \tag{3.11}$$

where

$$G_c(q) = \frac{P(q)}{1 + P(q)C(q)} \tag{3.12}$$

$$H_c(q) = \frac{1}{1 + P(q)C(q)} \tag{3.13}$$

G_c is the closed-loop dynamics and H_c is the noise model. r and v are uncorrelated; therefore, (3.11) represents an open-loop system between r and y and any open-loop identification method can be used to identify G_c. Subsequently, the estimated closed-loop dynamics $\hat{G}_c$ and the known controller dynamics $C(q)$ can be used to estimate the plant dynamics $\hat{P}$, as shown below:

$$\hat{G}_c(q) = \frac{\hat{P}(q)}{1 + \hat{P}(q)C(q)} \rightarrow \hat{P}(q) = \frac{\hat{G}_c(q)}{1 - \hat{G}_c(q)C(q)} \tag{3.14}$$

If some *a-priori* knowledge of the structure of P is available, it is possible to first parametrize $G_c$in (3.11) using the known controller and the structure of P. The benefit of this is that the plant dynamics $\hat{P}$ is delivered directly in the first step and there is no need to perform the second step in (3.14), which can cause some estimation complexities [226, 229]. This method has been particularly attractive in the studies of postural control, as will be explained in 3.4.

There are several drawbacks with the indirect approach. First, the feedback pathway must be known perfectly and be TI. In practice, various nonlinearities cause the feedback to deviate from a linear TI structure. Moreover, in physiological systems, the controller dynamics are not usually known and it may not be possible to measure the external input [12].

3.3.3 The joint input-output approach

The joint input-output approach treats both the input and the output of a system as being driven by an external input. It first identifies the two systems separately using the external input and the two outputs, and then uses the identified dynamics to determine the plant.

Thus, in the joint input-output approach, both u and y are considered as outputs, driven by r, so that the following relationships hold:

$$y(t) = G_c(q)\, r(t) + \frac{1}{1 + P(q)C(q)}\, v(t) \tag{3.15}$$

$$u(t) = S_i(q)\, r(t) - \frac{C(q)}{1 + P(q)C(q)}\, v(t) \tag{3.16}$$

Where

$$G_c(q) = \frac{P(q)}{1 + P(q)C(q)} \tag{3.17}$$

$$S_i(q) = \frac{1}{1 + P(q)C(q)} \tag{3.18}$$

S_i is usually referred to as input sensitivity function [12]. It is evident that P is given by:

$$P(q) = \frac{G_c(q)}{S_i(q)} \tag{3.19}$$

Therefore, the approach is to first estimate G_c and S_i, and then estimate P using (3.19). In estimating G_c and S_i, it is assumed that r and v are uncorrelated, thus, any open-loop method can be used. For example, the FR of G_c and S_i are obtained using:

$$\widehat{G_c}\left(e^{j\omega}\right) = \frac{\Phi_{ry}\left(e^{j\omega}\right)}{\Phi_{rr}(e^{j\omega})} \tag{3.20}$$

$$\widehat{S_\iota}(e^{j\omega}) = \frac{\Phi_{ru}(e^{j\omega})}{\Phi_{rr}(e^{j\omega})} \tag{3.21}$$

Therefore, following (3.19), the FR of P is obtained using:

$$\hat{P}(e^{j\omega}) = \frac{\widehat{G_c}(e^{j\omega})}{\widehat{S_\iota}(e^{j\omega})} = \frac{\Phi_{ry}(e^{j\omega})}{\Phi_{ru}(e^{j\omega})} \tag{3.22}$$

It should be noted the application of the external input, r, provides an estimate of P. However, if the objective is to identify the controller C, another external input must be applied to the output (where v enters the system) and a similar joint input-output procedure can be used.

In contrast to the indirect approach, the joint input-output method does not require knowledge of the controller *a-priori*. However, the external input and the output must be linearly related as shown in (3.2). The joint input-output approach can be extended to cases with a nonlinear controller, however, the estimation problem becomes difficult [224]. In addition, as with the indirect approach, the external input must be measured.

3.4 REVIEW OF THE STUDIES OF POSTURAL CONTROL IDENTIFICATION

A variety of methods have been used to quantify the mechanism underlying human postural control. The indirect and joint input-output approaches were used most often to identify human postural control dynamics from data acquired in perturbed standing experiments. The direct identification method, however, has been used in a fewer studies and generally in an incorrect manner, which has led to misleading conclusions regarding the postural control. Below, I will provide an overview of these studies.

3.4.1 Indirect approach

The indirect approach is the most widely used method for closed-loop identification of human postural control [1, 32, 43, 48-55, 113, 115, 129, 134, 230-233]. Generally, an external input in the form of mechanical (base of support (BOS) rotation) or sensory perturbation (visual or vestibular) was used to evoke postural responses, which were measured as body angle, EMG, or

ankle torque. Subsequently, the dynamics of the closed-loop system was identified between the external perturbation and the measured output. The estimated closed-loop system is a combination of the body dynamics, passive and active controllers, and feedback pathways. Therefore, *a-priori* assumptions regarding the structure of each sub-system were incorporated to break the identified closed-loop system into its elements.

Most often, the first step of the indirect approach, the identification of the closed-loop system between the external perturbation and the output was done using non-parametric FR methods. FR methods are attractive, since they are relatively simple, and provide unbiased estimates of the closed-loop system with no need to make *a-priori* assumptions regarding the structure of the closed-loop system. In a second step, parametric representations of active and passive controllers as well as body dynamics were combined to give a parametric representation of the closed-loop system. Subsequently, the model parameters were estimated using a nonlinear minimization to fit the FR of the parametric system to the estimated FR in the first step. The estimated parameters generally have physical significance and are used to interpret the postural control behavior.

Many researchers have used this approach to examine postural control in both healthy subjects and those with impaired postural control [1, 32, 43, 48-55, 113, 115, 129, 134, 230-233]. For example, Peterka generated estimates of the closed-loop system in response to BOS/visual rotation and subsequently estimated parametric models for each experimental condition. He determined the gain of the three sensory systems and the passive stiffness and concluded that when perturbations are applied to a sensory system, higher gains are given to the inputs from unperturbed sensory systems [1]. Similarly, using mechanical rotation of the BOS, Pasma et al. showed that the elderly and patients with cataracts and impaired balance relied heavily on proprioceptive information for balance control [49]. Pasma et al. applied separate continuous BOS perturbation to quantify bilateral coordination and concluded that the proprioceptive information from each leg was independently weighted for postural control [52]. Using BOS rotation, Van der Kooij et al. showed significant asymmetries in dynamic balance control of individuals with Parkinson's disease [55].

The indirect approach however requires *a-priori* knowledge of the structure of both the active and passive controllers. Another problem with the indirect approach in the identification of

postural control is the need to identify all elements of the control loop, even if only one element (e.g. active controller) is of interest. Finally, the indirect approach may mask the dynamics of the controller due to the heavily low-pass filter dynamics of the body (inverted pendulum) [12].

3.4.2 Joint input-output approach

This approach estimates the controller and/or the body dynamics with no need for *a-priori* assumptions on their structures. However, this flexibility comes at a price; in contrast to the indirect approach, for the joint input-output approach, more than two signals must be measured; in addition, two perturbations are required, one to identify the controller and one to identify the body dynamics, making the experiments more demanding [12].

The joint input-output approach has been used in many studies of postural control, mostly in the context of multi-segment postural control [12, 32, 41, 42, 47, 51, 78, 234]. Fitzpatrick et al. used this approach to identify the active controller and plant dynamics; they reported that the gain of feedback pathway was too low to provide stability; and so feedforward pathways were needed for postural control [47]. Kiemel et al. determined the plant dynamics, relating the weighted sum of muscle EMGs to lower leg and trunk angles, using perturbed standing data with visual perturbations. They demonstrated that a single neural control strategy in ankle and hip muscles leads to multiple kinematic patterns, i.e. ankle and hip strategies [32]. Similarly, Hwang et al. studied the effect of the BOS conditions on postural control using a multi-segment model; they identified the body and the neural controller, and showed that the leg and trunk responses to visual perturbations changed dramatically with the BOS conditions; these changes were evident in the plant dynamics and not the neural controller [234]. Boonstra et al. used the joint input-output approach to examine multi-segment coordination in healthy individuals and a subject with Parkinson's disease, and demonstrated that Parkinson's disease was associated with asymmetry between left and right legs in balance control [42].

3.4.3 Direct approach

The Direct approach has been generally used incorrectly in the study postural control. Direct identification between any two signals from EMG, COM, COP, torque, or body angle will not provide accurate estimates of the postural control, unless PEM is used. However, most often cross-

correlation and linear regression methods, rather than PEM, have been used in a direct framework and so generated erroneous results [17, 33, 57, 235-237].

Several studies assumed that ankle stiffness was adequate to provide postural stability and used linear regression between ankle torque (COP) and body angle to estimate the stiffness in quiet standing [17, 33, 238, 239]. However, since there is no external perturbation in quiet standing, the direct approach using linear regression between ankle torque (or COP) and COM angle provides an estimate of the plant dynamics and not the controller as outlined in section 3.2. In perturbed standing, linear regression may be used, since the perturbation power is dominant; however, this approach is faulty, since the ankle torque is generated by both active and passive elements and linear regression between the torque and body angle generates the effective quasi-stiffness, not ankle intrinsic stiffness in standing [12].

Cross-correlation has also generated unrealistic results, as expected. Thus, Winter et al. used cross-correlation, to demonstrate that there was no lag between the COP and COM in quiet standing and concluded that there could not be any active contributions to the postural control. Therefore, passive stiffness was sufficient to stabilize standing [17]. Similarly, Massani et al. used cross-correlation and found that EMG led the COM angle by 198 ms [236]. Subsequently, in a simulation study, they showed that a PD controller with a large derivative gain would show this predictive behavior [235]. However, their simulation results did not correspond to the experimentally observed power spectra for COP and COM [12]. Gatev et al. also showed a lead of 250-300 ms between the EMG and body angle and proposed that this was due to feedforward pathways of postural control [57]. It seems likely that all these studies generated misleading results as a result of using the direct approach in closed-loop conditions.

PEM, the only valid direct method, has been used only in a few studies of quiet standing. Ishida and Miyazaki [240] and Ishida et al. [241] identified an ARMAX model structure using PEM to estimate of the control system in quiet standing. However, their identified system seemed to be combination of both the plant and controller [41]. van der Kooij et al. suggested that an external perturbation was required for PEM to work properly [12]. To date, no study has used PEM in perturbed standing experiments.

3.5 RATIONALE

The preceding review of the literature demonstrates the difficulty and challenges that arise in understanding the role of the many sub-systems that contribute to human postural control. Based on this review, I will formulate the following rationale for my PhD work.

The development of models to quantify postural control and elucidate the role of the different elements are important, since they (1) provide the knowledge of the mechanisms, underlying postural control and generate the basis for understanding the etiology of many diseases that can affect balance; (2) provide tools to objectively examine balance control, find the source of balance impairment, and subsequently design rehabilitative interventions to address the impairments; (3) are useful to understand the changes in postural control system, happening due to aging and subsequently can be used to develop strategies for fall prevention in the elderly; (4) provide means to develop assistive and rehabilitative devices such as orthoses and prostheses in a manner that replicates normal human postural control.

In this thesis, I will focus on the postural control in the context of an ankle strategy, since it is the most commonly used postural strategy during daily living. An important element in such condition is ankle intrinsic stiffness. It is generally agreed that the intrinsic stiffness contributes significantly to postural control, however, there is still controversy over its role and contribution. One reason is that ankle intrinsic stiffness generally has been assumed constant in the literature of human postural control and average stiffness values have been obtained. However, there is strong evidence that the intrinsic stiffness changes significantly with ankle operating conditions, defined by ankle angle and ankle torque, both of which undergo large continuous changes in standing. Therefore, it is expected that the intrinsic stiffness will change in standing with postural sway. This is important, since the modulation of ankle intrinsic stiffness with sway shows its contribution may change in a phase-dependent manner. This implies that the complementary active contributions, generated through muscle activations, also may change to provide the required corrective forces for postural control. However, there is no method to quantity ankle intrinsic stiffness and its possible modulation with postural sway.

Consequently, in Chapter 6, I will develop a method to estimate ankle intrinsic stiffness in standing, while accounting for the modulation of ankle operating conditions with postural sway.

Consequently, the method will show how the intrinsic stiffness changes with the modulation of ankle torque due to postural sway; the results also show if the observed changes in the stiffness are functionally important and serve postural control.

In Chapter 7, I will use the method developed in Chapter 6 to estimate ankle intrinsic stiffness across a range of postural operating conditions. This is important, since the intrinsic stiffness has been rarely estimated in a range postural tasks to provide a better view of its role, contribution, and adaptation to new conditions. I will show that in any operating condition, ankle intrinsic stiffness changes significantly with postural sway, whereas these modulation are associated with different patterns of ankle muscle activations. In addition, the intrinsic stiffness value changes in a large range across tasks, consequently, its contribution to postural control is highly variable.

It is important to quantify the contributions of central, and stretch reflex mechanisms to postural control. However, this is a difficult task, because the contributions of the pathways appear together and postural control is performed in closed-loop conditions. Consequently, in Chapter 8, I will develop a method to decompose the ankle torque into its central, stretch reflex, and intrinsic contributions. The method will use EMG activity of major ankle muscles during standing experiments as the inputs to predict the active ankle torque. Since the intrinsic stiffness is responsible for the generation of passive joint torque, the difference between the measured torque and the predicted active torque provides an estimate of the intrinsic torque. I will use this model to provide an estimate of the relative contributions of different elements to postural control. In addition, I will show that the dynamic relationship of the *central EMG-torque* and *reflex EMG-torque* are different for ankle plantar-flexor muscles, demonstrating an individual muscle respond differently to central and stretch reflex activations.

CHAPTER 4 MEASUREMENT OF SHANK ANGLE DURING STANCE USING LASER RANGE FINDERS

This chapter describes the design and implementation of a system that I developed to measure shank angles with high resolution and accuracy in standing. The development of such a system was essential, since we wanted to estimate ankle stiffness in standing, for which it was needed to measure ankle angle. Our standing apparatus was initially equipped with potentiometers to measure foot angles; therefore, I developed this system to measure shank angles, which can be used in combination with foot angles to determine ankle angles in standing. Thus, high-resolution laser range finders measure the linear movements of shanks, which are used subsequently to determine shank angles. The chapter provides the theory and analysis of the system, describes its static and dynamic calibration, and its overall performance to measure shank angles in quiet and perturbed standing. The chapter has been published in the 38th IEEE international Conference of Engineering in Medicine and Biology (IEEE EMBC) in 2016 in Orlando, Florida.

Measurement of Shank Angle during Stance Using Laser Range Finders

Authors: Pouya Amiri, Luke J. MacLean, and Robert E. Kearney.

Conference: 39th IEEE Engineering in Medicine and Biology Conference, Oralndo, 2016.

4.1 ABSTRACT

Ankle joint stiffness, the dynamic relationship between the joint angle and the torque acting about it, plays an important role in the control of upright stance. In order to identify the contribution of ankle joint stiffness to stance control, ankle joint must be perturbed externally. One way to do this is to displace the foot that will cause shank movement. For identification, the ankle angle must be measured with high accuracy, for which we need to measure both foot and shank angles. However, most motion capture systems do not have the resolution and accuracy needed to measure the small ankle joint movements that occur during stance. This paper describes a method for the high resolution measurement of ankle angle during standing that uses a laser range finder to track linear displacements, which is then used to compute shank angle with respect to the vertical. A theoretical analysis of different possible measurement configurations demonstrated that measurements of horizontal shank movement would provide the optimal resolution; a range finder with a linear resolution of 25 micros would provide an angle resolution better than 0.01 degree. We built a measurement system using this configuration and performed static and dynamic experiments that demonstrated angle measurements with a resolution of less than 0.01 degree, which outperforms other motion capture systems, such as IMUs, whose resolution is in the order of one degree. Utility of the method was then demonstrated by using it to measure shank ankle during quiet and perturbed stance. The results confirmed that the method tracks small shank movements during both quiet and perturbed conditions. Estimated shank angle then was used with the foot angle, measured with a potentiometer to obtain the ankle joint angle, needed to identify the joint stiffness.

4.2 INTRODUCTION

Postural control involves the control of body position in space to maintain stability and a desired orientation [18]. In response to small perturbations, the nervous system generates corrective forces in muscles that stabilize the body using an ankle strategy, where the main movement happens around the ankle joint [242]. Corrective forces include those generated by intrinsic and reflex muscle stiffness, and forces generated centrally as a result of feedback from other sensory modalities (somatosensory, visual, and vestibular systems). The response due to stiffness is a function of ankle joint angle, velocity and acceleration; The centrally generated response is a function of both ankle and upper body angles and velocities [12]. It was initially believed that ankle joint stiffness was adequate to maintain stable stance by itself [33]. Currently, it is generally agreed that joint stiffness may not be large enough to stabilize stance completely, although it contributes significantly to the task. However, the contribution of stiffness during different postural tasks has never been quantified.

In stance controlled with an ankle strategy, the movements are small, and upper body angle changes in the order of one degree [33], and high resolution sensors, with a resolution higher than 0.1 degree must be used to measure the angles. There are a variety of motion capture systems available to record the movement of body. However, most systems are designed to record motion during tasks, involving large body movements, such as gait, and consequently their resolution and accuracy are not sufficient to measure the small movements associated with quiet standing. Video motion capture systems, the most popular means for tracking human body movement, record the linear movements of markers attached to body segments and these linear displacements are converted to angles, using inverse kinematic calculations. These systems can be used to capture whole body movement for a variety of motor tasks; however, the resulting angular resolution has rarely been examined, they are expensive and their use requires a large calibration volume, which is not always available due to limitation of laboratory space. Mechanical and optical goniometers can also be used to measure joint angular movements directly; they are attached to two limb segments about a joint, to measure its angle [243]. Inertial measurement units are another group of sensors that are attached to body segments to measure their angles [244]; however, all these systems lack sufficient resolution and accuracy, needed to measure movements during stance. Our research aims to quantify the contribution of ankle joint stiffness to stance control and investigate

its modulation with task requirements, for which we must measure ankle joint angle. Therefore, we need to develop a system capable of capturing small movements during stance.

This paper presents a motion capture strategy that utilizes laser range finders to measure shank movement during standing with high resolution and accuracy. Our analysis showed that we could achieve an angle resolution less than 0.01 degrees using available range finders. We evaluated our method experimentally during controlled static and dynamic conditions. Finally, we measured the shank movement during quiet and perturbed stance experiments to demonstrate that the method can track movements during stance.

The paper is structured as follows. Section 4.3 explains the theory of the proposed method. Section 4.4 presents the steps taken to verify the performance of the method in experiments. Section 4.5 shows the results and section 4.6 gives a brief discussion.

4.3 THEORY

This section explains the theoretical basis for shank angle estimation using linear measurements and examines the performance of different measurement configurations.

Linear displacement sensitivity

Shank angle may be estimated from either its vertical or horizontal displacements using geometric constraints, as illustrated in Figure 4.1 (assuming that the ankle joint is fixed in space). The angle is obtained using the following equations:

$$\Delta_h = h \sin\theta \tag{4.1}$$

$$\Delta_v = h(1 - \cos\theta) \tag{4.2}$$

Where Δ_h and Δ_v are the horizontal and vertical displacements, and θ is the shank angle. The sensitivity of the displacements to shank rotation will determine which one is superior to obtain the angle. This is given by the derivative of the displacements with respect to shank angle:

$$\begin{cases} \frac{d\Delta_h}{d\theta} = h\cos\theta \\ \frac{d\Delta_v}{d\theta} = h\sin\theta \end{cases} \xrightarrow{\theta \cong 0} \frac{d\Delta_h}{d\theta} > \frac{d\Delta_v}{d\theta} \tag{4.3}$$

This derivative is much larger for horizontal displacements than for vertical displacements, for shank angles close to vertical, as is the case in stance. This higher sensitivity implies that a change in shank angle will generate a larger horizontal than vertical displacement. Consequently, a measurement device with any linear resolution will provide better angular resolution if it is used to measure horizontal rather than vertical displacements.

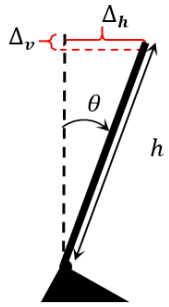

Figure 4.1 Shank rotation and the related horizontal and vertical displacements during stance

Implementation configurations

Figure 4.2 illustrates three configurations that could be employed to obtain shank angle using linear measurement by a range finder: attached sensor, vertical, and horizontal configurations.

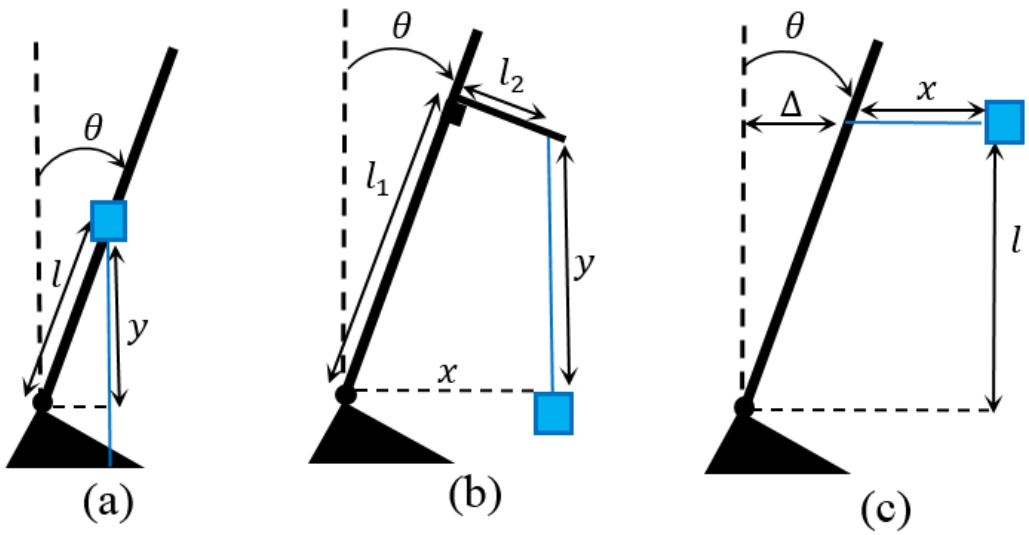

Figure 4.2 Implementation configurations for shank angle measurement using a range finder; (a) attached sensor, (b) vertical, and (c) horizontal strategies; the blue square and line show the range finder and its beam.

Attached sensor configuration

The range finder is attached to the upper shank and measures the vertical distance to the ground; the shank angle is given by:

$$\theta = \cos^{-1}\frac{y}{l} \tag{4.4}$$

Vertical configuration

The range finder is mounted to the environment at the same height as the ankle and a constant horizontal distance from it. It measures the vertical distance to a plate, firmly attached to the shank. The shank angle is given by:

$$\begin{cases} l_1 \sin\theta + l_2 \cos\theta = x \\ l_1 \cos\theta - l_2 \sin\theta = y \end{cases} \tag{4.5}$$

Solving these equations gives:

$$l_2 = \sqrt{x^2 + y^2 - {l_1}^2} \rightarrow \theta = \sin^{-1}\left(\frac{x}{\sqrt{{l_1}^2 + {l_2}^2}}\right) - \tan^{-1}\left(\frac{l_2}{l_1}\right) \quad (4.6)$$

Horizontal configuration

The range finder is mounted at constant horizontal and vertical distances from the ankle joint and measures the horizontal distance to the shank. The shank angle is given by:

$$\theta = \tan^{-1}\left(\frac{\Delta}{l}\right) = \tan^{-1}\left(\frac{x - x_0}{l}\right) \quad (4.7)$$

where x_0 is the distance of the laser to the shank when it is vertical.

Note that all three configurations assume that the range finder is not sensitive to small rotations of either the target or the laser; this is the case for commercially available lasers.

Configurations 1 and 2 rely on the measurement of vertical displacements, which, as demonstrated above, have lower sensitivity than horizontal measurements. In addition, either the range finder or a plate must be fixed firmly to the shank. This makes the experimental set-up more difficult and any motion due to soft tissue movement will contaminate the displacement signals. Third Configuration offers the highest sensitivity and requires nothing to be fixed to the shank. Therefore, we selected it for further exploration in experimental setting.

4.4 METHODS

4.4.1 Sensor selection

The movement of ankle during quiet stance has been shown to be in the order of one degree [33]. Therefore, we assumed that a resolution of >= 0.1 degree for angle measurement would be the minimum required to track shank movements.

Assuming that the height of the range finder relative to ankle is 25 cm, an angular resolution of 0.1 degree would require linear measurements with a resolution of 440 microns. Based on this, we chose a Micro-epsilon range finder (1401-50 model) [245] with a resolution of 25 microns and a bandwidth of 1 KHz, which should provide an angle resolution much better than our minimum requirement. The range finder provides an analog output that varies from 1 to 5 volts corresponding to a range of 45 mm to 95 mm.

4.4.2 Data acquisition

All signals were anti-aliasing filtered at 400Hz and sampled at 1 KHz with high performance 24-bit/8-channel, simultaneous-sampling, dynamic signal acquisition cards (NI 4472, National Instruments) with a dynamic range of 20 volts.

4.4.3 Linear calibration

Figure 4.3A illustrates the static linear calibration procedure. A caliper with a resolution of 10 microns was used to position a metal block at known distances from the range finder, ranging from 45 mm to 95 mm, in increments of 5 mm. The sensor output voltage was measured for 10 seconds at each position. The mean value of the voltage was computed for each trial and plotted against the corresponding distance. The slope and intercept of the best line fit were obtained to convert the range finder output voltage to distance.

4.4.4 Static angular testing

Figure 4.3B shows the setup used for static angular testing. A digital protractor with a resolution of 0.1 degrees was placed in front of the range finder and a piece of thick paper was attached to the protractor using two sided tape. The angle of the protractor was changed between 0 to 1 degree, in increments of 0.1 degrees and the range finder output was collected for 10 seconds. The procedure was repeated three times to examine the precision. We converted the measured laser voltages to the corresponding distances using the calibration constants and used the mean distance in each trial to find the corresponding angle using (4.7).

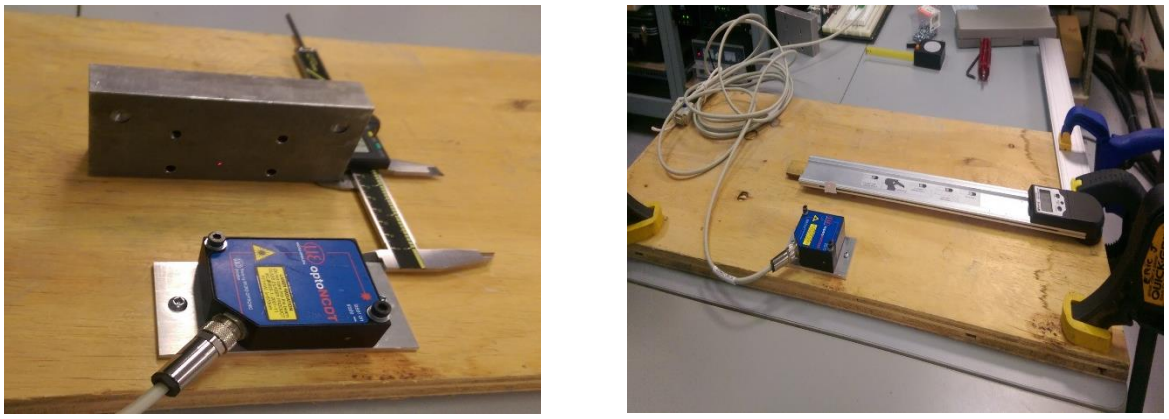

(a) (b)

Figure 4.3 (a) Calibration: the range finder, points to a block in known distances; (b) Static testing: the ranger finder points to a goniometer with known angles.

4.4.5 Dynamic testing

Figure 4.4 shows the standing actuator, comprising two foot pedals driven by independently-controlled electro-hydraulic rotary actuators, that we use to study joint stiffness during stance [246]. Transducers measure the torque of each actuator and the angle of pedals relative to horizontal. The apparatus is capable of applying independent, bilateral, perturbations having a bandwidth of 0-30 Hz [246].

To validate the performance of our angular measurement method in dynamic conditions, the range finder was attached to a frame, and aimed at the end of a pedal of the standing apparatus, illustrated in Figure 4.4A. The angle of the pedals was measured by a high performance potentiometer (Maurey Instruments 112-P19) attached to the shaft of the actuator. The pedal angle also was estimated using the measured distance by the range finder and compared to the true values from the potentiometer.

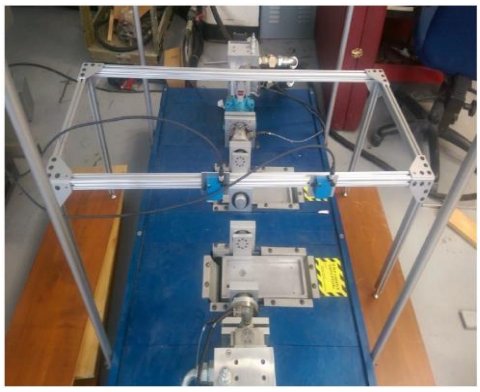

(a)

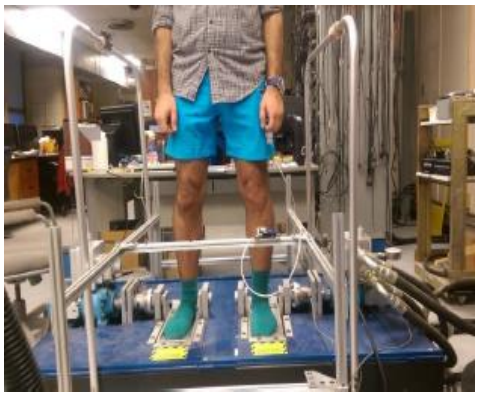

(b)

Figure 4.4 (a) Controlled dynamic testing: the range finder is attached to a frame, to measure the movement of the standing apparatus pedal (b) stance experiment: a subject, standing on the standing apparatus, with the laser measuring the linear displacement of a point on the shank

The input signals was chosen to have a sufficiently rich amplitude structure and enough power over the frequencies needed to identify joint stiffness. We performed 60-second dynamic experiments with four saw-tooth inputs with a period of 1 second and peak to peak amplitudes of 1.14, 1.72, 2.29, and 2.87 degrees. An offset trial was also performed with the pedal angle set to 0 to find the initial distance needed to estimate angle (x_0 in (4.7)). The range finder output was low pass filtered with a two-sided, zero phase shift, 10^{th} order Bessel filter with a cut-off frequency of 30 Hz. The angle was calculated in each dynamic trial using (4.7) and compared to the angle measured by the potentiometer.

4.4.6 Stance experiments

A subject stood on the standing apparatus and data was acquired in quiet stance and perturbed trials, shown in Figure 4.4B. A thick paper was attached to the shank using two sided tape, after the attachment point was shaved and the range finder, attached to a frame, recorded shank movement during the stance experiments. The vertical distance of the lasers to the rotation axis of the ankle joint was measured. The laser output voltage was converted to distance and then filtered. Finally, the shank angle was estimated using (4.7). The estimated shank angle then was used with pedal angle (measured by the potentiometer) to estimate ankle angle.

The input pedal perturbation was a pseudo random binary sequence (PRBS), where the input changes between two values, at intervals that are random multiples of a pre-set switching rate. The PRBS input has a wide band-width, appropriate to identify joint stiffness, while it is unpredictable and applies more power for a given amplitude compared to a Gaussian input. The switching rate of the PRBS input was 200 milliseconds and peak to peak amplitudes of 1.15, 1.38, and 1.72 degrees (0.02, 0.24, 0.03 radians) were used.

4.5 RESULTS

Figure 4.5A shows the results of the range finder calibration. The means and standard deviations of output corresponding to each distance are shown, demonstrating a linear input-output relationship. The line of best fit is also shown, having the following equation:

$$\mathrm{d} = 12.602\,\mathrm{v} + 32.278\ (R^2 = 0.9984)$$

Where d and v are distance in mm and voltage in volts, respectively. This relation was used for all subsequent experiments to obtain distance from the range finder output.

Figure 4.5B shows the estimated and true angles in static trials for the three measurements at each angle. The vertical green bars show the 0.1 degree uncertainty associated with setting the protractor. Each point shows the estimated mean angle using the range finder data during a 10 second trial and the bars around it show its standard deviation. The estimated angles lie inside the bars of true angles, showing accurate angle estimation in static conditions. Furthermore, the standard deviations of the estimated angles in each trial were less than 0.1 degrees, demonstrating that there is sufficient resolution in static conditions.

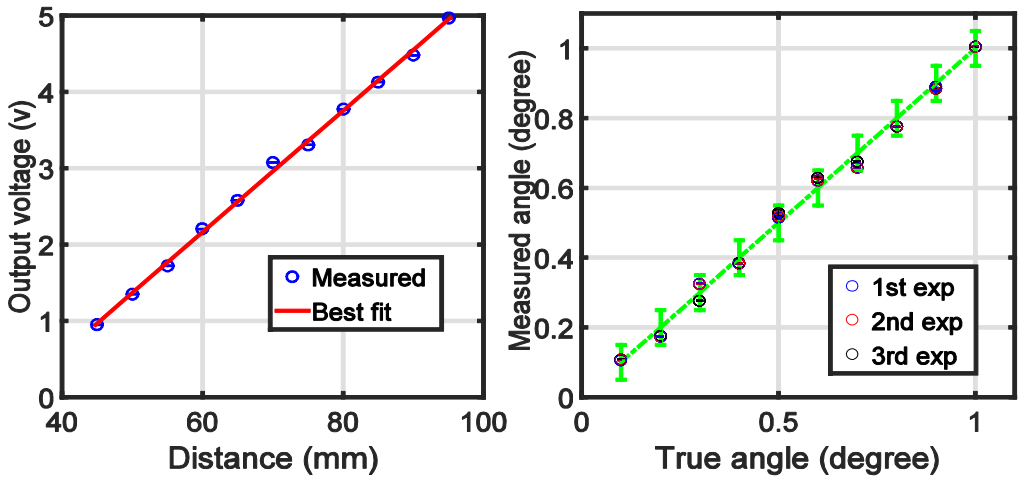

(a) (b)

Figure 4.5 (a) Calibration result: mean of the measured voltages and corresponding distances and the best line fit; (b) static experiment: estimated angles (mean± standard deviation) vs. true angles (green bars)

Figure 4.6 shows the results of a typical dynamic test performed with a saw-tooth input with a peak to peak amplitude of 1.72 degrees (0.03 radians). It is evident that the angle estimated using laser outputs accurately tracks this dynamic input, which has a bandwidth adequate for the identification of joint stiffness. Similar results were found for all input amplitudes.

Figure 4.7 shows the results of measurements made during quiet and perturbed stance. The left panels show the shank, foot, and ankle angles and the corresponding joint torque recorded during 60 seconds of quiet stance. The shank and ankle angle are identical since there is no pedal perturbations. Interestingly the shank angle shows a drift, which is consistent with the torque, indicating that the subject shifted his weight forward somewhat during the experiment, causing increased plantarflexion torque (shown as negative).

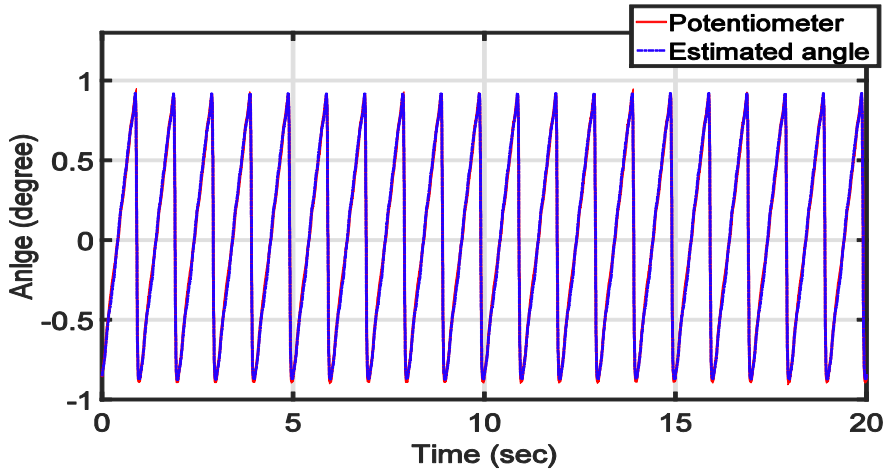

Figure 4.6 Dynamic experiment results: estimated angle using range finder data compared to the potentiometer angle for a sawtooth input with peak to peak amplitude of 1.72 degrees

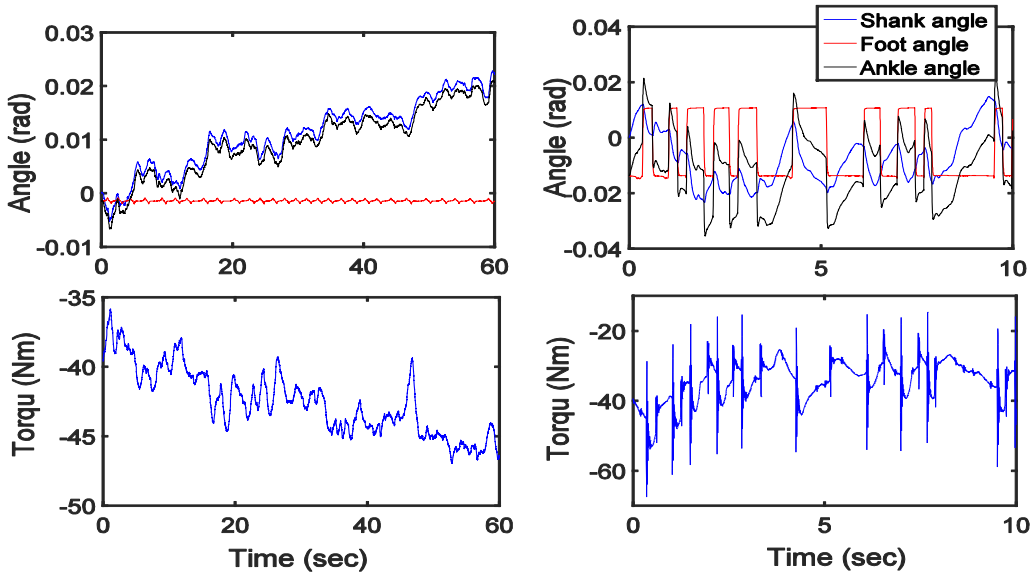

(Left) (Right)

Figure 4.7 Shank, foot, and ankle angles, and the corresponding joint torque in (left) quiet and (right) perturbed stance experiments

The right panels show the angles and the joint torque during a PRBS perturbed experiment with a peak to peak amplitude of 1.38 degrees (0.024 radians). There were significant shank

movements associated with the perturbations. Consequently, in contrast to quiet stance experiments, the ankle angle is different from shank and foot angles, meaning the true ankle angle must be used in identification studies.

4.6 DISCUSSION

Accurate measurement of joint angle is necessary to identify joint stiffness during stance. This paper presents the theoretical basis and experimental procedure for high resolution accurate measurement of shank angle during stance using a range finder. Our experiments demonstrated that our system can measure angles as small as 0.01 degree; other alternatives such as IMUs have resolutions in the order of one degree and are not suitable for measuring movements during stance. Future work will use the proposed method to better understand the underlying mechanism of stance control.

CHAPTER 5 EXPERIMENTAL METHODS TO STUDY HUMAN POSTURAL CONTROL

This chapter provides a detailed description of the experimental methods, used to study human postural control system. The aim of the chapter is to provide the researchers with the basic requirements and methods needed to study human postural control. Consequently, the chapter discusses the design characteristics of the bilateral hydraulic actuators we use to study ankle stiffness and evaluate proprioceptive contributions in standing. It also provides a description of a virtual reality device, which has been recently integrated to our bilateral actuator system, and will be used to study the role of vision in standing. The article then describes a systematic procedure to design and perform perturbed standing experiments, and to measure kinematics, kinetics and muscle EMG during the experiments. Finally, two identification procedures to investigate the role of vision and to estimate ankle intrinsic stiffness in standing are given, followed by some representative results of the two methods. The chapter has been accepted for publication in the Journal of Visualized Experiments (JOVE) in 2019. The published manuscript is accompanied by a video of the different steps of the protocols, which has been filmed in our lab, the Neuromuscular Control lab at McGill University. Below the link to the first draft of the video is found (not final yet):

https://www.jove.com/video/60078?status=a62084k

Experimental Methods to Study Human Postural Control

Authors: Pouya Amiri, Abolfazl Mohebbi, and Robert E. Kearney.

Journal: Journal of Visualized Experiments

5.1 ABSTRACT

Many components of the nervous and musculoskeletal systems act in concert to achieve the stable, upright human posture. Controlled experiments accompanied by appropriate mathematical methods are needed to understand the role of the different sub-systems involved in human postural control. This article describes a protocol for performing perturbed standing experiments, acquiring experimental data, and carrying out the subsequent mathematical analysis, with the aim of understanding the role of musculoskeletal system and central control in human upright posture. The results generated by these methods are important, because they provide insight into the healthy balance control, form the basis for understanding the etiology of impaired balance in patients and the elderly, and aid in the design of interventions to improve postural control and stability. These methods can be used to study the role of somatosensory system, intrinsic stiffness of ankle joint, and visual system in postural control, and may also be extended to investigate the role of vestibular system. The methods are to be used in the case of an ankle strategy, where the body moves primarily about the ankle joint and is considered a single-link inverted pendulum.

5.2 INTRODUCTION

Human postural control is realized through complex interactions between the central nervous and musculoskeletal systems [19]. The human body in standing is inherently unstable, subject to a variety of internal (e.g., respiration, heartbeat) and external (e.g., gravity) perturbations. Stability is achieved by a distributed controller with central, reflex, and intrinsic components (Figure 5.1).

Postural control is achieved by: an active controller, mediated by the central nervous system (CNS) and spinal cord, which changes muscle activation; and an intrinsic stiffness controller that resists joint movement with no change in muscle activation (Figure 5.1). The central controller uses sensory information to generate descending commands that produce corrective muscle forces

to stabilize the body. Sensory information is transduced by the visual, vestibular, and somatosensory systems. Specifically, the somatosensory system generates information regarding the support surface and joint angles; vision provides information regarding the environment; and the vestibular system generates information regarding the head angular velocity, linear acceleration, and orientation with respect to gravity. The central, closed-loop controller operates with long delays that may be destabilizing [15]. The second element of the active controller is reflex stiffness, which generates muscle activity with short latency and produces torques resisting joint movement.

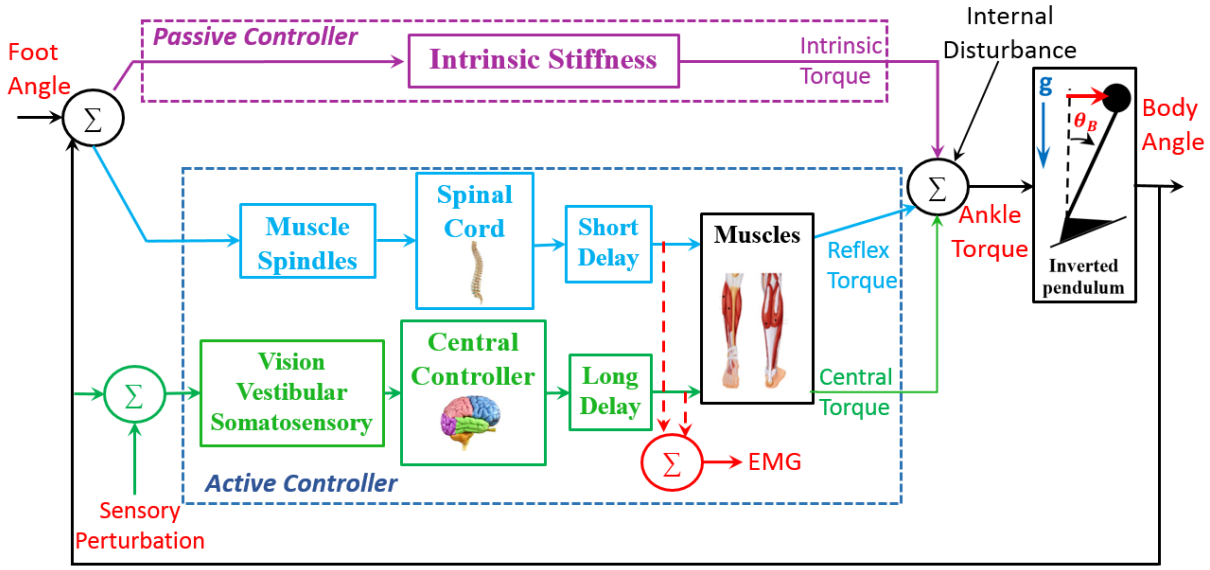

Figure 5.1 Postural control model: the body is inherently unstable and subject to destabilizing gravity torque (g) and disturbances. Stable upright posture is maintained by corrective muscle forces, generated by a central controller, spinal stretch reflexes, and intrinsic mechanical joint stiffness. Muscle activation due to stretch reflex and central contributions is evident in the EMG activity. Only the signals in red can be measured, whereas black signals cannot be measured.

There is a latency associated with both components of active controller; consequently, joint intrinsic stiffness, which acts with no delay, plays an important role in postural control [77]. Intrinsic stiffness is generated by passive visco-elastic properties of contracting muscles, soft tissues and inertial properties of the limbs, which generates resistive torques instantaneously in response to any joint movement [7]. The role of the joint stiffness (intrinsic and reflex stiffness) in

postural control is not clearly understood, since it changes with operating conditions, defined by muscle activation [4, 7, 180] and joint position [5-7], both of which change with the body sway, inherent to standing.

Identifying the roles of the central controller and joint stiffness in postural control is important, as it provides the basis for: diagnosing the etiology of balance impairments; the design of targeted interventions for patients; assessment of the risk of falls; the development of strategies for fall prevention in the elderly; and the design of assistive devices such as orthotics and prosthetics. However, it is difficult, because the different sub-systems act together and only the overall resulting body kinematics, joint torques, and muscle electromyography can be measured.

Therefore, it is essential to develop experimental and analytical methods that use the measurable postural variables to evaluate each subsystem's contribution. A technical difficulty is that the measurement of postural variables is done in closed-loop. As a result, the inputs and outputs (cause and effect) are interrelated. Consequently, it is necessary to: a) apply external perturbations (as inputs) to evoke postural reactions in responses (as outputs), and b) employ specialized mathematical methods to identify system models and disentangle cause and effect [41].

The present article focuses on postural control when an ankle strategy is used, that is, when the movements occur primarily about the ankle joint. In this condition, upper body and lower limbs move together, consequently, the body can be modeled as a single-link inverted pendulum in sagittal plane [32]. The ankle strategy is used when the support surface is firm and the perturbations are small [9, 19].

A standing apparatus capable of applying appropriate mechanical (proprioceptive) and visual sensory perturbations and recording the body kinematics, kinetics, and muscle activities has been developed in our laboratory. The device provides the experimental environment needed to study the role of ankle stiffness, central control mechanisms, and their interactions by generating postural responses using visual or/and somatosensory stimuli. It is also possible to extend the device to study the role of vestibular system by the application of direct electrical stimulation to the mastoid processes, that can generate a sensation of head velocity and evoke postural responses [47, 247].

Others have also developed similar devices to study human postural control, where linear piezo electric actuators [9], rotary electrical motors [10, 11], and linear electrical motors [40, 48, 190]

were used to apply mechanical perturbations to ankle in standing. More complex devices also have been developed to study multi-segment postural control, where it is possible to apply multiple perturbations to ankle and hip joints simultaneously [42, 78].

5.2.1 Standing apparatus

Two servo-controlled electrohydraulic rotary actuators move two pedals to apply controlled perturbations of ankle position. The actuators can generate large torques (>500 Nm) needed for postural control; this is especially important in cases such as forward lean, where the body's center of mass is far (anterior) from ankle axis of rotation, resulting in large values of ankle torque for postural control.

Each rotary actuator is controlled by a separate proportional servo valve, using pedal position feedback, measured by a high-performance potentiometer on the actuator shaft (Table 5.1). The controller is implemented using a MATLAB-based xPC real-time, digital signal processing system. The actuator/servo-valve together have a bandwidth of more than 40 Hz, much larger than bandwidth of the overall postural control system, ankle joint stiffness, and the central controller [248].

5.2.2 Virtual reality device and environment

A virtual reality (VR) headset (Table 5.1) is used to perturb the vision. The headset contains an LCD screen (dual AMOLED 3.6'' screen with a resolution of 1080 x 1200 pixels per eye) that provides the user with a stereoscopic view of the media sent to the device, offering three-dimensional depth perception. The refresh rate is 90 Hz, sufficient to provide a solid virtual sense to the users [249]. The field of view of the screen is 110°, enough to generate visual perturbations similar to real world situations.

The headset tracks the rotation of the user's head and alters the virtual view accordingly so that the user is fully immersed in the virtual environment; therefore, it can provide the normal visual feedback; and it can also perturb vision by rotating the visual field in sagittal plane.

Table 5.1 Table of materials

Name of Material/ Equipment	Company	Catalog Number	Comments/Description
5K potentiometer	Maurey	112P19502	Measures actuator shaft angle
8 channel Bagnoli surface EMG amplifiers and electrodes	Delsys		Measures the EMG of ankle muscles
AlienWare Laptop	Dell Inc.	P69F001-Rev. A02	VR-ready PC laptop
Data acquisition card	National instruments	4472	Samples the analogue signals from the sensors
Directional valve	REXROTH	4WMR10C3X	Bypasses the flow if the angle of actuator shaft goes beyond ±20°
Full body harness	Jelco	740	Protect the subjects from falling
Laser range finder	Micro-epsilon 1302-100	1507307	Measures shank linear displacement
Laser range finder	Micro-epsilon 1302-200	1509074	Measures body linear displacement
Load cell	Omega	LC302-100	Measures vertical reaction forces
Proportional servo-valve	MOOG	D681-4718	Controls the hydraulic flow to the rotary actuators
Rotary actuator	Rotac	26R21VDEISFTFLGMTG	Applies mechanical perturbations
Torque transducer	Lebow	2110-5k	Measures ankle torque
Virtual Environment Motion Trackers	HTC inc.	1551984681	Tracks the head motion
Virtual Reality Headset	HTC inc.	1551984681	Provides visual perturbations

5.2.1 Kinetic measurements

Vertical reaction force is measured by four load cells, sandwiched between two plates beneath the foot (Table 5.1). Ankle torque is measured directly by torque transducers with a capacity of 565 Nm and a torsional stiffness of 104 kNm/rad; it also can be measured indirectly from the vertical forces transduced by the load cells, using their distances to ankle axis of rotation [37], assuming that horizontal forces applied to the feet in standing are small [12, 15]. Center of pressure

(COP) is measured in sagittal plane by dividing the ankle torque by the total vertical force, measured by the load cells [37].

5.2.2 Kinematic measurements

Foot angle is the same as pedal angle, because when an ankle strategy is used, the subject's foot moves with the pedal. Shank angle with respect to the vertical is obtained indirectly from the linear displacement of the shank, measured by a laser range finder (Table 5.1) with a resolution of 50 μm and bandwidth of 750 Hz [245]. Ankle angle is the sum of the foot and shank angles. Body angle with respect to the vertical is obtained indirectly from the linear displacement of the mid-point between the left and right posterior superior iliac spines (PSIS), measured using a laser range finder (Table 5.1) with a resolution of 100 μm and bandwidth of 750 Hz [37]. Head position and rotation are measured with respect to the global coordinate system of the VR environment by the VR system base stations that emit timed infrared (IR) pulses at 60 pulses per second that are picked up by the headset IR sensors with sub-millimeter precision.

5.2.3 Data acquisition

All signals are filtered with an anti-aliasing filter with a corner frequency of 486.3 and then sampled at 1000 Hz with high performance 24-bit/8-channel, simultaneous-sampling, dynamic signal acquisition cards (Table 5.1) with a dynamic range of 20 V.

5.2.4 Safety mechanisms

Six safety mechanisms have been incorporated into the standing apparatus to prevent injuries to subjects; the pedals are controlled separately and never interfere with each other. (1) The actuator shaft has a cam, which mechanically activates a valve that disconnects hydraulic pressure if the shaft rotation exceeds ± 20° from its horizontal position. (2) Two adjustable mechanical stops limit the range of motion of the actuator; these are set to each subject's range of motion prior to each experiment. (3) Both the subject and the experimenter hold a panic button; pressing the button disconnects hydraulic power from the actuators and causes them to become loose, so they can be moved manually. (4) Handrails located at either side of the subject are available to provide support in case of instability. (5) The subject wears a full body harness (Table 5.1), attached to rigid crossbars in the ceiling to support them in case of a fall. The harness is slack and does not interfere with normal standing, unless the subject becomes unstable, where the harness prevents

the subject from falling. In the case of fall, the pedal movements will be stopped manually either by the subject, using the panic button or by the experimenter. (6) The servo-valves stop the rotation of the actuators using fail-safe mechanisms in case of electrical supply interruption.

5.3 PROTOCOL

All experimental methods have been approved by the McGill University Research Ethics Board and subjects sign informed consents before participating.

5.3.1 Experiments

NOTE: Each experiment involves the following steps.

Pre-test

1. Prepare a definite outline of all trials to be performed and make a checklist for data collection.

2. Provide the subject with a consent form with all the necessary information, ask them to read it thoroughly, answer any questions, and then have them sign the form.

3. Record the subject's weight, height, and age.

Subject preparation: Electromyography measurement

1. Use single differential electrodes (Table 5.1) with an inter-electrode distance of 1 cm for the measurement of electromyography (EMG) of ankle muscles.

2. Use an amplifier (Table 5.1) with an overall gain of 1000 and a bandwidth of 20−2000 Hz.

3. To ensure a high signal to noise ratio (SNR) and minimal cross-talk, locate and mark the electrode attachment areas according to guidelines provided by the Seniam project [250], as below: (1) for the medial gastrocnemius (MG), the most prominent bulge of the muscle; (2) for the lateral gastrocnemius (LG), 1/3 of the line between the head of the fibula and the heel; (3) for soleus (SOL), 2/3 of the line between the medial condyles of the femur and the medial malleolus; (4) for tibialis anterior (TA), 1/3 of the line between the tip of the fibula and the tip of the medial malleolus.

4. Shave the marked areas with a razor and clean the skin with alcohol. Allow the skin to dry thoroughly.

5. Shave a bony area on the patella for the reference electrode, and clean with alcohol.

6. Have the subject lie in a relaxed supine position.

7. Place the reference electrode on the shaved area of the patella.

8. Attach the electrodes one by one to the shaved areas of the muscles, using double sided tape, taking care to ensure that the electrodes are fixed to the skin securely.

9. After placing each electrode, ask the subject to perform a plantarflexing/dorsiflexing contraction against resistance and examine the waveforms on an oscilloscope to ensure that the EMG signal has a high SNR. If the signal SNR is poor, move the electrodes until a location with a high SNR is found.

10. Make sure that the subject's movements are not hindered by the EMG cables.

Subject preparation: Kinematic measurements

1. Attach a reflective marker to the shank with a strap, to be used for shank angle measurement.

NOTE: Place the shank marker as high as is possible on the shank to generate the largest possible linear displacement for a given rotation, therefore, improving angular resolution.

2. Have the subject put on the body harness.

3. Attach a reflect marker to the subject's waist with a strap, to be used for upper body angle measurement. Ensure that the waist reflective marker is placed at the mid-point between the left and right PSISs and that the subject's clothing does not cover the waist reflective surface.

4. Have the subject get on the standing apparatus.

5. Adjust the subject's foot position to align the lateral and medial malleoli of each leg to the pedal's axis of rotation.

6. Outline the subject's foot positions with a marker and instruct them to keep their feet in the same locations during the experiments. This ensures the axes of rotation of ankles and actuators remain aligned throughout the experiments.

7. Adjust the vertical position of the laser range finders to point to the center of the reflective markers. Adjust the horizontal distance between the laser range finder and reflective markers, so that the range finders work in their mid-range and do not saturate during quiet standing.

8. Have the subject lean forward and backward about the ankle and ensure that the lasers remain within their working range.

9. Measure the height of the laser range finders with respect to the ankle axis of rotation.

NOTE: These heights are used to convert linear displacements to angles.

5.3.2 Experimental protocols

1. Inform the subject of what to expect for each trial condition.

2. Instruct the subject to stand quietly with hands at the side while looking forward, and to maintain their balance as they do, when faced the real-world perturbations.

3. For perturbed trials, start the perturbation and allow the subject to adapt to it.

4. Start data acquisition once the subject has established a stable behavior.

5. Provide the subject with sufficient rest period after each trial to avoid fatigue. Communicate with them to see if they need more time.

6. Perform the following trials:

(A) For apparatus test, perform a 2-min test to examine the sensor data 2 h before subject's arrival. Look for irregularly large noises or offsets in the recorded sensor data. If there are problems, resolve them before the subject arrives.

(B) For quiet standing, perform a 2-min quiet standing trial with no perturbations.

NOTE: This trial provides a reference, needed to determine if/how postural variables change in response to perturbations.

(C) For perturbed experiments, run the perturbation and acquire data for 2−3 min. Apply pedal perturbations if the objective is to investigate the role of somatosensory system/ankle stiffness in standing. Apply visual perturbations if the objective is to examine the role of vision in

postural control. Apply visual and pedal perturbations simultaneously if the objective is to examine the interaction of the two systems in postural control.

NOTE: Pedal perturbations are applied as the rotation of the standing device pedals. Similarly, visual perturbations are applied by rotating the virtual visual field, using the VR headset. The angle of the pedal/visual field follows a signal, selected depending on the study objectives. The discussion section provides details regarding the perturbation types, used for the study of postural control and the merits of each perturbation.

7. Perform a minimum of 3 trials for each specific perturbation.

NOTE: Multiple trials is done to ensure reliability of the models when performing the analysis on the collected data; e.g., it is possible to cross validate the models.

8. Perform the trials in a random order to ensure the subjects do not learn to react to a specific perturbation; this also makes it possible to check for time-varying behavior.

9. Check the data visually after each trial to ensure that the acquired signals are of high quality.

5.4 IDENTIFICATION OF HUMAN POSTURAL CONTROL

5.4.1 Non-parametric identification of the dynamic relation of body angle to visual perturbations

Experiment

1. Acquire visually perturbed trials for 2 min according to the steps in sections 5.3.1and 5.3.2.

2. Use a trapezoidal signal (TrapZ) with a peak-to-peak amplitude of 0.087 rad and a velocity of 0.105 rad/s.

3. Hold the pedal position constant at the zero angle.

Analysis

NOTE: Data analysis is performed using MATLAB.

1. Decimate the raw body angle and visual perturbation signals (such that the highest observable frequency is 10 Hz), using the following commands:

$$VR = decimate(VR_{raw}, r) \tag{5.1}$$

$$\theta_b = decimate(\theta_{b\,raw}, r) \tag{5.2}$$

where

$$VR_{raw} = vector\ of\ raw\ VR\ perturbation\ signal$$

$$\theta_{b\,raw} = vector\ of\ raw\ body\ angle\ signal$$

$$r = decimation\ ratio$$

NOTE: For a sampling rate of 1 kHz, the decimation ratio must be 50 to have a highest frequency of 10 Hz.

2. Choose the lowest frequency of interest, which will determine the window length for power estimation.

NOTE: Here, a minimum frequency of 0.1 Hz is chosen, so the window length for power estimation is 1/0.1 Hz = 10 s. The frequency resolution is the same as the minimum frequency, and therefore, the calculations are done for 0.1, 0.2, 0.3, …, 10 Hz.

3. Choose the type of window and degree of overlap to find the power spectra.

NOTE: For a trial length of 120 s, 10 s Hanning windows with 50% overlap results in averaging of 23 segments for power spectrum estimation. Since we decimated the data to 20 Hz, a 10 s window has a length of 200 samples.

4. Use the $tfestimate$ function to find the frequency response (FR) of the system:

$$\left[FR_{VR\theta_b}, f\right] = tfestimate(VR, \theta_b, hann(window\ length), window\ length \times 0.5, f, F_s) \tag{5.3}$$

where

$$FR_{VR\theta_b} = FR\ of\ the\ VR\ perturbation - body\ angle$$

$$window\ length = 200$$

$$f = vector\ of\ frequecies\ of\ interest\ (in\ MATLAB\ use\ f = 0.1{:}\ 0.1{:}\ 10)$$

$$F_s = sampling\ frequency\ after\ the\ decimation\ (= 20\ Hz)$$

NOTE: The presented $tfestimate$ function computes the cross-spectrum between the decimated VR perturbation and body angle in the frequencies specified by f, using a Hanning window with the length specified by $window\ length$ and the number of overlaps equal to $window\ length \times 0.5$ (i.e., 50% overlap). Similarly, it computes the auto-spectrum of the VR input. Then, using the estimated cross-spectrum and auto-spectrum, it computes the FR of the system.

5. Find the gain and phase of the estimated FR in step 4, using the following commands:

$$gain = mag2db\ \left(abs\left(FR_{VR\theta_b}\right)\right) \tag{5.4}$$

$$phase = angle(FR_{VR\theta_b}) \times 180/pi \tag{5.5}$$

where

$$gain = gain\ of\ the\ FR_{VR\theta_b} in\ dB$$

$$phase = phase\ of\ the\ FR_{VR\theta_b} in\ degrees$$

6. Calculate the coherence function using the following command:

$$\left[C_{VR\theta_b}, f\right] = mscohere(VR, \theta_b, hann(window\ length), window\ length \times 0.5, f, F_s) \tag{5.6}$$

where

$$C_{VR\theta_b} = Coherence\ of\ the\ VR\ input - body\ angle$$

NOTE: $mscohere$ function follows a similar procedure as $tfetimate$ to find the coherence between VR and θ_b.

7. Plot the gain, phase, and coherence as a function of frequency.

$$plot(f, gain)$$

$$plot(f, phase)$$

$$plot(f, C_{VR\theta_b})$$

NOTE: The presented method can be extended to the case where both visual and mechanical perturbations are applied, where a multiple-input, multiple-output (MIMO) FR identification method must be used [41]. The identification can also be done using subspace method (which inherently deals with MIMO systems) [251] or using parametric transfer function methods such as MIMO Box-Jenkins [252]. Both subspace and Box-Jenkins (and other methods) are implemented in MATLAB system identification toolbox.

5.4.2 Parametric identification of ankle intrinsic stiffness in standing

Experiment

Perform mechanically perturbed trials for 2 min. Use a pseudo-random binary sequences (PRBS) perturbation with a peak-to-peak amplitude of 0.02 rad and a switching interval of 200 ms. Ensure that the pedal mean angle is zero.

Analysis

1. Differentiate the foot signal once to obtain foot velocity ($\dot{\theta}_F$), twice to obtain foot acceleration ($\ddot{\theta}_F$) and three times to obtain its jerk ($\dddot{\theta}_F$). Similarly differentiate the torque to obtain its velocity and acceleration, using the following command:

$$\dot{y} = diff(y)./diff(t) \tag{5.7}$$

where

$$y = vector\ of\ the\ signal$$

$$t = vector\ of\ the\ time$$

$$\dot{y} = derivative\ of\ the\ input\ signal\ with\ respect\ to\ time$$

2. Compute the location of the local maxima and local minima of the foot velocity to locate pulses, using the following command:

$$\begin{aligned} [v_{max}, locs_{max}] &= findpeaks(\dot{\theta}_F) \\ [v_{min}, locs_{min}] &= findpeaks(-\dot{\theta}_F) \end{aligned} \tag{5.8}$$

where

$$v_{max} = vector\ of\ the\ foot\ velocity\ local\ maxima$$

$$locs_{max} = vector\ of\ the\ locations\ of\ the\ foot\ velocity\ local\ maxima$$

$$v_{min} = vector\ of\ the\ foot\ velocity\ local\ minima$$

$$locs_{min} = vector\ of\ the\ locations\ of\ the\ foot\ velocity\ local\ minima$$

NOTE: $findpeaks$ function finds all the local maxima (positive foot velocity) and their locations. To find the local minima, the same function is used, but the sign of the foot angle velocity must be reversed.

3. Design an 8th order Butterworth low-pass filter with a corner frequency of 50 Hz, using the following command:

$$[fil_{num}, fil_{den}] = butter(8, f_c/(F_s/2)) \tag{5.9}$$

where

$$fil_{num} = filter\ numerator$$
$$fil_{den} = filter\ denominator$$
$$f_c = filter\ cut-off\ frequency\ (= 50)$$
$$F_s = sampline\ frequency (= 1000)$$

4. Filter all the signals with zero-phase shift using the Butterworth filter:

$$x_{filt} = filtfilt(fil_{num}, fil_{den}, x) \tag{5.10}$$

where

$$x = signal$$
$$x_{filt} = filtered\ signal$$

NOTE: *"filtfilt"* function does not cause any shift in the filtered signal. Do not use the *"filter"* function, because it generates a shift.

5. Plot the foot velocity, and visually find an estimate of the time period between the extrema of the foot velocity and the start of the pulse (which is the first point with zero foot velocity before the peak velocity). For the perturbation in this study, this point occurred 25 ms before the velocity extrema found in step 2.

6. For each pulse, compute the ankle background torque as the mean of the ankle torque of 25 ms prior to the start of the pulse, i.e., the mean of the torque in the segment starting 50 ms until 25 ms before the velocity extrema. Do this for the k^{th} pulse with a positive velocity using the following command:

$$TQ_{back}\ (k) = mean(TQ_{ankle}(locs_{max}(k) - 50 : locs_{max}(k) - 25)) \tag{5.11}$$

where

$$TQ_{back}\ (k) = ankle\ backgournd\ torque\ of\ the\ k^{th} pulse$$
$$TQ_{ankle} = vector\ of the\ ankle\ torque\ of\ the\ whole\ experiment$$

NOTE: This is done for both maximum and minimum velocities (negative foot velocity) found in step 2.

7. Find the minimum and maximum of all the background torques for all pulses, using the following command:

$$TQ_{back}^{max} = max(TQ_{back})$$
$$TQ_{back}^{min} = min(TQ_{back}) \quad (5.12)$$

8. For each pulse, extract the torque data of 65 ms after the pulse start (as the intrinsic torque segment), using the following command:

$$TQ_I^k = TQ_{ankle}(locs_{max}(k) - 25 : locs_{max}(k) + 40) \quad (5.13)$$

where

$$TQ_I^k = Intrinsic\ torque\ response\ to\ K^{th} pulse$$

NOTE: This is also done for the first and second derivative of the ankle torque (to provide the first and second derivate of the intrinsic torque), as well as, foot angle, foot velocity, foot acceleration, and foot jerk.

9. Compute the change in the k[th] intrinsic torque segment from its initial value, using the following command:

$$\Delta TQ_I^k = TQ_I^k - TQ_I^k(1) \quad (5.14)$$

NOTE: This is done similarly for foot angle to obtain $\Delta\theta_F^k$.

10. Divide the torque range (obtained in step 7) into 3 Nm wide bins and find the pulses with background torque in each bin.

NOTE: This is done using "*find"* function and indexing. It is assumed that the intrinsic stiffness is constant in each bin, since the ankle background torque does not change significantly.

11. Estimate the intrinsic stiffness parameters of the extended intrinsic model (EIM) [164], for the j[th] bin using the pulses in group j ($1 \leq j \leq p$).

11.1. Concatenate all the intrinsic torque responses in the j[th] bin to form the vector $\Delta\boldsymbol{TQ}_{\boldsymbol{I}}^{\boldsymbol{j}}$:

$$\Delta \boldsymbol{TQ_I^j} = \begin{bmatrix} \Delta TQ_{Ij}^1 \\ \Delta TQ_{Ij}^2 \\ \vdots \\ \Delta TQ_{Ij}^{m-1} \\ \Delta TQ_{Ij}^m \end{bmatrix} \tag{5.15}$$

where ΔTQ_{Ij}^i is the ith ($1 \leq i \leq m$) intrinsic torque response in group j.

NOTE: Similarly, concatenate foot angle, velocity, and acceleration, and first and second derivatives of the intrinsic torque of the jth group to be used in the next step.

11.2. Place the foot angle, velocity, acceleration and jerk, as well as the first and second derivative of the torque of the group j together to form the regressor matrix:

$$\boldsymbol{X_{EIM}^j} = \begin{bmatrix} \ddot{\boldsymbol{\theta}}_{\boldsymbol{F}}^{\boldsymbol{j}} & \ddot{\boldsymbol{\theta}}_{\boldsymbol{F}}^{\boldsymbol{j}} & \dot{\boldsymbol{\theta}}_{\boldsymbol{F}}^{\boldsymbol{j}} & \boldsymbol{\Delta\theta_F^j} & \boldsymbol{T\ddot{Q}_I^J} & \boldsymbol{T\dot{Q}_I^J} \end{bmatrix} \tag{5.16}$$

11.3. Find the intrinsic stiffness parameters for the jth group using the backslash (\) operator:

$$\boldsymbol{\theta_{EIM}^j} = \boldsymbol{X_{EIM}^j} \backslash \Delta \boldsymbol{TQ_I^j} \tag{5.17}$$

11.4. Extract the fourth element of $\boldsymbol{\theta_{EIM}^j}$ as the low frequency intrinsic stiffness K_{EIM}^j.

12. Perform steps 11 for all groups (bins) and estimate the corresponding low frequency intrinsic stiffness.

13. Divide all the estimated low frequency stiffness values by the subject's critical stiffness:

$$K_{cr} = mgh_{com} \tag{5.18}$$

where m is the subject's mass, g is gravitational acceleration, and h_{com} is the height of the body's center of mass above ankle axis of rotation, derived from anthropometric data [253]. This gives the normalized stiffness (K_{EIM}^{jN}).

14. Convert the ankle background torque to ankle background COP position (X_{cop}) by dividing the ankle background torques with the corresponding measured vertical forces.

15. Plot K_{EIM}^{N} as a function of center of pressure.

$$plot(X_{cop}, K_{EIM}^{N})$$

where

$$X_{cop} = vector\ of\ the\ position\ of\ the\ background\ COP$$

$$K_{EIM}^{N} = vector\ of\ normlized\ intrinsic\ stiffness$$

5.5 REPRESENTATIVE RESULTS:

5.5.1 Pseudo random ternary sequence (PRTS) and TrapZ signals

Figure 5.2A shows a PRTS signal, which is generated by integrating a pseudo random velocity profile. For each sample time Δt, the signal velocity may be equal to zero, or acquire a pre-defined positive or negative value, v. By controlling v and Δt, PRTS inputs with a wide spectral bandwidth can be generated and scaled to different peak-to-peak amplitudes. Furthermore, the PRTS is periodic, but unpredictable, which is desirable for the study of postural control. The reader is referred to the following article for detailed explanation of the PRTS signal [1].

Figure 5.2B shows a TrapZ signal. It starts at a zero value and after a random period δ (whose minimum is Δ), the signal ramps up randomly to its maximum amplitude ($+A$) with a velocity $+v$ or ramps down to its minimum amplitude ($-A$) with a velocity $-v$. The signal stays at its maximum or minimum for a random period, W (minimum of Δ) and then returns to zero with velocity $+v$ or $-v$. The loop starts again from zero. It is evident that unlike the PRTS, the TrapZ is a zero-mean signal, and therefore, does not cause non-stationarity in the postural response. In addition, it is unpredictable, as the timing of change of the signal value and the direction of the change (i.e., positive or negative velocity) are random.

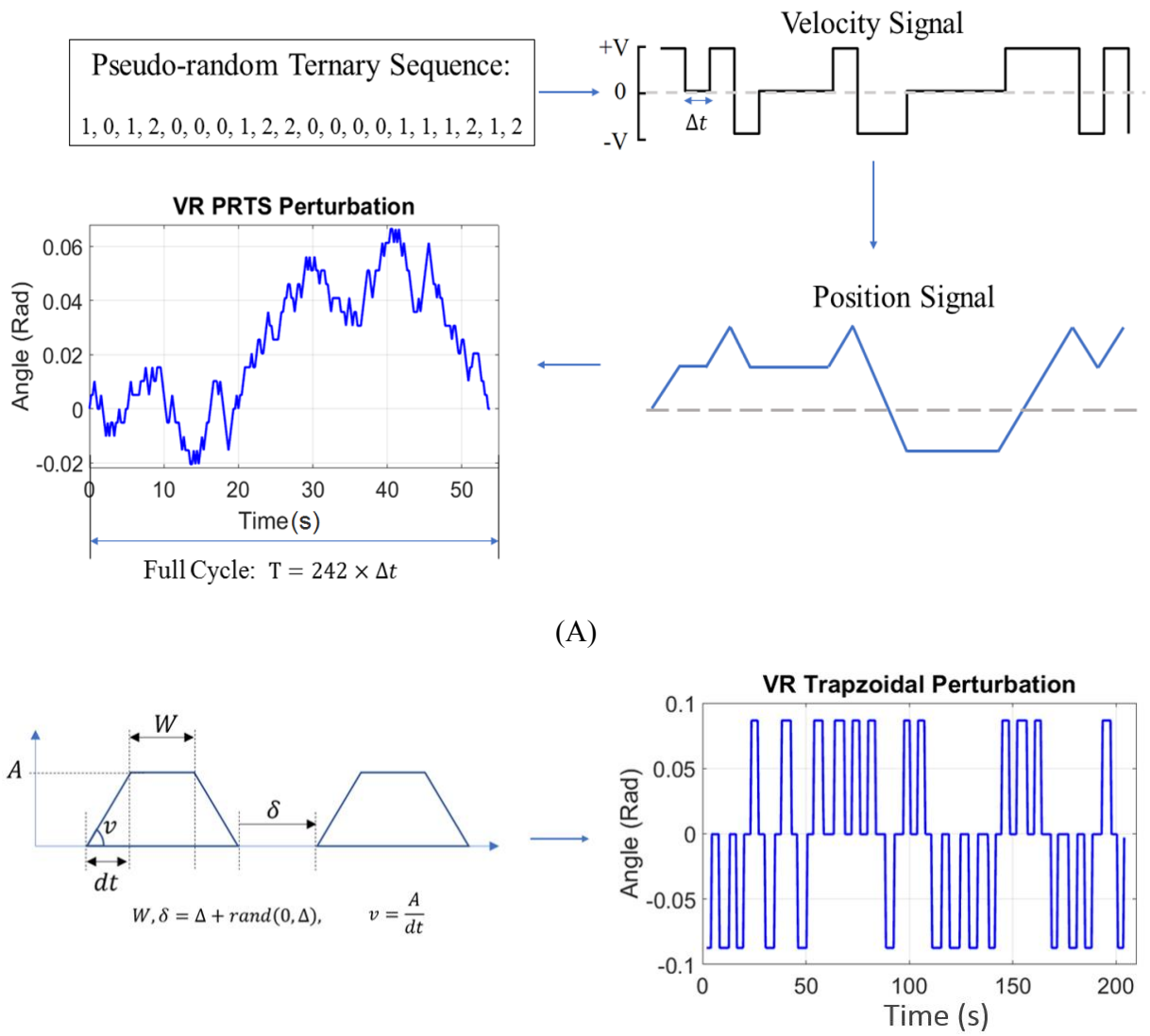

Figure 5.2 Generation of PRTS and TrapZ signals. (A) PRTS signal. A stimulus is created from a 242-length PRTS sequence, which includes values of 0, 1, and 2, corresponding to fixed velocities of 0, +v, and -v for a fixed duration of Δt. The velocity is integrated to generate the position, which is used as the perturbation signal. The period of the perturbation signal is equal to $(3^m - 1)\Delta t$, where m is the stage number of the shift registrar, determining the sequence of the velocity. (B) TrapZ signal. The signal starts at zero; after a random time interval (δ), it ramps up or down to its maximum ($+A$) or minimum value ($-A$) with a constant velocity; the signal goes back to zero after a random time interval (W) and the whole loop starts again.

5.5.2 Identification of the body angle to visual perturbations system

Figure 5.3 shows the signals from a typical standing trial with TrapZ visual perturbations. Figure 5.3A shows the VR perturbation, where the field of view rotates from 0 to ± 0.0435 rad (2.5°) in the sagittal plane. Figure 5.3C,E shows the ankle and body angles, which are very similar, since the foot angle is zero, and shank and upper body move together. Figure 5.3G shows the ankle torque, which is correlated with the shank and body angles. Figure 5.3B,D,F,H shows the EMGs from the ankle muscles. It is evident that SOL and LG are continuously active, MG periodically generates large bursts of activities with body sway, and TA is silent.

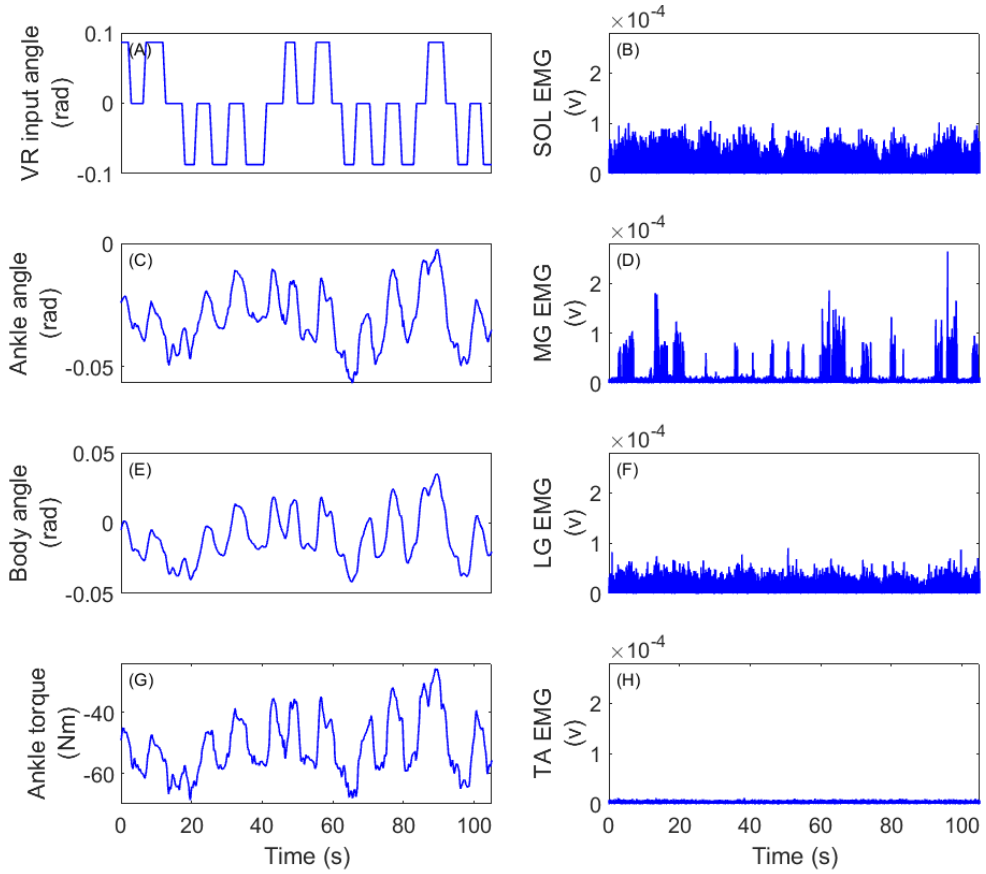

Figure 5.3 Typical experimental trial with TrapZ visual perturbation; the peak-to-peak perturbation amplitude is 0.087 rad, and the velocity is 0.105 rad/s. (A) VR perturbation angle, showing the rotation of the field of view in sagittal plane. (C) Ankle angle, which is the same as shank angle, as the foot does not move. (E) Body angle. (G) Ankle torque. (B, D, F, H) Raw rectified EMG of SOL, MG, LG, and TA; SOL and LG are continuously active, while MG shows burst of activity associated with body sway, and TA is silent.

Figure 5.4 shows the FR of the transfer function relating the visual input to the body angle for the data in Figure 5.3. The first step is to examine the coherence, because gain and phase are meaningful only when the coherence is high (when the coherence is 1, there is a linear noise- free relationship between the input and the output; a coherence less than 1 happens when the input output relationship is nonlinear or the data is noisy). The coherence is the highest at low frequency, between 0.1−1 Hz and drops significantly at higher frequencies. The gain increases initially from 0.1 Hz to 0.2 Hz and then decreases till 1 Hz, showing the expected low-pass behavior due to body's high inertia. The phase also starts at zero and decreases almost linearly with frequency, indicating that the output is delayed with respect to the input.

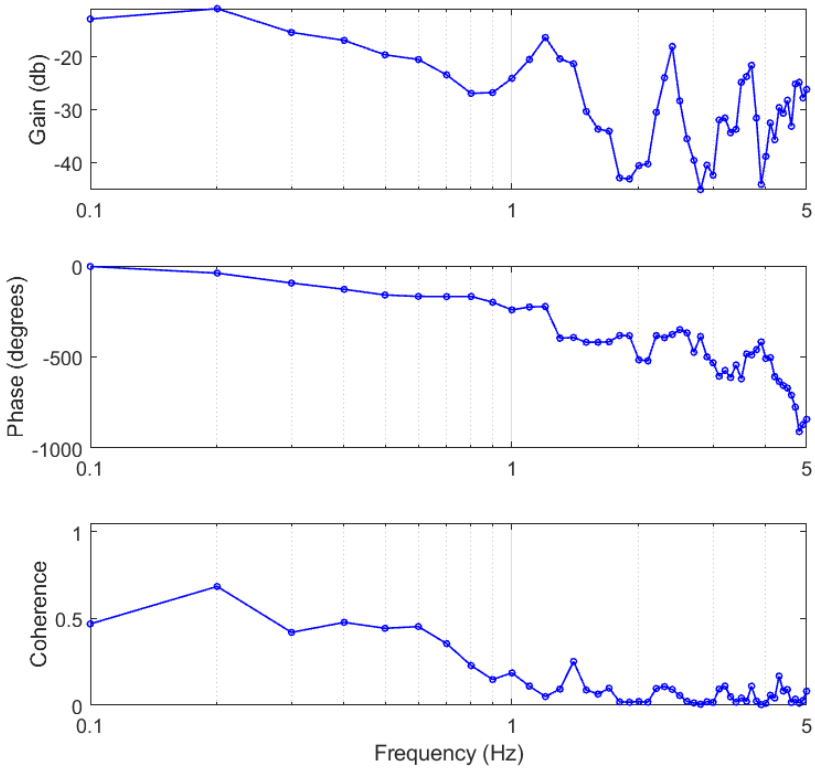

Figure 5.4 Frequency response of the dynamic relation of body angle to visual perturbation estimated from the data presented in Figure 3. Gain (top panel) shows ratio of the amplitude of the output to the input as a function of frequency; it shows a low pass behavior. Phase (middle panel) shows the difference between the input and output phase as a function of frequency. Coherence (bottom panel) provides an index measuring how much of the output power is linearly related to the input power at each frequency. A coherence of 1 shows perfect linear input-output relationship; however, the presence of noise or nonlinearity reduces it.

5.5.3 Identification of ankle intrinsic stiffness parameters

Figure 5.5 shows the signals measured for a typical perturbed standing trial. Figure 5.5A shows the pedal perturbation, a PRBS with a peak-to-peak amplitude of 0.02 rad and a switching interval of 200 ms. The pedal position switches between two values (-0.01 and 0.01) at integer multiples of the switching interval. Figure 5.5C shows the ankle angle, where the fast changes are due to the foot movement while the other changes are the result of shank movement with sway. Figure 5.5E shows the body angle in response to the perturbation with a peak-to-peak movement of around 0.04 rad. Figure 5.5G shows the measured ankle torque; two components are evident: the modulation of the torque with body sway, and large downward peaks, showing the stretch reflex torque response (generally happening after a dorsiflexing pulse). Figure 5.5B,D,F,H shows the SOL, MG, LG and TA EMGs. It is clear that the TS muscles are continuously active and display large bursts of activity due to stretch reflex responses. TA is mostly silent, except for a few peaks, which seem to be crosstalk from TS muscles, because they occur simultaneously with stretch reflex activity of TS muscles.

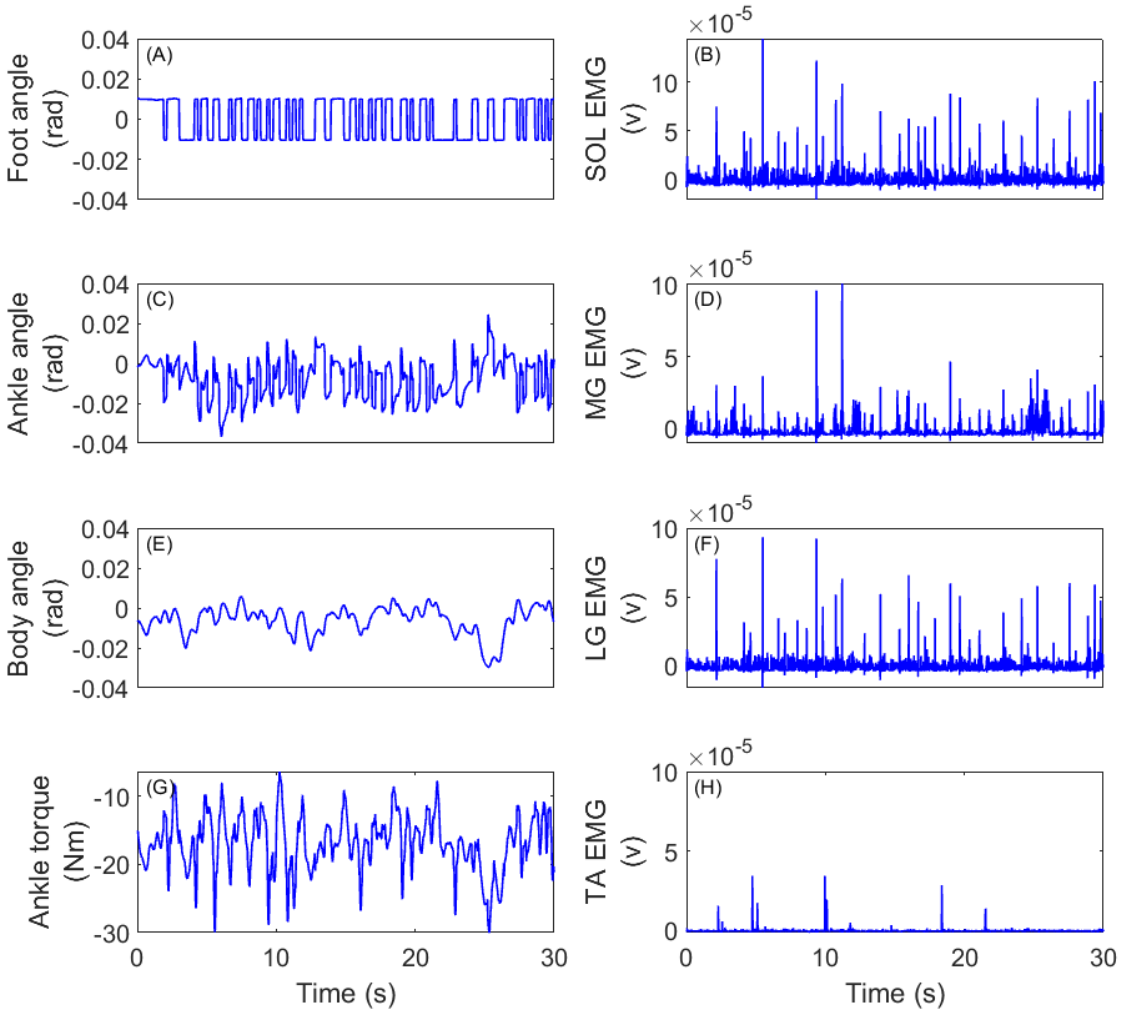

Figure 5.5 Typical PRBS position perturbation trial; the peak-to-peak perturbation amplitude is 0.02 rad, and the switching interval is 200 ms. (A) Foot angle, which is the same as the position perturbations since the foot moves with the pedal. (C) Ankle angle; the random changes are due to shank movement with sway. (E) Body angle, obtained assuming the body acts as an inverted pendulum. (G) Ankle torque measured form the load cells data. (B, D, F, H) Raw EMG of SOL, MG, LG, and TA; the TS muscles are all continuously active, while the large peaks reflect stretch reflex activity; TA is mostly silent.

Figure 5.6 shows a typical pulse position perturbation, its velocity and the corresponding SOL EMG and torque response. The intrinsic response starts 25 ms before and last until 40 ms after the peak foot velocity; the peak in the SOL EMG shows the presence of a reflex response. The pre-response segment, starting 50 ms before the peak velocity is used to find the background torque.

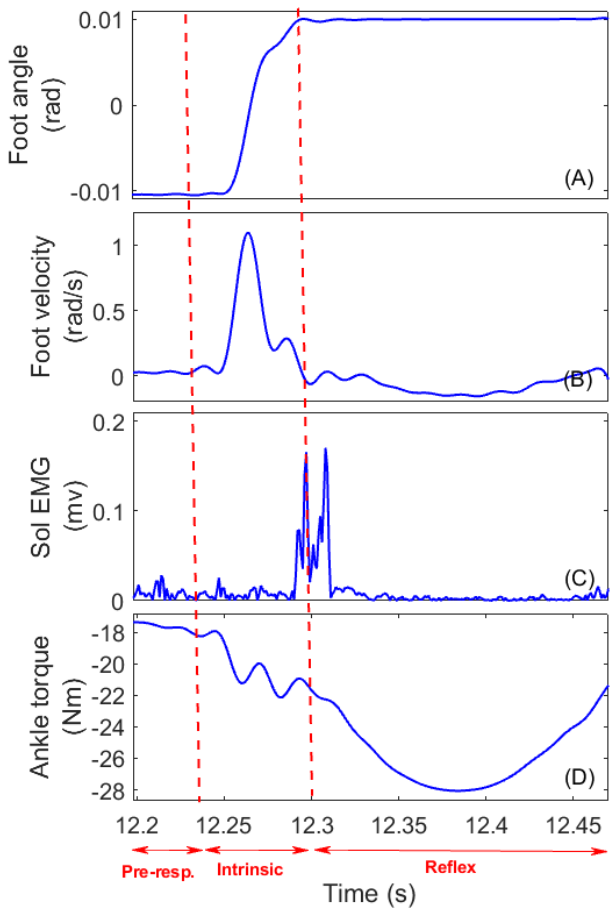

Figure 5.6 An individual pulse from the trial shown in Figure 5, on an expanded time scale. (A) Foot angle, (B) foot velocity, (C) SOL EMG, and (D) ankle torque. The vertical dotted lines separate the response into the pre-response (25 ms), intrinsic response (65 ms), and reflex response (300 ms); positive torque and angles correspond to dorsiflexion. The data for this figure are taken from Amiri and Kearney [37].

Figure 5.7 shows the intrinsic stiffness as a function the COP position for the left and right sides of the subject shown in Figure 5.5; the stiffness was estimated using the analysis method presented. It is evident that the intrinsic stiffness is not constant but changes significantly with postural sway. These changes appear functionally appropriate, because the stiffness increases as the COP moves farther from ankle axis of rotation, where there is higher possibility of fall.

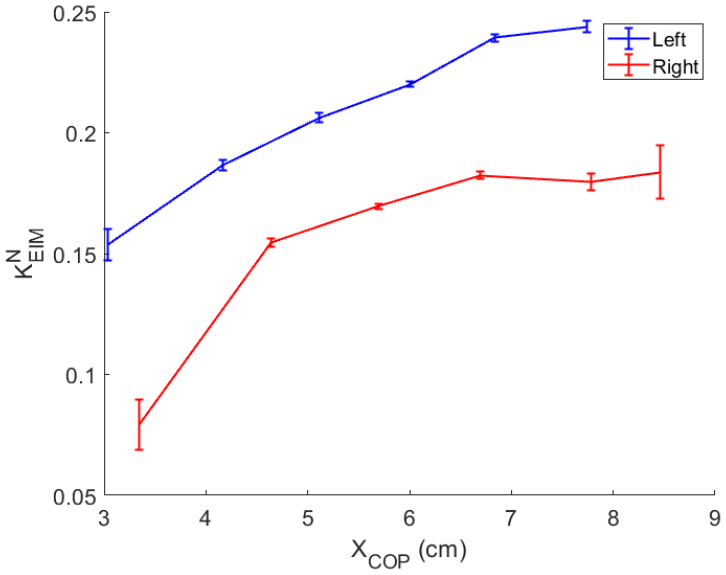

Figure 5.7 Estimated normalized intrinsic stiffness as a function of COP position for the left and right side of a typical subject, obtained from the data shown in Figure 5. Bars indicate the 95% confidence intervals of the stiffness values. The data for this figure are taken from Amiri and Kearney [37].

5.6 DISCUSSION

Several steps are critical in performing these experiments to study human postural control. These steps are associated with the correct measurement of the signals and include: 1) Correct alignment of the shank ankle axis of rotation to that of the pedals, for the correct measurement of ankle torques. 2) Correct set-up of the range finders to ensure they work in their range and are not saturated during the experiments. 3) Measurement of EMG with good quality and minimal cross talk. 4) Application of appropriate perturbations, which evoke sufficient responses, but not disrupt the normal postural control. 5) Selection of an appropriate trial length, based on the intended analysis, while avoiding body shift and fatigue. In addition to the experiments, the analysis also must be done carefully. For the estimation of the intrinsic stiffness from data acquired in mechanically perturbed standing, it is critical to select the length of the intrinsic response in a way that ensures NO reflex torque (which starts soon after a burst of activity in TS muscles) is included. In addition, although many studies have assumed that the intrinsic stiffness does not change in standing [9-11], a recent study showed that it is important to account for the modulation of the stiffness with changes in ankle torque associated with postural sway [37, 38, 254]. For determining

the FR of the dynamic relation from any input to the output, the most important step is to correctly estimate the cross-spectrum and power spectrum by selecting the window length and overlap, appropriate to the record length.

Design of the perturbations is an important step in human standing experiments. Different types of mechanical and visual perturbations have been used for the study of postural control, given as the angle of the support surface or the angle of the visual field. These include multi-sine, low-pass filtered noise, pseudo-random ternary sequence (PRTS) and others [1, 12, 32, 41, 47, 48, 77, 255, 256]. However, the use of a pseudo random binary sequence (PRBS) is advantageous for mechanical perturbations, because: 1) For a given peak-to-peak amplitude, it provides the highest power over a wide range of frequencies, which can be controlled by selecting the switching rate [77]; 2) It is unpredictable, yet repeatable, making it possible to reduce noise by averaging; 3) A PRBS input with low absolute mean velocity generates reflex responses, allowing quantification of stretch reflexes in standing. For the visual system, step pulses evoke no significant postural responses, because the visual system cannot follow fast changes of the visual field. In addition, predictable inputs such as sinusoids with one frequency can generate anticipatory behavior. Multi-sine signals are not effective for the study of visual responses, because their fast and continuous changes are hard to follow and can cause subjects to become motion sick. PRTS signals have been used extensively to study visual system in standing, as it is an informative input; the movements of the visual field are discrete rather than continuous and their velocity can be controlled to generate coherent visual responses. Although, the PRTS performs well, it is a non-zero mean signal, which may cause non-stationarities in the postural control and makes identification difficult. Therefore, the TrapZ was designed to address this problem, which is unpredictable, discrete, and has a zero-mean (Figure 5.2B). Another important consideration in designing the experiments is the perturbation amplitude. Generally, perturbations with low amplitudes should be used when the objective is to perform linear analysis and not to deviate from an ankle strategy. The validity of ankle strategy can be checked analytically [17], and if there are large deviations, which may be generated by larger perturbation amplitudes, nonlinear analysis methods, accompanied by multi-segment models of body in standing, may be required [257].

Another consideration for perturbation design is trial length, which must be long enough to allow reliable estimates of the model parameters. However, very long trials are undesirable,

because they may result in the subject shifting the body orientation, resulting in a non-stationarity that makes system modeling and identification difficult. A trial length between 2 and 3 minutes is optimal. This trial length does not generally result in fatigue, provided a sufficient resting period is enforced between trials. The analysis method also influences the required trial length. If a linear analysis using FR or impulse response function is used, then the lowest frequency of interest will determine the record length. The inverse of the window length is equal to the minimum frequency, so, if lower frequencies are to be examined, longer windows must be used. Moreover, the trial must be long enough to provide enough averaging to yield robust spectral estimates. Nonlinear analysis will, in general require even longer data records, because nonlinear models usually have more parameters than linear models.

The study of human postural control requires the selection of an appropriate identification method. Parametric and non-parametric linear identification methods can be used to study postural control [1, 32, 42, 43, 47-55, 78, 113, 115, 134, 230-234, 240, 241, 252]. **Non-parametric identification**, using FR estimation, has been used extensively to study postural control, because it is well suited for the identification of data acquired in the closed-loop condition of standing [12] and requires few *a-priori* assumptions (for the details of this method see [12]). The most commonly used method is to estimate the FR of the closed-loop system between an external (mechanical/sensory) perturbation and an output (e.g., body angle, ankle torque, or muscle EMG), which is a combination of controller, plant, and feedback. To provide physical significance and examine each component separately, many studies have used a parametric model of the closed-loop system and estimated the parameters that match the parametric model's FR to that of the estimated output sensitivity [1, 32, 43, 48-55, 113, 115, 134, 230-233]. **Parametric identification**, on the other hand, assumes that the system input and output are related by some model structure with a limited number of parameters, known *a-priori*. The prediction error method is used to find the model parameters that minimize the error between the measured output and model prediction [226]. In contrast to FR models, where the external perturbation must be measured and used for the analysis, these methods can be applied directly to any two signals, as long as a separate noise model, which is adequately parametrized, is estimated as well [59]. This means there is no need to measure the external perturbation. Although, the model orders must be determined *a-priori,* parametric models usually have fewer parameters than the FR models and hence provide more

robust parameter estimates. The main drawback of a parametric model is that a correct noise model must be used to obtain unbiased estimates of the parameters.

An important consideration in human postural control is its remarkable adaptability to new experimental and environmental conditions. This is achieved through multisensory integration, meaning that the CNS combines the information from somatosensory, visual, and vestibular systems, whereas it gives a larger weight to more accurate (and less variable) sensory inputs in any experimental conditions for postural control. For example, when proprioception is perturbed through foot rotation, the CNS relies more on visual and vestibular inputs. A method has been developed by Peterka [1] to quantify multisensory integration. For a standing experiment with a specific external perturbation, he identified the FR of the closed loop system and then fitted a parametric model to it (as explained in the previous paragraph). The parametric model comprised a central control, whose input was the weighted sum of the inputs from the three sensory systems; the weights were used to provide a means to quantify the importance of each sensory source to postural control, i.e., the higher the weight, the more important the sensory input. Application of this method to the experimental data showed that the perturbed sensory system has a lower weight and lower importance due to inaccuracy of its input and therefore, contributes less to postural control [1]. This method has been used to show how the postural control also changes due to ageing and diseases [50, 51]. A similar approach can be used with our experimental apparatus, where mechanical or/and visual perturbation are applied to investigate the role and interaction of the important sensory systems in postural control.

The presented methods have some limitations as the experimental and analytical methods are intended for the study of postural control when an ankle strategy is used. Therefore, the perturbations must be designed to avoid excessive body movement. However, when the perturbations are large or the support surface is compliant, a hip strategy is used, meaning both ankle and hip movements are significant. The hip strategy is characterized by anti-phase movement of the lower and upper body, which is specifically pronounced in frequencies larger than 1 Hz [3]. Study of hip strategy requires modeling the body with at least two links, i.e., a double-inverted pendulum model.

CHAPTER 6 ANKLE INTRINSIC STIFFNESS CHANGES WITH POSTURAL SWAY

Chapter 4 and 5 provide descriptions of the systematic protocols to study human postural control. Specifically, Chapter 5 briefly provides the steps of analytical approach to estimate ankle intrinsic stiffness in standing, while accounting for postural sway; however, it does not provide a thorough explanation of the approach. Consequently, the current chapter presents the details of this new method that I developed for the estimation of time varying ankle intrinsic stiffness in standing. The method identifies ankle intrinsic stiffness in each ankle separately in standing in response to pulses, while accounting for the modulation of ankle torque with postural sway. It utilizes a new intrinsic stiffness model and shows that it outperforms the commonly used mass-spring-damper (IBK) model of intrinsic stiffness. The application of the method to the perturbed standing data of healthy subjects demonstrates that ankle intrinsic stiffness is not constant and changes significantly with postural sway: ankle intrinsic stiffness increases as the center of pressure moves anteriorly with respect to ankle axis of rotation; the stiffness modulation seems functionally appropriate. It also shows the intrinsic stiffness is not adequate in itself to provide postural stability. This chapter is a manuscript, published in the Journal of Biomechanics in January 2019, as "*Amiri, P., Kearney, R. E. Ankle intrinsic stiffness changes with postural sway. Journal of Biomechanics. 85, 50-58 (2019)*".

Ankle Intrinsic Stiffness Changes with Postural Sway

Authors: Pouya Amiri, and Robert E. Kearney.

Journal: Journal of Biomechanics

6.1 ABSTRACT

In standing, the human body is inherently unstable and its stabilization requires constant regulation of ankle torque, generated by a combination of ankle intrinsic properties, peripheral reflexes, and central contributions. Ankle intrinsic stiffness, which quantifies the joint intrinsic properties, has been usually assumed constant in standing; however, there is strong evidence that it is highly dependent on the joint torque, which changes significantly with sway in stance. In this study, we examined how ankle intrinsic stiffness changes with postural sway during standing. Ten subjects stood on a standing apparatus, while subjected to pulse perturbations of ankle position. The mean torque of a short period before the start of each pulse was used as a measure of background torque. Responses with similar background torques were grouped together and used to estimate the parameters of an intrinsic stiffness model. Stiffness estimates were normalized to the critical stiffness and the background torque was transformed to the center of pressure location. We found that in most subjects, the normalized stiffness increased linearly with the movement of center of pressure towards the toes, with an average slope of 2.11±0.80 1/m.rad. This modulation of ankle intrinsic stiffness seems functionally appropriate, since the intrinsic stiffness increases quickly, as the center of pressure moves toward the toes and the limits of stability. These large changes of ankle intrinsic stiffness with postural sway must be incorporated in any model of stance control.

6.2 INTRODUCTION

During stance, the human body acts as an unstable inverted pendulum that is subject to internal and external perturbations. Consequently, ankle torque must be modulated continuously to maintain stability [8]. Ankle torque has two components. The first is intrinsic torque, generated by ankle intrinsic stiffness, which is the joint mechanical resistance to its movement with no intervention from the nervous system, generated by visco-elastic properties of the joint, active

muscle fibers, and inertial properties of the limbs [8]. The second is active torque, generated by changes in muscle activations, resulting from spinal reflexes and descending motor commands from brain. It is difficult to determine ankle intrinsic stiffness in functional tasks, such as standing, since the intrinsic and active torque appear together and cannot be separated easily. One method to quantify ankle intrinsic stiffness is to apply pulse perturbations of ankle position that generates an instantaneous intrinsic torque, followed by a delayed active torque response. The relationship between the joint angle and intrinsic torque defines the joint intrinsic stiffness and has been generally modelled as a mass-spring-damper [9, 10].

Ankle intrinsic stiffness has been demonstrated to change dramatically with joint background torque [7, 180] and joint mean position [7, 164] in supine experiments. In standing ankle torque and angle change continuously with sway, therefore, it is likely that ankle intrinsic stiffness changes with sway. Despite this, some previous studies of standing have assumed that ankle intrinsic stiffness is constant in standing [1, 10]; Others examined the modulation of the stiffness with sway but found no consistent relation [9]. Recently Sakanaka et el., 2016 showed that the elastic component of ankle intrinsic stiffness increased with ankle torque in standing, when the body sway was artificially increased by continuous rotation of base of support. Consequently, we felt it important to determine the extent to which ankle intrinsic stiffness changes with sway in normal standing. To do so, we first developed a parametric model that captures the dynamics of ankle intrinsic stiffness during stance accurately. Then, we used this model to characterize how the stiffness changes with postural sway.

6.3 METHODS

6.3.1 Participants

Ten subjects (6 male), aged between 18 to 40 years, with no history of neuromuscular disease were examined. Table 6.1 presents their anthropomorphic data. Subjects gave prior written consent to the experimental procedures, which had been approved by the McGill University's Research Ethics Board.

Table 6.1 Anthropometric data of the subjects (STD = standard deviation). For gender, M stands for male and F stands for female.

Subject Number	Gender (M/F)	Age (years)	Height (m)	Mass (Kg)
1	F	31	1.65	57.0
2	M	27	1.68	64.5
3	M	25	1.75	93.7
4	M	23	1.67	67.0
5	M	29	1.77	68.6
6	M	23	1.72	72.0
7	M	27	1.82	79.7
8	F	25	1.76	67.1
9	F	24	1.59	60.1
10	F	30	1.52	56.0
Average ± STD	-	26.4±2.9	1.69±0.09	68.6±11.3

6.3.2 Standing apparatus

Figure 6.1A illustrates the experimental apparatus, which comprised two pedals, driven by servo-controlled, electro-hydraulic rotary actuators, capable of applying independent, bilateral angular position perturbations (Forster et al., 2003). Subjects stood with a foot on each pedal and their ankle axis of rotation aligned with that of the actuator. High performance rotary potentiometers (Maurey Instruments 112-P19) measured foot angle (θ_F), the pedal angle with respect to the horizontal (Figure 6.1C). Each pedal was equipped with four load cells (The Omega™ LC302-100) that measured the vertical forces, used to compute ankle torque and the center of pressure (COP) position (Figure 6.1B). Shank angles were measured using laser range finders as described in [245]. Figure 6.1C shows the ankle angle, θ_A, the angle between the foot and the shank, given by:

$$\theta_A = \theta_F - \theta_S \tag{6.1}$$

where θ_S is the angle of the shank with respect to the vertical. By convention, dorsiflexing ankle angles and torques were taken as positive; a right angle between the foot and shank was taken as the zero ankle angle.

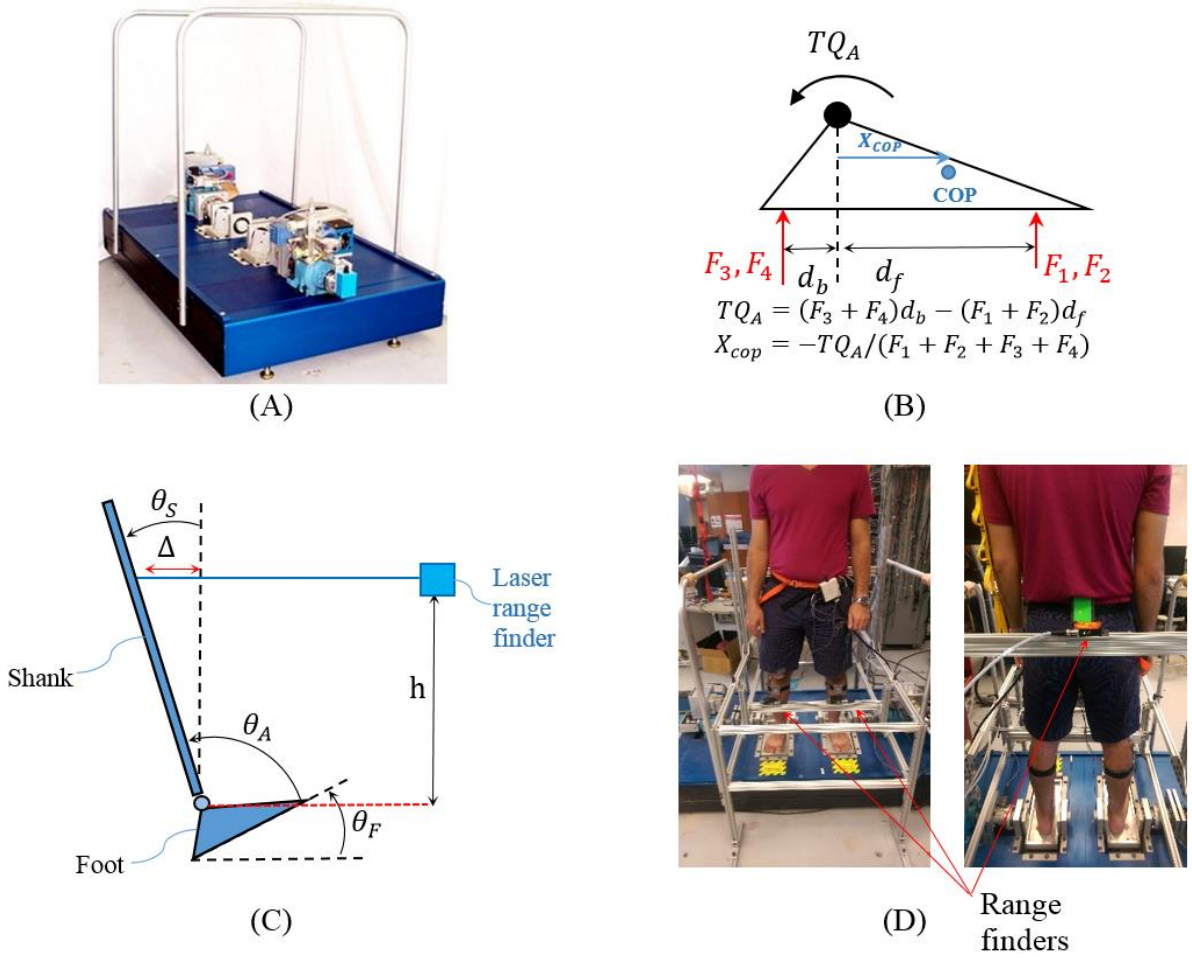

Figure 6.1 Experimental apparatus, (B) Schematic of the forces, measured by the load cells and the equation to calculate ankle torque and COP location; (C) The shank angle (θ_S) was estimated by measuring its linear discplacement Δ and dividing it by the range finder height, h, above the ankle axis of rotation; foot angle (θ_F) was measured by the actuator potentiometer; ankle angle (θ_A) was obtained using equation (3); (D) The laser range finders used to measure shank and body movements

Body angle (θ_B) was determined by dividing the displacement of the mid-point between left and right posterior superior iliac spines, measured using another laser range finder (1302-200

Micro-epsilon, Figure 6.1D), by the vertical distance between the laser and the ankle axis of rotation.

6.3.3 EMG

Surface EMGs were measured from the major muscles about the ankle joint: the tibialis anterior (TA), and the three triceps surae (TS) muscles: the medial (MG) and lateral (LG) gastrocnemius, and soleus. Single differential Delsys electrodes with an inter-electrode distance of 1 cm were placed on the muscles, according to the Seniam guidelines [250]. EMGs were amplified with a gain of 1000 and filtered with a bandwidth of 20-2000 Hz.

6.3.4 Experiments

Subjects stood comfortably on the apparatus, looking forward, with their hands at their sides, and the mean foot angles set to 0 degree (Figure 6.1D). First, a 60-second quiet standing trial (no perturbations) was performed for each subject. Then, the actuators applied uncorrelated, random position perturbations to both ankles simultaneously. Perturbations were pseudo random binary sequences (PRBS), where the actuator input switched between two values (peak-to-peak amplitude of 0.02 rad) at random multiples of 200 ms (Figure 6.2A). The perturbations were not intended to emulate any real world situation but rather to measure the intrinsic stiffness while minimizing postural disturbances. We chose to use low amplitude perturbations with independent, random time courses to each ankle, since these evoke smaller postural disturbances than coherent perturbations to both ankles [11]. Three two-minute trials, each with a different realization of the PRBS perturbation were acquired for each subject. Trials were separated by two minute rest periods to avoid fatigue.

6.3.5 Data acquisition

All signals were anti-alias filtered at 486.3 Hz and sampled at 1 KHz with 24-bit dynamic resolution. All sampled signals were low pass filtered at 50 Hz by a zero-phase shift 10^{th} order Butterworth filter. Derivatives of the torques and angles were estimated using a digital differentiator [258].

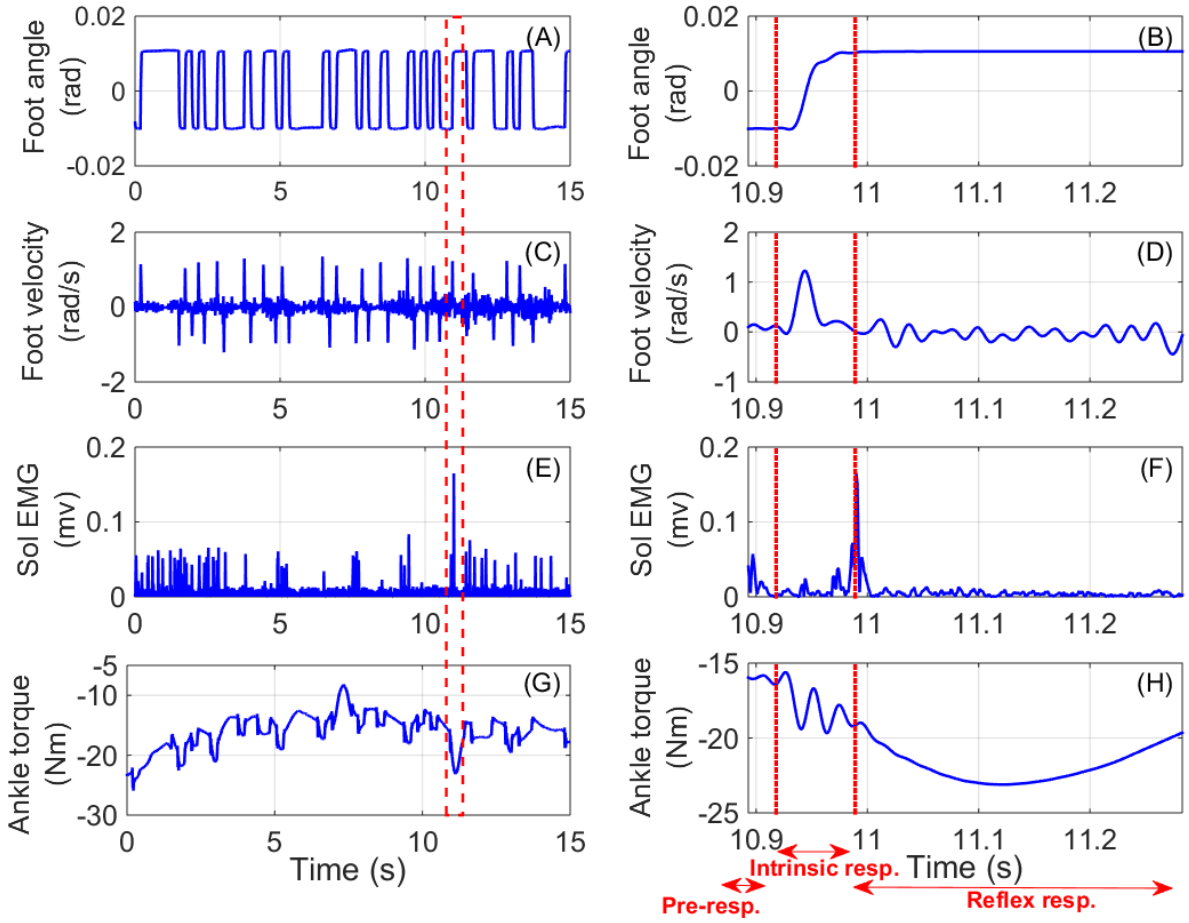

Figure 6.2 Typical experimental trial. Left column shows 15 seconds of a typical trial, (A) Foot angle, (C) Foot velocity, (E) Soleus EMG, and (G) Ankle torque; The right column shows an individual pulse, encompassed by the red dashed box in the left column, on an expanded time scale: (B) Foot angle, (D) Foot velocity, (F) Soleus EMG, and (H) Ankle torque. The vertical dotted lines separate the response into the pre-response (0 to 25 ms), intrinsic response (26 to 90 ms), and reflex response (91 to 390 ms); positive torque and angles correspond to dorsiflexion.

6.3.6 Postural activity

Postural activity was quantified in terms of the mean and standard deviation of the body angle and rectified EMG. For the perturbed trials, the postural component of the EMG was estimated by eliminating the synchronous burst of reflex activity from the EMG record as described in [180].

6.3.7 Data segmentation and grouping

Ankle torque changed significantly throughout trials, due to postural sway as Figure 6.2G shows. Such changes significantly change intrinsic stiffness [7, 180].

Figure 6.2A shows that the PRBS position perturbation consisted of a sequence of pulse perturbations in alternating directions. Therefore, to account for changes in the ankle torque, we analyzed each pulse separately by finding local extrema of the foot velocity, and extracting signals for 50 ms before and 40 ms after the displacement. The right hand column of Figure 6.2 shows a typical pulse response.

For analysis, we divided the responses into the two segments, shown in Figure 6.2:

1. Pre-response segment: started 50 ms before the peak velocity and lasted for 25 ms. Foot position remained constant during this segment, so it defined the state of the ankle prior to the perturbation.
2. Intrinsic response segment: lasted from the end of the pre-response segment until 40 ms after the peak velocity. The reflex torques was substantial in some trials. However, our analysis only considered data from the intrinsic response segment before any reflex torque could be generated. Consequently, we are confident that our estimates of the intrinsic stiffness were not affected by reflex torques.

To eliminate possible long lasting interactions between pulses, only pulses occurring more than 400 ms after a previous pulse were analyzed.

We also computed descriptive statistics for each pre-response including the mean torque (as a measure of background torque), the sum of mean rectified EMG of TS muscles, and TA muscle. Subsequently, intrinsic torque responses to pulse perturbations with similar background torques were grouped together, in 3Nm bins, and used to estimate stiffness.

6.3.8 Intrinsic stiffness estimation

Due to the sluggish body dynamics, the perturbations should not evoke any significant shank movements during the intrinsic segment. Consequently, we modelled the stiffness as a function of foot angle only. Intrinsic stiffness has often been described using a mass-spring-damper (IBK) model [8, 38]:

$$\frac{\Delta TQ_I}{\Delta \theta_F} = (I_F + I_P)s^2 + Bs + K \tag{6.2}$$

where ΔTQ_I is the change in the ankle intrinsic torque, $\Delta\theta_F$ is the change in the foot angle, and I_F and I_P are the foot and pedal inertias.

However, recent evidence indicates that an *extended intrinsic model* (EIM), comprising a second order system with three zeros describes ankle intrinsic stiffness better [164]:

$$\frac{\Delta TQ_I}{\Delta \theta_F} = \frac{n_3 s^3 + n_2 s^2 + n_1 s + K_{EIM}}{d_2 s^2 + d_1 s + 1} \tag{6.3}$$

Therefore, we compared the performance of the EIM and IBK model in standing. Parameters of each model were estimated using the regression formulation:

$$\Delta \boldsymbol{TQ_I} = \boldsymbol{X_{model}}\, \boldsymbol{\theta_{model}} \tag{6.4}$$

where $\Delta\mathbf{TQ_I} = \begin{bmatrix} \cdots & \Delta TQ_I(k) & \cdots \end{bmatrix}^T$, k=1,…,N (N is the number of samples). For the IBK model the regression matrix $\mathbf{X_{model}}$ in (6.4) was:

$$\boldsymbol{X_{IBK}} = \begin{bmatrix} \vdots & \vdots & \vdots \\ \ddot{\theta}_F(k) & \dot{\theta}_F(k) & \Delta\theta_F(k) \\ \vdots & \vdots & \vdots \end{bmatrix},\ \boldsymbol{\theta_{IBK}} = \begin{bmatrix} I \\ B \\ K \end{bmatrix} \tag{6.5}$$

and for the EIM was:

$$\boldsymbol{X_{EIM}} = \begin{bmatrix} \vdots & \vdots & \vdots & \vdots & \vdots & \vdots \\ \dddot{\theta}_F(k) & \ddot{\theta}_F(k) & \dot{\theta}_F(k) & \Delta\theta_F(k) & T\ddot{Q}_I(k) & T\dot{Q}_I(k) \\ \vdots & \vdots & \vdots & \vdots & \vdots & \vdots \end{bmatrix}, \boldsymbol{\theta_{EIM}} = \begin{bmatrix} n_3 \\ n_2 \\ n_1 \\ n_0 \\ d_2 \\ d_1 \end{bmatrix} \tag{6.6}$$

Model parameters were estimated using the standard least squares solution:

$$\boldsymbol{\theta_{model}} = \left(\boldsymbol{X_{model}^T X_{model}}\right)^{-1} \boldsymbol{X_{model}^T}\, \boldsymbol{\Delta TQ_I} \tag{6.7}$$

The estimated parameters were used to predict the intrinsic torque ($\widehat{\Delta TQ_I}$). Model performance was evaluated in terms of percentage variance accounted for (VAF):

$$VAF = 100\left(1 - \frac{\sum_{k=1}^{N}(\Delta TQ_I(k) - \widehat{\Delta TQ_I}(k))^2}{\sum_{k=1}^{N} \Delta TQ_I{}^2(k)}\right) \tag{6.8}$$

Model performance was also evaluated in terms to the minimum description length (MDL) criterion, which balances the goodness of fit and the number of model parameters:

$$MDL(M) = \left(1 + \frac{Mlog(N)}{N}\right)\sum_{k=1}^{N}\left(\Delta TQ_I(k) - \widehat{\Delta TQ_I}(k, M)\right)^2 \tag{6.9}$$

where M is the number of model parameters (M=3 for IBK model and M=6 for EIM).

Given the low frequencies associated with postural control [12], the low frequency stiffness is of primary interest. For the IBK model, this is equal to K, whereas, for the EIM, it is equal to K_{EIM}. Values of K and K_{EIM} were normalized to the subjects' critical stiffness, the minimum intrinsic stiffness required to maintain upright posture [10], given by:

$$K_{cr} = mgh_{com} \tag{6.10}$$

where m is the subject's mass, g is gravitational acceleration, and h_{com} is the height of the body's center of mass above ankle axis of rotation, derived from anthropometric data [253].

6.4 RESULTS

6.4.1 Quiet vs perturbed standing

The peak-to-peak amplitude of the perturbations was 0.02 rad; this was smaller than the range of the body angle in quiet standing, whose minimum was 0.025 rad (subject 1) and maximum was 0.041 rad (subject 3).

Mean body angle was similar (p=0.965), but the RMS value of the angle was significantly greater in the perturbed (0.0l7±0.006 rad) than unperturbed trials (0.006±0.002 rad). LG and soleus EMG remained unchanged, but MG activity increased more than 50% in perturbed trials; the ratio of perturbed/unperturbed MG RMS EMG was 1.51±0.74 for the left and 1.61±0.81 for the right side.

TA was silent in all subjects in unperturbed trials and in 8/10 subjects in perturbed trails. For these 8 subjects, the ratio of TA RMS activity in perturbed trials to its baseline activity in unperturbed trials was 1.13±0.33 for the left and 1.33±0.53 for the right side. In the two remaining subjects, the TA ratios of the left and right ankles were 9.1 and 11.2 (subject 2), and 10.0 and 4.6 (subject 9), showing substantial TA activity was present in perturbed trials.

6.4.2 Shank movement in response to foot perturbation

Figure 6.3 shows the position and torque records from the intrinsic segment of a typical response group in blue and their ensemble averages in red. Figure 6.3A&B demonstrate that the foot angle traces were very repeatable. However, as Figure 6.3C&D show, the shank angles behaved differently. First, the ensemble average was almost completely flat, indicating that, during the intrinsic segment, there was no consistent shank movement in response to the foot perturbation. Thus, shank displacements cannot contribute to the intrinsic torque. Second, the mean shank angle varied from perturbation to perturbation, presumably reflecting postural sway. Figure 6.3E&F demonstrate that the torque responses were consistent in shape, although offset from one another, presumably because of differences in ankle position.

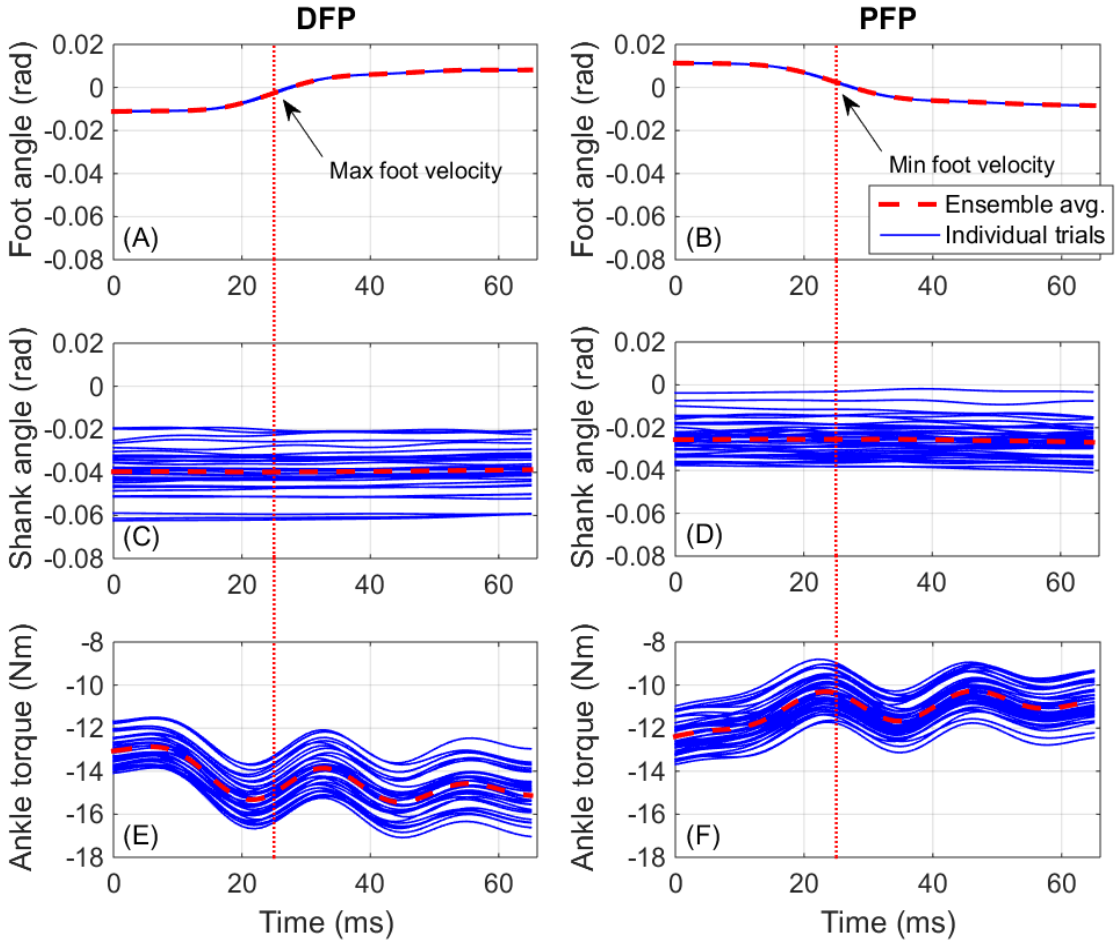

Figure 6.3 Typical group of intrinsic responses to dorsiflexing (DFP, left column) and plantar-flexing pulses (PFP, right column). (A,B) Foot angle, (C,D) Shank angle, (E,F) Ankle torque. Individual responses are shown in blue and their ensemble averages in red. Background torque range is 11 - 14 Nm for subject 1's left ankle.

6.4.3 Intrinsic stiffness model

Figure 6.4 shows typical position perturbations in dorsiflexing (Figure 6.4A) and plantar-flexing (Figure 6.4B) directions. Figure 6.4C&D show the measured torques, and those predicted by IBK model, and the EIM. Only a single pulse perturbation is shown, but all the perturbations in the group were used to estimate stiffness. The EIM prediction with a VAF of 99.4% was more accurate than IBK model, whose VAF was 98.3%. Figure 6.4E&F also shows that the EIM residual torques (RMS=0.17 Nm) were smaller than the IBK residuals (RMS=0.29 Nm). Furthermore, the

EIM estimate of low frequency stiffness (128.8 Nm/rad) was lower than that of the IBK model (138.4 Nm/rad).

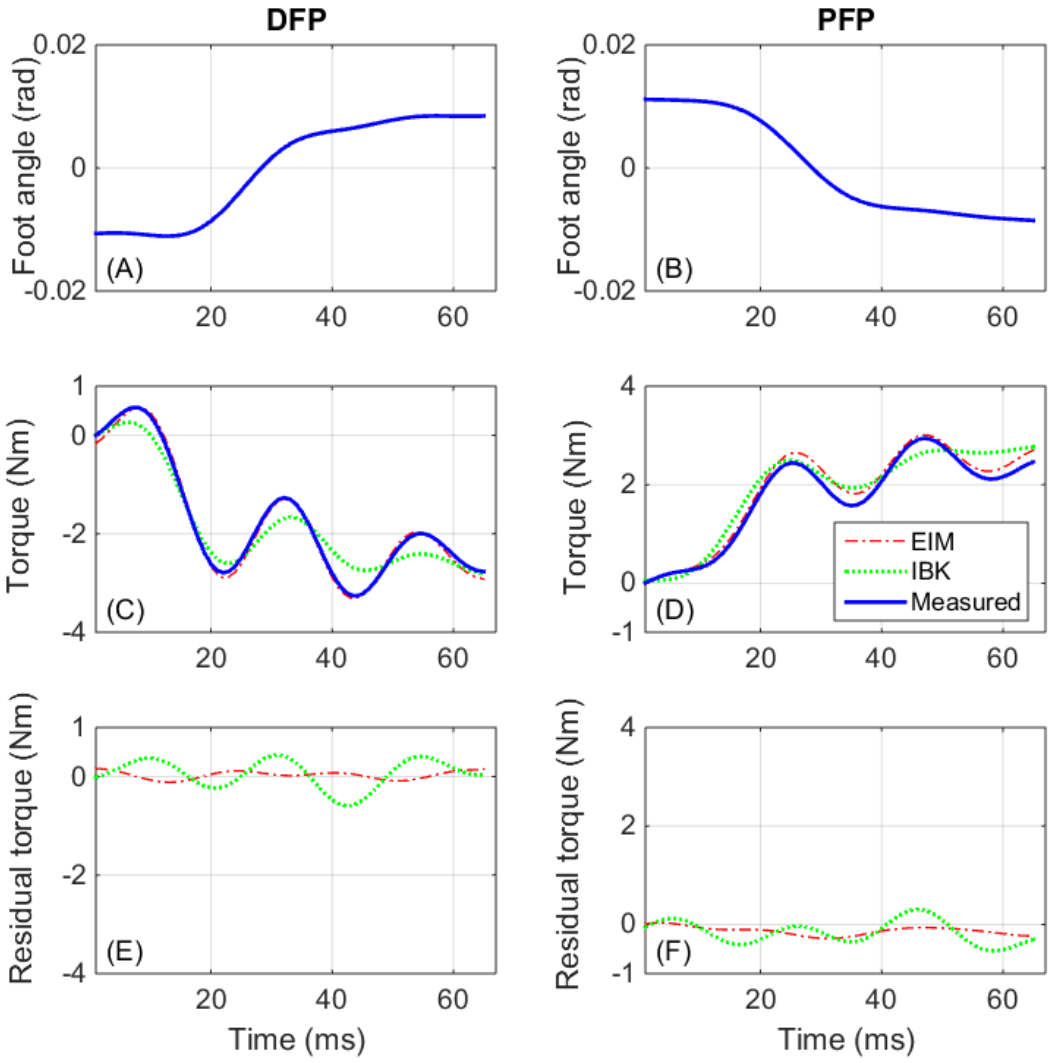

Figure 6.4 Torques predicted by the IBK model and EIM for typical dorsiflexing (DFP) and plantarflexing (PFP) pulses. (A,B) Foot angle, (C,D) Experimental, IBK model, and EIM torques, (E,F) Residual torques for the IBK model and EIM. The results belong to Subject 1's left ankle at background torque 22.5 Nm.

Table 6.2 summarizes the performance of the EIM and IBK model. Note that the data for S7R was discarded, since it was corrupted by a large, low frequency noise whose origin we could not determine. The EIM model always fits the data very well with a %VAF greater than 95%, which was always greater than that of the IBK model. In addition, the ratio of the MDL cost function of the IBK model to EIM was always greater than 1, indicating that increased %VAF did not result from the increased model complexity. Finally, the median of the ratio of K_{EIM} to K was less than 1, indicating that the K_{EIM} estimates were consistently lower than those of K.

Table 6.2 EIM and IBK model performance for all subjects. Min and max stand for minimum and maximum. IQR shows the interquartile range.

	Left ankle				**Right ankle**			
	Min	**Max**	**Median**	**IQR**	**Min**	**Max**	**Median**	**IQR**
%VAF	96.6	99.7	98.9	1.0	95.2	99.4	98.6	1.5
$\%VAF_{EIM}$-VAF_{IBK}	0.8	5.7	1.8	1.4	2.6	26.2	6.0	3.4
MDL_{IBK}/MDL_{EIM}	1.60	4.75	2.30	0.72	1.70	9.47	3.35	2.13
K_{EIM}/K	0.78	0.91	0.93	0.03	0.75	1.13	0.90	0.09

6.4.4 Low frequency ankle intrinsic stiffness

This section examines the relation between normalized K_{EIM} (K_{EIM}^{N}) and COP position. These variables, which normalize K_{EIM} and torque for differences in subjects' height and weight, reduce the inter-subject variability and simplify inter-subject comparisons.

Figure 6.5 shows K_{EIM}^{N} as a function of COP position. The small confidence intervals show the high sensitivity of the EIM for the low frequency stiffness. IBK model showed similar sensitivity. There were large COP movements in most subjects, associated with large changes in K_{EIM}^{N}. Left and right ankle stiffness followed similar patterns, increasing with COP displacement, although their ranges differed due to differences in COP displacement. In three subjects the left and right

stiffness were similar while in the other subjects the right ankle stiffness was consistently lower than the left at equivalent COP values.

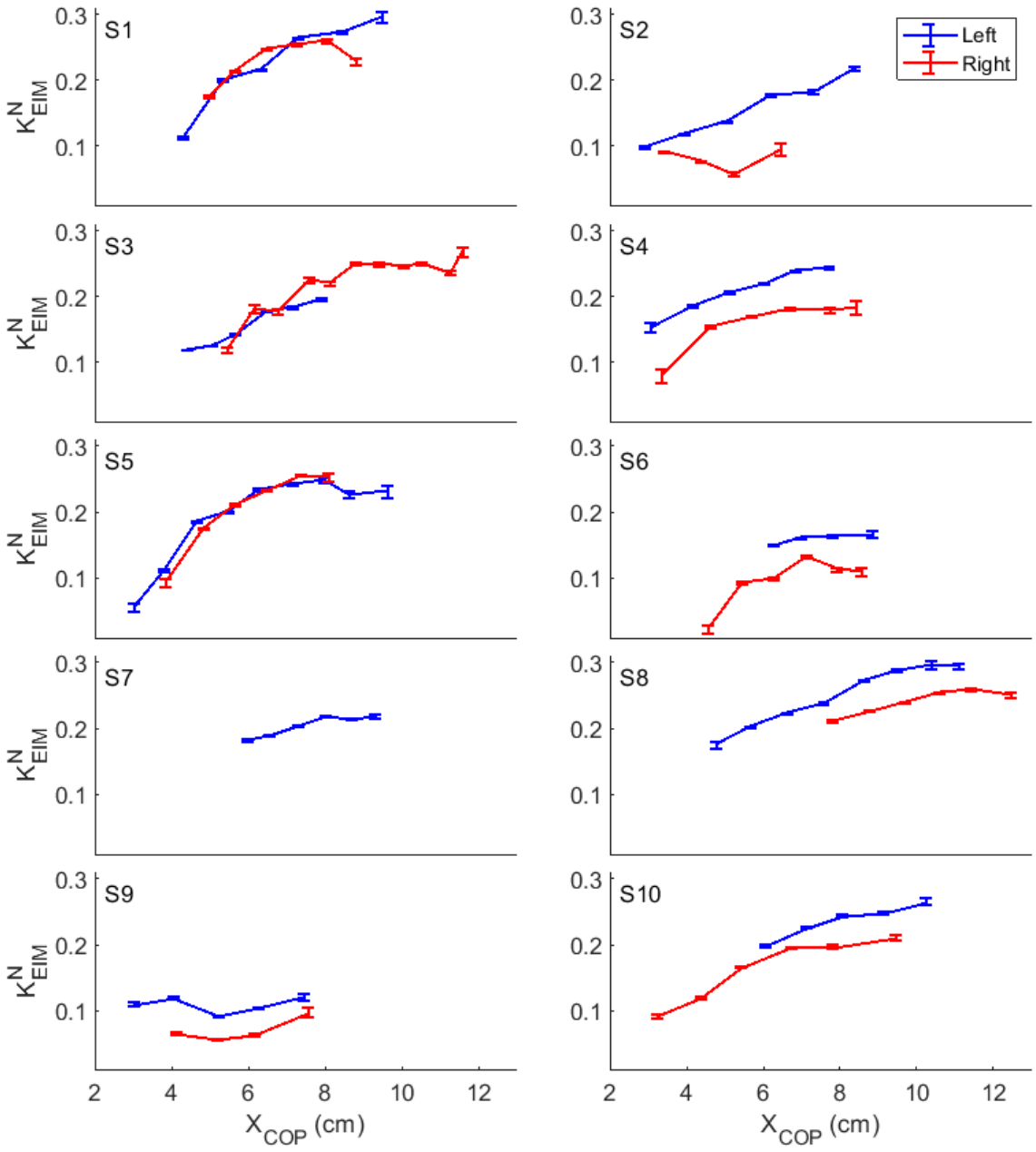

Figure 6.5 Relation between normalized intrinsic stiffness and COP position. Each panel shows the left (blue) and right (red) stiffness for one subject; bars indicate the 95% confidence intervals of the stiffness values. Note that S7R was discarded.

Table 6.3 summarizes the ratio of the maximum K_{EIM}^{N} to its minimum, ranges of $\overline{TQ}_A$, K_{EIM}^{N} and COP. The ratio of the maximum to minimum K_{EIM}^{N} was smallest for S7L (1.20) and largest for S6R (5.63). In addition, the range of COP displacement varied from 2.9 cm to 6.5 cm and the range of K_{EIM}^{N} varied from 3% to a maximum of 19%.

Table 6.3 also shows the regression results between K_{EIM}^{N} and COP, demonstrating that in most cases, K_{EIM}^{N} increased almost linearly with COP movement. In 15/19 cases, the coefficient of determination (COD) was greater than 0.639 and slopes were non-zero (P-value<0.05). In one case (S1R), the stiffness appeared to saturate for large COPs. In the remaining cases (S2R, S9L, and S9R), there was no significant change in stiffness with COP.

Table 6.3 Changes of K_{EIM} with COP for the left and right ankles of subjects. The ratio of maximum K^{N}_{EIM} (K^{max}_{EIM}) to minimum K^{N}_{EIM} (K^{min}_{EIM}) and the range (maximum-minimum) of the estimated parameters, including K^{N}_{EIM}, background torque ($\overline{TQ}_A$), and COP (X_{cop}); and the results of linear regressions analysis for the relation between K^{N}_{EIM} and X_{cop} for all subjects. P value is the probability of the slope being zero. The last column shows mean and standard deviation (std) of each parameter. To find the mean and standard deviation for slope, intercept, and R-squared, only the lines with a non-zero slope (i.e. with p-value<0.05) were used.

Subject			**1**	**2**	**3**	**4**	**5**	**6**	**7**	**8**	**9**	**10**	**mean± std**
Critical stiffness (Nm/rad)			471.6	548.1	832.9	563.2	601.6	617.4	721.5	590.3	478.8	432.0	**585.7± 120.6**
Left ankle	$K^{max}_{EIM}/K^{min}_{EIM}$		2.63	2.21	1.65	1.59	4.46	1.23	1.20	1.69	1.31	1.34	**1.93±1.00**
	Range	K^{N}_{EIM}	0.18	0.12	0.08	0.09	0.19	0.03	0.04	0.12	0.03	0.07	**0.10±0.06**
		$\overline{TQ}_A$ (Nm)	18	18	18	18	27	15	18	24	15	15	**19±4**
		X_{cop} (cm)	5.2	5.5	3.5	4.7	6.5	3.1	3.4	5.7	3.7	3.6	**4.5±1.2**
	Linear regression	**Slope (1/m.rad)**	3.26	2.15	2.41	1.93	2.51	0.97	1.14	2.22	0.08	1.75	**2.04±0.70**
		P Value	0.004	0.000	0.001	0.000	0.005	0.036	0.006	0.000	0.875	0.006	-
		Intercept $\times 10^{-2}$ (1/rad)	0.00	3.46	1.00	10.23	3.84	9.24	11.80	9.10	10.53	11.53	**6.69±4.61**
		R^2	0.897	0.977	0.957	0.968	0.695	0.816	0.879	0.961	0.001	0.942	**0.899± 0.093**
Right ankle	$K^{max}_{EIM}/K^{min}_{EIM}$		1.49	1.65	2.24	2.32	3.03	5.63	-	1.21	1.72	3.10	**2.49±1.35**
	Range	K^{N}_{EIM}	0.09	0.04	0.15	0.11	0.18	0.11	-	0.05	0.04	0.14	**0.10±0.05**
		$\overline{TQ}_A$ (Nm)	18	12	33	18	18	18	-	18	12	18	**18±6**
		X_{cop} (cm)	3.9	3.0	6.2	5.1	4.4	3.8	-	4.3	2.9	5.3	**4.3±1.1**
	Linear regression	**Slope (1/m.rad)**	1.51	0.00	1.86	1.77	3.98	2.11	-	1.04	1.11	2.59	**2.23±1.00**
		P Value	0.084	0.999	0.000	0.033	0.002	0.047	-	0.013	0.186	0.010	-
		Intercept $\times 10^{-2}$ (1/rad)	12.68	8.02	6.00	5.04	0.00	0.00	-	14.80	0.00	2.28	**4.69±5.55**
		R^2	0.475	0.000	0.764	0.719	0.935	0.639	-	0.822	0.662	0.840	**0.787± 0.103**

To understand this, we examined how COP and background EMGs varied. Figure 6.6A&C shows that for a typical subject, K^{N}_{EIM} and background TS EMG increased with COP, while the TA remained silent. In contrast, Figure 6.6B&D shows that for S9L, K^{N}_{EIM} stayed almost constant;

in this case, TA was active at low COP and decreased as COP increased, whereas TS activity increased. The same behavior was seen in S2R and S9R.

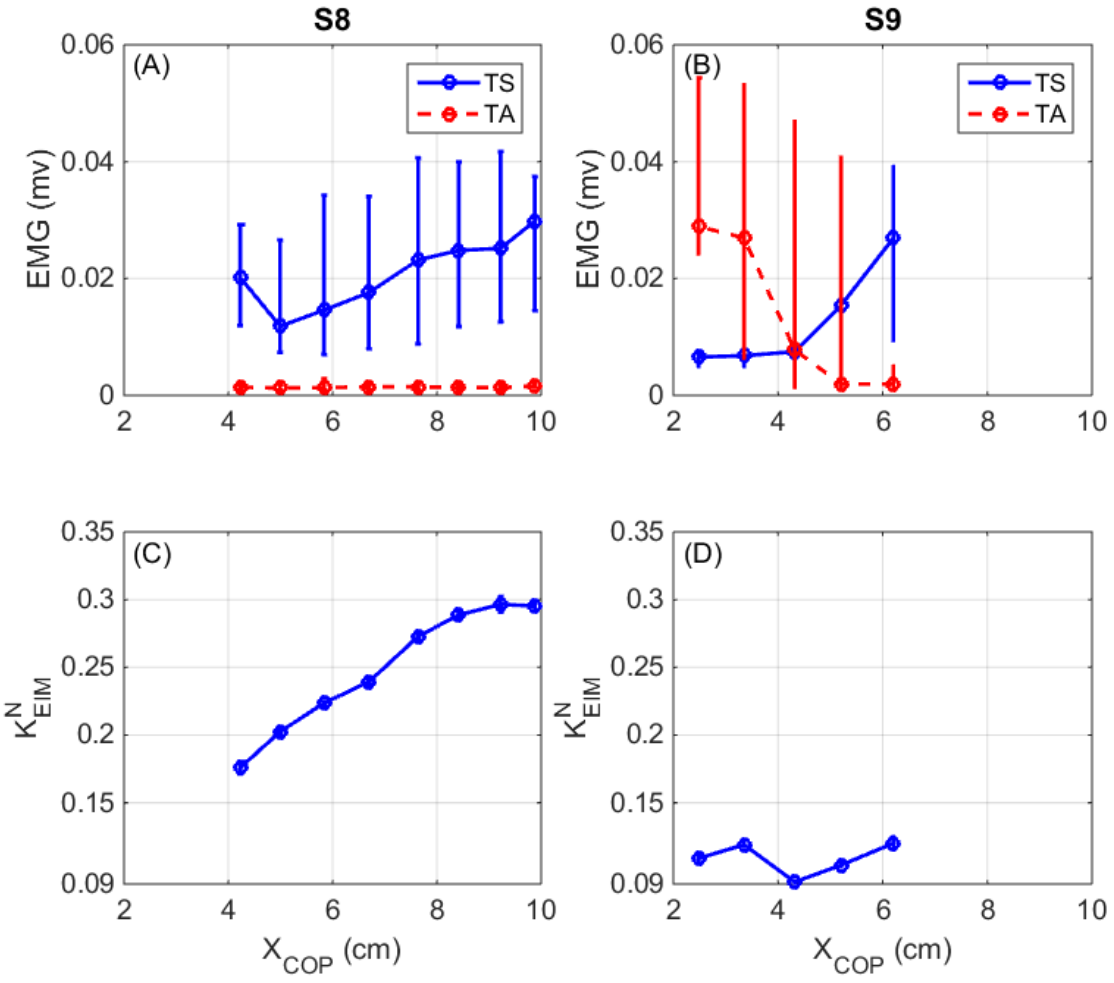

Figure 6.6 The influence of ankle muscle activity on the joint stiffness of subject 8's left ankle, (S8, left column) and subject 9' left ankle (S9, right column); (A, B) the EMG activity of the TS and TA muscles, and (C, D) the corresponding joint stiffness. In (A, B) the bars show the min and max and the circle shows the median of the background EMG activity at each background torque. In the bottom row, K^N_{EIM} is shown with its 95% confidence interval.

6.5 DISCUSSION

We showed that ankle intrinsic stiffness is not constant in standing, but changes significantly with postural sway; indeed in some subjects the intrinsic stiffness varied more than five-fold. These findings call into question the common assumption that ankle intrinsic stiffness is constant in stance [1, 9, 10, 32].

6.5.1 The intrinsic stiffness model

Ankle intrinsic stiffness has often been modelled as a mass-spring-damper system [8, 10, 38]. However, intrinsic dynamics may become more complex under certain operating conditions [164]. Our results showed that EIM is required to model the intrinsic stiffness during stance.

This conclusion is supported by the finding that the VAF of the EIM was higher than that of the IBK model. Moreover, this increase was not simply due to the added complexity, since, the MDL, which accounts for both the accuracy and complexity of a model, was always higher for the IBK model than the EIM. The stiffness estimates obtained with both the IBK and EIM models followed similar trends, but as Table 6.2 illustrates, the EIM estimates were consistently smaller than the IBK estimates. Sobhani-Tehrani et al., 2017 demonstrated that fits with the EIM model yields more accurate estimates of the low frequency gain. Consequently, we believe the EIM results provide a better indication of the contribution of intrinsic stiffness to postural control

6.5.2 Intrinsic stiffness

Our results demonstrated that ankle intrinsic stiffness changes with postural sway during stance. More specifically, the low frequency gain of intrinsic stiffness increases as the COP moves away from the ankle axis of rotation (Figure 6.5). This relationship between the stiffness and joint torque has been reported in supine conditions [7, 180]. However, many studies of stance have assumed ankle intrinsic stiffness to be constant [1, 32]. Some tried to show the stiffness changes with ankle torque in standing but they failed and concluded the stiffness was a biomechanical constant [65]. One study recently demonstrated that ankle intrinsic stiffness varied with background torque when body sway was increased by slowly rotating the support surface [40]. The current work systematically investigated the modulation of ankle intrinsic stiffness with postural sway in standing.

In most subjects, the left and right ankles showed similar trends, whereby stiffness increased with COP displacement. Two differences in behavior were evident. First, in some subjects, the range of COP changes was different between the limbs, resulting in differences in the range of stiffness (e.g. subject 3). We do not believe these differences result from the application of perturbations, since differences in the range of left and right COP displacements during perturbed trials were similar to those during unperturbed trials. Secondly, in six subjects, the trends were similar but there was an offset, so that the stiffness of the right ankle was lower than that of the left ankle at all COPs. We do not believe this was the result of the perturbations either, since EMG activity increased by a similar amount in the left and right MG in comparison to unperturbed trials and there was no evidence of co-contraction in most cases. Consequently, we believe that these differences likely represent inherent differences in the passive joint stiffness (i.e. stiffness with no muscle activity).

An important question is the extent to which ankle intrinsic stiffness contributes to overall stance control. Normalized stiffness (K_{EIM}^{N}) provides a convenient measure of this. We estimated the minimum contribution of the stiffness for each subject as the sum of the lowest normalized stiffness values of the left and right ankles. Similarly, we estimated the maximum contribution as the sum of the maximum values of the two sides. Figure 6.7 shows the range of combined stiffness values for each subject. Our estimates of the combined normalized stiffness of the two ankles ranged from a minimum of 14.7% (subject 5) to a maximum of 55.7% (subject 1). Other studies have reported higher values for the stiffness: Loram et al. 91% [9], Casadio 64% [10], Sakanaka et al. 45% to 80% [40], and Vlutters et al. 40% to 70% [11]. These differences likely arise from differences in the perturbation amplitudes. Ankle intrinsic stiffness decreases as perturbation amplitude increases [11, 178]. The peak to peak amplitude of the perturbations in our study was 1.15˚ (0.02 rad), which was larger than that used in other studies (Loram 0.055˚, Casadio 1˚, Sakanaka <0.6˚, and Vlutters 0.29˚-4.6˚).

Two other factors may also have contributed to the differences of low frequency stiffness estimates. First, other studies used an IBK model for the intrinsic stiffness, while we used the EIM, which yields lower values for the stiffness. Second, other studies obtained mean stiffness values by averaging torque responses to pulses, assuming that stiffness is constant. This approach masks

the dependency of the stiffness on ankle torque. Despite the difference in the stiffness values, consistent with other studies [9-11, 32], our results showed that although ankle intrinsic stiffness is not sufficient for stance control, it is large enough to contribute significantly to stance control.

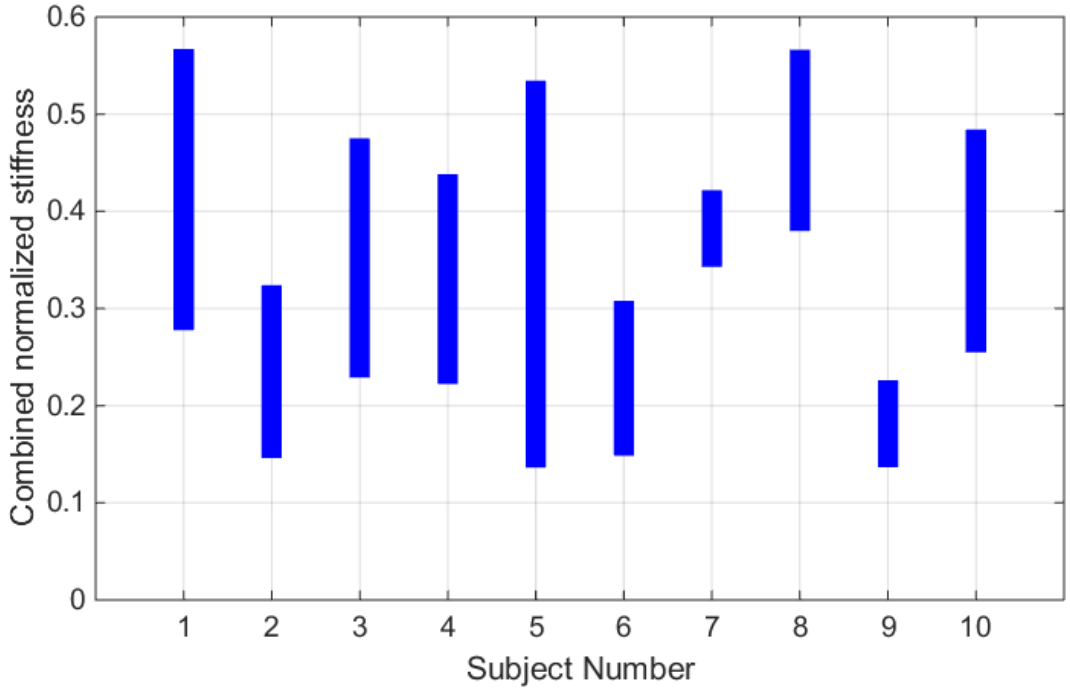

Figure 6.7 Range of combined normalized stiffness (left minimum stiffness + right minimum stiffness to left maximum stiffness + right maximum stiffness) for all subjects.

6.5.3 Functional significance of the modulation of ankle intrinsic stiffness in stance

We found that postural sway and MG activity increased when perturbations were applied, indicating that these made postural control more challenging. However, there was no change in mean body position and in all but two subjects only the plantar-flexors muscles were active, indicating that there was no major change in postural control strategy. Consequently, we believe that the results of our study are representative of changes to be expected in unperturbed standing.

The modulation of ankle intrinsic stiffness seems to be functionally appropriate for the control of stability in standing. Thus, when the COP is closer to the limits of stability and the body is more prone to fall, ankle intrinsic stiffness is higher. Therefore, the common assumption that the

contribution of intrinsic stiffness to stance control is constant may ignore an important feature of postural control.

CHAPTER 7 PATTERNS OF MUSCLE ACTIVATION AND MODULATION OF ANKLE INTRINSIC STIFFNESS IN STANDING

This chapter extends the findings of the previous chapter by investigating ankle intrinsic stiffness in several postural tasks, aimed at making postural control more difficult by changing the postural operating conditions. The method developed in Chapter 6 is used to estimate ankle intrinsic stiffness in normal standing, forward lean, backward lean, toe-up, and toe-down standing. The results demonstrate that ankle intrinsic stiffness changes with postural sway, however, the behavior is more complex than the patterns shown in Chapter 6 and depends on the postural operating condition. The results demonstrate that ankle intrinsic stiffness changes with the position of center of pressure in a manner, associated with one of three muscle activation patterns. In addition, the intrinsic stiffness is highest in forward lean and lowest in backward lean; as such, their stiffness values provide the range for ankle intrinsic stiffness in standing. Finally, the results show that the intrinsic stiffness can vary widely, from as little as 0.08 to as much as 0.75 of the critical stiffness, depending on the operating conditions, however, it is never adequate in itself for postural control. This chapter has been submitted to the Journal of Neurophysiology and is currently under review.

Patterns of Muscle Activation and Modulation of Ankle Intrinsic Stiffness at Different Standing Conditions

Authors: Pouya Amiri, and Robert E. Kearney

Journal: Submitted to the Journal of Neurophysiology

7.1 ABSTRACT

Ankle intrinsic stiffness describes the dynamic relationship between the joint angle and the torque acting about it, due to intrinsic mechanical stiffness of muscles and joints. Recently, we showed that ankle intrinsic stiffness changes significantly with postural sway in normal standing. The current article extends this work to document how intrinsic stiffness changes with postural operating conditions. Thus, subjects stood on an apparatus, while subjected to ankle position perturbations, in five conditions: normal standing, toe-up and toe-down standing, backward and forward lean. In each condition, ankle intrinsic stiffness was estimated while accounting for its modulation with postural sway. We found that the mean value of ankle intrinsic stiffness was the highest in forward lean and the lowest in backward lean. In addition, intrinsic stiffness changed as a function of center of pressure in one of three ways, associated with distinct muscle activation patterns. Most frequently, ankle intrinsic stiffness increased monotonically with center of pressure anterior displacement; this was associated with a progressive increase in triceps surae activation. In a second, less common pattern, intrinsic stiffness initially decreased and then increased with anterior movement of center of pressure; this was associated with alternating activation of tibialis anterior and triceps surae. In the third, least common pattern, intrinsic stiffness decreased monotonically with center of pressure anterior displacement; this was associated with decreasing activation of tibialis anterior. Finally, the results demonstrated that ankle intrinsic stiffness can vary widely in standing, from as little as 0.08 to as much as 0.75 of the critical stiffness, depending on the operating conditions.

7.2 INTRODUCTION

The coordinated action of the central nervous (CNS) and musculoskeletal systems is required to ensure stability and maintain orientation during human standing [18]. The body behaves as an unstable inverted pendulum, subject to internal and external perturbations. Therefore, ankle torque must be regulated continuously to maintain stability. This is achieved by a combination of

mechanisms including intrinsic musculoskeletal properties, peripheral spinal reflexes, and central motor commands generated in response to somatosensory, visual, and vestibular feedback. The relative contribution of each mechanism to postural control is unclear, since their effects appear together and are difficult to dissociate, and each mechanism has a complex response that is strongly dependent on the operating conditions [129, 259-261].

Joint stiffness is the joint resistance to movement, quantified as the dynamic relationship between the joint angle and the torque acting about it [74]. It has an intrinsic component, resulting from the passive visco-elastic properties of active muscles, joint, and connective tissues, as well as inertial properties of the limbs; and a reflex component due to changes in muscle activity, mediated by spinal reflex circuits [77]. It was initially suggested that ankle intrinsic stiffness was sufficient to maintain postural stability [17, 33]. However, it was subsequently demonstrated that, while intrinsic torque contributes significantly to the task, it is not adequate in itself [9-11, 15, 32, 213]. Nonetheless, there remains controversy over the importance of intrinsic stiffness to postural control, a question that can only be addressed by measuring ankle joint intrinsic stiffness.

Studies of postural control have often assumed that ankle intrinsic stiffness remains constant during standing [1, 9-12, 32, 47]. However, there is strong evidence that stiffness changes dramatically with operating conditions, defined by joint torque [4, 7, 180], joint mean position [5-7], and perturbation properties [11, 178]. Standing is accompanied by persistent sway, resulting in large changes of ankle torque and angle that would be expected to alter the stiffness. Indeed, we showed recently that ankle intrinsic stiffness is modulated significantly by postural sway in normal standing [37, 38]. However, the study examined the modulation of intrinsic stiffness for only the limited range of operating conditions present in normal upright standing, where intrinsic contributions were found to be rather modest in size. Nonetheless, it is not clear how ankle intrinsic stiffness changes with the operating conditions, associated with more demanding postural tasks. There has been much emphasis on the importance of the sensory systems in stance control, as revealed by their contributions to challenging postural tasks, such as lean [262-264], inclined surface standing [264-266] and load carriage [267, 268]. However, the intrinsic contributions to these tasks have been assumed constant and/or insignificant. Therefore, we felt it important to measure ankle intrinsic stiffness for a wide range of postural operating conditions.

The objective of this study was to investigate the modulation of ankle intrinsic stiffness in postural control when the operating conditions were modified by having subjects stand on inclined surfaces or lean forwards and backwards. Since intrinsic stiffness changes with sway, we estimated the stiffness as a function of center of pressure (COP) in each operating condition and characterized how this relation changed.

The paper is structured as follows: Section 7.3 explains the experimental methods and the analysis procedures, Section 7.4 presents the results, and Section 7.5 discusses the findings and summarizes the conclusions.

7.3 METHODS

7.3.1 Participants

Nine subjects, aged between 18 to 40 years, with no history of neuromuscular diseases participated in the study. Table 7.1 shows the subjects' anthropometric data. All participants gave prior written informed consent to the experiments, which had been approved by McGill University's Research Ethics Board.

Table 7.1 Anthropometric data of the subjects (STD = standard deviation).

Subject Number	Sex M=Male F=Female	Age (years)	Height (m)	Mass (Kg)
1	M	27	1.68	64.5
2	M	25	1.75	93.7
3	M	23	1.67	67.0
4	M	29	1.77	68.6
5	M	23	1.72	72.0
6	M	27	1.82	79.7
7	F	25	1.76	67.1
8	F	24	1.59	60.1
9	F	30	1.52	56.0
Average ± STD	-	25.9±2.5	1.70±0.10	69.9±11.2

7.3.2 Dual-actuator apparatus

Figure 7.1A illustrates the dual-actuator apparatus whose two pedals, each driven by servo-controlled hydraulic actuator, were capable of applying independent, bilateral perturbations of ankle angular position [248]. Participants stood with a foot on each pedal and the ankle axis of rotation aligned with that of the actuator, as shown in Figure 7.1C. High performance rotary potentiometers (Maurey Instruments 112-P19), mounted in series with the pedals, measured the foot angle with respect to horizontal. Four load cells (The Omega™ LC302-100) sandwiched between two plates beneath each foot measured the vertical forces, which were used to calculate the vertical force, ankle torque, and the position of COP with respect to the ankle axis of rotation [37].

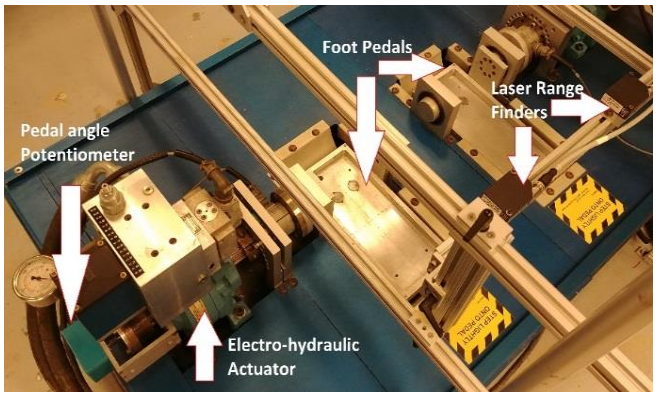

(A)

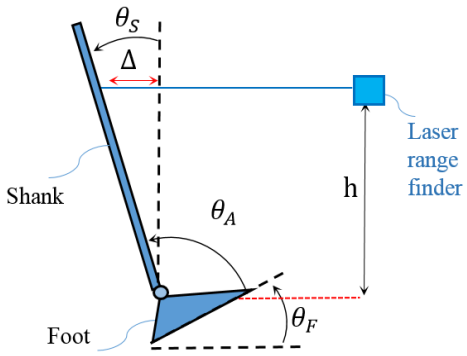

(B)

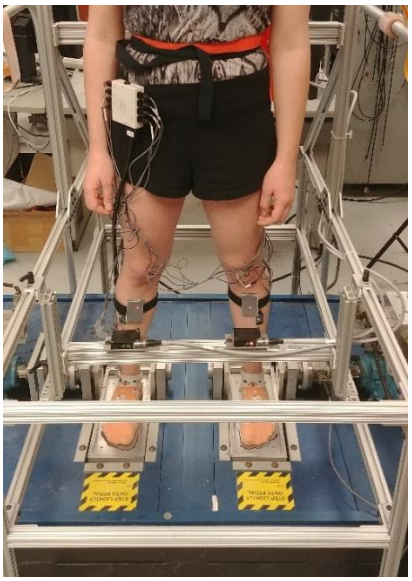

(C)

Figure 7.1 (A) Experimental apparatus, (B) The shank angle (θ_s) was estimated by measuring its linear discplacementand Δ dividing it by the range finder height above the ankle axis of rotation, h; foot angle (θ_F measured by the actuator potentiometer, (C) A participant during the experiments

As Figure 7.1B shows, the angle between the foot and the shank, is given by:

$$\theta_A = \theta_F - \theta_S \tag{7.1}$$

where θ_A is the ankle angle, the angle between the foot and the shank; θ_F is the foot angle with respect to the horizontal, controlled by the actuator, and θ_S is the shank angle with respect to the vertical. To determine θ_S, the linear displacement of each shank was measured using a laser range finder (1302-100, Micro-epsilon) and converted to shank angle [245]. By convention, angular displacements and torques in the dorsiflexing direction were taken as positive; zero was occurring when the foot and shank were perpendicular.

7.3.3 EMG collection

Surface EMG activity of the tibialis anterior (TA), and the three triceps surae (TS) muscles (medial and lateral gastrocnemius, and soleus) were measured using single-differential Delsys electrodes with an inter-electrode distance of 1 cm. Electrodes were placed in accordance with the guidelines provided by the Seniam project [250]. EMGs were measured using a total gain of 1000 and band-pass filtered 20-2000 Hz.

7.3.4 Data acquisition

All signals were filtered with an anti-aliasing filter with a corner frequency of 486.3 Hz and then sampled at 1000 Hz with 24-bit resolution (NI 4472, National Instruments). All subsequent data analysis was performed using MATLAB [269]. The sampled signals were filtered at 50 Hz by a 10^{th} order zero-shift Butterworth filter to remove noise. A digital differentiator with a frequency response (FR) close to that of a true differentiator from 0-100 Hz was used to calculate derivatives of the torque and angle signals [258].

7.3.5 Experiments

Participants were instructed to stand comfortably, looking forward, with their hands at their sides. A 60-second quiet standing trial, with no perturbations, was acquired for reference purposes. Then, a series of perturbed trials were acquired, in which the actuators applied uncorrelated position perturbations to both ankles simultaneously. Perturbations were pseudo random binary

sequences (PRBS), where the input changed between two values (peak to peak of 0.02 rad) at random multiples of a switching interval of 200 ms (Figure 7.2A). Perturbed trials were performed while subjects performed five operating conditions:

1- Normal standing: with the mean foot angle ($\overline{\theta_F}$) set to zero. This task was used as a reference to examine how the stiffness changed in other tasks.
2- Toe-up Standing: the actuator set the mean foot angle to +0.15 rad ($\overline{\theta_F}$=+0.15 rad).
3- Toe-down Standing: the actuator set the mean foot angle was set to -0.15 rad ($\overline{\theta_F}$= -0.15 rad).
4- Forward Lean: the mean foot angle was set to zero and subjects were instructed to lean forward maximally by rotating about the ankle (not the hip) and keep their posture constant for the trial.
5- Backward Lean: the mean foot angle was set to zero and subjects were instructed to lean backward by rotating about the ankle (not the hip) and keep their posture constant for the trial.

Three trials, each lasting two minutes and using a different realization of the PRBS input, were acquired for each operating condition, resulting in a total of 15 trials, performed in randomized order for each subject. A two-minute rest period was imposed between trials to prevent fatigue.

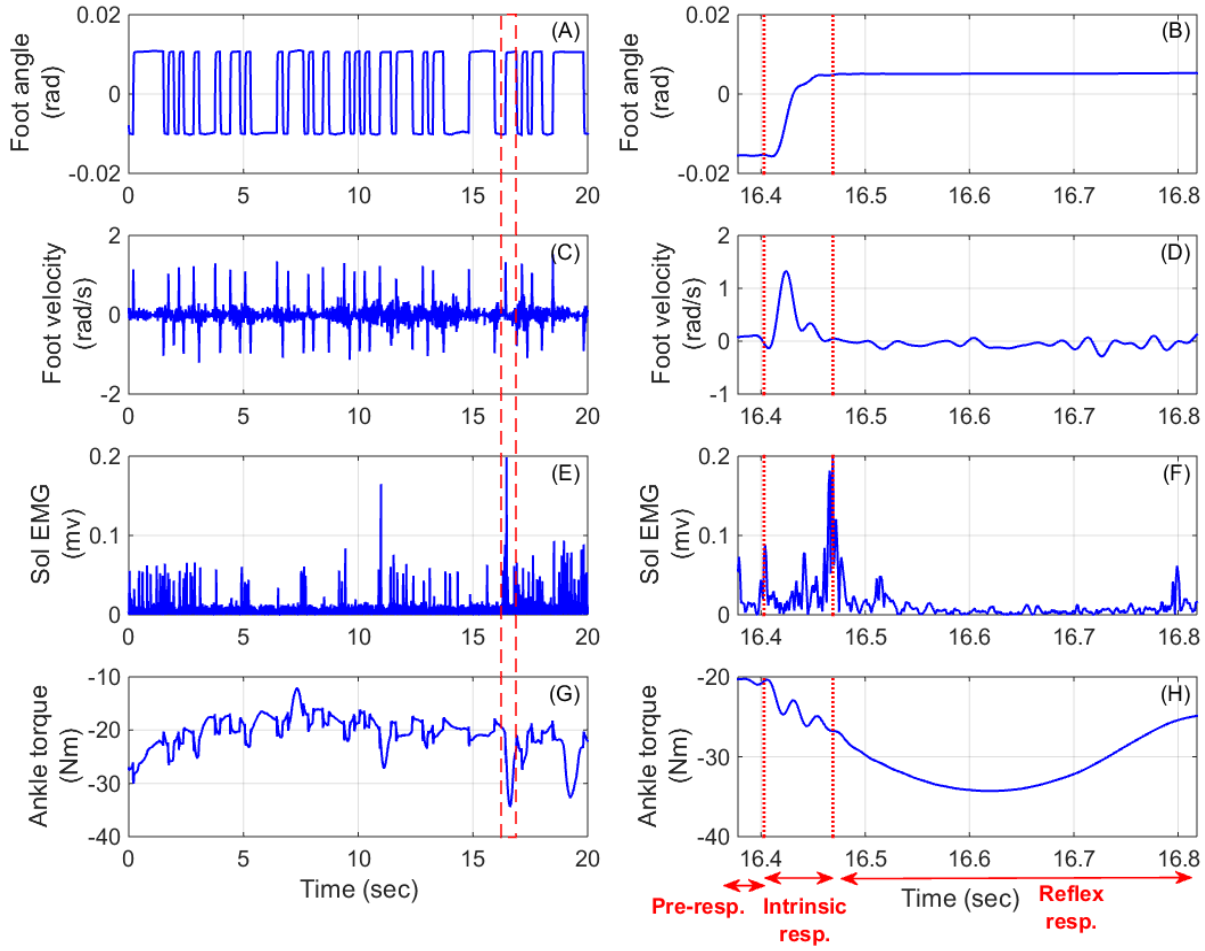

Figure 7.2 Typical experimental trial. Left column shows 15 seconds of a typical trial, (A) Foot angle, (C) Foot velocity, (E) Soleus EMG, and (G) Ankle torque; The right column shows an individual pulse, encompassed by the red dashed box in the left column, on an expanded time scale: (B) Foot angle, (D) Foot velocity, (F) Soleus EMG, and (H) Ankle torque. The vertical dotted lines separate the response into the pre-response segment (0 to 25 ms), intrinsic responses segment (26 to 90 ms), and reflex response segment (91 to 390 ms); positive torque and angles correspond to dorsiflexion.

7.3.6 Data analysis

The analysis procedures are fully described in [37], and so are described only briefly here.

Postural sway is associated with large changes in ankle torque, which causes significant changes in ankle intrinsic stiffness [37, 38]. Therefore, to account for these changes, we divided each PRBS perturbation into a sequence of pulse perturbations in alternating directions and

analyzed the torque response to each pulse. Pulses were located based on local extrema of the foot velocity. The associated torque response (starting 50 ms before the peak pulse velocity) was divided into three segments: pre-response (0 to 25 ms), intrinsic response (26 to 90 ms), and reflex response (91 to 390 ms), as the right column of Figure 7.2 illustrates. Descriptive statistics computed from the pre-response segment of each pulse included:

1- Background torque: the mean ankle torque ($\overline{TQ_A}$)
2- Background COP: the mean COP position ($\bar{X}_{cop}$)
3- Background TS EMG: the sum of the mean rectified EMG of the three TS muscles ($\overline{EMG_{TS}}$)
4- Background TA EMG: the mean rectified EMG of the TA ($\overline{EMG_{TA}}$)
5- Background ankle angle: the mean ankle angle ($\bar{\theta}_A$)

Subsequently, position and torque data of the intrinsic response from all pulses with similar background torques ($\overline{TQ_A}$) for each operating condition were grouped together. Groups were defined by dividing the range of the joint background torque into 3 Nm-wide bins; each pulse was assigned to the bin associated with its background torque. Groups with less than 8 pulse perturbations were discarded. A separate intrinsic stiffness model was fitted to all position-torque data in each group.

We showed previously that the traditional mass-spring-damper model does not describe ankle intrinsic stiffness adequately during standing. Rather, an extended intrinsic model (EIM) is needed to describe the stiffness accurately. The model has the form [37, 164]:

$$\frac{\Delta TQ_I(s)}{\Delta \theta_F(s)} = \frac{n_3 s^3 + n_2 s^2 + n_1 s + K_{EIM}}{d_2 s^2 + d_1 s + 1} \tag{7.2}$$

where ΔTQ_I is the change in ankle intrinsic torque, $\Delta\theta_F$ is the change in the foot angle, and s is Laplace operator. For the rapid perturbations used in the these experiments, only the foot angle contributes to ΔTQ_I, since the perturbations evoked no shank movements during the short intrinsic response segments [37].

We estimated the parameters of the EIM model for each group of responses using least squares. These parameter estimates were used to predict the intrinsic torque and the model performance was evaluated in terms of the percentage variance accounted for (%VAF):

$$\%VAF = 100\left(1 - \frac{\sum_{k=1}^{N}(\Delta TQ_I(k) - \widehat{\Delta TQ_I}(k))^2}{\sum_{k=1}^{N}\Delta TQ_I{}^2(k)}\right) \tag{7.3}$$

where $\widehat{\Delta TQ_I}$ is the predicted intrinsic torque, and N is the number of samples.

Because postural control has a low bandwidth [12], our analysis focused on the low frequency stiffness, K_{EIM}. Estimates of K_{EIM} were normalized to the participant's critical stiffness, the overall joint stiffness required to maintain upright posture [15], by:

$$K_{cr} = mgh_{com} \tag{7.4}$$

where m is subject's mass, h_{com} is the height of the whole body center of mass (COM) above the ankle axis of rotation, and g is gravitational acceleration. Values of h_{com} were derived from anthropometric data from NASA [253]. The normalized low frequency stiffness is denoted as K_{EIM}^{N}.

Results are presented in terms of the relation between K_{EIM}^{N} and background COP, because these variables normalize K_{EIM} and background torque for the mass and height of each subject.

An important question is the extent to which ankle intrinsic stiffness contributes to postural control. To address this, for each standing operating condition, we estimated the minimum contribution of each subject's stiffness as the sum of the lowest normalized stiffness observed for the two sides; the maximum contribution was estimated similarly.

7.3.7 Statistical analysis

To compare intrinsic stiffness across postural conditions, we pooled the stiffness values from both sides of all subjects in each operating condition. The stiffness for each condition did not follow a normal distribution. Thus, we performed Kruskal-Wallis test (one-way analysis of

variance on ranks) to determine if the stiffness was the same for all conditions. If the stiffness was different among conditions, Dunn-Sidak rank comparison test was applied to data from all pairs of conditions to establish if and how intrinsic stiffness differed among operating conditions.

7.4 RESULTS

7.4.1 Typical experimental trial

Figure 7.2 shows a 15 second segment of data for a typical perturbed standing trial. Figure 7.2A and C show the position and velocity of the PRBS foot perturbation. Figure 7.2E shows the EMG of soleus muscle; continuous activation of soleus muscle is evident, while large peaks show bursts of activity due to stretch reflex responses. Figure 7.2G shows ankle torque, where significant changes in the torque due to postural sway are clearly seen.

The right column of Figure 7.2 shows, on an expanded time scale, a response to an individual pulse perturbation as indicated in the left column. The vertical red lines show the three segments of the response: pre-response (0-25), intrinsic response (26-90), and reflex response (91-390).

7.4.2 Performance of the EIM

Figure 7.3 shows position and torque records for typical perturbations in the dorsiflexing (left column) and the plantar-flexing (right column) directions. The position perturbations (Figure 7.3A&B) evoked the torque responses shown in blue in Figure 7.3C&D; the torques predicted by the EIM are superimposed in red. The torque predictions were very accurate; the %VAFs were very high (99.1%) and the residual torques (Figure 7.3E&F) were very small. Figure 7.3 shows a single pulse perturbation but all the perturbations in the group were used to estimate the stiffness parameters. Such excellent fits were typical. The EIM predicted the intrinsic torque with a %VAF of 98.3±1.6% (mean ± standard deviation) for all trials and subjects.

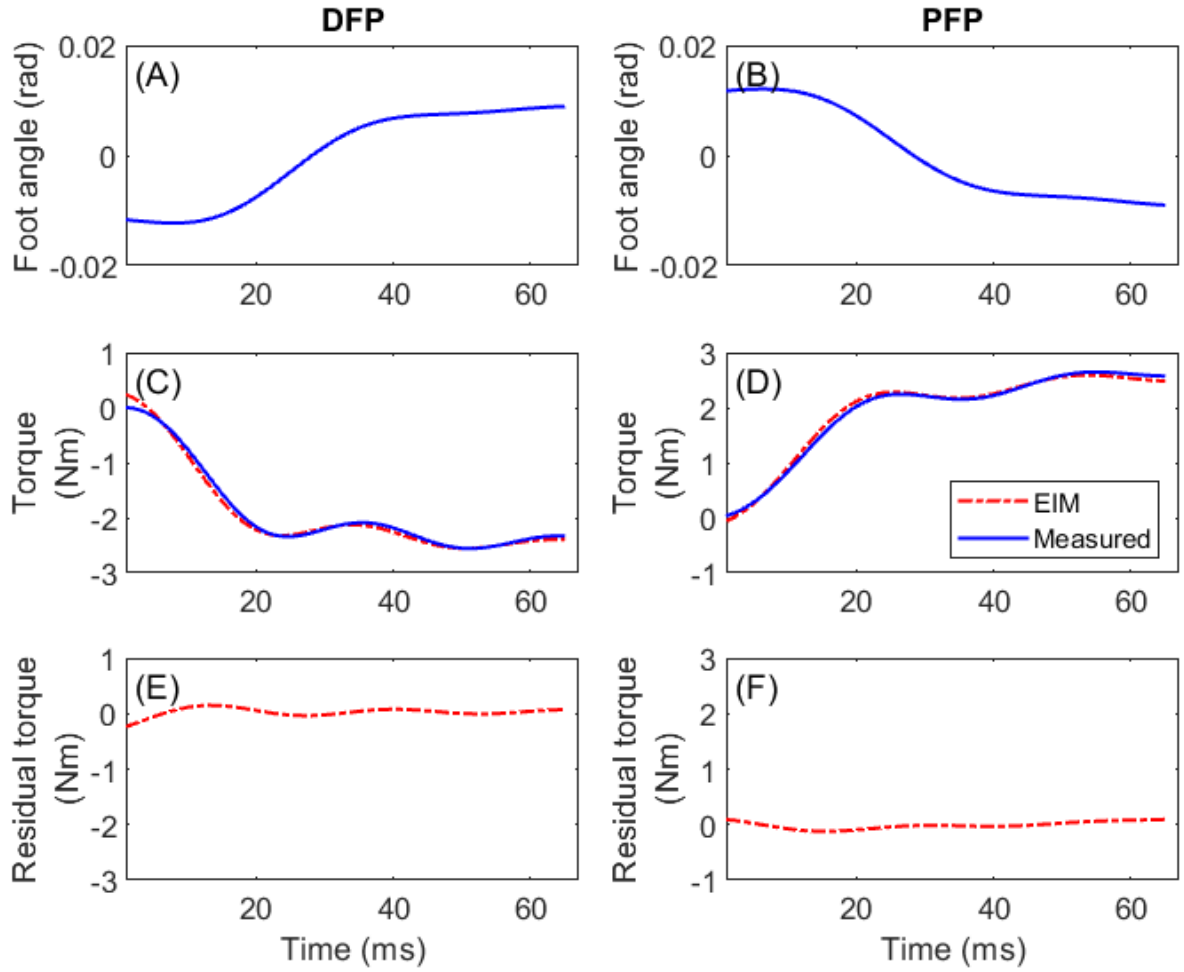

Figure 7.3 Torques predicted by the EIM for typical dorsiflexing (DFP) and plantarflexing (PFP) pulses. (A,B) Foot angle, (C,D) Experimental and EIM torques, (E,F) Residual torques for the EIM. The results belong to Subject 2's left ankle at background torque 19.5 Nm.

7.4.3 Intrinsic stiffness modulation

Examination of the results from individual subjects showed that K_{EIM}^{N} changed significantly and systematically with changes in COP. It became apparent that these changes occurred in three distinct patterns, as illustrated in the results from the two subjects presented in Figure 7.4 and Figure 7.5.

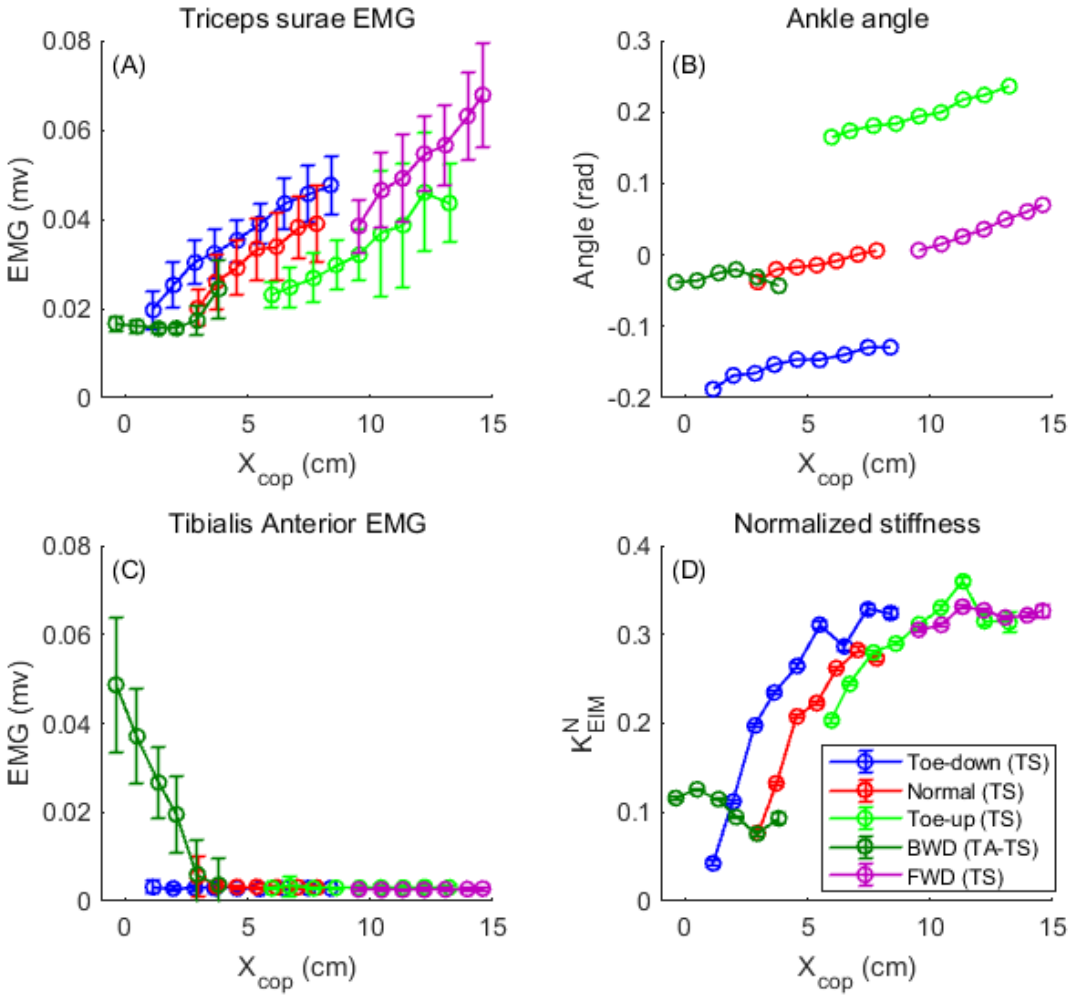

Figure 7.4 Modulation of (A) TS muscles background EMG, (B) Ankle background angle, (C) TA muscle background EMG, and (D) normalized intrinsic stiffness with COP position for S4L. The red curves show normal standing, blue curves show toe-down and the light green curves show toe-up. In addition, the dark green curves show backward lean (BWD) and purple curves show forward lean (FWD). TS and TA-TS inside the parenthesis in the legend show the muscle activation pattern used in the tasks.

A- TS-only stiffness modulation

The first pattern involved activation of only TS with little or no activation of TA and was associated with a monotonic increase in K^{N}_{EIM} with anterior COP displacement. This pattern is evident during the normal, toe-up, toe-down standing, and forward lean in Figure 7.4A. It is also

clear that anterior displacement of COP was accompanied by an increase in background TS EMG (Figure 7.4A), while TA remained silent (Figure 7.4C). In addition, ankle angle changed less than 0.1 rad (5.7°) in each operating condition; thus, angle changes seemed too small to affect intrinsic stiffness (Figure 7.4B). Figure 7.5 demonstrates that this TS-only modulation pattern was used by Subject 8 only in forward lean.

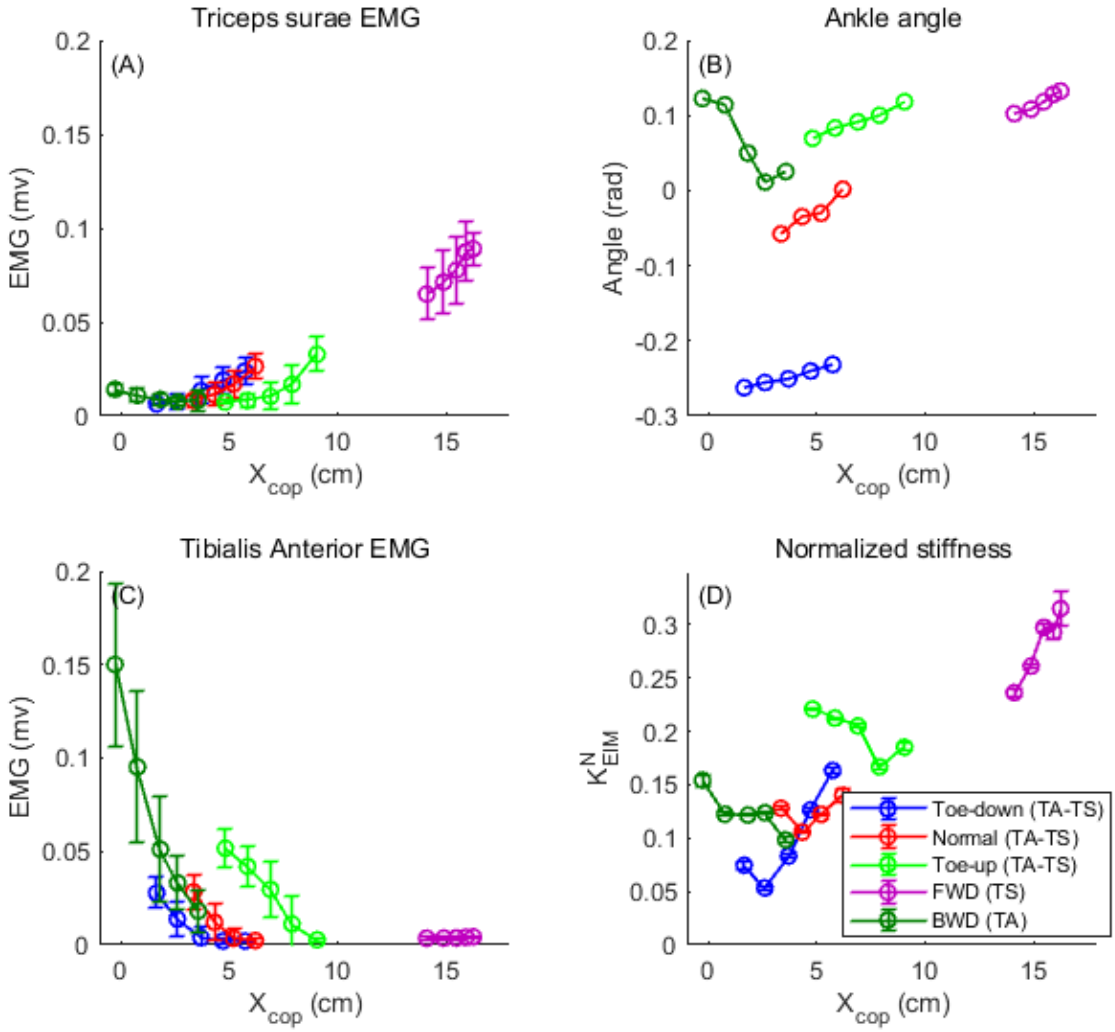

Figure 7.5 Modulation of (A) TS muscles background EMG, (B) Ankle background angle, (C) TA muscle background EMG, and (D) normalized intrinsic stiffness with COP position for S8L. The red curves show normal standing, blue curves show toe-down and the light green curves show toe-up. In addition, the dark green curves show backward lean (BWD) and purple curves show forward lean

(FWD). TS, TA and TA-TS inside the parenthesis in the legend show the muscle activation pattern used in the tasks.

B- TA-TS stiffness modulation

The second pattern involved the activation of both TS and TA and was associated with less systematic changes of intrinsic stiffness with COP. Figure 7.5 illustrates this pattern for the normal, toe-up, and toe-down standing. When the COP was close to the ankle axis of rotation, stiffness decreased with COP anterior displacement; and when the COP moved farther from the axis of rotation, intrinsic stiffness increased with COP anterior displacement (Figure 7.5D). TA activity (Figure 7.5C) was high when the COP was close to the ankle axis of rotation and decreased as the COP moved anteriorly; TS behaved in the inverse manner (Figure 7.5A).

C- TA-only stiffness modulation

In the third pattern, illustrated in the backward lean shown in Figure 7.5, subjects activated only TA with little or no activation of TS. Intrinsic stiffness decreased as the COP displaced anteriorly. This pattern was only observed in backward lean, where TA activity and stiffness decreased as the COP moved anteriorly, while TS remained silent.

Figure 7.6 summarizes the frequency with which each muscle activation pattern was observed in each operating condition. Note that the data for S6R[1] was discarded, since it was corrupted by a large, low frequency noise whose origin we could not determine. Overall, the TS-only pattern was used most frequently in 57/85 (67%) cases[2], followed by TA-TS in 22/85 (26%) and the TA-only pattern 6/85 (7%).

[1] Snp shows the p side (p=left or right) of subject n (n=1, … ,9).
[2] Case here means one ankle of a subject.

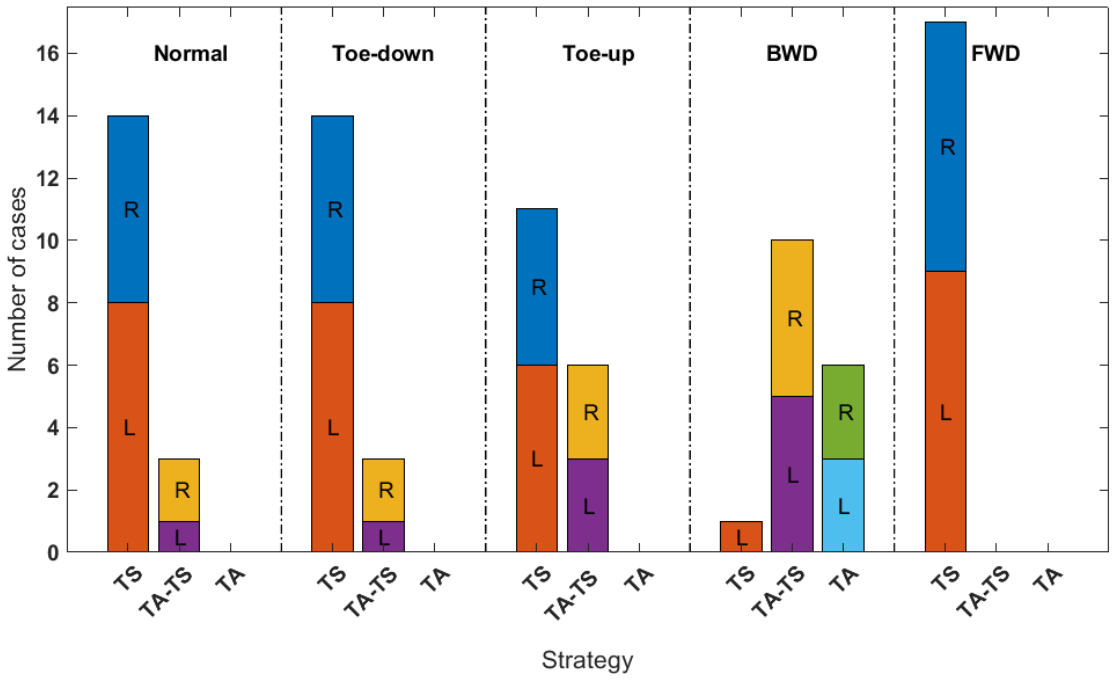

Figure 7.6 Number of cases for each muscle activation pattern in each postural task; TS, TA-TS, and TA stand for TS-only pattern, TA-TS pattern, and TA-only pattern, respectively. L and R shows the number of cases happening for left and right ankles.

The TS-only pattern predominated in normal standing (17/17), toe-down standing (14/17) and forward lean (17/17). The TA-TS pattern was used in the remaining six cases in these three operating conditions.

In toe-up standing, the TS-only pattern was still used most common (11/17), but the TA-TS pattern was used more frequently (6/17).

In backward lean, the TA-TS pattern was used in 10/17 cases, the TA-only pattern in 6/17 cases, and the TS-only pattern was used in only one case.

7.4.4 Intrinsic stiffness across operating conditions

Figure 7.7 shows the range of normalized total ankle stiffness (sum of the left and right sides) for each subject and operating condition. For most subjects, intrinsic stiffness was highest in forward lean and lowest either in backward lean or toe-down. The range of total intrinsic stiffness

was 0.21-0.66 in normal standing, 0.19-0.75 in toe-up standing, 0.08-0.74 in toe-down standing, 0.14-0.44 in backward lean, and 0.42-0.75 in forward lean.

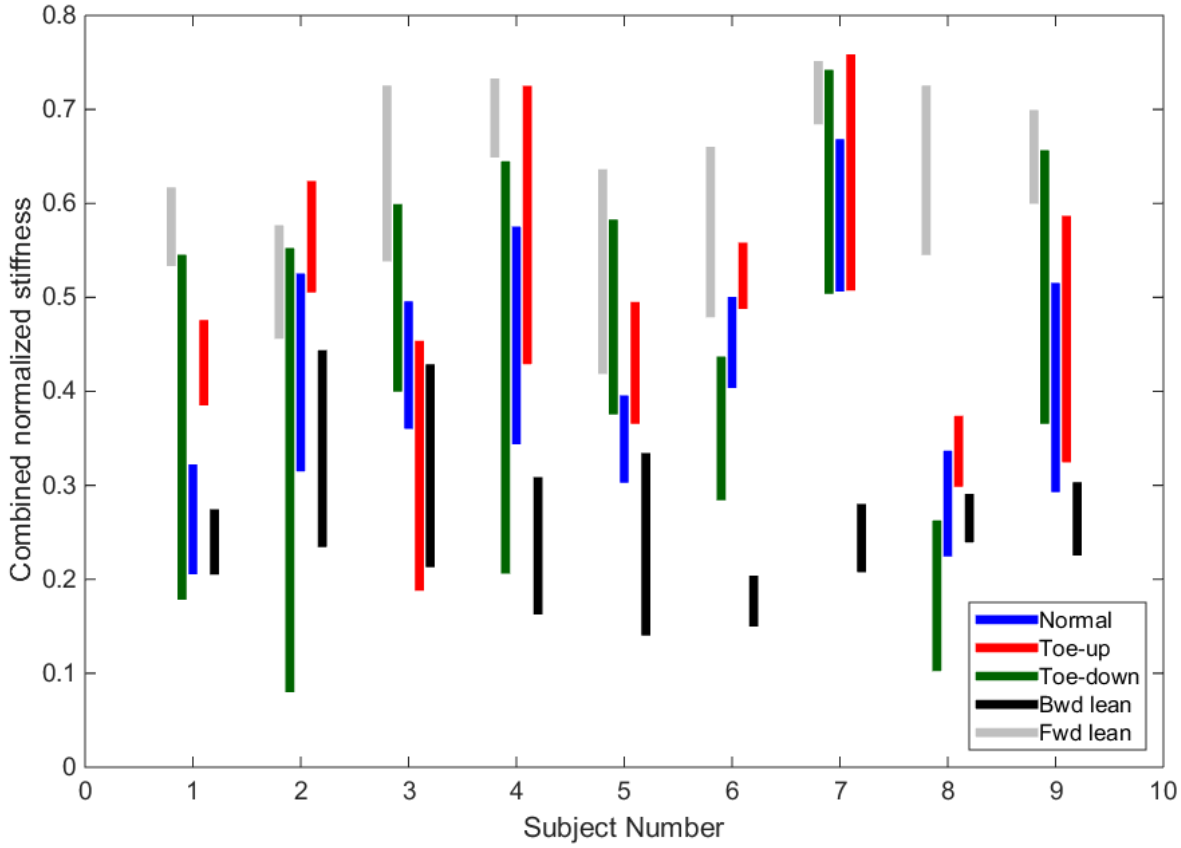

Figure 7.7 Range of combined normalized stiffness (left minimum stiffness + right minimum stiffness to left maximum stiffness + right maximum stiffness) for all subjects in normal standing, toe-up and toe-down experiments, and forward (shown by Fwd lean) and backward (shown by Bwd lean) lean.

The Kruskal-Wallis test revealed that K_{EIM}^{N} was significantly different among the operating conditions ($p<0.000$). Figure 7.8 demonstrate the results of the post hoc Dunn-Sidak multiple pairwise comparison with an adjusted significance level ($\alpha = 1-(1-0.05)^{\frac{1}{10}} = 0.005$). Intrinsic stiffness was greater in forward lean than all other conditions while stiffness during backward lean was smaller than in all other conditions. Toe-up stiffness was significantly higher than the stiffness in normal standing, but no different from toe-down standing. The stiffness in normal standing and toe-down conditions were not different.

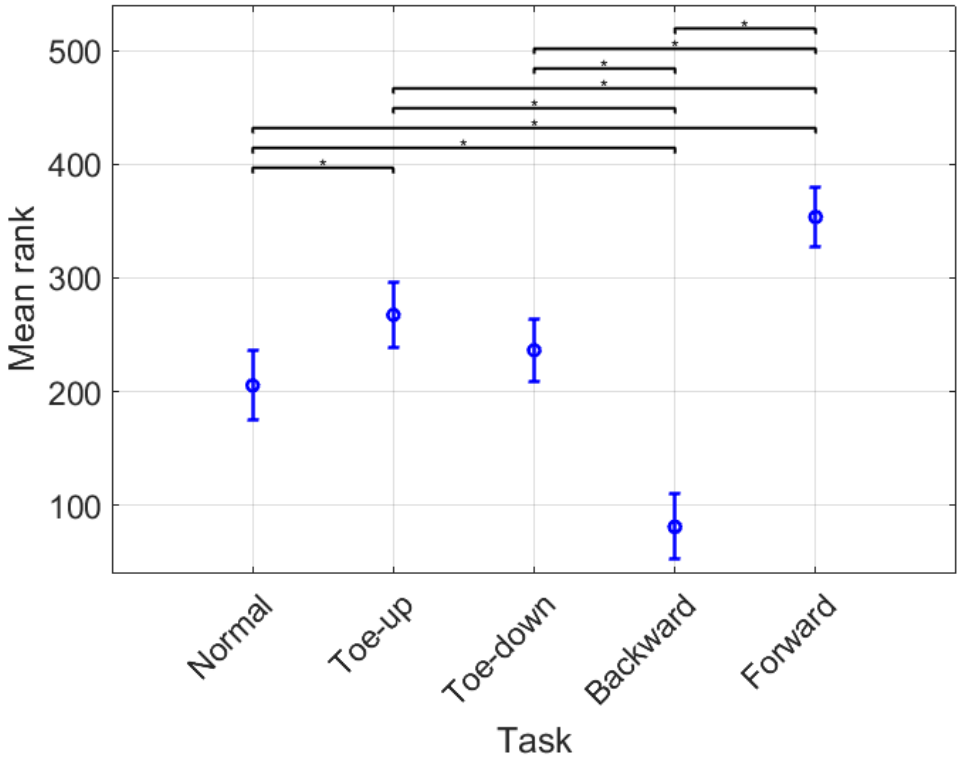

Figure 7.8 Results of Dunn-Sidak multiple pairwise comparison of normalized low frequency stiffness. The circles show the mean ranks for each operating condition and the bars show two standard errors. The black horizontal lines and stars indicate pairs of operating condtions, which were significantly different ($p \leq 0.005$).

7.5 DISCUSSION

The first important finding of this study was the observation that the modulation of muscle activation and intrinsic stiffness with COP followed three patterns. The most common pattern was activation of TS; this was observed in all cases in forward lean, and on the majority of cases during normal, toe-down and toe-up standing. The second most common pattern was alternating activation of TA and TS; this was used mostly in backward lean, but was also observed in some toe-up and toe-down standing trials. The least common pattern was activation of TA; this was observed only in backward lean trials. The pattern of ankle intrinsic stiffness modulation with COP varied consistently with the muscle activation patterns. Thus the TS-only pattern was associated with a monotonic, increasing stiffness-COP relationship; the TA-TS pattern was associated with a

less systematic stiffness-COP relationship (decreasing-increasing trend); and the TA-only pattern was associated with a monotonic decreasing stiffness-COP relationship.

The second important contribution of this study was the quantification of ankle intrinsic stiffness across a range of postural operating conditions. The mean intrinsic stiffness was greatest (0.42-0.75) when the mean COP was close to the anterior limits of stability in forward lean and it was lowest (0.14-0.44) when the mean COP was close to the posterior limits of stability in backward lean. The mean stiffness value in the other three operating condition was between its two extremes, which were observed in lean experiments. Thus, in agreement with others [9-11, 40], the stiffness was never large enough to maintain stability by itself, but it could make a substantial contribution to postural control in some operating condition, such as forward lean (75% of the critical stiffness).

7.5.1 Intrinsic stiffness in inclined surface standing

We demonstrated that for each support surface angle, ankle intrinsic stiffness changed significantly with postural sway. Six participants used the TS-only pattern, in all surface inclinations; therefore, the intrinsic stiffness increased with COP anterior displacement. However, three subjects used the TA-TS pattern in all inclinations, resulting in a bell shape stiffness-COP profile.

The modulation of intrinsic ankle stiffness with support surface angle has not been previously documented extensively. Several studies did use prolonged standing on inclined surfaces to examine the adaptation of postural control to sensory inputs [264, 265, 270, 271], however, only two studies examined the effect of support surface angle on ankle stiffness [39, 272]. Thus, Sakanaka et al. reported that mean ankle intrinsic stiffness was significantly higher in toe-up than normal standing [39]. Our results are in agreement with Sakanaka's; as Figure 7.8 illustrates, mean ankle intrinsic stiffness in toe-up was larger than normal standing. Moreover, our results extends Sakanaka's by characterizing the pattern of modulation of stiffness with sway in toe-up standing. Sakanaka et al. also observed a significant increase in TA activity from normal to toe-up standing; however, they concluded that higher stiffness resulted only from increased stretch of TS muscles in toe-up standing and ignored the contribution of TA to the joint stiffness. However, our results showed that the pattern of TA activation and intrinsic stiffness were highly correlated.

Consequently, we believe that the increase in TA activation in toe-up standing contributes to the increased stiffness.

In a second study, Sasagawa et al. examined EMG of medial gastrocnemius and soleus [272] and found that it was greater in toe-down than toe-up. This is consistent with our results, illustrated in Figure 7.4 and Figure 7.5, which show that TS activity at the same COPs was higher in toe-down than toe-down. However, Sasagawa et al. did not estimate the intrinsic stiffness in the two inclined surface conditions. Thus, our results extended theirs by measuring the intrinsic stiffness directly during inclined surface standing. We showed that in toe-up and toe-down standing the intrinsic stiffness-COP had a monotonically increasing or decreasing-increasing relation, associated with two muscle activation patterns.

7.5.2 Intrinsic stiffness in lean

We demonstrated that all subjects used the TS-only pattern during forward lean. In addition, ankle intrinsic stiffness wa greatest for this task. Others have shown that stiffness increases from normal to forward lean conditions [10, 39, 213, 273]. Thus, Sinha and Maki used a system identification approach to show that mean ankle intrinsic stiffness increased almost two-fold from normal standing to forward lean [273]. Casadio et al. [10] and Sakanaka et al. [39] estimated the average stiffness from responses to transient perturbations and showed that the average stiffness significantly increased from normal standing to forward lean [10].

Our estimates of total K_{EIM}^{N} during forward lean ranged 0.42-0.75, while Casadio et al. [10], and Sakanaka et al. [39] reported average combined normalized stiffness (for both legs) of 0.86 and 0.81, respectively, while Sinha did not report the normalized stiffness value [273]. It is difficult to compare our values to these studies, as our results document how stiffness changes with COP, whereas the previous work presented only average values. Nonthelese, our estimates of low frequency stiffness seem close and consistent with these studies.

Our results demonstrated that the TA-TS pattern predominated in backward lean with the TA-only pattern used infrequently. These muscle activation patterns were associated with a decreasing-increasing or all-decreasing trend for the stiffness-COP relationship. Similar activation patterns

have been associated with increased stiffness and stability in ankle [274], spine [275, 276], and knee [277].

Our results demonstrate that the predominant use of TA in backward lean was associated with lower intrinsic stiffness. This is consistent with the results of Sakanaka et al. who reported a decrease in the average stiffness in backward lean, compared to normal standing [39]. The lower stiffness was likely due to the fact that TA has a physiological cross-sectional area much smaller than the TS muscles [278].

7.5.3 Functional importance of intrinsic stiffness modulations

We demonstrated that the relative importance of ankle intrinsic stiffness varies across postural operating conditions, which are associated with different COP positions and muscle activation patterns. The highest combined stiffness (ranging 0.42-0.75) was observed in forward lean, where TS-only activation pattern was used. This seems functionally appropriate, since in forward lean, COP is located close to the anterior limits of stability and there is a high possibility of fall; high intrinsic stiffness would help reject perturbations that would endanger stability.

In contrast, during backward lean, where the TA-TS or TA-only pattern was used, the stiffness was the lowest (ranging 0.14-0.44) of any operating condition. In this situation, the COP was close to the posterior limits of stability, and there was high risk of falling. Despite this, intrinsic stiffness was low, which would not seem to be functionally appropriate. This may partly explain why it is more difficult to stand with backward lean and why people rarely do so.

In the normal, toe-up, and tow-down conditions, the stiffness was greater than backward and less than forward lean, which appears functionally appropriate, since the COP is farther from the limits of stability.

Finally, within any postural operating condition, ankle intrinsic stiffness increased as the COP moved towards the limits of stability (or as the margin of stability decreased). Thus, the change of stiffness within each condition seems functionally appropriate.

In summary, changes of intrinsic stiffness in different standing operating conditions must be accounted for in any attempt to quantify the interplay between the intrinsic and neural contribution to postural control.

CHAPTER 8 IDENTIFICATION OF CENTRAL, STRETCH REFLEX, AND INTRINSIC CONTRIBUTIONS TO HUMAN POSTURAL CONTROL

Chapter 6 and 7 provide a thorough investigation of ankle intrinsic stiffness in standing, while the current chapter deals with the identification of central and stretch reflex, i.e. active, contributions to human postural control. Thus, it introduces a novel multiple-input, single-output, closed-loop method to identify EMG-torque dynamics of ankle muscles in standing. The model provides an estimate of central and stretch reflex torques and their contributions to human postural control. It also provides an estimate of the noisy intrinsic torque by removing the active torque from the total measured torque. The application of the method to the experimental perturbed standing data of nine healthy subjects demonstrates that it performs very well. The relative contributions of central, stretch reflex, and intrinsic components, as well as, the contribution of individual muscles to postural control will be provided. Finally, it will be demonstrated that stretch *reflex EMG-torque* and *central EMG-torque* of ankle plantar-flexors dynamics are different. We will shortly submit this chapter to IEEE Transactions on Neural Systems and Rehabilitation Engineering (IEEE TNSRE) Journal.

Identification of Central, Stretch Reflex, and Intrinsic Contributions to Human Postural Control

Authors: Pouya Amiri, and Robert E Kearney

Journal: To be submitted to IEEE Transactions on Neural Systems and Rehabilitation Engineering Journal

8.1 ABSTRACT

Human postural control requires continuous modulation of ankle torque to stabilize the inherently unstable upright stance. The torque is generated by two components: active contributions, due to central control and stretch reflex mechanisms, and passive mechanisms, due to the joint intrinsic mechanical stiffness. Identifying the role and contribution of each component is difficult, since their effects appear together and standing is controlled in closed-loop conditions. This article presents a novel multiple-input, single-output, closed-loop method to identify central and stretch reflex EMG-torque dynamic relations and use them to determine the contributions of the two pathways. These are then removed from the total torque to estimate the intrinsic contribution. The method uses EMGs as its inputs, requires no kinematic data, and has few parameters, resulting in robust performance. Nine subjects stood on a standing apparatus, while subjected to uncorrelated bilateral perturbations of ankle position. The application of the method to the experimental data of the subjects showed that the model performed very well to capture the active contributions, with a variance accounted for of 84.0±5.5%. Thus, the active contributions to ankle torque were much larger than passive contributions. In addition, ankle plantar-flexors produced the largest portion of the active torque through central control, although there was large inter-subject variability in the relative contributions of the medial and lateral gastrocnemius, and soleus among the subjects. In contrast, activation of the ankle dorsi-flexor, was not necessary for postural control and was significant in only a few cases. Reflex contributions of the plantar-flexors also displayed large inter-subject variably; it was significant in half of the subjects. Finally, EMG-torque dynamic relation of ankle plantar-flexors were different for central and stretch reflex activation: central EMG-torque dynamics had higher DC gain and smaller bandwidth. The study provides the tools to understand the contribution of different components to postural control. Moreover, it demonstrates that the contributions of the different components, including central,

stretch reflex, and intrinsic stiffness vary greatly among the subjects. While the overall plantar-flexors central torque was consistently the highest in all subjects, the contribution of individual muscles differed. In addition, stretch reflex torques could be substantial and contribute significantly to postural control. Thus, any investigation of postural control must account for the heterogeneity of the different components contributing to the task.

8.2 INTRODUCTION

In standing, the human body resembles an unstable inverted pendulum, subject to internal and external perturbations. Yet, ankle muscles generate corrective forces that effectively resist the perturbations and allow humans to keep their balance easily. These stabilizing forces are generated by three mechanisms: 1) Central activation of the muscles, evoked in response to the information regarding body position and orientation, transduced by vision, vestibular, and somatosensory systems [19]; 2) Peripheral spinal activation of the muscles, generated by stretch reflexes; 3) Ankle intrinsic stiffness, the joint mechanical resistance to the movement, generated by visco-elastic properties of the joint active muscles, connective tissues, and inertial properties of the limbs [77]. Quantifying the contribution of each component is key to understanding healthy and impaired postural control and provides the possibility to objectively design interventions, targeted to address deficiencies in postural control for those with balance problems [50]. Quantifying central, stretch reflex, and intrinsic contributions to postural control is difficult, because all the contributing systems act simultaneously, while only global variables, describing the overall behavior of postural control (including body kinematics, ankle torque, and muscle electromyography (EMG)) can be recorded. Therefore, methods must be developed to manipulate these signals and extract information regarding each sub-system.

Active ankle torque, the torque generated by neural activation, is the sum of central and stretch reflex components. EMG provides a measure of the activation of muscles; therefore, it may feasible to estimate the active torque from EMG measurements. If so, the intrinsic torque could be determined as the residual after the active torque is subtracted from the total ankle torque. The possibility of using EMG for this decomposition has been recently shown by Pasma et al. [13], who showed that intrinsic parameters could not be estimated reliably without using EMG. Others who studied postural control without using EMG, have been unable to generate reliable estimates of intrinsic stiffness [32, 49, 279].

A few studies have used EMG to study human postural control [13, 32, 47, 273]. These generally examined the EMG response to external perturbations to identify the central controller in standing. However, they did not quantify the contribution of central and intrinsic controllers in terms of their generated torques. Moreover, these studies used the EMG from only one muscle [47, 273] or assumed that ankle plantar-flexors and dorsi-flexors have the same activation dynamics [13, 32]. In addition, a fixed, second-order structure for EMG-torque dynamics were used, which may not be the case in standing.

The role of stretch reflex in human postural control has been generally investigated by examining the reflex EMG amplitude, evoked by imposed rotation of ankle joint or electrical stimulation to the tibial nerve [198, 206-208, 280]. However, reflex EMG provides little information about the mechanical contribution of the stretch reflex mechanism to human postural control, and its relation with torque can be complex and nonlinear. Indeed, it has been shown that with increased muscle background activation, reflex EMG amplitude becomes saturated while the torque amplitude starts to diminish [7].

This study presents a multiple-input, single-output (MISO), closed-loop Box-Jenkins identification method that decomposes the ankle torque in standing into its central and stretch reflex components. The model also estimates the noisy intrinsic torque. The method has several advantages: 1) it estimates different EMG-torque relations for ankle plantar-flexors, dorsi-flexors, and stretch reflex, 2) it models the contribution from all major ankle muscles, 3) does not assume an *a-priori* second order structure for EMG-torque relations, 4) does not need kinematic measurements of posture, and 5) directly quantifies the mechanical contribution of central and stretch reflex mechanisms to human postural control.

The paper is structured as follows: section 8.3 provides details of the experimental procedure for the perturbed standing experiments, as well as, a model of balance control and the details of the identification. Section 8.4 presents the results, and section 8.5 discusses the findings.

8.3 METHODS

8.3.1 Subjects

Nine subjects (6 males), aged between 18-40 years, with no history of neuromuscular disease participated in the study. Subjects gave written consent to the experiments, which had been approved by McGill University's Research Ethics board.

8.3.2 Standing Apparatus

Figure 8.1 illustrates the apparatus, comprising two pedals, driven by servo controlled electro-hydraulic rotary actuators (Rotac 26R-2 1V), able to apply independent bilateral position perturbation to subjects' ankles during standing experiments [246, 281]. High performance rotary potentiometers (Maurey Instruments 112-P19) measured foot angle (θ_f), the pedal angle with respect to the horizontal. Each pedal had four load cells (The Omega™ LC302-100), which measured the vertical forces, which were used to calculate the ankle torque and the position of center of pressure (COP) relative to the ankle axis of rotation [37].

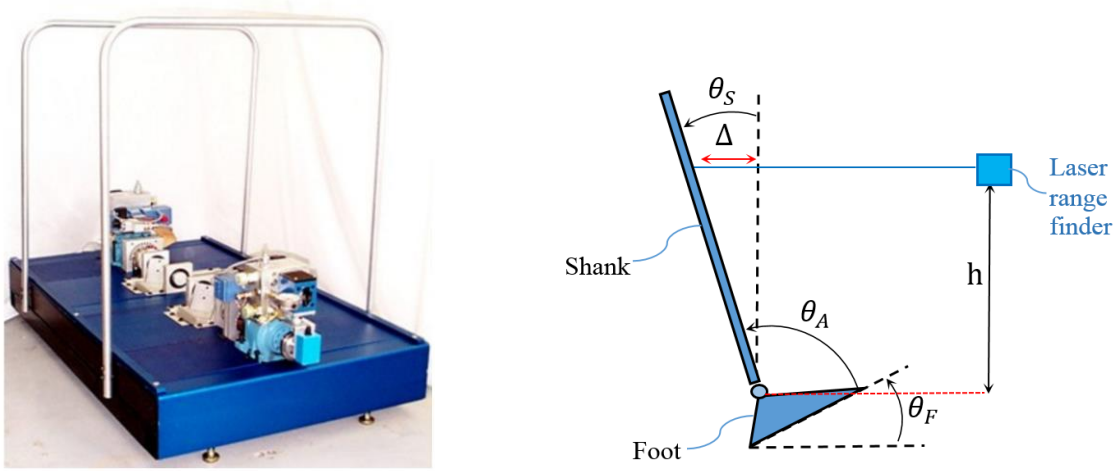

(A) (B)

Figure 8.1 (A) Experimental standing apparatus, (B) The shank angle (θ_s) was estimated by measuring its linear displacement (Δ) and dividing it by the range finder height, h, above the ankle axis of rotation; foot angle (θ_f) was measured by the actuator potentiometer; ankle angle (θ_A) was obtained using (8.1).

The ankle angle is the angle between the foot and shank, given by:

$$\theta_A = \theta_F - \theta_S \tag{8.1}$$

where θ_S is the shank angle with respect to the vertical. The shank angle was determined by measuring the horizontal displacement of a point on each shank using a high performance laser range finder (1302-100, Micro-epsilon), giving an angular resolution greater than 0.01 degree [245]. By convention, we took ankle dorsiflexion angle and torque as positive; a right angle between the foot and shank was taken as zero ankle angle.

8.3.3 EMG Recording

Surface EMG activity from the four major muscles about the ankle joint were measured. These included: Tibialis Anterior (TA), and the three muscles comprising the triceps surae (TS): medial and lateral gastrocnemius (MG and LG), and soleus (SOL). Single differential Delsys electrodes (with an inter-electrode distance of 1 cm) were placed at the locations suggested by the Seniam project [250]. Electrode locations were verified by having the subjects perform manual resistance tests, while observing the EMG waveforms on an oscilloscope to ensure there was a high signal to noise ratio and minimal cross talk. EMG signals were amplified, using a Bagnoli amplifier with an overall gain of 1000 and band-pass filtered between 20-2000 Hz.

8.3.4 Data Acquisition

To prevent aliasing, all signals were filtered at 486.3 Hz and then sampled at 1 KHz using 24 bit/8 channel, simultaneous-sampling, signal acquisition card (NI 4772, National Instrument). All subsequent analysis was performed in MATLAB. All signals were decimated to 100 Hz by first low pass filtering the signals with a zero-shift 6th-order Chebyshev Type I filter with a cut-off frequency of 40 Hz and a passband ripple of 0.05 dB and then down-sampling to 100 Hz.

8.3.5 Experiments

Participants stood comfortably on the standing apparatus, looking forward, with their hands at their sides, and mean foot angle set to 0 degree. The actuators applied uncorrelated random position perturbations to both ankles simultaneously. We used pseudo random binary sequences (PRBS) as perturbations, where pedal position switched between two values (-0.01, 0.01 rad) at random

multiples of 200 ms. The PRBS input has a wide bandwidth, is unpredictable, and provides the greatest input power for a given amplitude [74, 77]. The perturbation switching interval and amplitude were selected to ensure sufficient input bandwidth for the identification, to keep the mean absolute velocity low enough to avoid suppressing reflex responses [76], and to minimize postural disturbances. Two trials, each lasted two minutes, with a different realization of the PRBS input were acquired for each subject. The trials were separated by at least two minutes of rest to prevent fatigue.

8.3.6 Human Postural Control Model

Figure 8.2 illustrates a model of human postural control, considered in this study. The human body acts as an unstable inverted pendulum that must be stabilized in the presence of internal (e.g. respiration) and external disturbances (e.g. a push), and destabilizing gravity torque. Stabilizing torques are generated by ankle muscles due to three main mechanisms:

1- Intrinsic torque (tq_{int}): due to ankle intrinsic stiffness, which acts as soon as there is a change in joint angle.

2- Active torque (tq_{act}): due to neural activation of muscles, mediated through two feedback mechanisms:

A- Stretch Reflex torque (tq_r): generated by phasic activation of TS muscles, generated by stretch reflex mechanism, when the muscle spindles are stretched. The stretch reflex has a short delay (δ_r) of about 40 ms [74].

B- Central torque (tq_c): generated by activation of muscles, in response to the information about body position and orientation. The central torque is usually assumed to act with a neural delay (Δ_c) of 100-200 ms [1, 115, 235].

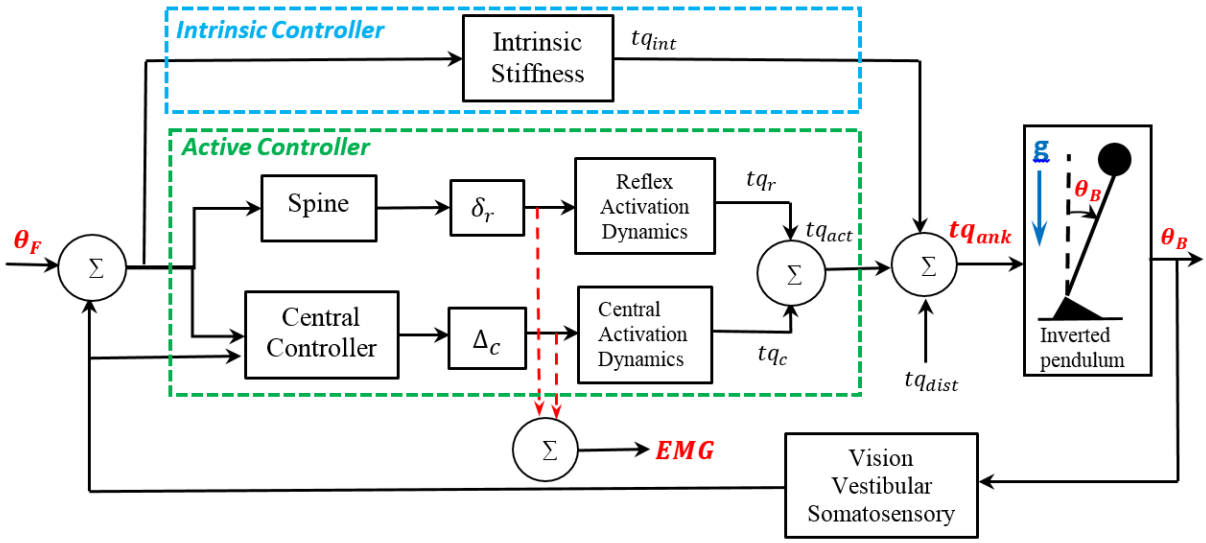

Figure 8.2 Postural control model: the body, an inverted pendulum, is unstable and subject to destabilizing gravity torque (g) and disturbances (tq_{dist}); therefore, corrective muscle forces are generated by a central controller, stretch reflexes, and intrinsic mechanical stiffness to achieve stable upright posture. The stretch reflex and central contributions are captured by muscle EMG activity. The red signals are measured, whereas the black signals cannot be measured.

It is difficult to determine the contribution of each component to the control of posture, since the individual torques cannot be measured. Only the total ankle torque (tq_{ank}), which is the sum of the intrinsic (tq_{int}), active (tq_{act}), and disturbance torque (tq_{dist}), and measurement noise (n_m) can be measured:

$$tq_{ank}(t) = tq_{act}(t) + tq_{\text{int}}(t) + tq_{dist}(t) + n_m(t) \tag{8.2}$$

However, active torque is directly related to EMG [282-284]. Therefore, the measured ankle torque can be considered as comprising an active torque generated in response to the EMG inputs, and a residual, composed of intrinsic and disturbance torques, as well as, measurement noise, which is not generated by muscle activation. Therefore, the EMG can be used to estimate the active torque, sum of central and stretch reflex torque, and removing it from the total torque provides a noisy estimate of the intrinsic torque.

The active torque is the sum of the active torque generated by all muscles about the ankle:

$$tq_{act}(t) = \sum_{i=1}^{4} r_i\left(\underline{\theta}(t)\right) f_i\left(\underline{\theta}(t), \underline{\dot{\theta}}(t), a_i(t)\right) \tag{8.3}$$

where r_i and f_i and are moment arm and force of muscle i, where i can be MG, LG, SOL, and TA. a_i is the muscle activation, and $\underline{\theta}$ and $\underline{\dot{\theta}}$ are the joint angle and velocity vectors.

Muscle moment arms (r_i) are nonlinear static functions of the angles of the joints they span; and muscle forces, f_i, are nonlinear dynamic functions of muscle length, muscle contraction velocity, and activation [211]. TA and SOL span the ankle, whereas LG and MG are bi-articular muscles and span both ankle and knee angles. We recently demonstrated that joint movement was small during our perturbed standing experiments (< 0.08 rad~4°) [37]. Consequently, it can be assumed that the ankle and knee angles are constant. With this assumption (8.3) is greatly simplified, since the muscle moment arms become constant and muscle force is then a function of activation only.

In addition, it has been shown that muscle force (torque) can be predicted from rectified EMG using a low-pass dynamic relation for low activation levels (which is the case in standing) [284]. Therefore, we assumed that the muscle forces to be described by linear transfer functions (TF). Consequently, (8.3) in Laplace domain was transformed into:

$$TQ_{act}(s) = \sum_{i=1}^{4} r_i TRF_i(s) E_i(s) \tag{8.4}$$

where s is Laplace operator, TRF_{i} is the transfer function of the i^{th} muscle, with its rectified EMG, E_i, as input. We made the following additional assumptions:

1- The EMG-force relations of the three TS muscles (MG, LG, and SOL) are the same.

2- The EMG-force relationship for central and reflex activation of TS muscles are different. So that separate TFs must be used to model the two activations.

3- There is no reflex torque in TA [76].

With these assumptions, (8.4) becomes a multiple-input single-output (MISO) system:

$$TQ_{act}(s) = G^c_{TS}(s)E^c_{TS}(s) + G^r_{TS}(s)E^r_{TS}(s) + G^c_{TA}(s)E^c_{TA}(s) \tag{8.5}$$

where G^c_{TS}, G^r_{TS}, and G^c_{TA} are the TFs between central TS input (E^c_{TS}), reflex TS input (E^r_{TS}), and central TA EMG (E^c_{TA}) to torque. The central and reflex TS inputs are given by:

$$\begin{aligned} E^c_{TS}(s) &= w^c_1 EMG^c_{SOL}(s) + w^c_2 EMG^c_{MG}(s) + w^c_3 EMG^c_{LG}(s) \\ E^r_{TS}(s) &= w^r_1 EMG^r_{SOL}(s) + w^r_2 EMG^r_{LG}(s) \end{aligned} \tag{8.6}$$

where w^c_j and w^r_j are the gains of the individual muscles (accounting for maximum isometric force and moment arm). EMG^c_{SOL} and EMG^r_{SOL} are the central and reflex EMG of SOL (similarly defined for MG and LG). MG did not generate reliable reflex responses; therefore, only SOL and LG were used to estimate the reflex input.

8.3.7 EMG decomposition

The measured EMG of TS muscles is the combination of their central and reflex activities. Therefore, to generate the inputs in (8.6), each muscle's EMG must be decomposed into its reflex and central components.

During standing, central activation of TS muscles appears continuously with postural sway. When a perturbation is applied, the central activity does not change any time sooner than 100 ms afterwards [13]. In contrast, reflex activity occurs in bursts, following only dorsi-flexing perturbations and reaches its peak at 40 ms after the pulse peak velocity, lasting for a total of approximately 80 ms [165]. Therefore, we assumed that central activation of TS muscles does not change during reflex responses. Thus, we located the reflex activities by finding the peak velocity of dorsi-flexing pulses. Then, to estimate the central EMG, samples of the EMG for 80 ms after the peak velocity were replaced with a randomly permuted activity of the same muscle, 80 ms right before the peak velocity. Finally, the estimated central EMG was subtracted from the total EMG and the residual was used as an estimate of the reflex EMG. Note that the reflex EMG was zero everywhere, except in 80 ms periods after peak dorsi-flexing pulses of the PRBS perturbations.

8.3.8 Identification

In standing, sensory inputs regarding body movements are used to generate stabilizing muscle forces, which in turn generate body movements, sensed by the sensory systems. Consequently, the postural control is performed under closed-loop conditions. In such conditions, direct identification between muscle EMG and ankle torque generates unbiased results, only if the prediction error method (PEM) is used [59]. PEM will give unbiased estimates from closed-loop data with an arbitrary feedback, provided the model parameterization is flexible enough. Therefore, we selected MISO Box-Jenkins structure illustrated in Figure 8.3, since it provides separate dynamics for the system and noise. Since the identification was performed using discrete experimental data, we formulated the model (8.2) in discrete time as:

$$tq_{ank}(t) = H^c_{TS}(q)e^c_{TS}(t) + H^c_{TA}(q)e^c_{TA}(t) + H^r_{TS}(q)e^r_{TS}(t) + \frac{C(q)}{D(q)}e(t) \tag{8.7}$$

where q is the shift operator, and $e(t)$ is a white random sequence. $H^c_{TS}(q)$, $H^c_{TA}(q)$, and $H^r_{TS}(q)$ are discrete TFs of TS central, TA central, and TS reflex dynamics. The term $C(q)/D(q)\,e(t)$ captures the intrinsic torque, internal disturbances, and noise.

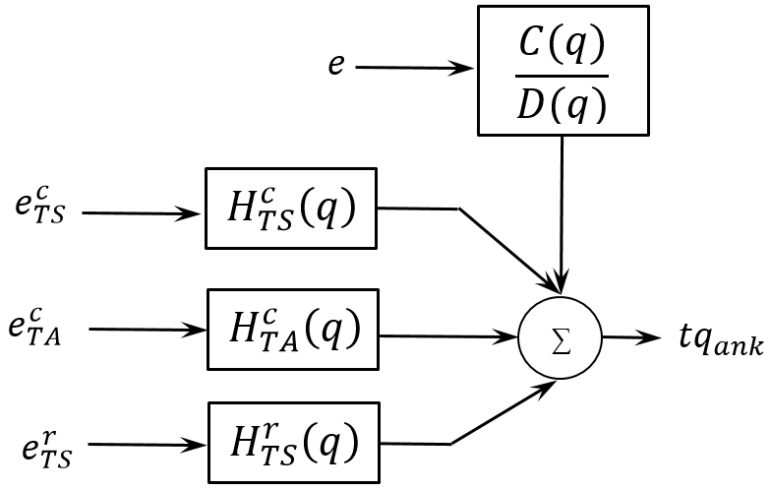

Figure 8.3 Box-Jenkins structure for central and reflex EMG-torque relationships

The weights in (8.6) and the TFs (the number of poles and zeros and parameters) in (8.7) are unknown. This results in a large search space for the model. Consequently, to reduce the complexity of the search, we performed the identification in three steps:

1- We used optimization to determine the weights in (8.6), assuming a fixed structure (i.e. number of poles and zeros) for all TFs.
2- Using these the weights, we identified the TFs in (8.7), where many possible model structures for the TFs were estimated and the best model was selected.
3- The TFs identified in step 2 were used to re-optimize the weights in (8.6) to minimize the error of model predictions. The obtained weights were used to find the final TFs.

Re-identifying the TFs using the final inputs, obtained in step 3 above, did not improve the model in terms of the goodness of fit. Therefore, we stopped at 3rd step and did not iterate more. The detailed steps are provided below.

(1) Identification of the input weights

To determine the weights in (8.6), we first normalized the EMG of each muscle to its total RMS activity in the trial. We then assumed that the structure (number of poles and zeros) of all the TFs in (8.7) were known and fixed; and performed optimization to find the weights that minimized the RMS error between the measured torque and the model prediction. The optimization was done using a gradient descent search using MATLAB fmincon solver with five random initial conditions and the weights giving the lowest objective function were selected. The optimization used MATLAB Identification Toolbox to find the TFs corresponding to the weights in each step of the search.

By trial and error, we found that a Box-Jenkins structure, where EMG-torque TFs had 3 poles and 3 zeros and the noise model had 10 zeros and 25 poles, provided good torque prediction for all subjects. This model structure may have been over-parameterized, but it provided good prediction accuracy and therefore, was effective to find the optimal weights for the inputs in the first step.

(2) Identification of EMG-torque transfer functions

In the second step, we identified EMG-torque and noise TFs using the obtained inputs and the output. This required selecting the number of poles and zeros for each TF, not known *a-priori*. Previous studies of postural control assumed the EMG-torque relationship to be a 2nd order continuous TF [32, 47]; however, our pilot results demonstrated that more complex structures could be required. To examine this, since the identification was done using sampled data, we first identified discrete TFs and at the end, transformed them to continuous TFs to investigate the model structures.

Therefore, we estimated the parameters for all the possible combinations of EMG-torque discrete TFs with 2 or 3 poles, and the number of zeros from 0 to the number of poles. We found that having more number of poles and zeros did not improve model performance. Noise model having 0-10 zeros and 5-25 poles were examined to ensure that it was flexible enough to deliver unbiased estimates of the dynamics. This resulted in the identification resulting in 118,041 models. We selected three candidate models, using the following three criteria:

1- Percentage variance accounted for (%VAF)

$$\%VAF(M) = 100\left(1 - \frac{\sum_{t=1}^{N}\left(tq_{ank}(t) - \hat{tq}(t,M)\right)^2}{\sum_{t=1}^{N} tq_{ank}^2(t)}\right) \tag{8.8}$$

2- Minimum description length (MDL)

$$MDL(M) = \left(1 + \frac{M\log(N)}{N}\right)\sum_{t=1}^{N}\left(tq_{ank}(t) - \hat{tq}_{act}(t,M)\right)^2 \tag{8.9}$$

3- Akaike information criterion (AIC)

$$AIC(M) = N\log\left(2\pi\sum_{t=1}^{N}\left(tq_{ank}(t) - \hat{tq}_{act}(t,M)\right)^2\right) + 2M + N \qquad (8.10)$$

Where M is the number of model parameters, $N = 12000$ is the number of samples, and $\hat{tq}_{act}$ is the total predicted active torque. We used the three criteria, since they do not necessarily select a unique model; the %VAF picks the model with the best fit; however, MDL and AIC account for both the fit and model complexity. It is believed that MDL favors fewer parameters over the goodness of the fit, while AIC favors the goodness of the fit.

For the %VAF criterion, the models were sorted, the first being the one with the highest %VAF. Then, the %VAF sorted models were examined for several necessary conditions:

1- All EMG-torque TFs must be stable.

2- The power spectrum of $\hat{e}$ should be near white and it should have no correlation with any of the inputs.

3- The frequency response (FR) and impulse response function (IRF) of all EMG-torque models must have a stable low pass behavior.

4- The noise model must be inversely stable, since it is used in one-step ahead prediction of PEM and an unstable noise model will cause the method to fail.

The model with the highest %VAF that satisfied these three conditions, was selected as the %VAF candidate model. A similar procedure was performed to find AIC and MDL candidate models; one must note that in these cases, the better models have lower AIC and MDL values.

To select the final model from the three candidate models (selected using VAF, MDL, AIC), data from a new trial were used; the three models used the EMG of the new trial to predict the torque and the model with the highest %VAF and lowest number of parameters was selected as the final model.

In some cases TA or/and stretch reflex contribution to the torque were very small. In such cases, the identification did not generate reliable estimates of the corresponding dynamics. This also might have affected the estimates of TS central EMG-torque dynamics. In such a cases, the

identification procedure was repeated using only those inputs, which made significant contributions to the output.

(3) Re-identifying the input weights

After finding the best model in step 2, we used the identified TFs and performed optimization using MATLAB fmincon function again to re-identify the weights, so that the RMS of error between the measured torque and the model prediction was minimized. The obtained weights and corresponding TFs were then used to generate the final output of the model.

The discrete identified TFs were converted to their continuous representation using the inverse of the bilinear transform, by substituting the shift operator as:

$$q = \frac{2 + st_s}{2 - st_s} \tag{8.11}$$

where t_s is the sampling time, which is 0.01 s after the decimation.

Some poles and zeros of the continuous TFs may not contribute to the dynamic response due to their high frequency. Therefore, we modified the continuous time TFs by removing high frequency poles and zeros. We then compared 1) the FR of the modified TF with that of the initial continuous TF, and 2) the simulated output of the initial and modified TF. Any continuous pole or zero with no significant effect on the FR and simulated output was discarded and the modified TF was considered the final continuous TF. The FR of the final TFs were determined by substituting $S = j\omega$ in a frequency range $\omega = 0.1 - 50$ Hz.

8.4 RESULTS

8.4.1 Experimental data

Figure 8.4 shows 15 seconds of the data from typical trials from two subjects S1L and S4L[3]. The ankle angles have two components: fast transients due to foot perturbations and low frequency

[3] Sip stands for p (L=Left, R=Right) side of subject i (i=1,…,9).

movement of shank due to body sway. The range of ankle angle dispalcement was less than 0.08 rad (<4.6°), verifying our assumption of small joint movement, used to tranfrom (8.3) to (8.4).

Figure 8.4C&D illustrates that the SOL had continuous baseline activity for both subjects. Peaks in SOL EMG, showing burst of reflex activity (happening after dorsi-flexing pulses) are evident in S1L, whereas reflex EMG was not evident in S4L. Figure 8.4E&F show that MG was intermittently active for both subjects; moreover, it is evident from Figure 8.4E that even for S1L, who had large SOL reflex EMG, the MG did not generate reliable reflex activity in response to all dorsi-flexing pulese. As shown in Figure 8.4G&H, LG had little central activity in both subjects, while its reflex activity was similar to SOL. Figure 8.4I&J show that S1L had large TA activity, whereas S4L did not use TA. Finally, Figure 8.4K&L show the measured ankle torque, where two components are evident: the modulation of the torque with body sway, and large downward peaks, showing reflex torque (the reflex torques are much more evident in S1L).

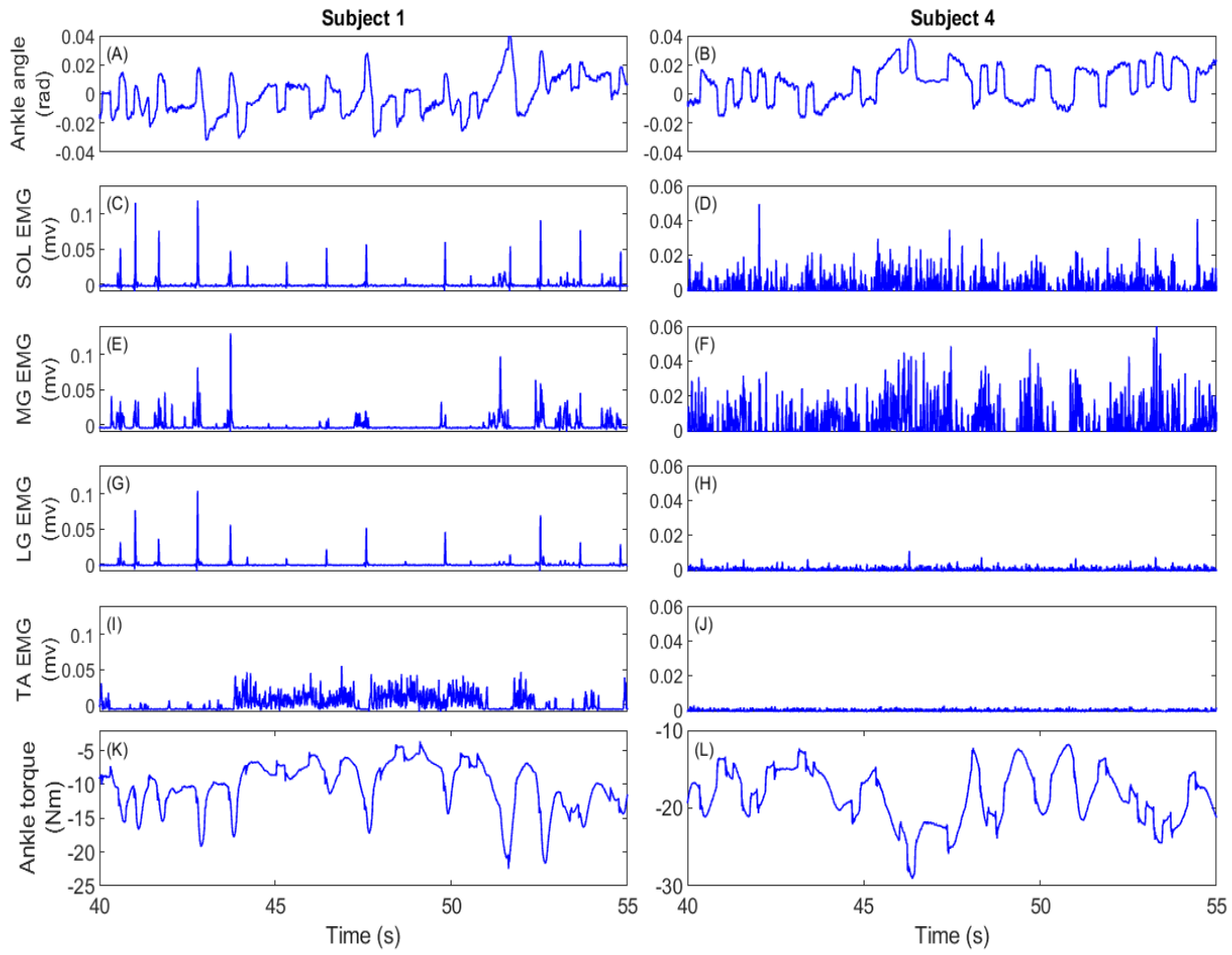

Figure 8.4 Sample experimental data; (A, B) ankle angle, (C, D) SOL rectified EMG, (E, F) MG rectified EMG, (G, H) LG rectified EMG, (I, J) TA rectified EMG, (K, L) ankle torque; left column shows the data of S1L, and right column shows the data of S4L.

8.4.2 EMG decomposition

Figure 8.5 illustrates the results of decomposing of TS EMGs into its central (red) and stretch reflex (blue) components. If the decomposition performed well, there should be no correlation between the central and reflex EMG components, since the reflex response has a delay of 40 ms after the pulse, while the delay is greater than 100 ms for the central response. Figure 8.6 shows that this was the case, as the correlation between the central and reflex components activities were negligible for all TS muscles of S1L.

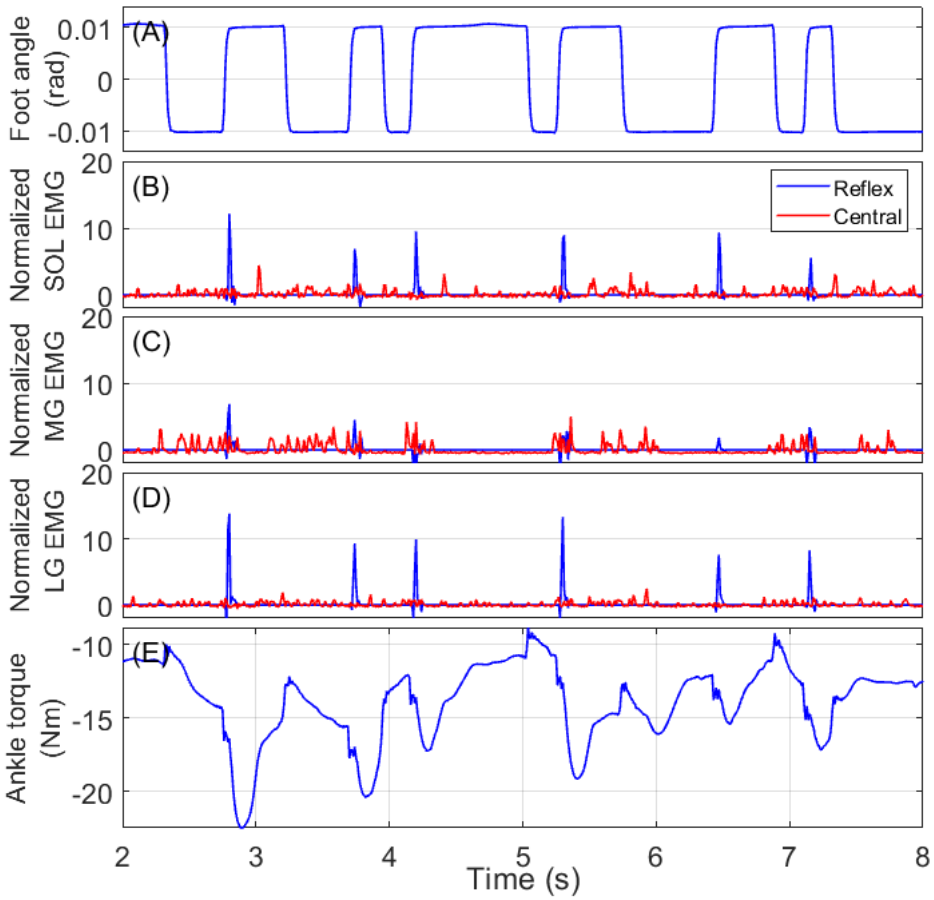

Figure 8.5 Decomposition of TS muscles EMG to central and reflex components for S1L; (A) foot angle, (B) SOL, (C) MG, and (D) LG normalized EMG, (E) ankle torque. Blue shows estimated reflex EMG, and red shows the estimated central EMG.

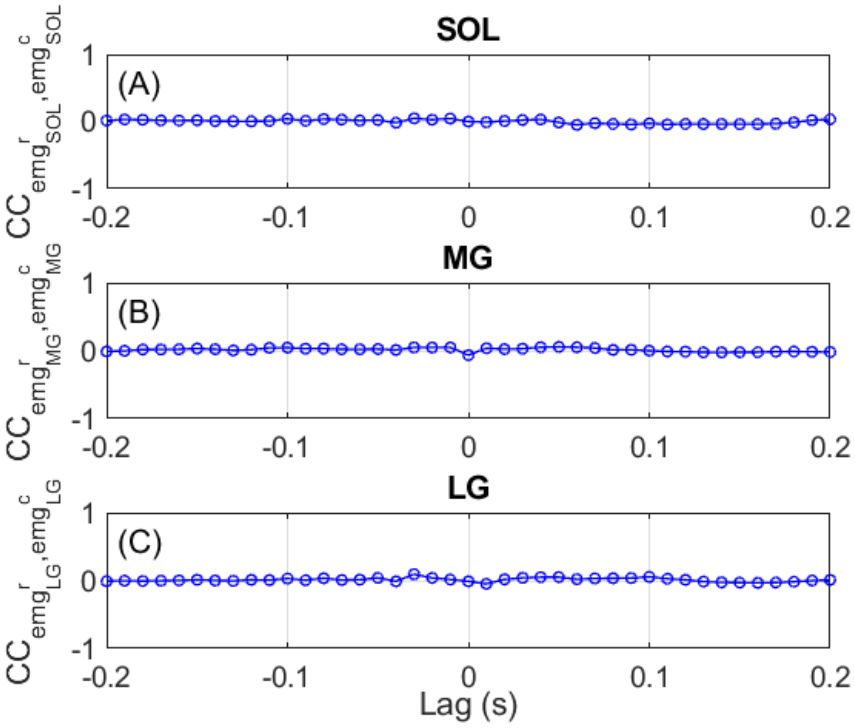

Figure 8.6 Cross-correlation between the estimated reflex and central EMG for (A) SOL (B) MG (C) LG of S1L. CC stands for cross-correlation.

8.4.3 Typical identification results

Figure 8.7 shows the results of the identification procedure applied to the data from Figure 8.4 (S1L). Figure 8.7A shows the ankle angle. The three input are shown in Figure 8.7B: e^c_{TS}, the TS central input, Figure 8.7C, e^r_{TS}, the TS reflex input, and Figure 8.7D, e^c_{TA}, the TA central input. The central input signals show that TS and TA were intermittently active; when one was active, the other was silent. Figure 8.7D shows TS reflex input, comprising bursts, lasting 80 ms, with the peaks at 40 ms after dorsi-flexing pulses.

Panels E-G in Figure 8.7 illustrate active torque components, predicted by the identified model and the inputs. The TS central torque (tq^c_{TS}, Figure 8.7E), generated the largest torque, while TA central torque (tq^c_{TA}, Figure 8.7F) and TS reflex torque (tq^r_{TS}, Figure 8.7G) were smaller, but still contributed significantly.

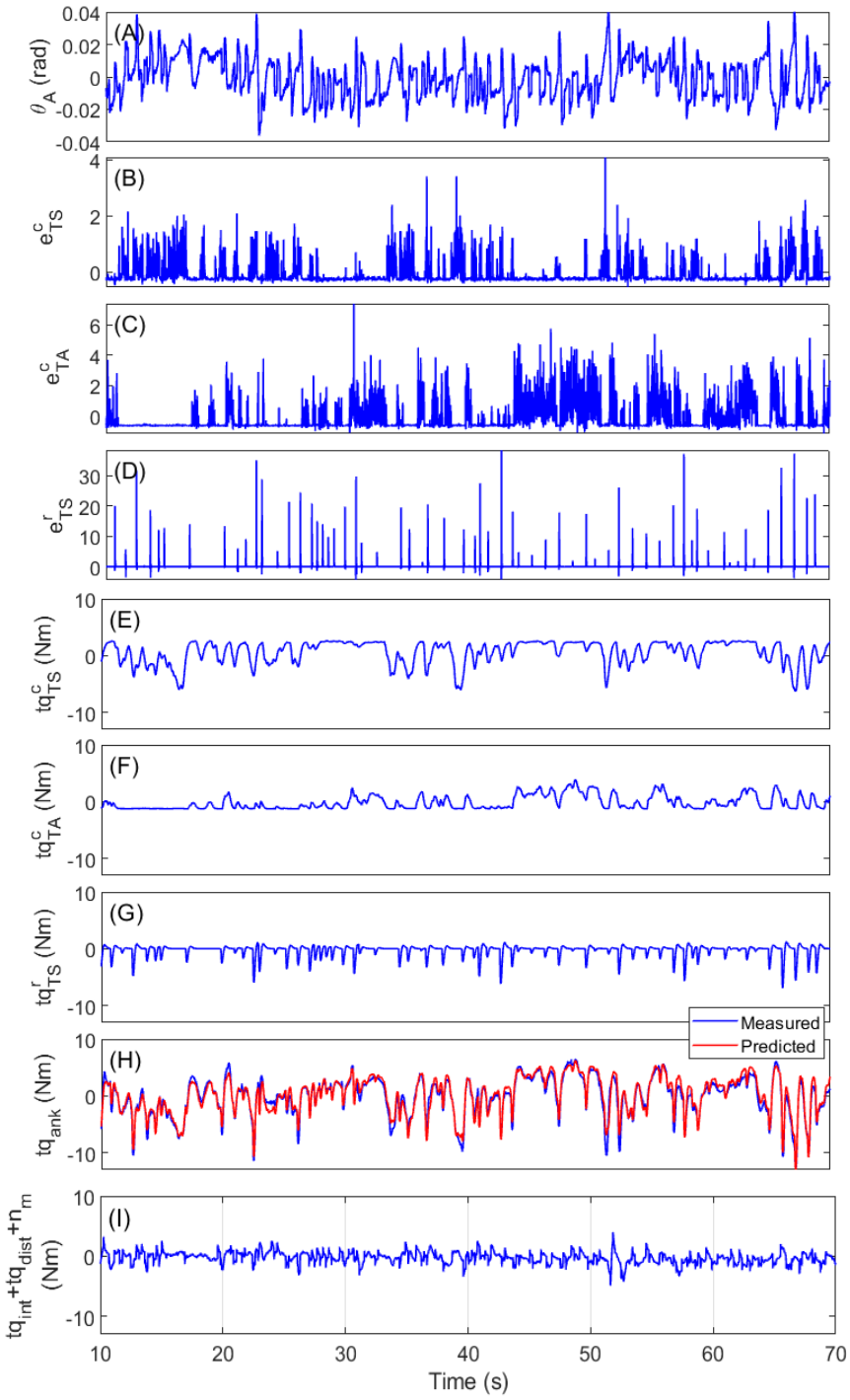

Figure 8.7 Identification results for S1L (A) ankle angle, (B) TS central input, (C) TA central input, (D) TS reflex input, (E) predicted TS central torque, (F) predicted TA torque, (G) predicted TS reflex torque, (H) measured torque (blue) and total predicted active torque (red), (I) residual torque.

Figure 8.7H shows the total predicted active torque (red) superimposed on the measured torque (blue) and the similarity of the two signals; the predicted active torque accounted for 92.8% of the measured torque variance.

Figure 8.7I illustrates the residual, $C(q)/D(q)\ e(t)$ in (8.4), which accounted for 9.1% of the torque variance. Figure 8.8 shows the residual torque and ankle angle in an expanded time scale for 5 seconds. The residual torque has an intrinsic component, in response to each pulse perturbation; and, another component, which is correlated with the movement of the ankle in between pulses, which seems to be the passive torque. In addition, there is additive noise.

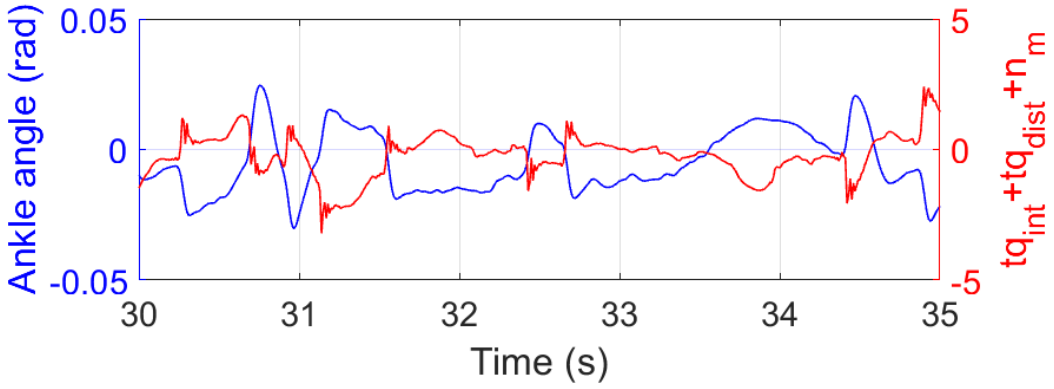

Figure 8.8 Ankle angle vs. residual torque in an expanded time scale for S1L.

Figure 8.9 shows the elements of the TS central torque for S1L. It is clear that MG and LG explained the highest and lowest torque variance. The %VAF of the MG torque relative to the ankle total torque was 55.4%, while it was 16.0% for SOL, and 3.3% for LG.

Figure 8.10 shows the FR of the identified EMG-torque TFs for S1L. These had low pass behavior, with corner frequencies 1.1 Hz, 1.4 Hz, and 3.1 Hz for G_{TS}^{c}, G_{TA}^{c}, and G_{TS}^{r}. Moreover, the phases started at 0˚ for all TFs and then decreased at higher frequencies.

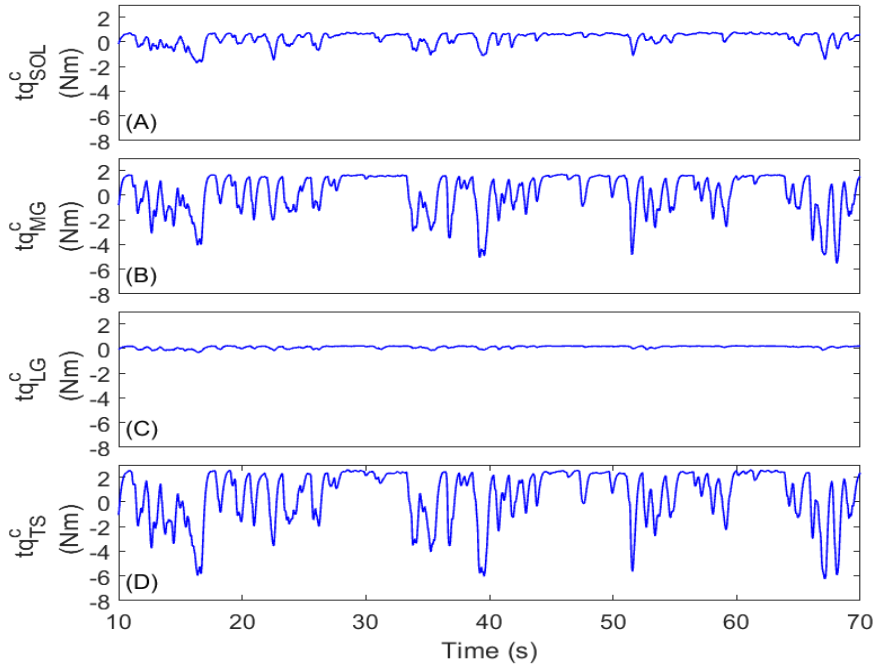

Figure 8.9 TS muscle central torques for S1L; (A) SOL, (B) MG, (C) LG, and (D) total TS central torque.

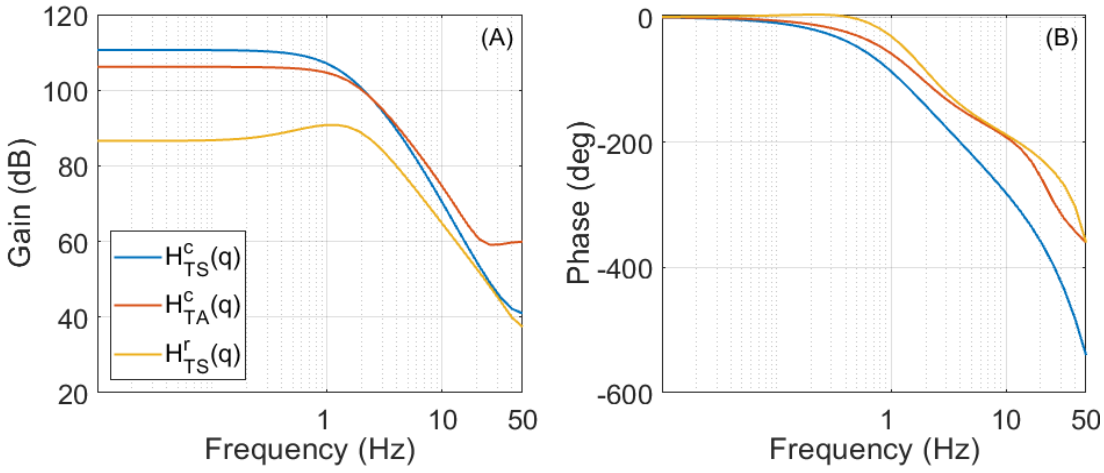

Figure 8.10 FR of the identified transfer functions for S1L, (A) Gain, (B) Phase.

8.4.4 Identification results for all subjects

Table 8.1 demonstrates the number of poles and BW of the continuous TFs and %VAF for the predicted active torques of all subjects. Zeros were never significant, therefore, are not shown in table. Note that the data for S6R was discarded, since it was corrupted by a large, low frequency noise, whose origin we could not determine. The table shows that the identified models predicted the active torque very accurately; the %VAF was 84.0±5.5% (mean ± standard deviation) for all subjects (min=72.0%, max=92.8%).

Table 8.1 Identification results for all subjects; S stands for subject; L and R shows left and right ankles. p and BW show the number of poles and bandwidth of the identified TFs. %VAF correspond to the the total active torque.

S		G_{TS}^{c}		G_{TA}^{c}		G_{TS}^{r}		%VAF
		p	BW (Hz)	p	BW (Hz)	p	BW (Hz)	
1	L	3	0.9	2	1.4	3	3.1	92.8
	R	2	1.2	3	0.5	2	2.5	85.2
2	L	3	0.4	-	-	2	1.5	81.7
	R	3	0.7	-	-	3	1.5	87.3
3	L	2	1.0	2	0.6	3	1.0	82.6
	R	3	0.6	2	2.7	2	2.7	86.1
4	L	3	0.6	-	-	2	1.9	89.8
	R	3	0.5	-	-	2	2.2	80.2
5	L	3	0.8	-	-	2	2.5	79.1
	R	2	0.7	-	-	3	2.3	79.2
6	L	2	1.0	-	-	3	2.8	80.5
7	L	2	0.5	-	-	2	2.1	78.7
	R	2	0.5	-	-	2	2.0	72.0
8	L	2	0.7	3	1.0	3	2.4	91.5
	R	2	0.9	2	1.0	2	1.7	88.0
9	L	3	0.3	-	-	2	1.1	84.8
	R	3	0.6	2	0.6	2	1.8	88.6

Table 8.1 also shows that the EMG-torque TF structures differed among the subjects and even between the legs of the same subject. The number of poles ranged 2-3, showing there was large

variation among the cases. The noise model structure was also variable, with zeros and poles ranging 0-9 and 5-15. In addition, TA transfer function was reliably estimated in only 7/17 cases, showing TA contribution to the torque was small in the other 10 cases.

All EMG-torque relations showed low-pass behavior similar to Figure 8.10, but with different BW. The BW of G_{TS}^{c} was 0.7±0.2 Hz, whereas the BW of G_{TS}^{r} was 2.1±0.6 Hz, showing central EMG-torque dynamics were slower than stretch reflex EMG-torque dynamics. Moreover, similar to Figure 8.10, the phase of all TFs for all subjects started at 0 and then dropped to larger lags at higher frequencies.

8.4.5 Central, stretch reflex, and intrinsic contributions

Figure 8.11A compares the %VAF of the total active and residual torques for all subjects. It is clear that the active torque accounted for most of the total ankle torque. The %VAF of the left and right active torques were 84.6±5.5% and 82.8±6.3%. Similar results as Figure 8.8 was observed for all subjects.

Figure 8.11B compares the %VAF of tq_{TS}^{c}, tq_{TA}^{c},and tq_{TS}^{r} relative to the total ankle torque for all cases. It is clear that there was substantial difference among active torque components, not only between the subjects, but also between the ankles of the same subject. tq_{TS}^{c} contributed the most with a mean %VAF of 71.8±8.4% and 63.0±12.8% for the left and right ankles.

The contribution of tq_{TS}^{r} was generally less than tq_{TS}^{c}; however, in some cases it was quite large, such as S8R, where it had a %VAF of 32.8%. For cases with significant reflex contributions, the minimum and maximum %VAF were 2.5% and 23.2% for the left ankle, and 13.0%, and 37.5% for the right ankles. TA torque explained large variation of ankle torque through central activation in 7/17 cases.

Figure 8.11C summaries the contributions of SOL, MG, and LG to the ankle torque. MG accounted for the highest torque variation in 11/17 cases; the %VAF of MG torque was 57.6±12.5% and 39.9±16.8% for the left and right ankles.

SOL and LG contributed the highest in the remaining 6 cases. In 4/17 cases, SOL contributed the most to the torque, while LG was responsible for the highest torque variation in 2/17 cases.

This showed that there was high variability among the subjects in using their individual TS muscles for postural control.

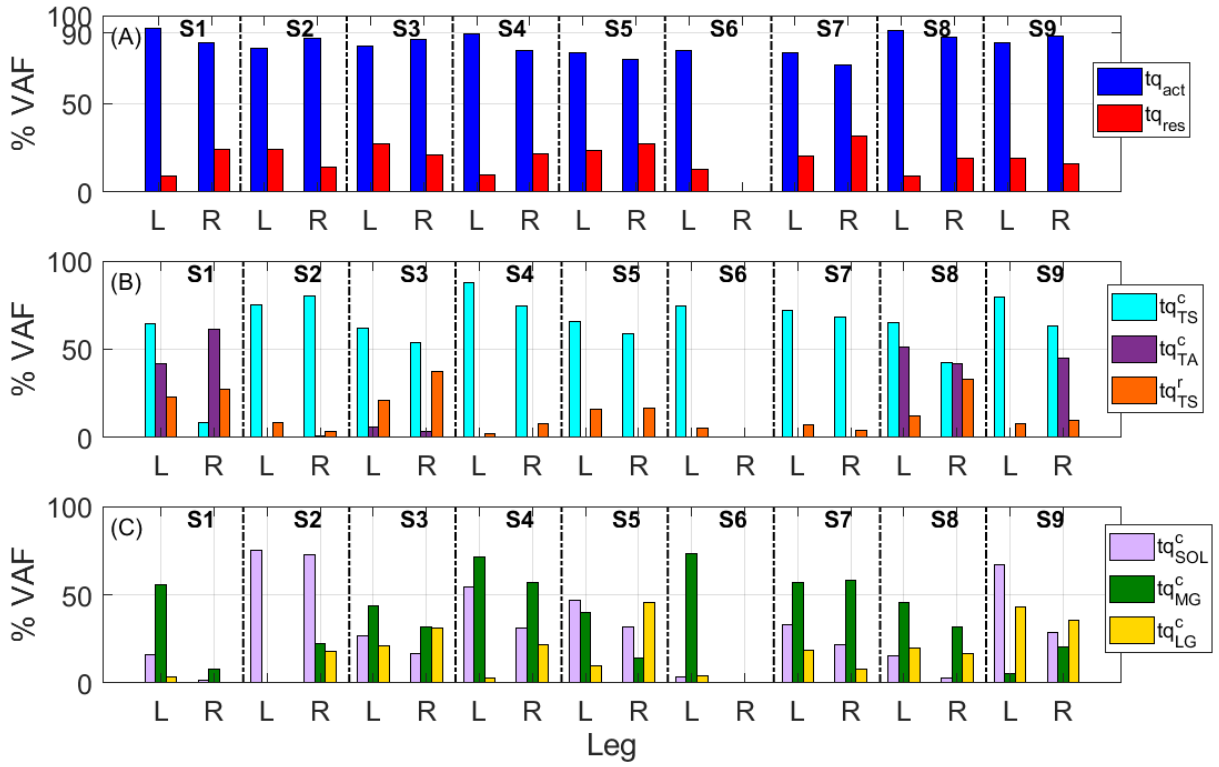

Figure 8.11 %VAF of the preidcted torque components; (A) %VAF of the total active (blue) and the residual (red) torques, (B) %VAF of the TS central (tq^c_{SOL}, cayan), TA central (tq^c_{TA}, purple), and TS reflex (tq^r_{TS}, orange) torque; (C) %VAF SOL (light purple), MG (green), and LG (yellow) central torque; L and R show left and right sides. Si (i=1,…,9) shows subject i.

8.4.6 Soleus reflex and central EMG-torque dynamics

Figure 8.12A shows the BW of SOL central and reflex EMG-torque relations of all cases. It is evident that reflex EMG-torque dynamic had a higher BW than central EMG-torque relation. The median of reflex BW was around 2.1 Hz, while it was 0.7 Hz for the central dynamics.

Figure 8.12B shows that DC gain of SOL central EMG-torque dynamics were always larger than that of reflex EMG-torque relation (note that these these are the gains from the dynamic relation between raw rectified EMG to corresponding torques). The median DC gains were 117.4

and 105.8 dB for central and reflex TFs of the left ankle and 113.0 and 103.5 dB for those of the right ankle.

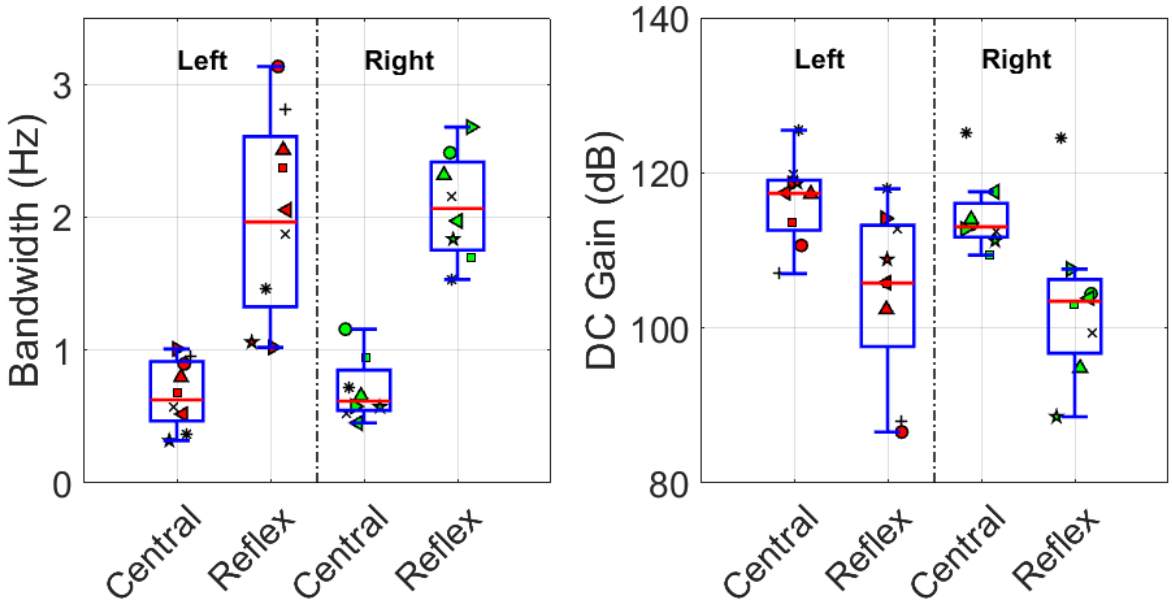

Figure 8.12 Comparison of SOL central and reflex BW and DC gain; (A) BW, and (B) DC gain; the results are shown for left and right ankles. The individual points show the values for the individual cases, whereas identical markers belong to the same case.

8.5 DISCUSSION

We developed a novel method to decompose the central and stretch reflex contributions to ankle torque during postural control. The method takes as the EMGs from the ankle muscles as inputs, without the need of any kinematic data. The model had few parameters, resulting in a robust estimation performance. Applying this method to data from normal standing led to the following main findings:

1. Active contributions to ankle torque were much larger than that from intrinsic stiffness (%VAF=84.0±5.5% vs. 16.3±4.2%).
2. The active torque was mostly generated by ankle plantar-flexor muscles, while TA, the ankle dorsi-flexor muscle, also contributed to a few cases (7/17).
3. Stretch reflex contributions were significant in almost half of the subjects.

4. Plantar-flexors EMG-torque dynamics were different for reflex and central activation; reflex activation dynamics had higher bandwidth but lower DC gain.

8.5.1 EMG decomposition

Our method performed well to decompose TS muscles EMG to central and reflex components; this was shown with the lack of short latency cross-correlation between the two components. In addition, the reflex activity is generally much larger than central activity; consequently, our assumption for the decomposition probably did not affect the estimated EMG components substantially. Even if, the decomposition generated some input noise, the closed-loop identification approach takes care of the noise.

We initially used interpolation to estimate central EMG in the reflex period; however, this method did not generate good results; because, first, the EMG was very noisy and interpolation caused negative central EMG values in some cases; second, high correlations between the reflex and central EMGs reduced the performance of identification.

8.5.2 Identification performance

Using only EMG of ankle muscles, without the need of any kinematic data, our method generated a set of inputs and TFs with few parameters that predicted the active torque with a %VAF of 84.0±5.5%. We observed minimal cross-correlation between the inputs and e in (8.7). Thus, high %VAF and low input-e correlation showed that the assumptions of our method are valid.

In addition, the residual showed the expected characteristics of the intrinsic response and was consistent with the movement of the ankle [7, 38, 285]. Finally, visual inspection of the FR of the identified EMG-torque relations showed the expected low pass behavior, which was consistent with other studies [273, 283, 284, 286, 287].

Parametric models can be criticized, because they require *a-priori* knowledge of the model structure. We addressed this drawback by identifying a variety of model structures, then selecting three candidate models using three widely used model selection criteria, and choosing the final model by cross-validation using the data of a new trial. This procedure helped to objectively select

a structure from a large pool and avoid *a-priori* assumptions, often used when parametric identification is used.

A few studies of postural control have examined ankle EMG-torque dynamics in standing [32, 47, 273, 288]. However, they usually estimated the experimental closed-loop FR of postural control system and then estimated the EMG-torque dynamics indirectly by fitting a parametric model to the experimental FR [32, 47, 288]. Therefore, it is hard to compare the performance of our model with theirs. Only one study by Sinha and Maki reported that their model predicted ankle torque in standing with a %VAF between 52-95% in four subjects [273]. These %VAF were obtained for the contribution from the sum of both intrinsic and active components, and the model inputs were EMG of EMG and kinematics. In contrast, for our model, which used EMG of 4 major ankle muscles and no kinematics, the generated %VAF by the only active contributions (and not the intrinsic contributions) was much higher. This showed it is important to include all ankle muscle activity to model torque variation in standing.

In addition, our results showed that the subjects employed a variety of TS muscle recruitment strategies for postural control, i.e. the contribution of individual muscles in the generation of ankle torque was very subject-specific. Therefore, we believe that any model of postural control must include all the major ankle muscles. Previous work has failed to do so. Thus, Sinha and Maki [273] used only MG, and Fitzpatrick et al. [47] used only SOL. Two other studies used a weighted sum of all ankle muscles as their input [32, 288]. However, they assumed that the EMG-torque dynamics of TS and TA muscles were the same, while our results showed their low-pass dynamics relation were clearly different; most importantly, they had very different DC gain and corner frequencies.

8.5.3 EMG-torque dynamics

We selected the parametric structures of EMG-torque relations objectively using three performance criteria. Our results showed that 2^{nd} or 3^{rd} order discrete EMG-torque TFs with variable number of zeros are needed. However, conversion to continuous TFs revealed that the zeros were at high frequencies and so contributed little to the dynamic response of the TFs. It was the poles that determined the dynamics of the continuous TFs. Therefore, the final EMG-torque TFs were 2^{nd} or 3^{rd} order with no zeros. Previous studies of standing generally assumed an *a-priori*

fixed 2nd order structure for EMG-torque relation [32, 36, 47, 288] based on the results provided during controlled isometric contractions [283, 289, 290]. Our results clearly demonstrate that such an assumption may result in inaccurate estimate of EMG-torque dynamics of muscles in standing.

The estimated EMG-torque relations were low pass in nature; however, they had different gain and phase properties. We found that G_{TA}^{c}, G_{TS}^{c}, and G_{TS}^{r} had bandwidth equal to 1.0±0.7 Hz, 0.7±0.2 Hz, and 2.1±0.7 Hz. The only few studies of postural control, which used EMG to estimate the torque showed similar values: 1.48 Hz [288], 0.95-1.43 Hz [32], 0.95 Hz [36], and 1 Hz [47]. It should be noted that these values were reported where it was assumed that all ankle muscles share the same dynamics [32, 288] or only one muscle contributes to postural control [47]. Other studies in isometric conditions reported TA BW to be less than 2 Hz [284], or 2.4-3.6 Hz [290], and TS BW to be 1.27-1.91 [283] and 2-2.5 Hz [290]. Although, these values are similar to ours, the results must be interpreted with care, because estimated EMG-torque dynamics in a task is dependent the contraction BW [284], depth of torque modulation [283], and ankle joint position [290], which may be different in controlled isometric experiments.

8.5.4 Central and reflex EMG-torque dynamics

Our results demonstrated that EMG-torque dynamics were different for central and stretch reflex activations of TS muscles in human postural control. The stretch reflex EMG-torque dynamics had a higher BW, but lower DC gain. These differences could be the due to differences in motor-unit (MU) recruitment between central and stretch reflex mechanisms. Slow muscle contractions are characterized by initial recruitment of slow small MUs, followed by recruitment of larger MUs, having faster contraction time [291]. However, during rapid ballistic muscle contractions, the large fast MUs are recruited at a much lower force threshold [292, 293]. The reduction in the activation threshold is specifically significant in muscle with a large proportion of type I slow twitch fibers, such as SOL [294]. Therefore, it is expected that rapid reflex activation engages large fast MUs with lower force thresholds, and therefore, generates output forces with smaller gain, but higher BW.

Differences in motor-unit synchronization could also explain the differences. Yao et al. investigated the effect of motor-unit synchronization on surface EMG and the resulting isometric muscle force, using a computer model of muscle. They demonstrated that motor-unit

synchronization increased the amplitude of the EMG, but not the force [295]. Consequently, higher level of synchronization in stretch reflex compared to central control with similar torque magnitudes may have resulted in a lower DC gain for stretch reflex dynamics.

Consistent with our results, Toft et al. showed that the EMG-torque DC gain was lower for stretch reflex than for voluntary contractions [75, 296]. In addition, Genadry et al. and Sinkjaer et al. showed that increased rate of muscle force development resulted in higher BW of EMG-torque dynamics [282, 283]; this is similar to the stretch reflex mechanism, where the force is generated quickly and EMG-torque relation has a high BW.

8.5.5 Central, reflex, and intrinsic contributions to ankle torque

Our results demonstrated that active mechanisms contributed more than intrinsic stiffness to the ankle torque for the postural control. Active torque accounted for an average 84% of the total torque generated, whereas the residual, which provided an estimate of noisy intrinsic torque, explained the rest of the measured torque.

Several studies of postural control have reported that due to its small contribution to postural control, intrinsic stiffness is difficult to estimate in standing [1, 32, 49, 56]. It was recently shown that EMG provides the means to separate the active and intrinsic contributions [13]. Some studies estimated the intrinsic stiffness from the response to transient perturbations in standing, reporting normalized stiffness values 64% [10], 91% [9], 15-55% [37]. However, these values do not provide a representation of generated intrinsic torque, because the intrinsic torque depends on the joint movement. Only one study found an average active contributions of 74% using EMG, whereas the remaining torque was attributed to the intrinsic mechanism [273].

Our results demonstrated that the muscle recruitment strategy varied among subjects. In most cases, the TS central contribution to the total ankle torque was highest, where MG generated the most torque, while SOL and LG contributed significantly. TA was generally silent, but in some individuals contributed significantly to the torque.

Individual muscle contributions to postural control have been rarely quantified. Few studies used only one muscle's EMG [47, 273] or even when used all muscles, provided no indication of muscles mechanical contribution to the ankle torque [13, 32]. Sinha and Maki used EMG of MG

and kinematics to model both intrinsic and central torque and reported %VAF between 52-95%; however, did not show the contribution of the individual components; Kiemel et al. showed that gastrocnemius muscles generated the highest coherence with visual perturbations [32]. In addition, consistent with our results, TA was reported to be silent mostly and sometimes active [32, 47, 273], with small contributions in most cases [32, 47].

Our results demonstrated that the stretch reflex contribution to control was quite variable among the subjects. Although, the reflex torque was not present for some subjects, in some cases, it made large contributions up to 37.5%. This shows that stretch reflex torque could be significant and potentially have important role in the postural control. It was previously shown that the stretch reflex could contribute significantly to the ankle torque in supine conditions [7, 74]; however, to the best of our knowledge, this is the first study to quantify the mechanical contribution of stretch reflex to human postural control. This is important, since stretch reflex has been generally investigated by examining its EMG amplitude in TS muscles (evoked by Hoffman-reflex or fast ankle rotations) in standing [198, 207, 208]. This method may generate misleading results, since EMG does not quantify the mechanical contribution of stretch reflex to ankle torque and may even have a different trends from its corresponding torque [7, 74, 212]. Future work should focus on the functional importance of stretch reflex in the postural control by further investigation into its role and effect on postural stability, similar to what was shown by Nashner for long latency stretch reflex in standing [114].

8.6 CONCLUSIONS

We developed a method to decompose the ankle torque to its central, stretch reflex, and intrinsic contributions in human standing. The application of the method to the experimental data of healthy individuals showed that active contributions were much higher than passive contributions, and were mostly generated by central control of plantar-flexors; whereas, dorsi-flexors and stretch reflex contributions were also significant in some individuals. Moreover, we found that ankle plantar-flexors responds differently to central and stretch reflex activations, probably due to differences in motor-unit recruitment strategies. The study provides the tools and basis for systematic study of standing and demonstrates that a correct understanding of postural control requires accounting for the large heterogeneity in the contribution of the different elements.

CHAPTER 9 DISCUSSION AND CONCLUSIONS

This chapter provides a summary of the objectives and accomplishments of this thesis, followed by a discussion of their significance and original contributions. The chapter ends with some recommendations for future work.

9.1 SUMMARY OF ACCOMPLISHMENTS

The overall objectives of this thesis were to:

1. Develop a method to identify ankle intrinsic stiffness in standing, while accounting for its change with postural sway.
2. Use the new method to estimate ankle intrinsic stiffness and characterize its behavior in different postural operating conditions.
3. Develop a method to use ankle muscle EMGs, recorded during stance to decompose ankle torque into its central, stretch reflex, and intrinsic contributions.

Thus, in the first part of the thesis (Chapter 6 and 7), I developed a method to identify time-varying (TV) ankle intrinsic stiffness in standing and used it to estimate intrinsic stiffness in a range of postural operating conditions. The results demonstrated that in each postural condition, ankle intrinsic stiffness changed significantly with postural sway in a manner dependent on muscle activation patterns. Moreover, across operating conditions, the stiffness varied widely from very little to large values. In the second part (Chapter 8), I developed a closed-loop method to determine active (i.e. central and stretch reflex mechanisms) and intrinsic contributions to postural control. Details of each part are given.

I started my thesis work by developing a system to measure shank angles in standing. Estimation of ankle intrinsic stiffness in standing requires measurements of ankle angle. Our standing device was equipped with potentiometers to measure only pedal (foot) angles. Therefore, I built a system that used two high-resolution laser range finders to measure shank angles, which in combination with foot angles delivered bilateral ankle angles. The system measured shank angles with a resolution of less than 0.01 degree and performed well to capture the movement in both quiet and perturbed standing.

In Chapter 6, I developed a method to estimate TV ankle intrinsic stiffness in standing. The method estimates the intrinsic stiffness by determining the dynamic relationship between pulse perturbations of ankle position and the corresponding intrinsic torque responses. To account for the modulation of intrinsic stiffness with sway, the stiffness parameters were estimated for groups of responses with similar ankle background torque. Application of the method to the data from normal standing demonstrated that ankle intrinsic stiffness changed significantly (15-56% of critical stiffness) with the modulation of ankle torque, induced by postural sway. These changes were functionally appropriate: stiffness increased as the center of pressure (COP) moved anteriorly from ankle axis of rotation. However, the intrinsic stiffness was never large enough to provide postural stability by itself.

Chapter 7 extended the work by delineating how intrinsic stiffness changed with postural operating conditions. I used the method developed in Chapter 6 to estimate the intrinsic stiffness in five operating conditions: normal standing, toe-up standing, toe-down standing, backward lean, and forward lean. I showed that the mean value of ankle intrinsic stiffness varied with the operating condition: it was the highest in forward lean and lowest in backward lean. Moreover, the modulation of intrinsic stiffness within a postural operating condition was more complex than normal standing in Chapter 6. Thus, the intrinsic stiffness changed as a function of COP, in one of three patterns associated with distinct muscle activations. These include an increasing stiffness-COP relationship, associated with activation of triceps surae (TS) muscles, a less systematic stiffness-COP relationship (decreasing-increasing trend), associated with alternating activation of TS and tibialis anterior (TA), and finally, a decreasing stiffness-COP relationship, associated with activation of only TA. Finally, I demonstrated that ankle intrinsic stiffness vary in a large range across operating conditions, and consequently, the importance of its contribution depended on the operating condition. Intrinsic stiffness was small at intermediate COP positions (i.e. when COP was close to mid-point between the limits of stability) and so could make only modest contributions to postural control. However, the stiffness increased quickly as the COP approached the limits of stability where it contributed substantially to postural control.

The objective of Chapter 8 was to investigate the active contributions, generated by central control and stretch reflex mechanisms, to postural control. To do so, I developed a method that used EMG activity of ankle muscles to estimate the torques generated by central and stretch reflex

mechanisms. The method also generated an estimate of noisy intrinsic torque through its residuals (i.e. the different between the measured ankle torque and the predicted central and stretch reflex torques using the model). Thus, the model was a multiple-input, single-output Box-Jenkins structure with three dynamic relationships: *central EMG-torque* of ankle plantar-flexors, *central EMG-torque* of ankle dorsi-flexors, and *reflex EMG-torque* of ankle plantar-flexors. The intrinsic pathway was modelled as noise with a separate dynamic model. I used a multi-step identification approach to identify a variety of dynamic models and the final model was selected using three commonly used model selection criteria and cross-validation, using the data of a second experimental trial. The identified model then was used to predict the contribution of active contributions. The results showed that active mechanisms contributed, on average 85%, to the total ankle torque so that intrinsic contributions were small. Most of the active torque was generated through central activation of the plantar-flexors; stretch reflex contribution of the plantar-flexors was significant in half of the subjects. A few subjects also generated large torques through central activation of the dorsi-flexors. Moreover, there was large variation in the strategies that the subjects utilized to activate their plantar-flexors, i.e. the three TS muscles were used to different degrees by different subjects. Finally, I demonstrated that the *central EMG-torque* and *stretch reflex EMG-torque* dynamic relations of ankle plantar-flexors were different; the stretch reflex EMG-torque dynamics had a higher bandwidth and a lower DC gain.

9.2 DISCUSSION

This thesis aimed to investigate passive and active contributions to human postural control. Thus, in the first part, I characterized ankle intrinsic stiffness in standing, and in the second part, I developed methods to determine the active contributions.

Ankle intrinsic stiffness is an important element in human postural control. Indeed, it was initially proposed that intrinsic stiffness is adequate for postural control [17, 33]. However, many studies have shown that intrinsic stiffness is too small to maintain upright posture by itself. However, its contribution can be significant and simplify the control task [8-10, 15, 39, 40]. Nonetheless, the role and contribution of intrinsic stiffness to postural control is not completely understood. This is partly due to lack of appropriate methods to quantify ankle intrinsic stiffness in standing. Two approaches have been used to identify intrinsic stiffness in standing.

The first group of studies performed standing experiments with *continuous* mechanical perturbations of ankle positions, with the aim of characterizing different elements of human postural control, using linear time invariant identification methods. They modelled ankle intrinsic stiffness as controller with proportional and derivative terms with ankle position as input and determined the stiffness parameters. They found that ankle intrinsic stiffness contribution was small, between 10-15% [1]. Some studies even suggested that the intrinsic contribution was too small to allow the reliable estimation of the intrinsic stiffness and ignored it [32, 49, 56]. A second group of studies performed standing experiments using *discrete* mechanical perturbations of ankle position with the sole objective of estimating ankle intrinsic stiffness in standing. The approach consisted of the application of rapid pulse perturbations of ankle position and estimating the intrinsic stiffness as the dynamic relation between ankle position and ankle torque before there could be any active contribution due stretch reflex and central control. Numerous studies have employed this approach and determined the value of intrinsic stiffness in standing [8-10, 15, 39, 40]. Their results consistently demonstrated that ankle intrinsic stiffness was not sufficient to provide postural stability.

However, both groups of studies overlooked the possible modulation of ankle intrinsic stiffness in standing. There is ample evidence that ankle intrinsic stiffness changes dramatically with ankle operating conditions, defined by mean ankle angle and mean ankle torque [4-7]. Both ankle torque and angle change significantly with postural sway in standing. Consequently, it is likely that intrinsic stiffness changes with postural sway. Therefore, these modulations need to be investigated.

Moreover, there is lack of information regarding the modulation of ankle intrinsic stiffness when the operating conditions of standing change. There has been much emphasis on the importance of the sensory systems in stance control, as revealed by their contributions to challenging postural tasks, such as lean [262-264], inclined surface standing [264-266] and load carriage [267, 268]. However, the intrinsic contributions to these conditions have been assumed constant and/or insignificant.

Together Chapter 6 and 7 answered two important questions: (i) how does intrinsic stiffness change with postural sway in standing? (ii) how does intrinsic stiffness change when postural operating conditions change?

In response to the first question, I demonstrated that within any given standing condition, ankle intrinsic stiffness changed as a function of COP, in one of three ways associated with distinct muscle activation patterns. Most frequently, ankle intrinsic stiffness increased monotonically as the COP moved anterior to the ankle axis of rotation; this was associated with a progressive increase in TS activation. In a second, less common pattern, observed mostly in backward lean and toe-up standing, intrinsic stiffness initially decreased and then increased as the COP moved anterior to the ankle axis of rotation; this was associated with alternating activation of TA and TS. In the third, least common pattern, observed only during backward lean, intrinsic stiffness decreased monotonically as the CP moved anterior to the ankle axis of rotation and was associated with decreasing activation of TA.

In response to the second question, I found that the mean value of ankle intrinsic stiffness varied with postural operating conditions: it was highest in forward lean when the mean COP was close to the anterior limits of stability and was lowest in backward lean when the mean COP was close to the posterior limits of stability. Thus, the results demonstrated that ankle intrinsic can vary widely with the operating condition, from as low as 8% to as much as 75% of the critical stiffness. Consequently, the intrinsic stiffness may not be significant in some conditions, but, it can generate substantial contributions in others, such as forward lean. These findings show that ankle intrinsic stiffness can not be treated as having constant contribution and ignoring its modulation will generate erroneous results regarding the mechanism of postural control.

In the second part of the thesis, I investigated the role and contribution of active elements to postural control. Decomposing ankle torque to its central, stretch reflexes and intrinsic components in human postural control is difficult, because the contributions of all pathways appear together and cannot be measured in isolation. Only global variables such as ankle torque (COP), body center of mass, joint angles, or muscle EMGs can be measured, providing information regarding the overall effect of all components. In addition, the development of mathematical models to disentangle the roles of the different pathways is challenging, because ankle stiffness changes with

postural sway and has a nonlinear structures, large non-stationarities are present in the measured waveforms, and postural control is performed in closed-loop conditions.

There has been many attempts to identify the human postural control system using kinematic and kinetic measurement (angle and torque) as input and output measures [1, 41-43, 49, 52, 53, 55, 78, 128, 234, 297-300]. However, the methods were generally unable to decompose active and passive contributions effectively; it was claimed this was due to small contribution of passive relative to active components, which makes it difficult to reliably estimate intrinsic stiffness parameters [13]. It was recently proposed that ankle muscle EMGs could be used to perform the decomposition effectively [13]. However, only a few studies have utilized EMG to study postural control and they generally used the activity of only one muscle in their models [47], and assumed that all muscles have similar EMG-torque dynamic relationships [13, 32].

Moreover, the contribution of stretch reflexes in standing has been rarely examined. Many studies have tried to investigate spinal excitability using direct electrical stimulation or by imposed joint rotations; these have provided evidence for the presence and complex behavior of reflexes in standing [198, 207, 208, 301, 302]. However, reflex responses were usually characterized by examining the amplitude of the evoked EMG response. The problem with such approach is that EMG amplitude itself does not provide a direct measure of the mechanical contribution of the reflexes, since muscle forces (torques) have complicated nonlinear relationship with EMG that change with muscle length and velocity [211].

Chapter 8 developed a multiple-input, single-output closed-loop method to decompose ankle torque to its central, stretch reflex, and intrinsic components. The method identified *central EMG-torque* dynamics of ankle plantar-flexors, *central EMG-torque* dynamics of ankle dorsi-flexors, and *reflex EMG-torque* dynamics of ankle plantar-flexors. Subsequently, the torque of each pathway was estimated. A separate dynamic noise model was considered to account for intrinsic torque and other noises. Inclusion of a separate transfer function to account for noise was important in closed-loop conditions of standing, since direct identification between EMG and ankle torque provides unbiased estimates of the dynamics only if an independent noise model with flexible parameterization is used in the context of the prediction error methods (PEM).

Using EMG as input to our model has some advantages. Reflex stiffness may change with postural sway (similar to intrinsic stiffness) and EMG seems to capture TV behavior of stretch reflexes in standing, i.e. the amplitude of stretch reflex EMGs, evoked by similar pulse perturbations (used in our experiments), changes with sway. This is desirable, since EMG and torque (force) are assumed to have a time invariant relationship that can be used to estimate stretch reflex torques. On the other hand, if ankle angle is used as the input for the identification of stretch reflexes in standing, it is essential to use TV identification approaches, since the reflex stiffness may change with ankle torque due to postural sway.

In Chapter 8, I showed that active contributions are much larger than passive contributions in normal perturbed standing. This agrees with the results of previous studies, claiming that intrinsic torque contribution to torque is around 15% in normal standing [1, 13]. This value provides an estimate of average intrinsic torque contributions, while, in Chapter 6, I showed that ankle intrinsic stiffness value changes between 15-56% of the critical stiffness in normal standing due to postural sway. Therefore, the results of the two chapters complement each other.

Subjects generated most of the active torque through central activation of TS, but used different muscle recruitment strategies, i.e. the contributions of individual TS muscles to the torque were very subject-dependent. Some subjects also used TA, whose activation is not necessary for postural stability, since the COP is always located in front of ankle axis of rotation in standing. Thus, all ankle muscles may contribute to postural control and their role and contribution is very subject dependent. Consequently, any investigation of postural control, using muscle EMGs, must include all ankle muscles. Most previous studies measured EMGs of only one plantar-flexor muscle in standing and did not account for the contribution of other muscles [47, 273]. A few studies measured all the major ankle muscles, but assumed that ankle plantar-flexors and dorsi-flexors had the same EMG-torque dynamics [13, 32]. This is not true, as I demonstrated that dynamic relationships for dorsi-flexors, and plantar-flexor are significantly different, i.e. although they both show low pass behavior, they have very different EMG-torque relations.

The EMG-torque modelling approach provided estimates of the reflex torque, generated by ankle plantar-flexor muscles in standing. The results showed that the generated reflex torque amplitude could be substantial for some subjects. This is the first study to quantify mechanical

contribution of stretch reflex in postural control; most previous studies examined reflex responses in terms of EMG amplitudes, which provides no direct information regarding their mechanical contribution.

Finally, the method demonstrated that ankle plantar-flexors possess different EMG-torque dynamics in response to central and stretch reflex activations. Both relations have low-pass behavior, but, the stretch reflex dynamics has higher bandwidth and lower DC gain. Our study provided evidence for such a difference for the first time in a functional task. These differences seem to be due to differences in motor unit recruitment strategies for central and reflex activation.

Overall this thesis provided important insights into human postural control. First, ankle intrinsic stiffness is time varying due to sway in any postural conditions. The pattern of modulations is different in different postural operating conditions, and are associated with distinct muscle activation patterns. Stiffness changes can be functionally important, i.e. it provides higher resistance to perturbations in more unstable postures. Therefore, these changes must be considered in any analysis of postural control. Failure to account for such changes will ignore an important feature of human postural control and generate misleading results. In addition, the average stiffness value changes significantly when postural operating conditions change, and in some conditions, (e.g. forward lean), the stiffness can generate substantial contributions. Therefore, it must be considered as an important contributing factor to the postural control. Whereas, in other conditions, for example in backward lean, its value and contribution are much smaller, thus, ignoring it will produce much less error in the study of postural control.

Second, the results demonstrated that active contributions consistently generate the largest portion of the torque required for normal postural control. Subjects often generated this torque, using only TS, however, the contribution of individual TS muscles to the torque was subject-specific. Moreover, the stretch reflex of TS and TA central contributions are not required for postural control. However, some subjects produce large torques through the two mechanisms. This implies that a correct understanding of postural control requires accounting for the contribution of all ankle muscles, through both central and stretch reflex contributions. Omitting any muscle or mechanism may result in the ignorance of an important contributing factor to postural control, and

results in low performance of the models in terms of goodness of fit and probably affects the estimated dynamic relationships for the muscles, since an insufficient model structure is used.

Finally, the results showed that the dynamic relationship of EMG-force (torque) of the TS muscles are not the same for stretch reflex and central activations. Therefore, it is not correct to simply assume reflex and central EMGs can be used as input to one dynamic relation to obtain muscle forces (torques). In addition, when studying the postural control and probably other functional tasks, assessing the central and stretch reflex contributions based on only the amplitude of their EMG amplitude do not generate correct understanding of their relative mechanical contribution to the task.

9.3 ORIGINAL CONTRIBUTIONS

This section outlines the original contributions of this thesis and their significance.

9.3.1 Intrinsic stiffness in standing

The first contribution was to quantify ankle intrinsic stiffness in a variety of postural operating conditions.

Thus, I developed a method to directly identify ankle intrinsic stiffness in standing that accounted for its modulation with postural sway. I showed that the mass-spring-damper (IBK) model, commonly used to model intrinsic stiffness, does not fully capture the dynamics of intrinsic stiffness in standing. Rather, a 2^{nd} order model with three zeros must be used. I used the developed method to identify intrinsic stiffness across a range of postural operating conditions, including normal standing, forward and backward lean, and toe-up and toe-down standing. The results demonstrated that the intrinsic stiffness changes within each operating condition as a function of COP in a manner dependent on muscle activation patterns. Consequently, the intrinsic stiffness-COP relation may be monotonically increasing, monotonically decreasing, or decreasing-increasing within a given operating condition; these patterns are associated with the activation of TS muscles, TA muscles, or alternating activation of both muscle groups, respectively; In addition, the mean stiffness was the highest in forward lean, and lowest in backward lean, while base of support inclination did not change the mean stiffness value. The intrinsic stiffness ranged from as little as 0.08 to as large as 0.75 of the critical stiffness. Therefore, its contribution changed significantly in different operating conditions. And although the stiffness was not sufficient to

provide postural stability, it could generate substantial contributions to the ankle torque and significantly simplify postural control.

These findings provide important insight into human postural control. First, the use of an IBK model to estimate intrinsic stiffness in standing will provide biased estimates of the stiffness parameters. Previous studies used an IBK model for the intrinsic stiffness, therefore, their results must be interpreted with care. Second, the assumption of constant intrinsic stiffness is not correct, since the stiffness changes substantially with postural sway and muscle activation. Hence, any model of postural control needs to account for the time varying nature of the intrinsic stiffness. Previous studies of postural control overlooked these changes and assumed a constant intrinsic stiffness value. This will ignore an important feature of postural control. Third, COP movement toward both anterior and posterior limits of stability results in an increase in the stiffness. This is functionally important, since higher involuntary intrinsic resistance against external perturbations, when the margin of stability is smaller (due to movement of COP toward limits of stability) seems appropriate. Moreover, the contribution of ankle intrinsic stiffness is much more significant during forward lean, less important in backward lean, and modest in other operating conditions. These differences must be considered when studying postural control in different conditions. Finally, the observed modulation of ankle intrinsic stiffness provides guidelines for biomimetic design of orthoses and prostheses in a manner that replicates the normal behavior of the joint.

9.3.2 Identification of central, stretch reflex, and intrinsic contributions to human postural control

The second contribution was the development of a multiple-input, single-output, closed-loop method to identify EMG-torque dynamic relationship of ankle muscles in standing and subsequently estimate the active contributions, generated by central and stretch reflex mechanisms.

I used this model in normal standing conditions to show that (i) active contributions to ankle torque, generated by central and stretch reflex mechanisms, were much larger than passive contributions. (ii) Plantar-flexors central torque accounted for most of the ankle torque, while dorsi-flexor central torque was smaller and only present in half of the subjects. (iii) Stretch reflex torque contributions were variable among the subjects; it was significant in some subjects, but very small in others. (iv) There were large variability in the strategy subjects used to activate their TS

muscles. (v) C*entral EMG-torque* and *reflex EMG-torque* dynamic relationships of ankle plantar-flexors were different: the former had a lower bandwidth but a higher DC Gain.

Several important conclusions can be drawn from this study. First, the new method is a powerful tool to decompose ankle torque to its central, stretch reflex, and intrinsic components in human postural control. It provides the means to investigate the role and importance of each pathway in isolation in any experimental conditions. For example, the central torque can be examined alone in a variety of experimental conditions to study multisensory integration. Or the adaptation of stretch reflexes in different postural tasks could be studied. Second, the method generates noise-free estimates of central torque and stretch reflex torque; consequently, open-loop identification methods, which are much simpler compared to closed-loop methods can be used to identify stretch reflex and central pathways. This is particularly desirable for reflex stiffness, since it has a non-linear structure, which makes its identification difficult even in open-loop conditions. Third, we found that subjects consistently generated most of the active torque using their TS muscles, however, the contribution of individual TS muscles to the torque depends strongly on the subject. In addition, some subjects may have significant TA and stretch reflex contributions. This indicates that in contrast to previous studies of postural control, which usually used only the EMG of medial gastrocnemius or soleus in their models (and ignored the role of other muscles), it is very important to include all ankle muscles in any model of postural control. Finally, the difference between *central* and *reflex EMG-torque dynamics* of the plantar-flexor muscles must be considered in the study of the two mechanisms. The differences may be caused by different motor-unit recruitment strategies. In addition, the amplitude of the measured central and reflex EMG do not provide an indication of their relative mechanical contribution (torque). Instead, correct dynamic models must be used to estimate each pathway's torque (force), which provides a better understanding of the role and contribution of each pathway. Thus, it is crucial to model the two mechanisms separately.

9.4 FUTURE WORK

Following this thesis, several recommendations can be formulated for the future work.

9.4.1 Development of a global ankle intrinsic stiffness model for standing

I developed a model to estimate ankle intrinsic stiffness and used the model to characterize the intrinsic stiffness in several postural tasks. My results demonstrated that the intrinsic stiffness changed with the position of COP and activation of ankle muscles. Consequently, it should be possible to develop models that can predict ankle intrinsic stiffness in standing as a function of COP position, EMG of the triceps surae and EMG of tibialis anterior muscles. Such a global model, when calibrated for an individual, could generate ankle intrinsic stiffness value in standing, and therefore, could be used to design assistive devices such as orthoses and prostheses. It could also provide insight for the generation of appropriate scheduling variables that can be used for linear parameter varying or time varying identification of ankle intrinsic stiffness in standing.

9.4.2 Identification of stretch reflex stiffness in standing

One of the outputs of the EMG-torque model developed in the last phase of this thesis is the reflex torque. Since the predicted reflex torque is simulated by the model, it is noise-free, therefore, open-loop identification methods can be used to identify reflex stiffness in standing. The reflex stiffness has a nonlinear Hammerstein structure and probably changes with postural sway. Consequently, the predicted reflex torques can be first used with the available open-loop nonlinear identification methods for time invariant Hammerstein systems; if the model residuals show time varying characteristics, then available time varying and linear parameter varying open-loop methods for Hammerstein systems can be used for the identification. The identification of a linear parameter varying model is still challenging, because finding the right scheduling variable for reflexes is difficult. This is due to the fact that reflexes are very complex and dependent on many factors. The first scheduling variable candidates can be ankle torque and the direction of postural sway (found by the derivative of ankle torque).

Development of such a method is important, since the functional role of the stretch reflex in standing is still unclear. A correct characterization of ankle reflex stiffness in standing provides a means to assess its role in postural control. This can be done by developing realistic simulations of postural control with and without the identified reflexes and subsequently developing metrics that provide quantified measures of reflex influence on postural stability.

9.4.3 Identification of intrinsic stiffness from the residual of the EMG-torque model

The method developed in the first phase of this thesis provides estimates of ankle intrinsic stiffness in standing in response to discrete pulse perturbations; however, it does not characterize the intrinsic stiffness for the whole length of the experiments. A more systematic approach would be to use the whole record of the data during an experiment and identify the intrinsic stiffness in standing. Our EMG-torque model gives an estimate of the noisy intrinsic torque. Since the intrinsic stiffness changes with sway and there is noise in the closed-loop system, closed-loop time varying or linear parameter varying identification methods must be developed to identify the intrinsic stiffness. In doing so, the possible nonlinear behavior of the intrinsic stiffness due to its short-range and long-range behavior must be accounted for. This means that the structure of the intrinsic stiffness may need to be switched when there is pulse perturbation during an experiment.

9.4.4 Adaptation of human postural control

A fundamental property of human postural control is its adaptation to new experimental conditions and postural tasks. The EMG-torque method estimates the contributions of central, and stretch reflex mechanisms (and indirectly intrinsic stiffness) to the postural control in any given conditions. Consequently, the method can be used in a range of postural tasks (such as the one we performed in phase 2 of this thesis) to investigate the contribution of different pathways and their adaptations to different conditions.

Another application of the method is to investigate the modulation of postural control due to ageing (or diseases) and develop methods for fall prevention. Thus, the method could be used to generate subject-specific estimates of the contribution of different components in postural control and examine their changes due to ageing. This can be followed by targeted interventions, aimed at improving the impaired component to improve balance and prevent falls.

9.4.5 Application of the EMG-torque model to standing experiments with continuous perturbations

A challenge in the identification of human postural control in standing when using continuous perturbation the difficulty in estimating the intrinsic contributions. Our EMG-torque model should be used with the data in standing experiments with continuous perturbations to separate intrinsic contributions from active contributions. Subsequently, the contribution of all pathways can be

examined and compared to see if the application of discrete and continuous perturbations generate different effects on human postural control.

REFERENCES

[1] Peterka, R.J., *Sensorimotor integration in human postural control.* J Neurophysiol, 2002. **88**(3): p. 1097-118.

[2] Peterka, R.J., *Chapter 2 - Sensory integration for human balance control*, in *Handbook of Clinical Neurology*, B.L. Day and S.R. Lord, Editors. 2018, Elsevier. p. 27-42.

[3] Horak, F.B. and L.M. Nashner, *Central programming of postural movements: adaptation to altered support-surface configurations.* Journal of neurophysiology, 1986. **55**(6): p. 1369-1381.

[4] Weiss, P.L., I.W. Hunter, and R.E. Kearney, *Human ankle joint stiffness over the full range of muscle activation levels.* J Biomech, 1988. **21**(7): p. 539-44.

[5] Weiss, P.L., R.E. Kearney, and I.W. Hunter, *Position dependence of ankle joint dynamics--I. Passive mechanics.* J Biomech, 1986. **19**(9): p. 727-35.

[6] Weiss, P.L., R.E. Kearney, and I.W. Hunter, *Position dependence of ankle joint dynamics--II. Active mechanics.* J Biomech, 1986. **19**(9): p. 737-51.

[7] Mirbagheri, M.M., H. Barbeau, and R.E. Kearney, *Intrinsic and reflex contributions to human ankle stiffness: variation with activation level and position.* Exp Brain Res, 2000. **135**(4): p. 423-36.

[8] Loram, I.D., C.N. Maganaris, and M. Lakie, *The passive, human calf muscles in relation to standing: the non-linear decrease from short range to long range stiffness.* J Physiol, 2007. **584**(Pt 2): p. 661-75.

[9] Loram, I.D. and M. Lakie, *Direct measurement of human ankle stiffness during quiet standing: the intrinsic mechanical stiffness is insufficient for stability.* Journal of Physiology-London, 2002. **545**(3): p. 1041-1053.

[10] Casadio, M., Morasso, P. G., Sanguineti, V., *Direct measurement of ankle stiffness during quiet standing: implications for control modelling and clinical application.* Gait Posture, 2005. **21**(4): p. 410-24.

[11] Vlutters, M., T.A. Boonstra, A.C. Schouten, and H. van der Kooij, *Direct measurement of the intrinsic ankle stiffness during standing.* J Biomech, 2015. **48**(7): p. 1258-63.

[12] van der Kooij, H., E. van Asseldonk, and F.C. van der Helm, *Comparison of different methods to identify and quantify balance control.* J Neurosci Methods, 2005. **145**(1-2): p. 175-203.

[13] Pasma, J.H., J. van Kordelaar, D. de Kam, V. Weerdesteyn, A.C. Schouten, and H. van der Kooij, *Assessment of the underlying systems involved in standing balance: the additional value of electromyography in system identification and parameter estimation.* J Neuroeng Rehabil, 2017. **14**(1): p. 97.

[14] Shumway-Cook, A. and M.H. Woollacott, *Motor control: translating research into clinical practice*. 2007: Lippincott Williams & Wilkins.

[15] Morasso, P.G. and M. Schieppati, *Can muscle stiffness alone stabilize upright standing?* J Neurophysiol, 1999. **82**(3): p. 1622-6.

[16] Mochizuki, G., J.G. Semmler, T. Ivanova, and S. Garland, *Low-frequency common modulation of soleus motor unit discharge is enhanced during postural control in humans.* Experimental brain research, 2006. **175**(4): p. 584-595.

[17] Winter, D.A., A.E. Patla, F. Prince, M. Ishac, and K. Gielo-Perczak, *Stiffness control of balance in quiet standing.* J Neurophysiol, 1998. **80**(3): p. 1211-21.

[18] HORAK, F. and J. MACPHERSON, *Postural orientation and equilibrium.* In: Handbook of Physiology. Exercise: Regulation and Integration of Multiple Systems, edited by Rowell LB and Shepherd JT., 1996.

[19] Horak, F.B., *Postural orientation and equilibrium: what do we need to know about neural control of balance to prevent falls?* Age and Ageing, 2006. **35**: p. 7-11.

[20] Benda, B.J., P.O. Riley, and D.E. Krebs, *Biomechanical relationship between center of gravity and center of pressure during standing.* IEEE Transactions on Rehabilitation Engineering, 1994. **2**(1): p. 3-10.

[21] Scholz, J., G. Schöner, W. Hsu, J. Jeka, F. Horak, and V. Martin, *Motor equivalent control of the center of mass in response to support surface perturbations.* Experimental brain research, 2007. **180**(1): p. 163-179.

[22] Pai, Y.-C., B. Maki, K. Iqbal, W. McIlroy, and S. Perry, *Thresholds for step initiation induced by support-surface translation: a dynamic center-of-mass model provides much better prediction than a static model.* Journal of biomechanics, 2000. **33**(3): p. 387-392.

[23] Horak, F.B., H. Diener, and L. Nashner, *Influence of central set on human postural responses.* Journal of neurophysiology, 1989. **62**(4): p. 841-853.

[24] Creath, R., T. Kiemel, F. Horak, R. Peterka, and J. Jeka, *A unified view of quiet and perturbed stance: simultaneous co-existing excitable modes.* Neuroscience letters, 2005. **377**(2): p. 75-80.

[25] McIlroy, W. and B. Maki, *Task constraints on foot movement and the incidence of compensatory stepping following perturbation of upright stance.* Brain research, 1993. **616**(1-2): p. 30-38.

[26] Anne Shumway-Cook, M.H.W., *Motor Control: Translating Research into Clinical Practice*. 2007: Lippincott Williams & Wilkins. 612.

[27] Nashner, L.M., *Fixed patterns of rapid postural responses among leg muscles during stance.* Experimental Brain Research, 1977. **30**(1): p. 13-24.

[28] Saffer, M., T. Kiemel, and J. Jeka, *Coherence analysis of muscle activity during quiet stance.* Experimental brain research, 2008. **185**(2): p. 215-226.

[29] Crutchfield, C., A. Shumway-Cook, and F. Horak, *Balance and coordination training.* Physical therapy, 1989: p. 825-843.

[30] Runge, C., C. Shupert, F. Horak, and F. Zajac, *Ankle and hip postural strategies defined by joint torques.* Gait & posture, 1999. **10**(2): p. 161-170.

[31] Zhang, Y., T. Kiemel, and J. Jeka, *The influence of sensory information on two-component coordination during quiet stance.* Gait & posture, 2007. **26**(2): p. 263-271.

[32] Kiemel, T., A.J. Elahi, and J.J. Jeka, *Identification of the plant for upright stance in humans: multiple movement patterns from a single neural strategy.* J Neurophysiol, 2008. **100**(6): p. 3394-406.

[33] Winter, D.A., A.E. Patla, S. Rietdyk, and M.G. Ishac, *Ankle muscle stiffness in the control of balance during quiet standing.* J Neurophysiol, 2001. **85**(6): p. 2630-3.

[34] Carpenter, M.G., J.S. Frank, D.A. Winter, and G.W. Peysar, *Sampling duration effects on centre of pressure summary measures.* Gait & Posture, 2001. **13**(1): p. 35-40.

[35] Loram, I.D., C.N. Maganaris, and M. Lakie, *Paradoxical muscle movement during postural control.* Med Sci Sports Exerc, 2009. **41**(1): p. 198-204.

[36] Vette, A.H., K. Masani, K. Nakazawa, and M.R. Popovic, *Neural-mechanical feedback control scheme generates physiological ankle torque fluctuation during quiet stance.* IEEE Trans Neural Syst Rehabil Eng, 2010. **18**(1): p. 86-95.

[37] Amiri, P. and R.E. Kearney, *Ankle intrinsic stiffness changes with postural sway.* Journal of Biomechanics, 2019. **85**: p. 50-58.

[38] Amiri, P. and R.E. Kearney, *Ankle intrinsic stiffness is modulated by postural sway.* Conf Proc IEEE Eng Med Biol Soc, 2017: p. 70-73.

[39] Sakanaka, T.E., J. Gill, M.D. Lakie, and R.F. Reynolds, *Intrinsic ankle stiffness during standing increases with ankle torque and passive stretch of the Achilles tendon.* PloS one, 2018. **13**(3): p. e0193850-e0193850.

[40] Sakanaka, T.E., M. Lakie, and R.F. Reynolds, *Sway-dependent changes in standing ankle stiffness caused by muscle thixotropy.* J Physiol, 2016. **594**(3): p. 781-93.

[41] Engelhart, D., T.A. Boonstra, R.G.K.M. Aarts, A.C. Schouten, and H. van der Kooij, *Comparison of closed-loop system identification techniques to quantify multi-joint human balance control.* Annual Reviews in Control, 2016. **41**: p. 58-70.

[42] Boonstra, T.A., A.C. Schouten, and H. van der Kooij, *Identification of the contribution of the ankle and hip joints to multi-segmental balance control.* Journal of Neuroengineering and Rehabilitation, 2013. **10**.

[43] Fujisawa, N., T. Masuda, Y. Inaoka, H. Fukuoka, A. Ishida, and H. Minamitani, *Human standing posture control system depending on adopted strategies.* Med Biol Eng Comput, 2005. **43**(1): p. 107-14.

[44] Park, S., F.B. Horak, and A.D. Kuo, *Postural feedback responses scale with biomechanical constraints in human standing.* Exp Brain Res, 2004. **154**(4): p. 417-27.

[45] van der Kooij, H., R. Jacobs, B. Koopman, and F. van der Helm, *An adaptive model of sensory integration in a dynamic environment applied to human stance control.* Biol Cybern, 2001. **84**(2): p. 103-15.

[46] Mihelj, M., Z. Matjacic, and T. Bajd, *Postural activity of constrained subject in response to disturbance in sagittal plane.* Gait Posture, 2000. **12**(2): p. 94-104.

[47] Fitzpatrick, R., D. Burke, and S.C. Gandevia, *Loop gain of reflexes controlling human standing measured with the use of postural and vestibular disturbances.* J Neurophysiol, 1996. **76**(6): p. 3994-4008.

[48] Peterka, R.J., C.F. Murchison, L. Parrington, P.C. Fino, and L.A. King, *Implementation of a Central Sensorimotor Integration Test for Characterization of Human Balance Control During Stance.* Frontiers in Neurology, 2018. **9**(1045).

[49] Pasma, J.H., D. Engelhart, A.B. Maier, A.C. Schouten, H. van der Kooij, and C.G. Meskers, *Changes in sensory reweighting of proprioceptive information during standing balance with age and disease.* J Neurophysiol, 2015. **114**(6): p. 3220-33.

[50] Pasma, J.H., D. Engelhart, A.C. Schouten, H. van der Kooij, A.B. Maier, and C.G.M. Meskers, *Impaired standing balance: The clinical need for closing the loop.* Neuroscience, 2014. **267**: p. 157-165.

[51] Engelhart, D., J.H. Pasma, A.C. Schouten, C.G.M. Meskers, A.B. Maier, T. Mergner, and H. van der Kooij, *Impaired Standing Balance in Elderly: A New Engineering Method Helps to Unravel Causes and Effects.* Journal of the American Medical Directors Association, 2014. **15**(3): p. 227.e1-227.e6.

[52] Pasma, J.H., T.A. Boonstra, S.F. Campfens, A.C. Schouten, and H.V.d. Kooij, *Sensory reweighting of proprioceptive information of the left and right leg during human balance control.* Journal of Neurophysiology, 2012. **108**(4): p. 1138-1148.

[53] Goodworth, A.D. and R.J. Peterka, *Sensorimotor integration for multisegmental frontal plane balance control in humans.* Journal of neurophysiology, 2012. **107**(1): p. 12-28.

[54] Kiemel, T., Y. Zhang, and J.J. Jeka, *Identification of neural feedback for upright stance in humans: stabilization rather than sway minimization.* J Neurosci, 2011. **31**(42): p. 15144-53.

[55] van der Kooij, H., E.H.F. van Asseldonk, J. Geelen, J.P.P. van Vugt, and B.R. Bloem, *Detecting asymmetries in balance control with system identification: first experimental results from Parkinson patients.* Journal of Neural Transmission, 2007. **114**(10): p. 1333.

[56] Engelhart, D., J.H. Pasma, A.C. Schouten, R.G. Aarts, C.G. Meskers, A.B. Maier, and H. van der Kooij, *Adaptation of multijoint coordination during standing balance in healthy young and healthy old individuals.* J Neurophysiol, 2016. **115**(3): p. 1422-35.

[57] Gatev, P., S. Thomas, T. Kepple, and M. Hallett, *Feedforward ankle strategy of balance during quiet stance in adults.* The Journal of Physiology, 1999. **514**(Pt 3): p. 915-928.

[58] Van Der Kooij, H. and E. De Vlugt, *Postural responses evoked by platform pertubations are dominated by continuous feedback.* Journal of neurophysiology, 2007. **98**(2): p. 730-743.

[59] Forssell, U. and L. Ljung, *Closed-loop identification revisited.* Automatica, 1999. **35**(7): p. 1215-1241.

[60] Nashner, L.M., *Adaptation of human movement to altered environments.* Trends in neurosciences, 1982. **5**: p. 358-361.

[61] Belenkii, V., V. Gurfinkel, and E. Paltsev, *ON THE CONTROL ELEMENTS OF VOLUNTARY MOVEMENTS.* Biofizika, 1967.

[62] Asai, Y., Y. Tasaka, K. Nomura, T. Nomura, M. Casadio, and P. Morasso, *A model of postural control in quiet standing: robust compensation of delay-induced instability using intermittent activation of feedback control.* PLoS One, 2009. **4**(7): p. e6169.

[63] Bottaro, A., Y. Yasutake, T. Nomura, M. Casadio, and P. Morasso, *Bounded stability of the quiet standing posture: An intermittent control model.* Human Movement Science, 2008. **27**(3): p. 473-495.

[64] Loram, I.D., P.J. Gawthrop, and M. Lakie, *The frequency of human, manual adjustments in balancing an inverted pendulum is constrained by intrinsic physiological factors.* J Physiol, 2006. **577**(Pt 1): p. 417-32.

[65] Bottaro, A., M. Casadio, P.G. Morasso, and V. Sanguineti, *Body sway during quiet standing: Is it the residual chattering of an intermittent stabilization process?* Human Movement Science, 2005. **24**(4): p. 588-615.

[66] Héroux, M.E., C.J. Dakin, B.L. Luu, J.T. Inglis, and J.-S. Blouin, *Absence of lateral gastrocnemius activity and differential motor unit behavior in soleus and medial gastrocnemius during standing balance.* Journal of Applied Physiology, 2014. **116**(2): p. 140-148.

[67] Vieira, T.M.M., I.D. Loram, S. Muceli, R. Merletti, and D. Farina, *Recruitment of motor units in the medial gastrocnemius muscle during human quiet standing: is recruitment intermittent? What triggers recruitment?* Journal of Neurophysiology, 2012. **107**(2): p. 666-676.

[68] Forbes, P.A., A. Chen, and J.-S. Blouin, *Chapter 4 - Sensorimotor control of standing balance*, in *Handbook of Clinical Neurology*, B.L. Day and S.R. Lord, Editors. 2018, Elsevier. p. 61-83.

[69] Mergner, T., *A neurological view on reactive human stance control.* Annual Reviews in Control, 2010. **34**(2): p. 177-198.

[70] Dietz, V., M. Trippel, and G. Horstmann, *Significance of proprioceptive and vestibulo-spinal reflexes in the control of stance and gait*, in *Advances in Psychology*. 1991, Elsevier. p. 37-52.

[71] Nashner, L., M. Woollacott, and G. Tuma, *Organization of rapid responses to postural and locomotor-like perturbations of standing man.* Experimental Brain Research, 1979. **36**(3): p. 463-476.

[72] Nashner, L.M. and P. Wolfson, *Influence of head position and proprioceptive cues on short latency postural reflexes evoked by galvanic stimulation of the human labyrinth.* Brain Research, 1974. **67**(2): p. 255-268.

[73] Dokka, K., R.V. Kenyon, E.A. Keshner, and K.P. Kording, *Self versus environment motion in postural control.* PLoS computational biology, 2010. **6**(2): p. e1000680.

[74] Kearney, R.E., R.B. Stein, and L. Parameswaran, *Identification of intrinsic and reflex contributions to human ankle stiffness dynamics.* IEEE Trans Biomed Eng, 1997. **44**(6): p. 493-504.

[75] Toft, E., T. Sinkjaer, S. Andreassen, and K. Larsen, *Mechanical and electromyographic responses to stretch of the human ankle extensors.* J Neurophysiol, 1991. **65**(6): p. 1402-10.

[76] Stein, R.B. and R.E. Kearney, *Nonlinear Behavior of Muscle Reflexes at the Human Ankle Joint.* Journal of Neurophysiology, 1995. **73**(1): p. 65-72.

[77] Kearney, R.E. and I.W. Hunter, *System identification of human joint dynamics.* Crit Rev Biomed Eng, 1990. **18**(1): p. 55-87.

[78] Engelhart, D., A.C. Schouten, R.G. Aarts, and H. van der Kooij, *Assessment of Multi-Joint Coordination and Adaptation in Standing Balance: A Novel Device and System Identification Technique.* IEEE Trans Neural Syst Rehabil Eng, 2015. **23**(6): p. 973-82.

[79] Günther, M., S. Grimmer, T. Siebert, and R. Blickhan, *All leg joints contribute to quiet human stance: a mechanical analysis.* Journal of biomechanics, 2009. **42**(16): p. 2739-2746.

[80] Pintelon, R. and J. Schoukens, *System identification: a frequency domain approach*. 2012: John Wiley & Sons.

[81] van Asseldonk, E.H., J.H. Buurke, B.R. Bloem, G.J. Renzenbrink, A.V. Nene, F.C. van der Helm, and H. van der Kooij, *Disentangling the contribution of the paretic and non-paretic ankle to balance control in stroke patients.* Experimental neurology, 2006. **201**(2): p. 441-451.

[82] Boonstra, T.A., J.P.P. van Vugt, H. van der Kooij, and B.R. Bloem, *Balance Asymmetry in Parkinson's Disease and Its Contribution to Freezing of Gait.* PLOS ONE, 2014. **9**(7): p. e102493.

[83] Boonstra, T.A., A.C. Schouten, J.P.P.v. Vugt, B.R. Bloem, and H.v.d. Kooij, *Parkinson's disease patients compensate for balance control asymmetry.* Journal of Neurophysiology, 2014. **112**(12): p. 3227-3239.

[84] Löwenstein, O. and A. Sand, *The mechanism of the semicircular canal. A study of the responses of single-fibre preparations to angular accelerations and to rotation at constant speed.* Proceedings of the Royal Society of London. Series B-Biological Sciences, 1940. **129**(855): p. 256-275.

[85] Wilson, V.J., *Mammalian vestibular physiology*. 2013: Springer Science & Business Media.

[86] Lowenstein, O.E. and R. Saunders, *Otolith-controlled response from the first-order neurons of the labyrinth of the bullfrog (Rana catesbeiana) to changes in linear acceleration.* Proceedings of the Royal Society of London. Series B. Biological Sciences, 1975. **191**(1105): p. 475-505.

[87] Dietz, V., M. Schubert, M. Discher, and M. Trippel, *Influence of visuoproprioceptive mismatch on postural adjustments.* Gait & Posture, 1994. **2**(3): p. 147-155.

[88] Osler, C.J. and R.F. Reynolds, *Postural reorientation does not cause the locomotor after-effect following rotary locomotion.* Experimental Brain Research, 2012. **220**(3): p. 231-237.

[89] Fitzpatrick, R.C. and B.L. Day, *Probing the human vestibular system with galvanic stimulation.* Journal of Applied Physiology, 2004. **96**(6): p. 2301-2316.

[90] Fetter, M., H.-C. Diener, and J. Dichgans, *Recovery of postural control after an acute unilateral vestibular lesion in humans.* J Vestib Res, 1991. **1**(4): p. 373-83.

[91] Black, F., C. Shupert, F. Horak, and L. Nashner, *Abnormal postural control associated with peripheral vestibular disorders*, in *Progress in brain research*. 1988, Elsevier. p. 263-275.

[92] Herdman, S.J., P. Blatt, M.C. Schubert, and R.J. Tusa, *Falls in patients with vestibular deficits.* Otology & Neurotology, 2000. **21**(6): p. 847-851.

[93] Herdman, S.J., R.A. Clendaniel, D.E. Mattox, M.J. Holliday, and J.K. Niparko, *Vestibular adaptation exercises and recovery: acute stage after acoustic neuroma resection.* Otolaryngology—Head and Neck Surgery, 1995. **113**(1): p. 77-87.

[94] Krebs, D.E., K.M. Gill-Body, P.O. Riley, and S.W. Parker, *Double-blind, placebo-controlled trial of rehabilitation for bilateral vestibular hypofunction: preliminary report.* Otolaryngology—Head and Neck Surgery, 1993. **109**(4): p. 735-741.

[95] Horak, F., C. Jones-Rycewicz, F.O. Black, and A. Shumway-Cook, *Effects of vestibular rehabilitation on dizziness and imbalance.* Otolaryngology–Head and Neck Surgery, 1992. **106**(2): p. 175-180.

[96] Houk, J.C., W.Z. Rymer, and P.E. Crago, *Dependence of dynamic response of spindle receptors on muscle length and velocity.* Journal of Neurophysiology, 1981. **46**(1): p. 143-166.

[97] Day, J., L.R. Bent, I. Birznieks, V.G. Macefield, and A.G. Cresswell, *Muscle spindles in human tibialis anterior encode muscle fascicle length changes.* Journal of Neurophysiology, 2017. **117**(4): p. 1489-1498.

[98] Burgess, P. and F. Clark, *Characteristics of knee joint receptors in the cat.* The Journal of Physiology, 1969. **203**(2): p. 317-335.

[99] Macefield, V.G., *Physiological characteristics of low-threshold mechanoreceptors in joints, muscle and skin in human subjects.* Clinical and Experimental Pharmacology and Physiology, 2005. **32**(1-2): p. 135-144.

[100] Iggo, A. and A.R. Muir, *The structure and function of a slowly adapting touch corpuscle in hairy skin.* The Journal of Physiology, 1969. **200**(3): p. 763-796.

[101] Johansson, R.S., U. Landstro¨m, and R. Lundstro¨m, *Responses of mechanoreceptive afferent units in the glabrous skin of the human hand to sinusoidal skin displacements.* Brain Research, 1982. **244**(1): p. 17-25.

[102] Edin, B.B., *Cutaneous afferents provide information about knee joint movements in humans.* The Journal of Physiology, 2001. **531**(1): p. 289-297.

[103] Loewenstein, W.R. and R. Skalak, *Mechanical transmission in a Pacinian corpuscle. An analysis and a theory.* The Journal of Physiology, 1966. **182**(2): p. 346-378.

[104] IGGO, A., *CUTANEOUS AND SUBCUTANEOUS SENSE ORGANS.* British Medical Bulletin, 1977. **33**(2): p. 97-102.

[105] Roudaut, Y., A. Lonigro, B. Coste, J. Hao, P. Delmas, and M. Crest, *Touch sense: functional organization and molecular determinants of mechanosensitive receptors.* Channels, 2012. **6**(4): p. 234-245.

[106] Kennedy, P.M. and J.T. Inglis, *Distribution and behaviour of glabrous cutaneous receptors in the human foot sole.* The Journal of Physiology, 2002. **538**(3): p. 995-1002.

[107] Fallon, J.B., L.R. Bent, P.A. McNulty, and V.G. Macefield, *Evidence for Strong Synaptic Coupling Between Single Tactile Afferents From the Sole of the Foot and Motoneurons Supplying Leg Muscles.* Journal of Neurophysiology, 2005. **94**(6): p. 3795-3804.

[108] Anderson, J.H., *Dynamic characteristics of Golgi tendon organs.* Brain Research, 1974. **67**(3): p. 531-537.

[109] Loram, I.D., M. Lakie, I.D. Giulio, and C.N. Maganaris, *The Consequences of Short-Range Stiffness and Fluctuating Muscle Activity for Proprioception of Postural Joint Rotations: The Relevance to Human Standing.* Journal of Neurophysiology, 2009. **102**(1): p. 460-474.

[110] Diener, H., J. Dichgans, B. Guschlbauer, and H. Mau, *The significance of proprioception on postural stabilization as assessed by ischemia.* Brain research, 1984. **296**(1): p. 103-109.

[111] Asai, H., *Limiting factor for movable range of the center of foot pressure in backward direction.* Vestibular and Neural Front., 1994: p. 525-528.

[112] Magnusson, M., H. Enbom, R. Johansson, and J. Wiklund, *Significance of pressor input from the human feet in lateral postural control: The effect of hypothermia on galvanically induced body-sway.* Acta oto-laryngologica, 1990. **110**(3-4): p. 321-327.

[113] Werness, S.A. and D.J. Anderson, *Parametric analysis of dynamic postural responses.* Biol Cybern, 1984. **51**(3): p. 155-68.

[114] Nashner, L.M., *Adapting reflexes controlling the human posture.* Exp Brain Res, 1976. **26**(1): p. 59-72.

[115] Johansson, R., M. Magnusson, and M. Akesson, *Identification of human postural dynamics.* IEEE Trans Biomed Eng, 1988. **35**(10): p. 858-69.

[116] Kavounoudias, A., J.C. Gilhodes, R. Roll, and J.P. Roll, *From balance regulation to body orientation: two goals for muscle proprioceptive information processing?* Exp Brain Res, 1999. **124**(1): p. 80-8.

[117] Jeka, J.J., *Light Touch Contact as a Balance Aid.* Physical Therapy, 1997. **77**(5): p. 476-487.

[118] Jeka, J.J. and J.R. Lackner, *Fingertip contact influences human postural control.* Experimental Brain Research, 1994. **79**(2): p. 495-502.

[119] Lee, D.N. and J.R. Lishman, *Visual proprioceptive control of stance.* Journal of Human Movement Studies, 1975. **1**(2): p. 87-95.

[120] PAULUS, W.M., A. STRAUBE, and T. BRANDT, *VISUAL STABILIZATION OF POSTURE: PHYSIOLOGICAL STIMULUS CHARACTERISTICS AND CLINICAL ASPECTS.* Brain, 1984. **107**(4): p. 1143-1163.

[121] Lishman, J.R. and D.N. Lee, *The Autonomy of Visual Kinaesthesis.* Perception, 1973. **2**(3): p. 287-294.

[122] Bronstein, A.M. and D. Buckwell, *Automatic control of postural sway by visual motion parallax.* Experimental Brain Research, 1997. **113**(2): p. 243-248.

[123] Dichgans, J. and T. Brandt, *Visual-Vestibular Interaction: Effects on Self-Motion Perception and Postural Control*, in *Perception*, R. Held, H.W. Leibowitz, and H.-L. Teuber, Editors. 1978, Springer Berlin Heidelberg: Berlin, Heidelberg. p. 755-804.

[124] Peterka, R.J. and M.S. Benolken, *Role of somatosensory and vestibular cues in attenuating visually induced human postural sway.* Experimental Brain Research, 1995. **105**(1): p. 101-110.

[125] Mergner, T., G. Schweigart, C. Maurer, and A. Blümle, *Human postural responses to motion of real and virtual visual environments under different support base conditions.* Experimental Brain Research, 2005. **167**(4): p. 535-556.

[126] Day, B.L., T. Muller, J. Offord, and I. Di Giulio, *Dual processing of visual rotation for bipedal stance control.* The Journal of Physiology, 2016. **594**(19): p. 5661-5671.

[127] Stoffregen, T.A. and G.E. Riccio, *An ecological theory of orientation and the vestibular system.* Psychological review, 1988. **95**(1): p. 3.

[128] Mergner, T., C. Maurer, and R.J. Peterka, *A multisensory posture control model of human upright stance*, in *Progress in Brain Research*. 2003, Elsevier. p. 189-201.

[129] Oie, K.S., T. Kiemel, and J.J. Jeka, *Multisensory fusion: simultaneous re-weighting of vision and touch for the control of human posture.* Brain Res Cogn Brain Res, 2002. **14**(1): p. 164-76.

[130] Kiemel, T., K.S. Oie, and J.J. Jeka, *Multisensory fusion and the stochastic structure of postural sway.* Biol Cybern, 2002. **87**(4): p. 262-77.

[131] Kuo, A.D., R.A. Speers, R.J. Peterka, and F.B. Horak, *Effect of altered sensory conditions on multivariate descriptors of human postural sway.* Exp Brain Res, 1998. **122**(2): p. 185-95.

[132] Nashner, L.M., F.O. Black, and C. Wall, 3rd, *Adaptation to altered support and visual conditions during stance: patients with vestibular deficits.* J Neurosci, 1982. **2**(5): p. 536-44.

[133] Fitzpatrick, R. and D. McCloskey, *Proprioceptive, visual and vestibular thresholds for the perception of sway during standing in humans.* The Journal of physiology, 1994. **478**(1): p. 173-186.

[134] Peterka, R.J. and M.S. Benolken, *Role of somatosensory and vestibular cues in attenuating visually induced human postural sway.* Exp Brain Res, 1995. **105**(1): p. 101-10.

[135] Kuo, A.D., *An optimal control model for analyzing human postural balance.* IEEE Transactions on Biomedical Engineering, 1995. **42**(1): p. 87-101.

[136] van der Kooij, H., R. Jacobs, B. Koopman, and H. Grootenboer, *A multisensory integration model of human stance control.* Biol Cybern, 1999. **80**(5): p. 299-308.

[137] van der Kooij, H., R. Jacobs, B. Koopman, and F. van der Helm, *An adaptive model of sensory integration in a dynamic environment applied to human stance control.* Biological Cybernetics, 2001. **84**(2): p. 103-115.

[138] Kuo, A.D., *An optimal state estimation model of sensory integration in human postural balance.* J Neural Eng, 2005. **2**(3): p. S235-49.

[139] Fong, D.T.-P., Y. Hong, L.-K. Chan, P.S.-H. Yung, and K.-M. Chan, *A systematic review on ankle injury and ankle sprain in sports.* Sports medicine, 2007. **37**(1): p. 73-94.

[140] Adams, J.G., *Emergency Medicine E-Book: Clinical Essentials (Expert Consult-Online and Print)*. 2012: Elsevier Health Sciences.

[141] Swartz, M.H., *Textbook of Physical Diagnosis, History and Examination.* Journal of General Internal Medicine, 1995. **10**(7): p. 416-416.

[142] Winter, D.A., *Biomechanics and motor control of human movement*. 2009: John Wiley & Sons.

[143] Maughan, R., J.S. Watson, and J. Weir, *Strength and cross-sectional area of human skeletal muscle.* The Journal of physiology, 1983. **338**(1): p. 37-49.

[144] Pearson Education, I. *Lower leg muscles, http://web.uaccb.edu/academicdivisions/mathscience/science/bwheeler/ess/figs/0620figure-u.jpg]*. 2009.

[145] Latash, M.L. and V.M. Zatsiorsky, *Joint Stiffness - Myth or Reality.* Human Movement Science, 1993. **12**(6): p. 653-692.

[146] Yeung, M., K.-M. Chan, C. So, and W. Yuan, *An epidemiological survey on ankle sprain.* British journal of sports medicine, 1994. **28**(2): p. 112-116.

[147] Nichols, T.R., N.E. Bunderson, and M.A. Lyle, *Neural Regulation of Limb Mechanics: Insights from the Organization of Proprioceptive Circuits.* Neuromechanical Modeling of Posture and Locomotion, 2016: p. 69-102.

[148] Zehr, E.P. and R.B. Stein, *What functions do reflexes serve during human locomotion?* Progress in neurobiology, 1999. **58**(2): p. 185-205.

[149] Sinkjær, T., J.B. Andersen, and B. Larsen, *Soleus stretch reflex modulation during gait in humans.* Journal of neurophysiology, 1996. **76**(2): p. 1112-1120.

[150] Dietz, V., K.-H. Mauritz, and J. Dichgans, *Body oscillations in balancing due to segmental stretch reflex activity.* Experimental brain research, 1980. **40**(1): p. 89-95.

[151] Kearney, R.E. and I.W. Hunter, *System-Identification of Human Joint Dynamics.* Critical Reviews in Biomed Eng, 1990. **18**(1): p. 55-87.

[152] Perreault, E.J., R.F. Kirsch, and A.M. Acosta, *Multiple-input, multiple-output system identification for characterization of limb stiffness dynamics.* Biological Cybernetics, 1999. **80**(5): p. 327-337.

[153] Westwick, D.T. and R.E. Kearney, *Identification of physiological systems: A robust method for non-parametric impulse response estimation.* Medical & Biological Eng. & Comp., 1997. **35**(2): p. 83-90.

[154] Westwick, D.T. and E.J. Perreault, *Estimates of Acausal Joint Impedance Models.* IEEE Trans Biomed Eng, 2012. **59**(10): p. 2913-2921.

[155] Perreault, E.J., P.E. Crago, and R.F. Kirsch, *Estimation of intrinsic and reflex contributions to muscle dynamics: A modeling study.* IEEE Trans Biomed Eng, 2000. **47**(11): p. 1413-1421.

[156] Lee, H., P. Ho, M. Rastgaar, H.I. Krebs, and N. Hogan, *Multivariable Static Ankle Mechanical Impedance With Active Muscles.* IEEE Trans Neural Sys Rehab Eng, 2014. **22**(1): p. 44-52.

[157] Lee, H., P. Ho, M.A. Rastgaar, H.I. Krebs, and N. Hogan, *Multivariable static ankle mechanical impedance with relaxed muscles.* J. Biomech., 2011. **44**(10): p. 1901-1908.

[158] Lee, H. and N. Hogan, *Time-Varying Ankle Mechanical Impedance During Human Locomotion.* IEEE Trans Neural Sys Rehab Eng, 2015. **23**(5): p. 755-764.

[159] Weiss, P.L., R.E. Kearney, and I.W. Hunter, *Position dependence of ankle joint dynamics—I. Passive mechanics.* J. Biomech., 1986. **19**(9): p. 727-735.

[160] Weiss, P.L., R.E. Kearney, and I.W. Hunter, *Position dependence of ankle joint dynamics—II. Active mechanics.* J. Biomech., 1986. **19**(9): p. 737-751.

[161] Pfeifer, S., H. Vallery, M. Hardegger, R. Riener, and E.J. Perreault, *Model-Based Estimation of Knee Stiffness.* IEEE Trans Biomed Eng, 2012. **59**(9): p. 2604-2612.

[162] Wang, D., G. De Vito, M. Ditroilo, D.T.P. Fong, and E. Delahunt, *A comparison of muscle stiffness and musculoarticular stiffness of the knee joint in young athletic males and females.* Journal of Electromyography and Kinesiology, 2015. **25**(3): p. 495-500.

[163] de Vlugt, E., S. van Eesbeek, P. Baines, J. Hilte, C.G.M. Meskers, and J.H. de Groot, *Short range stiffness elastic limit depends on joint velocity.* J. Biomech., 2011. **44**(11): p. 2106-2112.

[164] Sobhani Tehrani, E., K. Jalaleddini, and R.E. Kearney, *Ankle Joint Intrinsic Dynamics is More Complex than a Mass-Spring-Damper Model.* IEEE Trans Neural Syst Rehabil Eng, 2017. **25**(9): p. 1568-1580.

[165] Kearney, R.E. and I.W. Hunter, *System identification of human triceps surae stretch reflex dynamics.* Exp Brain Res, 1983. **51**(1): p. 117-27.

[166] Berardelli, A., M. Hallett, C. Kaufman, E. Fine, W. Berenberg, and S.R. Simon, *Stretch reflexes of triceps surae in normal man.* Journal of Neurology, Neurosurgery, and Psychiatry, 1982. **45**(6): p. 513-525.

[167] Kearney, R.E. and I.W. Hunter, *System-Identification of Human Triceps Surae Stretch Reflex Dynamics.* Exp. Brain Res., 1983. **51**(1): p. 117-127.

[168] Mirbagheri, M.M., H. Barbeau, and R.E. Kearney, *Modulation of spastic anke stiffness dynamics with voluntary contraction in spinal cord injury.* Proceedings of the 23rd Annual International Conference of the Ieee Engineering in Medicine and Biology Society, Vols 1-4, 2001. **23**: p. 1260-1262.

[169] Mirbagheri, M.M., H. Barbeau, M. Ladouceur, and R.E. Kearney, *Intrinsic and reflex stiffness in normal and spastic, spinal cord injured subjects.* Exp. Brain Res., 2001. **141**(4): p. 446-459.

[170] Kearney, R.E. and I.W. Hunter, *System identification of human stretch reflex dynamics: tibialis anterior.* Exp Brain Res, 1984. **56**(1): p. 40-9.

[171] Jalaleddini, K., E. Sobhani Tehrani, and R.E. Kearney, *A Subspace Approach to the Structural Decomposition and Identification of Ankle Joint Dynamic Stiffness.* IEEE Trans. Biomed. Eng., 2017. **64**(6): p. 1357-1368.

[172] Mrachacz-Kersting, N. and T. Sinkjaer, *Reflex and non-reflex torque responses to stretch of the human knee extensors.* Experimental Brain Research, 2003. **151**(1): p. 72-81.

[173] Guarin, D.L., K. Jalaleddini, and R.E. Kearney, *Identification of a Parametric, Discrete-time Model of Ankle Stiffness.* 35th IEEE EMBC Conf., 2013: p. 5065-5070.

[174] Zhao, Y., *Identification of Ankle Joint Stiffness Using Subspace Methods*, in *Department of Biomedical Engineering*. 2009, McGill University: Montreal, Canada.

[175] Tehran, E.S., *Nonlinear Parameter Varying Identification of Time-Varying Ankle Dynamic Stiffness*. 2018, McGill University.

[176] Hunter, I.W. and R.E. Kearney, *Dynamics of human ankle stiffness: Variation with mean ankle torque.* Journal of Biomechanics, 1982. **15**(10): p. 747-752.

[177] van der Helm, F.C.T., A.C. Schouten, E. de Vlugt, and G.G. Brouwn, *Identification of intrinsic and reflexive components of human arm dynamics during postural control.* Journal of Neuroscience Methods, 2002. **119**(1): p. 1-14.

[178] Kearney, R.E. and I.W. Hunter, *Dynamics of human ankle stiffness: variation with displacement amplitude.* J Biomech, 1982. **15**(10): p. 753-6.

[179] Guarin, D.L. and R.E. Kearney, *Identification of a Time-Varying, Box-Jenkins Model of Intrinsic Joint Compliance.* Ieee Transactions on Neural Systems and Rehabilitation Engineering, 2017. **25**(8): p. 1211-1220.

[180] Golkar, M.A., E. Sobhani Tehrani, and R.E. Kearney, *Linear Parameter Varying Identification of Dynamic Joint Stiffness during Time-Varying Voluntary Contractions.* Front Comput Neurosci, 2017. **11**: p. 35.

[181] Sobhani Tehrani, E., K. Jalaleddini, and R.E. Kearney, *Linear parameter varying identification of ankle joint intrinsic stiffness during imposed walking movements.* Conf Proc IEEE Eng Med Biol Soc, 2013. **2013**: p. 4923-7.

[182] Ludvig, D., T.S. Visser, H. Giesbrecht, and R.E. Kearney, *Identification of time-varying intrinsic and reflex joint stiffness.* IEEE Trans Biomed Eng, 2011. **58**(6): p. 1715-23.

[183] Sobhani Tehrani, E., K. Jalaleddini, and R.E. Kearney. *Linear parameter varying identification of ankle joint intrinsic stiffness during imposed walking movements*. in *35th IEEE EMBS Conf.* 2013.

[184] Kirsch, R.F. and R.E. Kearney, *Identification of time varying stiffness dynamics of the human ankle joint during an imposed movement.* Experimental Brain Research, 1997. **114**(1): p. 71-85.

[185] Jalaleddini, K., M.A. Golkar, and R.E. Kearney, *Measurement of dynamic joint stiffness from multiple short data segments.* IEEE Transactions on Neural Systems and Rehabilitation Engineering, 2017. **25**(7): p. 925-934.

[186] Rouse, E.J., L.J. Hargrove, E.J. Perreault, and T.A. Kuiken, *Estimation of Human Ankle Impedance During the Stance Phase of Walking.* IEEE Trans Neural Sys Rehab Eng, 2014. **22**(4): p. 870-878.

[187] Kirsch, R.F. and R.E. Kearney, *Identification of Time-Varying Dynamics of the Human Triceps Surae Stretch Reflex .2. Rapid Imposed Movement.* Experimental Brain Research, 1993. **97**(1): p. 128-138.

[188] Kirsch, R.F., R.E. Kearney, and J.B. Macneil, *Identification of Time-Varying Dynamics of the Human Triceps Surae Stretch Reflex .1. Rapid Isometric Contraction.* Experimental Brain Research, 1993. **97**(1): p. 115-127.

[189] Kearney, R.E., M. Lortie, and R.B. Stein, *Modulation of stretch reflexes during imposed walking movements of the human ankle.* J Neurophysiol, 1999. **81**(6): p. 2893-902.

[190] Sakanaka, T.E., *Causes of variation in intrinsic ankle stiffness and the consequences for standing*, in *School of Sport, Exercise and Rehabilitation Sciences*. 2017, University of Birmingham. p. 213.

[191] Warner, J. and A.W. Wiegner, *Effects of muscle thixotropy on afferent activity in the hindlimb of the rat.* Experimental physiology, 1990. **75**(2): p. 223-230.

[192] Whitehead, N., J. Gregory, D. Morgan, and U. Proske, *Passive mechanical properties of the medial gastrocnemius muscle of the cat.* The Journal of physiology, 2001. **536**(3): p. 893-903.

[193] Stein, R.B., *Presynaptic inhibition in humans.* Progress in Neurobiology, 1995. **47**(6): p. 533-544.

[194] Schieppati, M., *The Hoffmann reflex: a means of assessing spinal reflex excitability and its descending control in man.* Progress in neurobiology, 1987. **28**(4): p. 345-376.

[195] Zehr, P.E., *Considerations for use of the Hoffmann reflex in exercise studies.* European journal of applied physiology, 2002. **86**(6): p. 455-468.

[196] Palmieri, R.M., C.D. Ingersoll, and M.A. Hoffman, *The Hoffmann reflex: methodologic considerations and applications for use in sports medicine and athletic training research.* Journal of athletic training, 2004. **39**(3): p. 268.

[197] Morita, H., N. Petersen, L. Christensen, T. Sinkjær, and J. Nielsen, *Sensitivity of H-reflexes and stretch reflexes to presynaptic inhibition in humans.* Journal of neurophysiology, 1998. **80**(2): p. 610-620.

[198] Shimba, S., N. Kawashima, Y. Ohta, S.-I. Yamamoto, and K. Nakazawa, *Enhanced stretch reflex excitability in the soleus muscle during passive standing posture in humans.* Journal of Electromyography and Kinesiology, 2010. **20**(3): p. 406-412.

[199] Cecen, S., I.K. Niazi, R.W. Nedergaard, A. Cade, K. Allen, K. Holt, H. Haavik, and K.S. Türker, *Posture modulates the sensitivity of the H-reflex.* Experimental Brain Research, 2018. **236**(3): p. 829-835.

[200] Miles, T. and K. Türker, *Does reflex inhibition of motor units follow the "size principle"?* Experimental brain research, 1986. **62**(2): p. 443-445.

[201] Türker, K., *A method for standardization of silent period measurements in human masseter muscle.* Journal of oral rehabilitation, 1988. **15**(1): p. 91-101.

[202] Stein, R.B., K.L. Estabrooks, S. McGie, M.J. Roth, and K.E. Jones, *Quantifying the effects of voluntary contraction and inter-stimulus interval on the human soleus H-reflex.* Experimental brain research, 2007. **182**(3): p. 309-319.

[203] Lowrey, C.R. and L.R. Bent, *Modulation of the soleus H-reflex following galvanic vestibular stimulation and cutaneous stimulation in prone human subjects.* Muscle & Nerve: Official Journal of the American Association of Electrodiagnostic Medicine, 2009. **40**(2): p. 213-220.

[204] Scarpini, C., R. Mazzocchio, M. Mondelli, D. Nuti, and A. Rossi, *Changes in alpha motoneuron excitability of the soleus muscle in relation to vestibular stimulation assessed by angular acceleration in man.* ORL, 1991. **53**(2): p. 100-105.

[205] Nakazawa, K., N. Kawashima, H. Obata, K. Yamanaka, D. Nozaki, and M. Akai, *Facilitation of both stretch reflex and corticospinal pathways of the tibialis anterior muscle during standing in humans.* Neuroscience Letters, 2003. **338**(1): p. 53-56.

[206] Kawashima, N., H. Yano, Y. Ohta, and K. Nakazawa, *Stretch reflex modulation during imposed static and dynamic hip movements in standing humans.* Experimental Brain Research, 2006. **174**(2): p. 342-350.

[207] Tokuno, C.D., S.J. Garland, M.G. Carpenter, A. Thorstensson, and A.G. Cresswell, *Sway-dependent modulation of the triceps surae H-reflex during standing.* J Appl Physiol (1985), 2008. **104**(5): p. 1359-65.

[208] Tokuno, C.D., M.G. Carpenter, A. Thorstensson, S.J. Garland, and A.G. Cresswell, *Control of the triceps surae during the postural sway of quiet standing.* Acta Physiol (Oxf), 2007. **191**(3): p. 229-36.

[209] Mynark, R.G., *Reliability of the soleus H-reflex from supine to standing in young and elderly.* Clinical neurophysiology, 2005. **116**(6): p. 1400-1404.

[210] Tokuda, T., K. Tako, R. Hayashi, and N. Yanagisawa, *Disturbed modulation of the stretch reflex gain during standing in cerebellar ataxia.* Electroencephalography and Clinical Neurophysiology/Evoked Potentials Section, 1991. **81**(6): p. 421-426.

[211] Buchanan, T.S., D.G. Lloyd, K. Manal, and T.F. Besier, *Neuromusculoskeletal Modeling: Estimation of Muscle Forces and Joint Moments and Movements from Measurements of Neural Command.* Journal of Applied Biomechanics, 2004. **20**(4): p. 367-395.

[212] Bock, P.J., R.E. Kearney, S.M. Forster, and R. Wagner, *Modulation of stretch reflex excitability during quiet human standing.* Conf Proc IEEE Eng Med Biol Soc, 2004. **7**: p. 4684-7.

[213] Lang, C.B. and R.E. Kearney, *Modulation of ankle stiffness during postural sway.* Conf Proc IEEE Eng Med Biol Soc, 2014. **2014**: p. 4062-5.

[214] Lang, C.B., *The Modulation of Dynamic Ankle Stiffness with Postural Sway During Upright Stance*. 2014, McGill Univeristy.

[215] Westwick, D.T. and R.E. Kearney, *Separable Least Squares Identification of Nonlinear Hammerstein Models: Application to Stretch Reflex Dynamics.* Annals of Biomedical Engineering, 2001. **29**(8): p. 707-718.

[216] Westwick, D.T. and R.E. Kearney, *Identification of nonlinear physiological systems*. Vol. 7. 2003: John Wiley & Sons.

[217] Jalaleddini, K. and R.E. Kearney, *Subspace identification of SISO Hammerstein systems: application to stretch reflex identification.* IEEE transactions on biomedical engineering, 2013. **60**(10): p. 2725-2734.

[218] Jalaleddini, K., E.S. Tehrani, and R.E. Kearney, *A subspace approach to the structural decomposition and identification of ankle joint dynamic stiffness.* IEEE transactions on biomedical engineering, 2016. **64**(6): p. 1357-1368.

[219] Macneil, J.B., R.E. Kearney, and I.W. Hunter, *Identification of Time-Varying Biological-Systems from Ensemble Data.* Ieee Transactions on Biomedical Engineering, 1992. **39**(12): p. 1213-1225.

[220] Lortie, M. and R.E. Kearney, *Identification of Time-Varying Hammerstein Systems from Ensemble Data.* Annals of Biomedical Engineering, 2001. **29**(7): p. 619-635.

[221] Ludvig, D., T.S. Visser, H. Giesbrecht, and R.E. Kearney, *Identification of Time-Varying Intrinsic and Reflex Joint Stiffness.* Ieee Transactions on Biomedical Engineering, 2011. **58**(6): p. 1715-1723.

[222] Guarín, D.L. and R.E. Kearney, *Estimation of Time-Varying, Intrinsic and Reflex Dynamic Joint Stiffness during Movement. Application to the Ankle Joint.* Frontiers in Computational Neuroscience, 2017. **11**(51).

[223] Verahegen, M. and P. Dewilde, *Subspace model identification. Part I: The output-error state-space model identification class of algorithm.* Int. J. Control, 1992. **56**: p. 1187-1210.

[224] Forssell, U., *Closed-loop Identification*

Methods, Theory, and Applications, in *Department of Electrical Engineering*

1999, Linkoping University.

[225] Chou, C.T. and M. Verhaegen, *Subspace algorithms for the identification of multivariable dynamic errors-in-variables models.* Automatica, 1997. **33**(10): p. 1857-1869.

[226] Ljung, L., *System identification: theory for the user*. 1986: Prentice-Hall, Inc.

[227] Westwick, D.T. and E.J. Perreault, *Closed-Loop Identification: Application to the Estimation of Limb Impedance in a Compliant Environment.* Ieee Transactions on Biomedical Engineering, 2011. **58**(3): p. 521-530.

[228] Van Wingerden, J.-W., *Control of wind turbines with'Smart'rotors: Proof of concept & LPV subspace identification.* 2008.

[229] Van Donkelaar, E.T. and P.M. Van den Hof, *Analysis of closed-loop identification with a tailor-made parameterization.* European Journal of Control, 2000. **6**(1): p. 54-62.

[230] Johansson, R., M. Magnusson, P.A. Fransson, and M. Karlberg, *Multi-stimulus multi-response posturography.* Mathematical Biosciences, 2001. **174**(1): p. 41-59.

[231] Jeka, J., K. Oie, G. Schöner, T. Dijkstra, and E. Henson, *Position and Velocity Coupling of Postural Sway to Somatosensory Drive.* Journal of Neurophysiology, 1998. **79**(4): p. 1661-1674.

[232] Maki, B.E. and G.R. Fernie, *A system identification approach to balance testing.* Prog Brain Res, 1988. **76**: p. 297-306.

[233] Maki, B.E., P.J. Holliday, and G.R. Fernie, *A Posture Control Model and Balance Test for the Prediction of Relative Postural Stability.* IEEE Transactions on Biomedical Engineering, 1987. **BME-34**(10): p. 797-810.

[234] Hwang, S., P. Agada, T. Kiemel, and J.J. Jeka, *Identification of the Unstable Human Postural Control System.* Frontiers in Systems Neuroscience, 2016. **10**(22).

[235] Masani, K., A.H. Vette, and M.R. Popovic, *Controlling balance during quiet standing: proportional and derivative controller generates preceding motor command to body sway position observed in experiments.* Gait Posture, 2006. **23**(2): p. 164-72.

[236] Masani, K., M.R. Popovic, K. Nakazawa, M. Kouzaki, and D. Nozaki, *Importance of body sway velocity information in controlling ankle extensor activities during quiet stance.* J Neurophysiol, 2003. **90**(6): p. 3774-82.

[237] Barin, K., *Evaluation of a generalized model of human postural dynamics and control in the sagittal plane.* Biological Cybernetics, 1989. **61**(1): p. 37-50.

[238] Loram, I.D., S.M. Kelly, and M. Lakie, *Human balancing of an inverted pendulum: is sway size controlled by ankle impedance?* The Journal of physiology, 2001. **532**(3): p. 879-891.

[239] Mihelj, M., Z. Matjačić, and T. Bajd, *Postural activity of constrained subject in response to disturbance in sagittal plane.* Technology and Health Care, 1999. **7**(6): p. 437-442.

[240] Ishida, A. and S. Miyazaki, *Maximum likelihood identification of a posture control system.* IEEE Trans Biomed Eng, 1987. **34**(1): p. 1-5.

[241] Ishida, A., S. Imai, and Y. Fukuoka, *Analysis of the posture control system under fixed and sway-referenced support conditions.* IEEE Trans Biomed Eng, 1997. **44**(5): p. 331-6.

[242] Sousa, A.S., A. Silva, and J.M. Tavares, *Biomechanical and neurophysiological mechanisms related to postural control and efficiency of movement: a review.* Somatosens Mot Res, 2012. **29**(4): p. 131-43.

[243] Mohamed, A.A., J. Baba, J. Beyea, J. Landry, A. Sexton, and C.A. McGibbon, *Comparison of strain-gage and fiber-optic goniometry for measuring knee kinematics during activities of daily living and exercise.* J Biomech Eng, 2012. **134**(8): p. 084502.

[244] Cooper, G., I. Sheret, L. McMillan, K. Siliverdis, N. Sha, D. Hodgins, L. Kenney, and D. Howard, *Inertial sensor-based knee flexion/extension angle estimation.* J Biomech, 2009. **42**(16): p. 2678-85.

[245] Amiri, P., L.J. MacLean, and R.E. Kearney, *Measurement of shank angle during stance using laser range finders.* International Conference of the IEEE Engineering in Medicine and Biology, 2016.

[246] Forster, S.M., R. Wagner, and R.E. Kearney, *A bilateral electro-hydraulic actuator system to measure dynamic ankle joint stiffness during upright human stance.*

[247] Dakin, C.J., G.M.L. Son, J.T. Inglis, and J.S. Blouin, *Frequency response of human vestibular reflexes characterized by stochastic stimuli.* The Journal of physiology, 2007. **583**(3): p. 1117-1127.

[248] Forster, S.M., R. Wagner, and R.E. Kearney, *A bilateral electro-hydraulic actuator system to measure dynamic ankle joint stiffness during upright human stance.* Proceedings of the 25th Annual International Conference of the IEEE Engineering in Medicine and Biology Society, Cancun, Mexico, 2003: p. 1507-1510.

[249] Davis, J., Y.-H. Hsieh, and H.-C. Lee, *Humans perceive flicker artifacts at 500 Hz.* Scientific reports, 2015. **5**: p. 7861.

[250] http://www.seniam.org/.

[251] Jalaleddini, K., E.S. Tehrani, and R.E. Kearney, *A Subspace Approach to the Structural Decomposition and Identification of Ankle Joint Dynamic Stiffness.* IEEE Trans Biomed Eng, 2017. **64**(6): p. 1357-1368.

[252] Amiri, P. and R.E. Kearney, *A Closed-loop Method to Identify EMG-Ankle Torque Dynamic Relation in Human Balance Control.* Conf Proc IEEE Eng Med Biol Soc, 2019.

[253] NASA. *Anthropometry and biomechanics*. 1995; Available from: http://msis.jsc.nasa.gov/sections/section03.htm.

[254] Amiri, P. and R.E. Kearney, *Patterns of Muscle Activation and Modulation of Ankle Intrinsic Stiffness in Different Postural Operating Conditions*. Journal of Neurophysiology, 2019.

[255] Jeka, J.J., L.K. Allison, and T. Kiemel, *The dynamics of visual reweighting in healthy and fall-prone older adults.* Journal of motor behavior, 2010. **42**(4): p. 197-208.

[256] Jilk, D.J., S.A. Safavynia, and L.H. Ting, *Contribution of vision to postural behaviors during continuous support-surface translations.* Experimental brain research, 2014. **232**(1): p. 169-180.

[257] Pasma, J.H., T.A. Boonstra, J. van Kordelaar, V.V. Spyropoulou, and A.C. Schouten, *A Sensitivity Analysis of an Inverted Pendulum Balance Control Model.* Frontiers in Computational Neuroscience, 2017. **11**(99).

[258] Westwick, D.T. and R.E. Kearney, *An object-oriented toolbox for linear and nonlinear system identification.* Conf Proc IEEE Eng Med Biol Soc, 2004. **1**: p. 514-7.

[259] Horak, F.B., C.L. Shupert, V. Dietz, and G. Horstmann, *Vestibular and somatosensory contributions to responses to head and body displacements in stance.* Exp Brain Res, 1994. **100**(1): p. 93-106.

[260] Oie, K.S., T. Kiemel, and J.J. Jeka, *Human multisensory fusion of vision and touch: detecting non-linearity with small changes in the sensory environment.* Neurosci Lett, 2001. **315**(3): p. 113-6.

[261] Ludvig, D., I. Cathers, and R.E. Kearney, *Voluntary modulation of human stretch reflexes.* Exp Brain Res, 2007. **183**(2): p. 201-13.

[262] Riley, M.A., S. Mitra, T.A. Stoffregen, and M.T. Turvey, *Influences of Body Lean and Vision on Unperturbed Postural Sway.* Motor Control, 1997. **1**(3): p. 229-246.

[263] Duarte, M. and V.M. Zatsiorsky, *Effects of body lean and visual information on the equilibrium maintenance during stance.* Exp Brain Res, 2002. **146**(1): p. 60-9.

[264] Kluzik, J., F.B. Horak, and R.J. Peterka, *Differences in preferred reference frames for postural orientation shown by after-effects of stance on an inclined surface.* Exp Brain Res, 2005. **162**(4): p. 474-89.

[265] Kluzik, J., R.J. Peterka, and F.B. Horak, *Adaptation of postural orientation to changes in surface inclination.* Exp Brain Res, 2007. **178**(1): p. 1-17.

[266] Mezzarane, R.A. and A.F. Kohn, *Control of upright stance over inclined surfaces.* Exp Brain Res, 2007. **180**(2): p. 377-88.

[267] Al-Khabbaz, Y.S., T. Shimada, and M. Hasegawa, *The effect of backpack heaviness on trunk-lower extremity muscle activities and trunk posture.* Gait Posture, 2008. **28**(2): p. 297-302.

[268] Strube, E.M., A. Sumner, R. Kollock, K.E. Games, M.A. Lackamp, M. Mizutani, and J.M. Sefton, *The Effect of Military Load Carriage on Postural Sway, Forward Trunk Lean, and Pelvic Girdle Motion.* Int J Exerc Sci, 2017. **10**(1): p. 25-36.

[269] https://www.mathworks.com/.

[270] Earhart, G.M., J.M. Henckens, P. Carlson-Kuhta, and F.B. Horak, *Influence of vision on adaptive postural responses following standing on an incline.* Exp Brain Res, 2010. **203**(1): p. 221-6.

[271] Chong, R., B. Berl, B. Cook, P. Turner, and K. Walker, *Individuals with a vestibular-related disorder use a somatosensory-dominant strategy for postural orientation after inclined stance.* Acta Neurol Scand, 2017. **135**(6): p. 635-640.

[272] Sasagawa, S., J. Ushiyama, K. Masani, M. Kouzaki, and H. Kanehisa, *Balance control under different passive contributions of the ankle extensors: quiet standing on inclined surfaces.* Exp Brain Res, 2009. **196**(4): p. 537-44.

[273] Sinha, T. and B.E. Maki, *Effect of forward lean on postural ankle dynamics.* IEEE Trans Rehabil Eng, 1996. **4**(4): p. 348-59.

[274] Nielsen, J., T. Sinkjaer, E. Toft, and Y. Kagamihara, *Segmental reflexes and ankle joint stiffness during co-contraction of antagonistic ankle muscles in man.* Exp Brain Res, 1994. **102**(2): p. 350-8.

[275] McGill, S.M., S. Grenier, N. Kavcic, and J. Cholewicki, *Coordination of muscle activity to assure stability of the lumbar spine.* J Electromyogr Kinesiol, 2003. **13**(4): p. 353-9.

[276] Lee, P.J., E.L. Rogers, and K.P. Granata, *Active trunk stiffness increases with co-contraction.* J Electromyogr Kinesiol, 2006. **16**(1): p. 51-7.

[277] Hirokawa, S., M. Solomonow, Z. Luo, Y. Lu, and R. D'Ambrosia, *Muscular co-contraction and control of knee stability.* J Electromyogr Kinesiol, 1991. **1**(3): p. 199-208.

[278] Ward, S.R., C.M. Eng, L.H. Smallwood, and R.L. Lieber, *Are current measurements of lower extremity muscle architecture accurate?* Clin Orthop Relat Res, 2009. **467**(4): p. 1074-82.

[279] Peterka, R., *Sensorimotor integration in human postural control.* Journal of neurophysiology, 2002. **88**(3): p. 1097-1118.

[280] Chalmers, G.R. and K.M. Knutzen, *Soleus H-Reflex Gain in Healthy Elderly and Young Adults When Lying, Standing, and Balancing.* The Journals of Gerontology: Series A, 2002. **57**(8): p. B321-B329.

[281] Amiri, P., A. Mohebbi, and R.E. Kearney, *Experimental methods to study human postural control.* Journal of Visualized Experiments, 2019.

[282] Sinkjaer, T., E. Toft, K. Larsen, and S. Andreassen, *Emg-Torque Dynamics at Different Contraction Levels in Human Ankle Muscles.* Journal of Electromyography and Kinesiology, 1993. **3**(2): p. 67-77.

[283] Genadry, W.F., R.E. Kearney, and I.W. Hunter, *Dynamic Relationship between Emg and Torque at the Human Ankle - Variation with Contraction Level and Modulation.* Medical & Biological Engineering & Computing, 1988. **26**(5): p. 489-496.

[284] Golkar, M.A., K. Jalaleddini, and R.E. Kearney, *EMG-Torque Dynamics Change with Contraction Bandwidth.* IEEE Transactions on Neural Systems and Rehabilitation Engineering, 2018. **PP**(99): p. 1-1.

[285] Amiri, P. and R.E. Kearney, *Ankle Intrinsic Stiffness Changes with Postural Sway.* Journal of Biomechanics, 2018.

[286] Klomp, A., J.H. de Groot, E. de Vlugt, C.G. Meskers, J.H. Arendzen, and F.C. van der Helm, *Perturbation amplitude affects linearly estimated neuromechanical wrist joint properties.* IEEE Trans Biomed Eng, 2014. **61**(4): p. 1005-14.

[287] van Drunen, P., E. Maaswinkel, F.C. van der Helm, J.H. van Dieen, and R. Happee, *Identifying intrinsic and reflexive contributions to low-back stabilization.* J Biomech, 2013. **46**(8): p. 1440-6.

[288] Pasma, J.H., J. van Kordelaar, D. de Kam, V. Weerdesteyn, A.C. Schouten, and H. van der Kooij, *Assessment of the underlying systems involved in standing balance: the additional value of electromyography in system identification and parameter estimation.* Journal of NeuroEngineering and Rehabilitation, 2017. **14**(1): p. 97.

[289] Schouten, A.C., E. De Vlugt, J.J.B. Van Hilten, and F.C.T. Van der Helm, *Quantifying proprioceptive reflexes during position control of the human arm.* Ieee Transactions on Biomedical Engineering, 2008. **55**(1): p. 311-321.

[290] Tani, H. and H. Nagasaki, *Contractile properties of human ankle muscles determined by a systems analysis method for the EMG-force relationship.* Journal of Electromyography and Kinesiology, 1996. **6**(3): p. 205-213.

[291] De Luca, C.J., R.S. LeFever, M.P. McCue, and A.P. Xenakis, *Behaviour of human motor units in different muscles during linearly varying contractions.* The Journal of physiology, 1982. **329**: p. 113-128.

[292] Maffiuletti, N.A., P. Aagaard, A.J. Blazevich, J. Folland, N. Tillin, and J. Duchateau, *Rate of force development: physiological and methodological considerations.* European Journal of Applied Physiology, 2016. **116**(6): p. 1091-1116.

[293] Desmedt, J.E. and E. Godaux, *Ballistic contractions in man: characteristic recruitment pattern of single motor units of the tibialis anterior muscle.* The Journal of physiology, 1977. **264**(3): p. 673-693.

[294] Desmedt, J.E. and E. Godaux, *Ballistic contractions in fast or slow human muscles: discharge patterns of single motor units.* The Journal of physiology, 1978. **285**: p. 185-196.

[295] Yao, W., R.J. Fuglevand, and R.M. Enoka, *Motor-Unit Synchronization Increases EMG Amplitude and Decreases Force Steadiness of Simulated Contractions.* Journal of Neurophysiology, 2000. **83**(1): p. 441-452.

[296] Toft, E., T. Sinkjaer, and S. Andreassen, *Mechanical and electromyographic responses to stretch of the human anterior tibial muscle at different levels of contraction.* Exp Brain Res, 1989. **74**(1): p. 213-9.

[297] van der Kooij, H. and R.J. Peterka, *Non-linear stimulus-response behavior of the human stance control system is predicted by optimization of a system with sensory and motor noise.* Journal of Computational Neuroscience, 2011. **30**(3): p. 759-778.

[298] Mergner, T., *Modeling sensorimotor control of human upright stance.* Prog Brain Res, 2007. **165**: p. 283-97.

[299] Mergner, T., C. Maurer, and R.J. Peterka, *Sensory contributions to the control of stance: a posture control model.* Adv Exp Med Biol, 2002. **508**: p. 147-52.

[300] Morasso, P.G., L. Baratto, R. Capra, and G. Spada, *Internal models in the control of posture.* Neural Netw, 1999. **12**(7-8): p. 1173-1180.

[301] Nakazawa, K., T. Miyoshi, H. Sekiguchi, D. Nozaki, M. Akai, and H. Yano, *Effects of loading and unloading of lower limb joints on the soleus H-reflex in standing humans.* Clinical Neurophysiology, 2004. **115**(6): p. 1296-1304.

[302] Miyoshi, T., D. Nozaki, H. Sekiguchi, T. Kimura, T. Sato, T. Komeda, K. Nakazawa, and H. Yano, *Somatosensory graviception inhibits soleus H-reflex during erect posture in humans as revealed by parabolic flight experiment.* Experimental Brain Research, 2003. **150**(1): p. 109-113.